

UNIVERSITY OF NAPLES FEDERICO II

*Department of Structures
for Engineering and Architecture*

PH.D. PROGRAMME IN
SEISMIC RISK
COORDINATOR PROF. ALDO ZOLLO
XXVI CYCLE



CRESCENZO PETRONE

PH.D. THESIS

**NONSTRUCTURAL COMPONENTS: SEISMIC
CAPACITY AND DEMAND**

TUTOR: PROF. DR. GENNARO MAGLIULO

2014

*To Agnese, Carmela,
Raffaelina and Marianna*

ABSTRACT

Some research studies concerning nonstructural components are described in this thesis, based on several motivations: (a) the threat to life-safety that the collapse of nonstructural components can cause; (b) the attitude of these components in exhibiting damage (and the consequent evacuation of buildings) even for low-intensity earthquakes; (c) the huge economic loss connected to their damage.

Different experimental activities are carried out aiming at the evaluation of the seismic capacity of some nonstructural components, i.e. innovative plasterboard partitions, hollow brick partitions, standard high plasterboard partitions, hospital building contents and plasterboard continuous ceilings.

A test setup is defined for each test campaign in order to subject the specimen to the demand that it would experience in a building. Realistic boundary conditions of the specimen are reproduced. A testing protocol is defined according to AC 156, in case shake table tests are conducted, and FEMA 461 prescriptions, in case quasi-static tests are performed. A slight modification to the testing protocol provided by FEMA 461 is proposed, considering a set of European earthquakes in lieu of American ones, while a seismic input is derived based on AC 156 prescriptions for shake table testing. After each test of each campaign the visual damage is correlated to the occurrence of a given Damage State (DS) through the use of a damage scheme. A relationship between an Engineering Demand Parameter (EDP), e.g. the interstory drift ratio or the peak floor acceleration, and a predefined Damage State (DS), is established for the tested components. In case the number of specimens within a test campaign is adequate, the fragility curve of the tested specimens, that expresses the attitude that the specimens have to exhibit damage at different seismic demand levels, is also evaluated. The damage progression is correlated to different properties of the test setup, such as its natural frequency, damping ratio and the dissipated energy. Macro-models of the tested specimens are also defined based on the experimental results for an easy implementation in a structural model of the tested nonstructural components.

The evaluation of the seismic demand on nonstructural components is also a main objective of this research study. Nonstructural components should be subjected to a careful and rational seismic design, in order to reduce the economic loss and to avoid threats to the life safety, as well as what concerns the structural elements. A parametric study on five RC frame structures, designed according to Eurocode 8, is conducted. It

is found that the Eurocode formulation for the evaluation of the seismic demand on nonstructural components does not well fit the outcomes of the analyses. Some comments on the target spectrum provided by AC 156 for the seismic qualification of nonstructural components are also included and a modification is proposed. The counterintuitive approach of current building codes to the design of nonstructural components is highlighted. For this reason the seismic demand on acceleration-sensitive nonstructural components caused by frequent earthquakes is also investigated. Finally, a novel formulation for the evaluation of such a demand is proposed for an easy implementation in future building codes based on the actual Eurocode provisions. The proposed formulation gives a good estimation of the floor spectral accelerations that result from the analyzed structures.

Keywords: nonstructural components, seismic performance, seismic demand, shake table test, quasi-static test, seismic design.

TABLE OF CONTENTS

Abstract	I
Table of contents.....	III
List of figures	VIII
List of tables	XVI
Chapter 1 Introduction	1
1.1 Motivations	1
1.2 Objectives.....	4
1.3 Outline of the thesis.....	5
1.4 References.....	7
Chapter 2 Seismic capacity of nonstructural components.....	9
2.1 Shake table test on innovative plasterboard partitions	9
2.1.1 Introduction.....	9
2.1.2 Experimental facilities, test setup, specimen and input.....	10
2.1.2.1 Test frame: idea, design and parametric study	12
2.1.2.2 Test setup and specimen: mounting detailed description	15
2.1.2.3 Instrumentation.....	17
2.1.2.4 Input and testing protocol.....	18
2.1.3 Test results and observations	20
2.1.3.1 Dynamic identification	20
2.1.3.2 Results summary.....	26
2.1.3.3 Damage description	30
2.1.3.4 Analytical results	32

2.1.3.5	Frequency and damping evaluation.....	33
2.1.3.6	Base shear repartition	35
2.1.3.7	Evaluation of the frequency of the component.....	36
2.1.4	<i>Analytical modelling: post-test dynamic analyses.....</i>	37
2.1.5	<i>Conclusions</i>	39
2.1.6	<i>References.....</i>	40
2.2	Shake table test on hollow brick partitions.....	43
2.2.1	<i>Introduction</i>	43
2.2.2	<i>Experimental facilities and test set up, specimens and input</i>	44
2.2.2.1	Test setup and specimen	45
2.2.2.2	Instrumentation.....	47
2.2.2.3	Input and testing protocol.....	49
2.2.2.4	Definition of the partition dimensions.....	51
2.2.3	<i>Results and discussion.....</i>	52
2.2.3.1	Dynamic identification	52
2.2.3.2	Results summary.....	53
2.2.3.3	Damage description	57
2.2.3.4	Frequency and damping evaluation.....	61
2.2.3.5	Base shear distribution.....	63
2.2.3.6	Evaluation of the natural frequency of the component.....	64
2.2.4	<i>Conclusions</i>	65
2.2.5	<i>References.....</i>	66
2.3	Shake table test on hospital building contents.....	69
2.3.1	<i>Introduction.....</i>	69
2.3.1.1	State of the art research.....	72
2.3.2	<i>Test setup, specimen, instrumentation and input definition.....</i>	74
2.3.2.1	Test setup and specimens.....	74

2.3.2.2	Input and testing protocol	77
2.3.2.3	Test program.....	79
2.3.3	<i>Results and Discussion</i>	82
2.3.3.1	Dynamic identification	82
2.3.3.2	Numerical modelling of the components.....	88
2.3.3.3	Damage scheme definition	97
2.3.3.4	Test results.....	100
2.3.3.5	Fragility curve evaluation.....	104
2.3.3.6	Horizontal acceleration pattern on cabinet	106
2.3.4	<i>Conclusions</i>	112
2.3.5	<i>References</i>	113
2.4	In-plane test on high plasterboard partitions.....	117
2.4.1	<i>Introduction</i>	117
2.4.2	<i>Experimental facilities, test setup, specimens and testing protocol</i>	118
2.4.2.1	Test setup: concept, design and test on bare setup	119
2.4.2.2	Instrumentation.....	122
2.4.2.3	Testing protocol.....	123
2.4.2.4	Specimens.....	125
2.4.3	<i>Results and Discussion</i>	127
2.4.3.1	Damage description	127
2.4.3.2	Results summary.....	128
2.4.3.3	DS-EDP correlation.....	133
2.4.3.4	Fragility curve evaluation.....	135
2.4.4	<i>Conclusions</i>	136
2.4.5	<i>References</i>	137
2.5	Shake table test on plasterboard continuous ceilings	139
2.5.1	<i>Introduction</i>	139

2.5.2	<i>Experimental facilities and test set up, specimens and input</i>	140
2.5.2.1	Test setup and specimens.....	141
2.5.2.2	Instrumentation.....	143
2.5.2.3	Input and testing protocol.....	144
2.5.3	<i>Results, comparisons and observations</i>	146
2.5.4	<i>Conclusions</i>	152
2.5.5	<i>References</i>	152
Chapter 3	Seismic demand on nonstructural components	155
3.1	Floor response spectra in RC frame structures designed according to Eurocode 8	155
3.1.1	<i>Introduction</i>	155
3.1.2	<i>Methodology</i>	157
3.1.2.1	Description of the parametric study.....	157
3.1.2.2	Modeling.....	158
3.1.2.3	Ground motion records	159
3.1.2.4	Preliminary nonlinear static analyses	161
3.1.3	<i>Results and Discussion</i>	164
3.1.3.1	Elastic and inelastic floor response spectra	164
3.1.3.2	Floor amplification evaluation.....	167
3.1.3.3	Component amplification evaluation.....	169
3.1.3.4	Comparison with EC8 formula and limitations	170
3.1.3.5	Comparison with AC156 target spectrum	173
3.1.4	<i>Conclusions</i>	175
3.1.5	<i>References</i>	177
3.2	Code-oriented evaluation of the seismic demand on light acceleration-sensitive nonstructural components in ordinary buildings	180
3.2.1	<i>Introduction</i>	180
3.2.2	<i>Why to investigate floor spectra caused by frequent earthquakes?</i>	181

3.2.3	<i>Methodology</i>	183
3.2.3.1	Design of the benchmark structures	183
3.2.3.2	Modeling.....	184
3.2.4	<i>Ground motion records</i>	185
3.2.5	<i>Results and Discussion</i>	186
3.2.5.1	Elastic and inelastic floor response spectra	186
3.2.5.2	Floor amplification evaluation.....	189
3.2.5.3	Component amplification evaluation.....	190
3.2.5.4	Comparison with EC8 formula and limitations	190
3.2.5.5	Definition of a code formula.....	193
3.2.6	<i>Conclusions</i>	196
3.2.7	<i>References</i>	197
Chapter 4	Conclusions	199

LIST OF FIGURES

Figure 1. (a) Collapse of horizontal precast panels. (b) Collapse of vertical precast panels.....	2
Figure 2. Damage to (a) infill walls and to (b) internal partition after a 4.9 M_w Italian earthquake.....	3
Figure 3. Damage recorded in hollow brick partitions after 2009 L'Aquila earthquake in (a) a residential building and (b) in San Salvatore hospital.....	3
Figure 4. Typical distribution of costs in three different building typologies (Taghavi and Miranda, 2003).	4
Figure 5. (a) Earthquake simulator system used in the tests; (b) general (XYZ) view of the test setup.	11
Figure 6. Internal plasterboard partition: (a) overview; (b) graphical scheme; (c) horizontal cross section.	12
Figure 7. Scheme of test setup: (a) lateral view, (b) horizontal cross section.	13
Figure 8. Parametric study for the definition of the column cross sections: Equivalent Mass Required (EMR) and the Maximum Stress (MS) for each considered column cross section.....	14
Figure 9. Installation procedure: (a) base runner; (b) top and lateral runners; (c) vertical studs; (d) plasterboard second (outer) layer.	16
Figure 10. Scheme of test instrumentation: (a) lateral view; (b) horizontal cross section.	17
Figure 11. Input time histories and spectra for S_{DS} equal to 0.30 g: (a) acceleration, velocity and displacement time-history - X direction (blue) and Y direction (red); (b) input accelerogram spectra, RRS (bold line), upper and lower limits (dashed line), matching frequency range (vertical dashed line).....	19
Figure 12. Transmissibility ratios curve for the bare steel frame.	21
Figure 13. Ratio between theoretical Transmissibility ratio TR and Displacement response factor R_d for different damping values.	22
Figure 14. Transmissibility ratios curve for the infilled structure.	23
Figure 15. Transfer function generated by a white noise input on the bare structure. ...	23

Figure 16. Acceleration time history recorded at the base of the test frame, Filtered and recorded acceleration time histories at the top of the test frame. The black box indicates the region in which the free vibration decay method is applied.24

Figure 17. Input vs recorded time-histories in X-direction – test no. 4.27

Figure 18. Recorded response spectra vs the Test Response Spectrum (TRS) and the Required Response spectrum (Target Spectrum) in X-direction – test no. 4.27

Figure 19. Input vs recorded time-histories in X-direction – test no. 6.28

Figure 20. Recorded response spectra vs the Test Response Spectrum (TRS) and the Required Response spectrum (Target Spectrum) in X-direction – test no. 6.28

Figure 21. Recorded damage after different shaking tests: (a) acrylic silicone detachment; (b) gypsum dust fall; (c) cracking of the vertical joints between plasterboards; (d) crushing of the corners of the plasterboards.31

Figure 22. Partition rigid-body mechanism for moderate displacement demand level. 32

Figure 23. Top acceleration vs relative displacement plot for the different seismic tests in (a) X direction (b) Y direction.33

Figure 24. (a) Natural frequency evaluation according to Hashemi and Mosalam (2006) (H&M) procedure and transfer curve method (TC) for the different seismic tests; (b) damping ratio evaluation according to Hashemi and Mosalam (2006) (H&M) procedure and the energetic method (EM) for the different seismic tests.35

Figure 25. Base shear repartition between test frame and partition systems for the different seismic tests.36

Figure 26. Transfer function from the base to the partition center in the out of plane direction for the bidirectional tests.37

Figure 27. Comparison between experimental and numerical hysteresis loop: (a) test 6; (b) test 11.38

Figure 28. Comparison between experimental and numerical time histories: (a) test 6; (b) test 11.39

Figure 29. Global view of the test setup.44

Figure 30. Specimen: (a) plan view; (b) general view.46

Figure 31. Cross sections of the specimen: (a) front view of the larger partition; (b) cross sections of the larger partition: gaps filled with mortar to reproduce the presence of the orthogonal partitions.47

Figure 32. Instrumentation arrangement: (a) accelerometers position; (b) strain gauges arrangement; (c) displacement laser sensors layout.48

Figure 33. Input time histories and spectra for S_{DS} equal to 1.50 g: (a) acceleration, velocity and displacement time-history - X direction (blue) and Y direction (red); (b) input accelerogram spectra, RRS (bold line), upper and lower limits (dashed line), matching frequency range (vertical dashed line).50

Figure 34. Transfer functions between base and top acceleration time histories for a low-intensity random vibration applied to both bare and infilled test setups (a) in X direction and (b) in Y direction.53

Figure 35. Input vs recorded time-histories in Y-direction – test no. 2.....54

Figure 36. Recorded response spectra vs the Test Response Spectrum (TRS) and the Required Response spectrum (Target Spectrum) in Y-direction – test no. 2.54

Figure 37. Input vs recorded time-histories in Y-direction – test no. 3.....55

Figure 38. Recorded response spectra vs the Test Response Spectrum (TRS) and the Required Response spectrum (Target Spectrum) in Y-direction – test no. 3.55

Figure 39. Top acceleration vs relative displacement plot for different seismic tests in (a) X direction and (b) Y direction.56

Figure 40. Recorded damage after different shaking tests: (a) wide sliding cracks in mortar in the joints between the bricks; (b) crushing of mortar at the corner; (c) collapse of a brick in the top of the partition; (d) deep extended horizontal cracks in mortar in the lower part of the wall.58

Figure 41. Final damage state at the end of the seismic tests in the largest partition and in the smallest partitions.60

Figure 42. Test frame natural frequency evaluation according to the Transfer Curve method (TC) and to the Hashemi and Mosalam (H&M) procedure (Hashemi and Mosalam, 2006) and compared to the bare frame natural frequency (Bare) for the different seismic tests in (a) X and (b) Y directions; damping ratio evaluation according to the Energetic Method (EM) for the different seismic tests in (c) X and (d) Y directions.62

Figure 43. Transfer function for 7 seconds time windows for different time instants corresponding to test n. 2 in Y direction: (a) 3D view; (b) contour view.....63

Figure 44. Base shear distribution between test frame and partition systems for the different seismic tests in (a) X and (b) Y directions.64

Figure 45. Transfer function from the base to the partition center in the out of plane direction for random vibration tests.....65

Figure 46. Typical emergency response of hospitals in the aftermath of an extreme event, such as an earthquake (Pinto et al., 2011).....70

Figure 47. Damage to the building contents surveyed in the aftermath of the 2011 Van (Turkey) earthquake in the Yüzüncü Yıl University – Faculty of Medicine Hospital. .71

Figure 48. Global perspective of the test setup.....76

Figure 49. Tested hospital building contents: (a) double-windows cabinet, (b) single-window cabinet and (c) desk.77

Figure 50. Earthquake time history and spectra for a level of shaking corresponding to S_{DS} equal to 1.50g: (a) acceleration time-history; (b) input accelerogram spectrum (TRS) and RRS (bold line).....	78
Figure 51. Double-window cabinet in (a) test groups 100 and 400, (b) test groups 200 and 500 and in (c) test groups 300 and 600.....	80
Figure 52. Photo and plan view of the test setup: (a) and (c) configuration 1, adopted in test groups 100, 200 and 300 and (b) and (d) configuration 2, adopted in test groups 400, 500 and 600.	81
Figure 53. Transfer curves for (a) double-window cabinet – tests 1000, (b) single-window cabinet – tests 1000, (c) desk – tests 4000.....	84
Figure 54. 3D and contour plots of the spectrograms recorded on the double-window cabinet during test no. 1001.....	85
Figure 55. Contour plots of the spectrogram (a) on the single-window cabinet during test no. 1001 (b) on the desk during test no. 4001.....	86
Figure 56. Half power bandwidth method applied at the spline envelopes (in green) of the original transfer curves (in blue) for (a) double-window cabinet – tests 1000, (b) single-windows cabinet – tests 1000 and (c) desk – tests 4000.....	88
Figure 57. Desk (a) 3D view and (b) geometry (measures are in cm).....	89
Figure 58. Finite element model of the desk created through Sap 2000.	90
Figure 59. Tube-to-tube connection between the steel elements of the desk.	91
Figure 60. (a) 1 st mode and (b) 2 nd mode shapes, natural frequencies and participating mass ratios.	92
Figure 61. Global view of the considered cabinets.....	93
Figure 62. Connection between the steel elements and the glass window of the single-window cabinet.....	94
Figure 63. Single-window cabinet modal shapes in tests 1000: (a) I vibration mode which frequency is 6.18 Hz, (b) II vibration mode which frequency is 7.38 Hz, (c) III vibration mode which frequency is 23.12 Hz.....	95
Figure 64. Double-window cabinet modal shapes in tests 1000: (a) I vibration mode which frequency is 4.74 Hz, (b) II vibration mode which frequency is 5.08 Hz, (c) III vibration mode whose frequency is 10.35 Hz, (d) IV vibration mode which frequency is 19.90 Hz.....	97
Figure 65. Spectrum compatibility between the spectrum of the recorded acceleration time-history and the target spectrum for test 101, corresponding to a S_{DS} value equal to 0.15 g.	100
Figure 66. Ratio between peak component acceleration and peak shake table acceleration in (a) large cabinet, (b) small cabinet and (c) desk.....	102

Figure 67. Vertical acceleration time history recorded at the base of the single-window cabinet for the different tests of the test group 100.	103
Figure 68. Fragility curves for the damage states 1 and 3 considering mass variability.	105
Figure 69. Fragility curves evaluated considering gap and mass variability for the damage state 3.	106
Figure 70. Fragility curves evaluated considering both gap and mass variability in the same experimental data for the damage state 3.	106
Figure 71. Horizontal acceleration distribution on the double-window cabinet at different intensity levels for the different mass distribution.	107
Figure 72. Horizontal acceleration distribution on the single-window cabinet at different intensity levels for the different mass distribution.	107
Figure 73. Horizontal accelerograms recorded during the test group 1000 corresponding to a 0.45 g S_{DS} value on the double-window cabinet.	108
Figure 74. Horizontal accelerograms recorded during the test group 1000 corresponding to a 0.45 g S_{DS} value on the single-window cabinet.	109
Figure 75. Trend of the horizontal accelerations along the height for the different performed tests (gray and black lines) compared to the structural floor acceleration trend provisions included in ASCE 7 and EC8 (dotted lines) for (a) the double-window and (b) the single-window cabinets.	110
Figure 76. Comparison between the horizontal acceleration trend recorded during the tests (gray and black lines) compared to the current Eurocode 8 (EC8) provision for nonstructural components and to the proposed trend for (a) the double-window and (b) the single-window cabinets.	111
Figure 77. Global view of test setup.	119
Figure 78. (a) Conception scheme of the test setup; (b) kinematic mechanism of the test frame without partition.	120
Figure 79. Test frame 3D view.	120
Figure 80. Lateral view on the rollers of the out-of-plane reaction system.	121
Figure 81. Test on bare test setup: force – displacement relationship.	122
Figure 82. Strain gauge position on the steel vertical stud.	123
Figure 83. Comparison between the ordered normalized amplitudes resulting from the analyses and the amplitudes provided by equation (14).	125
Figure 84. Symmetric (a) and staggered (b) partitions cross sections.	126
Figure 85. Global view of the specimens from no. 1 to no. 6 (from top-left to bottom-right).	127
Figure 86. Damage in the specimen: (a) paper cracking along the perimeter (test no. 1); (b) paper cracking in the vertical and horizontal joints (test no. 6); (c) bearing failure of	

the boards-to-steel screwed connections (test no. 2); (d) local buckling of the partition (test no. 2); (e) global buckling of the partition (test no. 3); (f) buckling of the stud across plasterboard horizontal joints (test no. 2).129

Figure 87. Hysteretic loops from test 1 to test 6.....130

Figure 88. Comparison among (a) the backbones and the (b) secant stiffness recorded during the different tests.....131

Figure 89. Energy dissipated in test no. 1 for each cycle of the protocol and for each negative and positive semi-cycle.....132

Figure 90. Strain gauge recording in (a) Siniat steel studs and in (b) Siniat plasterboards in test no. 2.133

Figure 91. Fragility curves for the considered damage states for the tested specimens. The dashed thick lines are the fragility curve that fits the experimental data (dashed lines); the solid thick lines are the fragility curves that includes a larger standard deviation due to the use of the same loading protocol for the different specimen (Porter et al., 2006).....136

Figure 92. Suspended plasterboard continuous ceilings: (a) single frame ceiling (SFC); (b) double frame ceiling (DFC).....141

Figure 93. Technical scheme of the test setup: (a) plan view, (b) and (c) lateral views.142

Figure 94. (a) Test frame installed on the shake table; (b) SFC specimen detail.143

Figure 95. Triaxial accelerometers, plasterboard and hanger position in the case of single frame ceiling (a) and double frame ceiling (b) specimen.144

Figure 96. Earthquake time history and spectra for a level of shaking corresponding to S_{DS} equal to 1.50g: (a) acceleration time-history; (b) input accelerogram spectrum (TRS), RRS (bold line), upper and lower matching limits (dashed line).145

Figure 97. Tests corresponding to S_{DS} equal to 1.50g: shake table recorded acceleration time histories (a) zoomed in a 2 sec time range (b) for single frame ceiling tests compared to the shake table input; spectra for single frame (SFC) and double frame ceiling (DFC) compared to the RRS and the TRS (c).148

Figure 98. Tests corresponding to SDS equal to 1.50g: deformation time history recorded by SG3 in single frame ceiling test (a); maximum deformations recorded by strain gauges in (b) SFC tests and (c) DFC tests.150

Figure 99. Ceiling with undersized tiles (Badillo-Almaraz et al., 2007).....150

Figure 100. Ceiling fragility curve: ceiling with undersized tiles (Badillo-Almaraz et al. 2007).....151

Figure 101. Plan view of the benchmark structures.157

Figure 102. Lateral view of the considered building models and their design fundamental period (T_{des}). Dimensions of the cross sections are in [cm].....158

Figure 103. Comparison between the mean acceleration response spectrum of the adopted set of accelerograms and the design spectrum according to EC8.	160
Figure 104. Evaluation of the bilinear capacity curve according to the Italian Building Code (Consiglio Superiore dei Lavori Pubblici, 2009).	161
Figure 105. Overstrength ratios definition.	162
Figure 106. Capacity curves of the benchmark structures plotted in the Acceleration Displacement Response Spectrum plane.	163
Figure 107. Floor response spectra of the 5-story structure evaluated on both the elastic (dotted line) and inelastic models (solid line).	165
Figure 108. Floor response spectra of the (a) 1-story, (b) 2-story, (c) 3-story and (d) 10-story structures evaluated on both the elastic (dotted line) and inelastic models (solid line).	167
Figure 109. Ratio between peak floor acceleration and peak ground acceleration, versus the relative height (z/h) for the different considered structures compared to the provisions included in ASCE7 and EC8.	168
Figure 110. Floor acceleration magnification on nonstructural components.	169
Figure 111. Comparison between effective inelastic floor response spectra (solid lines) and floor response spectra evaluated according to Eurocode 8 (dashed lines) for the (a) 1-story, (b) 2-story, (c) 3-story, (d) 5-story and (e) 10-story structures.	171
Figure 112. AC156 horizontal Required Response Spectrum (RRS) for qualification testing of nonstructural components.	173
Figure 113. AC156 Required Response Spectrum (RRS), original and proposed, compared to the floor response spectrum at the top story of the different structures.	175
Figure 114. Lateral view of the considered building models and their design fundamental period (T_{des}). Dimensions of the cross sections are in [cm].	184
Figure 115. Comparison between design and mean natural spectrum at damage limit state.	186
Figure 116. Floor response spectra in elastic (dotted lines) and inelastic (solid lines) models for (a) 1-story, (b) 2-story, (c) 3-story, (d) 5-story and (e) 10-story structures.	188
Figure 117. Ratio between peak floor acceleration (PFA) and peak ground acceleration (PGA), versus the relative height (z/h) compared to the provisions included in ASCE7 and EC8.	189
Figure 118. Floor acceleration magnification on nonstructural components versus the relative height (z/h) compared to the provisions included in ASCE7 and EC8.	190
Figure 119. Floor response spectra (solid lines) on inelastic models compared to EC8 floor spectra (dashed lines) for the (a) 1-story, (b) 2-story, (c) 3-story, (d) 5-story and (e) 10-story structures.	192

Figure 120. Proposed floor spectral shape compared to the Eurocode 8 floor spectral shape and to a typical analytical floor spectrum.....193

Figure 121. Floor response spectra (solid lines) on inelastic models compared to formulation (23) (dashed lines) for the (a) 1-story, (b) 2-story, (c) 3-story, (d) 5-story and (e) 10-story structures.....195

LIST OF TABLES

Table 1. Test ID, typology and S_{DS} values for the different input test levels.	20
Table 2. Damping evaluation according to free vibration decay method – positive cycles.	25
Table 3. Damping evaluation according to free vibration decay method – negative cycles.	25
Table 4. Outcomes of the dynamic identification procedures performed on bare and infilled frame in terms of natural frequency f_n and damping ratio ξ (Magliulo et al., 2012).	26
Table 5. Maximum recorded accelerations at the test frame base and roof in X and Y directions and at the partition center both in plane (i.p.) and out of plane (o.o.p.) for the different test intensities.	29
Table 6. Maximum recorded relative displacements and interstory drifts in X and Y directions for the different test intensities.	30
Table 7. Gap dimension, stiffness of the acrylic silicone spring and of the partition system adopted in the model.	38
Table 8. S_{DS} values for five input test levels.	51
Table 9. Average acceleration ($a_{collapse}$) in the out of plane direction that causes the collapse of the specimen according to different formulations.	52
Table 10. Maximum recorded accelerations at the test frame roof and maximum recorded relative displacements in X and Y directions for the different test runs.	56
Table 11. Damage state definitions and their repercussions for hollow brick partitions.	59
Table 12. Interstory drifts and damage states in X and Y directions for the different tests.	61
Table 13. Test program definition.	82
Table 14. Random vibration tests ID, amplitude and root mean square.	82
Table 15. Natural frequency of the tested components for the different random test groups.	85
Table 16. Damping of the tested components for the different random test groups.	87
Table 17. Comparison between the natural frequencies resulting from modal applied to FEM and transfer curve.	92

Table 18. Dimensions of the investigated cabinets.	92
Table 19. Comparison between the frequency results from modal applied to FEM and transfer curve.	95
Table 20. Comparison between the frequency results from modal applied to FEM and transfer curve.	96
Table 21. Damage scheme for the correlation of the visual damage to the damage state.	98
Table 22. Damage table compiled after test no. 308.	99
Table 23. Peak floor acceleration (PFA) that causes the rocking mechanism initiation for the different test groups and for the two tested cabinets.	101
Table 24. Peak floor acceleration (PFA) that causes the cabinet overturning for the different test groups and for the two tested cabinets.	101
Table 25. Peak floor accelerations that induces damage state 1 (DS1) and damage state 3 (DS3) for the different test groups.	104
Table 26. Set of European ordinary ground motions considered in the input definition study.	124
Table 27. Loading history protocol.	124
Table 28. Description of the different components used for each tested specimen.	126
Table 29. Damage scheme for the correlation between the recorded damage in each component of the partition and the attained damage state.	134
Table 30. Interstory drift ratio (IDR) at which the considered damage states (DS) occur for the different performed tests.	135
Table 31. Maximum recorded accelerations on the specimen (<i>Ceiling</i>), test frame top (<i>Roof</i>) and at the shake table level (<i>Base</i>) as indicated in Figure 93: single frame ceiling test.	147
Table 32. Maximum recorded accelerations on the specimen (<i>Ceiling</i>), test frame top (<i>Roof</i>) and at the shake table level (<i>Base</i>) as indicated in Figure 93: double frame ceiling test.	147
Table 33. Form for recording damage observed during the test performed on single frame ceiling with intensity level S_{DS} equal to 1.50g.	149
Table 34. Comparison of the first and second vibrational periods evaluated according to different models of the considered structures.	159
Table 35. Waveform ID, earthquake ID (Eqk ID) and name, date, moment magnitude (MW), epicentral distance (R), horizontal direction (Dir.) and peak ground acceleration (PGA) of the accelerograms selected for dynamic analyses (Ambraseys et al., 2002).	160
Table 36. Overstrength ratios values for the analyzed structures.	163

Table 37. Ratio between the first two peak floor spectral accelerations obtained for the top floor of the different structures in both the elastic and in inelastic models. Comparison between maximum floor spectrum acceleration in the elastic and inelastic models. 165

Table 38. Information about earthquakes used for dynamic analyses (Ambraseys et al., 2002)..... 186

Table 39. Values of the parameters of the proposed formulation for different ranges of structural periods. 194

Chapter 1 *INTRODUCTION*

Nonstructural components are all the systems and components attached to the floors and walls of a building that are not part of the main structural system resisting both to vertical and lateral loads (Villaverde, 1997).

Different studies available in literature (e.g. (Filiatrault et al., 2013), among many others) classify these components into three categories:

- architectural components, such as interior partition systems, ceilings, cladding systems, windows, doors, egress stairways;
- mechanical and electrical equipment, such as HVAC, Engines, generators, piping systems;
- building contents, such as cabinets, desks, bookshelves.

Porter (2005) provides a detailed categorization, i.e. a taxonomy, of nonstructural components, focusing on those components that may contribute to earthquake-induced repair costs, casualties, or loss of use (dollars, deaths, or downtime).

Nonstructural components can also be classified in different categories according to the structural response parameter that is better correlated to their damage (Taghavi and Miranda, 2003). Acceleration-sensitive components, e.g. parapets and suspended ceilings, can be distinguished from (relative) displacement-sensitive components, e.g. windows and elevator cabin. Some components may be classified as both acceleration- and displacement-sensitive components (Magliulo et al., 2014b), such as fire sprinklers and brick infill walls.

1.1 MOTIVATIONS

The seismic performance of nonstructural components is nowadays recognized to be a key issue in the framework of the Performance-Based Earthquake Engineering (PBEE). Three main issues motivate this statement.

- The failure of nonstructural components can cause injuries or deaths; for instance, the failure of cladding panels in precast structure (Figure 1) was the main cause of fatalities in the 2012 Emilia earthquake (Northern Italy) (Magliulo et al., 2014a).

The threatening to the life safety due to nonstructural components increases if it is considered that suffocation is the most common cause of death due to an earthquake. The 64% of the fatalities caused by 1995 Great Hanshin Earthquake was due to the compression (suffocation) of the human body (Ikuta and Miyano, 2011). Such a phenomenon could be caused by the damage to nonstructural components, that may also obstruct the way out from the damaged building.



- Nonstructural components generally exhibit damage for low seismic demand levels. The seismic performance of nonstructural components is especially important in frequent, and less intense, earthquake, in which their damage can cause the inoperability of several buildings.

This evidence is caused by three main issues: (a) nonstructural components are typically subjected to acceleration larger than the ground acceleration due to the structural dynamic amplification; this phenomenon is emphasized in case a nonstructural component is in tune with the structure, i.e. the component period of vibration is close to one of the structural periods of vibration; (b) these components typically do not possess a significant amount of ductility; (c) such components are usually characterized by low level of damping ratio, that increase the seismic demand.

For instance, a 4.9 M_w earthquake, that struck the northern part Campania region in Italy on 29 December 2013 caused many building evacuations mainly due to nonstructural component damage, such as internal partitions and infill walls (Figure 2).



Figure 2. Damage to (a) infill walls and to (b) internal partition after a 4.9 M_w Italian earthquake.

L'Aquila earthquake, occurred on April the 6th, 2009, in central Italy, also widely confirmed this issue: the majority of the evacuated buildings showed undamaged structural elements and moderate-to-heavy damaged nonstructural components, especially ceiling systems (Magliulo et al., 2009). Furthermore, the earthquake clearly evidenced that brick partitions usually exhibit extensive damage jeopardizing the functionality of the whole building (Figure 3).



Figure 3. Damage recorded in hollow brick partitions after 2009 L'Aquila earthquake in (a) a residential building and (b) in San Salvatore hospital.

- The cost connected to nonstructural components represents the largest portion of a building construction. In Figure 4 a typical cost distribution is shown for the most common buildings: structural cost represents a small portion of the total one, corresponding to 18%, 13% and 8% for offices, hotels and hospitals respectively (Taghavi and Miranda, 2003). The economic loss due to the failure of nonstructural components may exceed the replacement cost of the building, in case the loss of inventory and the downtime loss caused by nonstructural components are taken into account (Earthquake Engineering Research Institute (EERI), 1984).

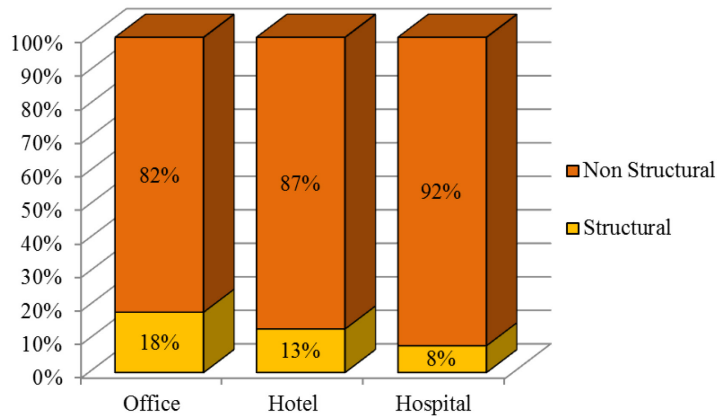


Figure 4. Typical distribution of costs in three different building typologies (Taghavi and Miranda, 2003).

Nonstructural components behavior is critical especially for strategic buildings, that must be operative immediately after an earthquake, also considering that these components usually exhibit damage even for low-intensity earthquakes.

The high vulnerability of nonstructural components, e.g. hollow brick partitions, may result in significant damages that are not acceptable in hospital buildings; San Salvatore hospital in L'Aquila (Figure 3b), struck by L'Aquila earthquake in 2009, clearly evidenced this issue.

For these reasons and especially for emergency or strategic buildings (that must be operative immediately after an earthquake), the knowledge of the seismic performance of nonstructural elements is essential. A confirmation of this urgent need is given by ASCE 7 (American Society of Civil Engineers, 2010), that prescribes the seismic qualification of nonstructural components installed in “important” buildings. The qualification could be performed according to experimental tests, analytical methods or experience data. In case the qualification is pursued via experimental tests, the AC 156 code (International Conference of Building Officials (ICBO), 2000) should be used. The qualification procedure is passed in case the component remains functional during and after a seismic event.

1.2 OBJECTIVES

The evaluation of the seismic capacity of some nonstructural components is a main objective of the research study. Since nonstructural components are typically not amenable of traditional numerical analyses, the seismic fragility of several components is pursued through the experimental method. Most of the experimental tests are

conducted through the shake table facility available at the Department of Structures for Engineering and Architecture.

The main objective of the experimental tests is the evaluation of a relationship between an Engineering Demand Parameter (EDP), e.g. the interstory drift ratio or the peak floor acceleration, and a predefined Damage State (DS), according to the PBEE approach. In case the number of tests within a test campaign is adequate, the fragility curve of the tested specimens, that expresses the attitude that the specimens have to exhibit damage at different seismic demand levels, is also evaluated.

This objective is pursued through different phases that typically characterize an experimental test: (a) the definition of a test frame that is able to subject the specimen to the demand that it would experience in a real building; (b) the testing protocol and the input accelerogram definition, in case a shake table test is performed; (c) the instrumentation of the test setup and the definition of a damage scheme, that allows correlating the visual damage to the occurrence of a given damage state; (d) the processing of the results.

The evaluation of seismic demand of nonstructural components is also a main objective of this research study. Nonstructural components should be subjected to a careful and rational seismic design, in order to reduce the economic loss and to avoid threats to the life safety, as well as what concerns the structural elements. Nonstructural components are subjected to severe seismic actions due to the dynamic interaction with the primary system. This study is mainly focused on acceleration-sensitive nonstructural components. The design of such components is based on the evaluation of the maximum inertia force, which is related to the floor spectral accelerations. The accuracy of actual building codes in predicting the maximum acceleration demand on a component placed at a given floor of a building is therefore investigated.

1.3 OUTLINE OF THE THESIS

The thesis is divided in two main Chapters: 0, that deals with some experimental activities aiming at the evaluation of the seismic capacity of some nonstructural components, and Chapter 3, that deals with the investigation of the seismic demand on acceleration-sensitive nonstructural components.

In Section 2.1 a shake table-test campaign on innovative plasterboard partition systems is described. Bidirectional input motion are defined and scaled at different intensity levels. The tested partition is an innovative partition system, that is designed in order to reduce the damage in such a component.

In Section 2.2 full-scale experimental tests on standard hollow brick partitions are described. The hollow brick internal partition systems are one of the most spread

partition system in the European area. Bidirectional shaking table tests are performed in order to investigate the seismic performance of typical hollow brick partitions, subjecting the partition simultaneously to interstorey relative displacements in their own plane and accelerations in the out of plane direction.

Section 2.3 deals with shake table test on hospital building contents, such as freestanding cabinets, aimed at establishing the limit states for a typical health care room and deriving empirical fragility curves by considering a systemic approach. At this purpose a typical ambulatory room is defined and tested via shake table test.

Quasi-static tests on high plasterboard internal partitions are detailed in Section 2.4. This partition typology is representative of typical partitions used in industrial and commercial buildings in the European countries. A steel test setup is designed in order to transfer the load, provided by the actuator, to the partition. The testing protocol provided by FEMA 461 (Federal Emergency Management Agency (FEMA), 2007) is adopted for the quasi-static tests.

Shaking table tests for the investigation of the seismic behavior of plasterboard continuous suspended ceiling systems are described in Section 2.5. Two kinds of ceiling systems, named single frame ceiling (SFC) and double frame ceiling (DFC), are tested. A steel test frame is properly designed in order to simulate the seismic effects at a generic building story.

In Section 3.1 a parametric study is conducted on five RC frame structures in order to evaluate the floor response spectra. The structures, designed according to Eurocode 8, are subjected to a set of earthquakes, compatible with the design response spectrum in order to assess the Eurocode formulation for the evaluation of the seismic demand on acceleration-sensitive nonstructural components. Some comments on the target spectrum provided by AC 156 for the seismic qualification of nonstructural components are also included.

In Section 3.2 a similar parametric study is performed. The seismic demand on light acceleration-sensitive nonstructural components caused by frequent earthquakes is assessed. The study is motivated by the counterintuitive approach of current building codes to the design of nonstructural components; moreover, the extensive nonstructural damage recorded after recent low intensity earthquakes also encouraged such a study. A novel formulation is proposed for an easy implementation in future building codes based on the actual Eurocode provisions.

Each Section includes a brief state-of-art related to the investigated topic in an introductory paragraph, that shows the main conclusions of past studies. The conclusions related to the different research activities are included in each Section. Chapter 4 includes the main conclusions of the research activities described in the thesis.

1.4 REFERENCES

- American Society of Civil Engineers (2010) ASCE/SEI 7-10: Minimum Design Loads for Buildings and Other Structures. Reston, Virginia, US
- Earthquake Engineering Research Institute (EERI) (1984) Nonstructural Issues of Seismic Design and Construction, Publication 84-04. Berkeley, CA, USA
- Federal Emergency Management Agency (FEMA) (2007) Interim protocols for determining seismic performance characteristics of structural and nonstructural components through laboratory testing. Report No. FEMA 461. Washington DC, US
- Filiatrault A, Tremblay R, Christopoulos C, Folz B, Pettinga D (2013) Elements of Earthquake Engineering and Structural Dynamics. 3rd Edition. Presses Internationales polytechnique, Quebec, Canada
- Ikuta E, Miyano M (2011) Study of Damage to the Human Body Caused by Earthquakes: Development of a Mannequin for Thoracic Compression Experiments and Cyber Mannequin Using the Finite Element Method. In: Spence R, So E, Scawthorn C (eds) Human Casualties in Earthquakes, vol 29. Advances in Natural and Technological Hazards Research. Springer Netherlands, pp 275-289. doi:10.1007/978-90-481-9455-1_19
- International Conference of Building Officials (ICBO) (2000) AC 156 Acceptance Criteria for the Seismic Qualification of Nonstructural Components. ICBO Evaluation Service, Inc., Whittier, California, USA
- Magliulo G, Ercolino M, Petrone C, Coppola O, Manfredi G (2014a) Emilia Earthquake: the Seismic Performance of Precast RC Buildings. Earthquake Spectra Online Early. doi:10.1193/091012EQS285M
- Magliulo G, Pentangelo V, Manfredi G (2009) Danneggiamento delle controsottiture a seguito del terremoto dell'Aquila dell'aprile 2009 V1.00, available on <http://www.reluis.it> (in Italian).
- Magliulo G, Petrone C, Capozzi V, Maddaloni G, Lopez P, Manfredi G (2014b) Seismic performance evaluation of plasterboard partitions via shake table tests. Bulletin of Earthquake Engineering:(online first). doi:10.1007/s10518-013-9567-8
- Porter K (2005) A Taxonomy of Building Components for Performance-Based Earthquake Engineering. PEER Report 2005/03. Pacific Earthquake Engineering Research Center, College of Engineering, University of California, Berkeley, US
- Taghavi S, Miranda E (2003) Response assessment of nonstructural building elements, PEER report 2003/05. College of Engineering, University of California Berkeley, USA
- Villaverde R (1997) Seismic design of secondary structures: State of the art. Journal of Structural Engineering-Asce 123 (8):1011-1019. doi:10.1061/(Asce)0733-9445(1997)123:8(1011)

Chapter 2 SEISMIC CAPACITY OF NONSTRUCTURAL COMPONENTS

2.1 SHAKE TABLE TEST ON INNOVATIVE PLASTERBOARD PARTITIONS

Shaking table tests are performed to investigate the seismic behavior of plasterboard partitions. A steel test frame is properly designed in order to simulate the seismic effects at a generic building story. The tests are performed shaking the table simultaneously along both the horizontal directions. The accelerograms are scaled at eleven different intensity levels, in order to investigate a wide range of interstory drift demand and seismic damage.

The tested plasterboard partitions exhibit a good seismic behavior, both in their own plane and out of plane, showing limited damage up to 1.1% interstory drift ratio. The correlation between the dynamic characteristics of the test setup and the recorded damage is evidenced. Finally, an interesting comparison between the experimental results and the analytical model is also performed.

2.1.1 INTRODUCTION

Few studies were conducted in the past on nonstructural components performance evaluation. Concerning plasterboard partitions some experimental tests were carried out in order to investigate their seismic behavior (Restrepo and Lang, 2011; Retamales et al., 2013; Adham et al., 1990; Anderson, 1981; Landolfo et al., 2006). A series of experimental tests are conducted by Lee et al. (2007): in order to characterize the seismic performance of drywall partitions typically used in Japanese buildings, to observe the entity of the damage under cyclic loading conditions and to quantify the corresponding repair costs, four full-scale drywall partitions sheathed with two layers of gypsum boards on both faces are constructed and tested. A full-scale shake table test on a specimen, consisting of both gypsum board partition walls and suspended ceiling systems, is carried out by McCormick et al. (2008). The test shows the main damages which occur at different drift levels and provides preliminary data for a test on a full-scale steel moment frame. An innovative set up for non-structural component testing is proposed by Mosqueda et al. (2009): a modular two-level shake platform is used in order to evaluate the behavior of both displacement and acceleration-sensitive

nonstructural components. Gypsum wall and piping systems are also tested to evaluate their seismic performance. Through the experimental results, reported in Filiatrault et al. (2010), the authors conduct a seismic fragility analysis of partition walls and propose innovative construction details in order to minimize the seismic damage. On the basis of tests experimental results, as those just described, several researchers (Fülöp and Dubina, 2004a, b; Restrepo and Bersofsky, 2011; Kanvinde and Deierlein, 2006) propose numerical and analytical model representative of the seismic behavior of these nonstructural components.

In this study (Magliulo et al., 2014) the seismic performance of innovative plasterboard partitions is investigated. Such partitions are designed in order to not interfere with the hosting structure up to moderate level of interstory drifts ($\sim 0.5\%$). The seismic performance evaluation is pursued via shake table tests with increasing intensity. The shake table tests, combined with the definition of a proper test frame in which the partitions are housed, allow investigating the seismic behavior of the systems subjecting them simultaneously to interstory drifts in their own plane and accelerations in the out of plane direction.

The recorded damage states are correlated to an engineering demand parameter; some considerations on the hysteretic curve are made through a complete analysis of the recorded quantities. Finally a model of the test setup is introduced comparing the experimental results with the analytical ones.

2.1.2 EXPERIMENTAL FACILITIES, TEST SETUP, SPECIMEN AND INPUT

The shake table tests, performed in order to investigate the seismic behavior of plasterboard internal partitions, are carried out at the laboratory of the Department of Structures for Engineering and Architecture of the University of Naples Federico II.

The tests are performed by the earthquake simulator system, consisting of two 3 m x 3 m square shake tables. Each table is characterized by two degrees of freedom in the two horizontal directions. The maximum payload of each shake table is 200 kN with a frequency range of 0 – 50 Hz, acceleration peak equal to 1 g at the maximum payload, velocity peak equal 1 m/sec and total displacement equal to 500 mm (± 250 mm). Only one shake table is used in this experimental testing program (Figure 5a).

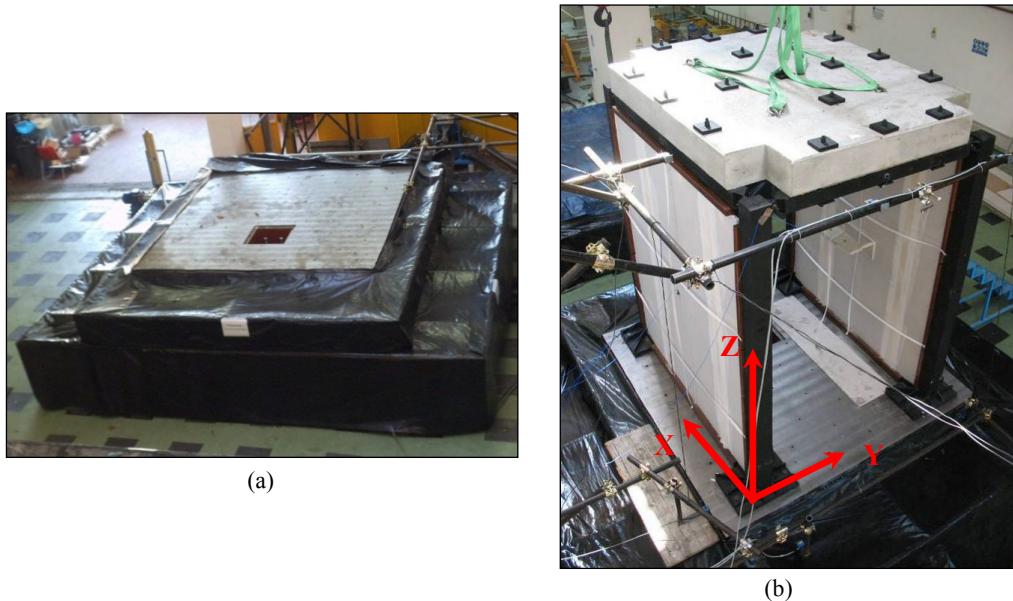


Figure 5. (a) Earthquake simulator system used in the tests; (b) general (XYZ) view of the test setup.

A general view of test setup is shown in Figure 5b, while a schematic representation of the tested specimen is presented in Figure 6. The main components of the tested partitions are: the “base and lateral runners”, U-steel section profiles screwed respectively to base floor and columns, with dimension 40-75-40 mm and 6/10 mm thick; the “top runner”, an U-steel section profile screwed to top floor, with dimension 80-75-80 mm and 10/10 mm thick; “vertical studs”, U-section profiles housed in the upper and lower runners, but not screwed to them, with dimension 47-74-50 mm, 6/10 mm thick, spaced 600 mm; the outer layer of “PREGYPLAC BA13” plasterboards, gypsum panels properly sized and horizontally jointed and weighing 90 N/m²; the inner layer of “PREGY LaDURA BA13” plasterboards, with high surface and mechanical resistance conferred by the presence of wooden fibers within the gypsum, properly positioned in order to prevent low resistance sections and weighing 128 N/m². Each layer is 12.5 mm thick and provides thinned edges. The plasterboards are screwed only on vertical studs through phosphated and drilling screws spaced 30 cm. Joints between boards of the external layer (PREGY LaDURA BA13) are sealed by the joint compound. The gap between the plasterboards and the perimeter is filled with acrylic silicone.

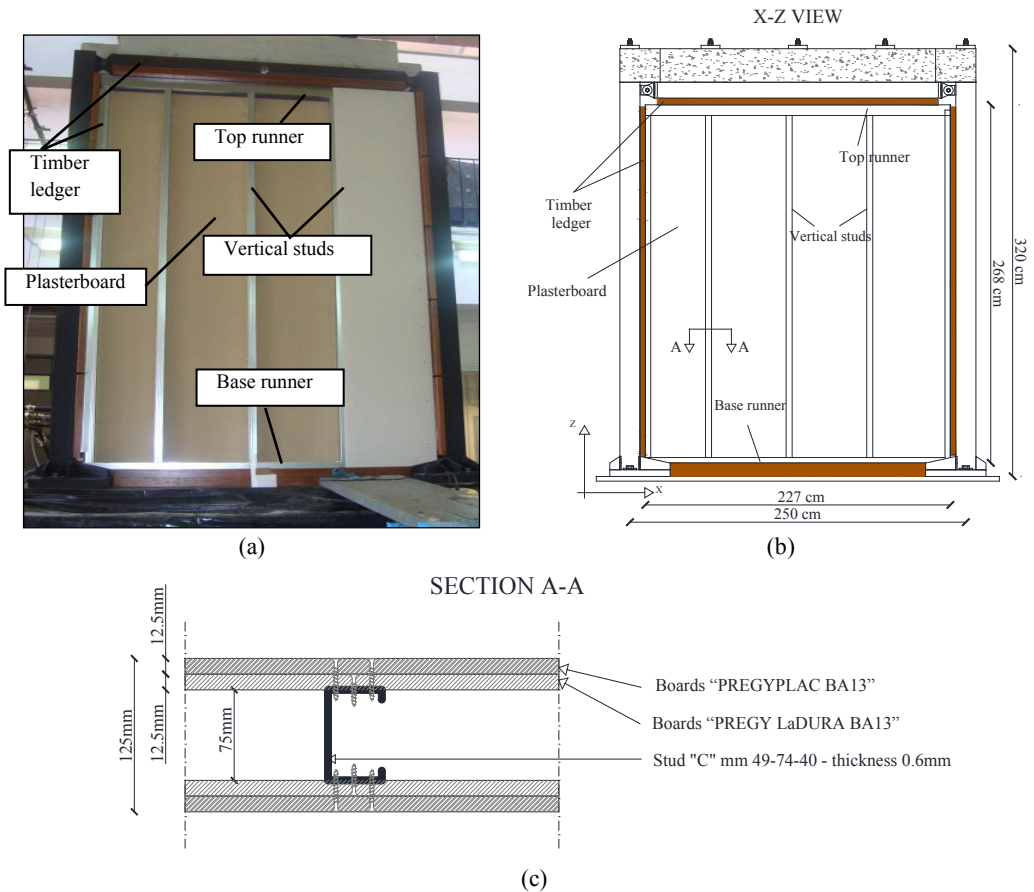


Figure 6. Internal plasterboard partition: (a) overview; (b) graphical scheme; (c) horizontal cross section.

2.1.2.1 TEST FRAME: IDEA, DESIGN AND PARAMETRIC STUDY

A steel test frame is properly designed and built (Figure 7) with the purpose of simulating the seismic effects on the partitions. The test frame is designed so as to simulate the behavior of a generic story of a building, in which the partitions are installed. The geometry of the test frame is defined taking into account three requirements: (i) realistic value of mass; (ii) realistic interstory height h , assumed equal to 2.74 m; (iii) realistic interstory displacement d_r , assumed equal to $0.005h$ for a Damage Limit State earthquake with 50 year return period.

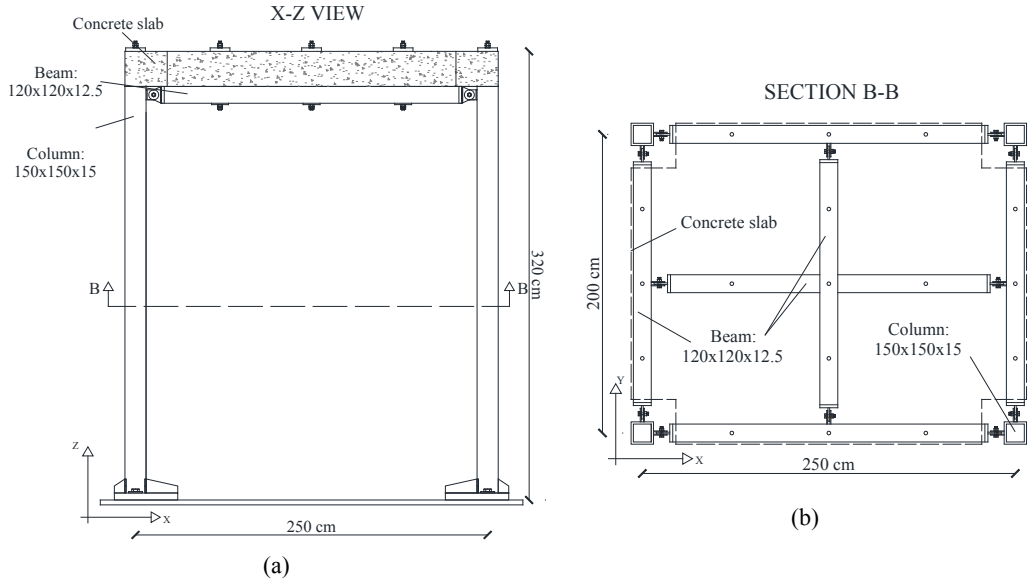


Figure 7. Scheme of test setup: (a) lateral view, (b) horizontal cross section.

In order to select the cross section dimensions of the columns of the test frame a parametric study is conducted to satisfy the before mentioned strict requirements. Firstly, a cantilever scheme is adopted, capable to reach the same displacement of a frame scheme with rigid beams, inducing a halved moment at the base of the columns with respect to the frame one. Hollow squared cross sections are chosen in order to guarantee the same lateral behavior in the two orthogonal directions. A high grade steel C45 is chosen for the columns, considering the high level of stress expected during the shakings.

The parametric study is prudently conducted assuming that the steel test frame does not interact with the partitions in sustaining the horizontal loads. The assumed quantities are:

- the maximum spectral ordinate $S_{a,max}$, equal to 2.40 g and obtained from the most intense seismic input at the shake table;
- the maximum spectral ordinate $S_{a,DLS}$, equal to 0.96 g corresponding to a Damage Limit State earthquake with 50-year return period;
- the maximum lateral displacement Δ , evaluated as $\Delta = S_{a,max} / S_{a,DLS} \cdot 0.005 \cdot h = 3.43cm$, considering that the test frame is designed to remain in the elastic range for all the shakings.
- A set of steel hollow square cross sections are considered. For each of them, the following quantities can be evaluated, using simple relationships:

- the equivalent mass of a SDOF system $EMR = 4 \cdot \frac{\Delta}{h^3} \cdot \frac{3 \cdot EI}{S_{a,\max}}$, required to reach the target displacement Δ , where I is the moment of inertia of the considered cross section and E is the Young modulus;
- the maximum stress (MS) in the cross section at the base, resulting from the linear dynamic analysis with the most intense seismic input.

Considering that the floor area is equal to 5 m² and in order to achieve the above mentioned requirements, the mass is limited to be in the range 4.0 t ÷ 6.0 t. Obviously, to prevent the yielding of the steel columns, the maximum stress is limited to be less than the yielding stress, i.e. 430 MPa. These two limitations lead to the choice of a steel profile with 150 mm x 150 mm x 15 mm cross section, as highlighted in red in Figure 8, where the parametric study is summarized.

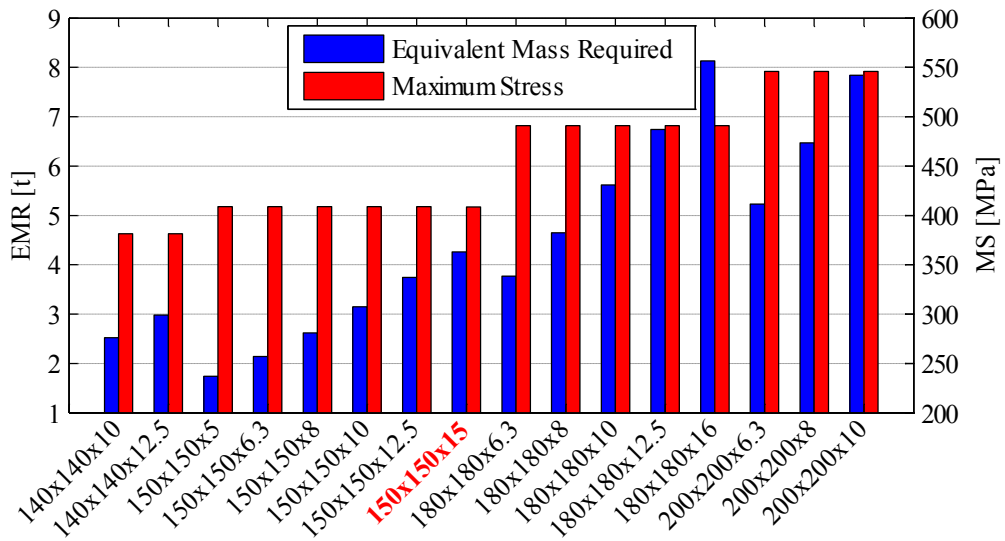


Figure 8. Parametric study for the definition of the column cross sections: Equivalent Mass Required (EMR) and the Maximum Stress (MS) for each considered column cross section.

The final result is a 2.50 m (X direction) x 2.00 m (Y direction) x 2.89 m (Z direction) inverted pendulum test fixture. The test frame is composed of welded square hollow columns (150 mm x 150 mm x 15 mm) of C45 steel material and rolled square hollow beams (120 mm x 120 mm x 12.5 mm) of steel S275; the beam-column connections are bolted. A horizontal frame made of rolled square hollow steel profiles (120 mm x 120 mm x 12.5 mm) is bolted to the principal beams of the test frame, as shown in Figure 7. A reinforced concrete slab with class C45/55 concrete is placed on the roof of the structure. Its plan dimensions are 2.15 m x 2.65 m with thickness equal to 0.25 m

suitably shaped to allow relative beam-column rotations. The concrete slab is connected to the test frame with prestressed bolts, in order to guarantee enough friction strength at the steel beams-to-slab interface for the transfer of inertia forces.

A FEM model of the test frame is assembled by means of the computer program SAP2000 (CSI Computer & Structures Inc., 2004). Each element of the test frame is implemented as elastic “beam” finite element. The FEM model is implemented in order to perform the design analysis and to obtain an estimation of the first period along both the orthogonal directions of the test frame. The two first translational periods are equal to 0.24 s (4.17 Hz). The test frame is designed according to Eurocode 3 (CEN, 2005a, b) and 8 (CEN, 2004b) provisions by dynamic linear elastic analysis. The total seismic weight of the test frame is equal to 42.5 kN.

2.1.2.2 TEST SETUP AND SPECIMEN: MOUNTING DETAILED DESCRIPTION

Two partitions are contemporary tested in order to maintain symmetry in the seismic behavior of test frame. The specimen is a plain drywall partition with dimensions of 2.68 m (height) by 2.27 m (width) with 12.5 cm thickness (Figure 6). It is installed between two columns, in particular along the longest side (2.50 m) of test fixture, connected by the perimeter U-section runners to a timber ledger covering the steel elements. Between the plasterboards and the wooden supports, a 0.8 cm to 1cm gap is left.

The installation procedure of the partition wall is as follows:

- a) Base, lateral and top runners are sequentially screwed to top and bottom beams and to columns (Figure 9a and b).
- b) Vertical studs are simply housed in the top and base runners; they are not attached to the runners through the use of screws (Figure 9c).
- c) The first (inner) layer (PREGY LaDURA BA13) of gypsum plasterboards is only attached to vertical studs by screws with 30cm step on each face of drywall partition; there is no screw that connects plasterboard to runners. This configuration allows the vertical studs to slide with respect to the lateral runner avoiding any collaboration between the partition and structure.
- d) The second (outer) layer (PREGYPLAC BA13) of gypsum boards is attached to the first one by screws on each face of the drywall partition. The installation is made in order to prevent the formation of low resistance sections. Therefore, they are arranged so that joints are staggered (Figure 9d).
- e) Joints between boards of the second layer are sealed by joint compound.
- f) The gap between the plasterboards and the perimeter is filled with acrylic silicone.

The above presented construction technology allows the partition to rigidly move within the bay in which it is installed without absorbing significant forces (neglecting the contribution of the silicone). In case the structure exhibits relative displacements larger than the separation gap, the partition can rigidly move within the bay up to relative displacement at least equal to twice the separation gap width. Hence, a 8 mm wide gap allows the partition to not absorb significant force at least up to 16 mm relative displacement, i.e. $\sim 0.5\%$ interstory drift ratio.



Figure 9. Installation procedure: (a) base runner; (b) top and lateral runners; (c) vertical studs; (d) plasterboard second (outer) layer.

The partitions are designed for the out-of-plane seismic force evaluated according to Eurocode 8 prescriptions on nonstructural components. The out-of-plane seismic demand on the nonstructural component is evaluated assuming a 0.3 g peak ground

acceleration and that the component is installed at the last story of a building. The resistance of the partition is evaluated according to Eurocode 3 (CEN, 2004a), neglecting the contribution of the boards to the out-of-plane strength of the partition.

2.1.2.3 INSTRUMENTATION

Accelerometers, strain gauges and laser-optical sensors are used to monitor the response of the test frame and partitions (Figure 10).

In order to control roof rigid rotation and its displacements adequately, two triaxial accelerometers (named TRI-103762, TRI-103765) are installed at the center of the principal beams in X and Y directions (Figure 10b). Other two accelerometers (named TRI-103763, TRI-103766) are also arranged in two different points of the test frame: one accelerometer is placed at the center of the partition (TRI-103763) and the other one at the column base (TRI-103766).

Eight strain gauges are adopted and indicated in Figure 10a: four strain gauges are placed on the vertical steel studs (SG-m1) and perimeter runners (SG-s1, SG-i1, SG-i2), two at the column base (SG-i3, SG-i4) and two on the plasterboard (SG-m2, SG-i5).

Six laser-optical sensors are used to monitor displacements of specific points of the test frame. Three of the six lasers are placed at steel base plate mid-height (base plate that connects column to shake table); the remaining three sensors monitor concrete slab displacement. In Figure 10b the exact sensors arrangement is presented.

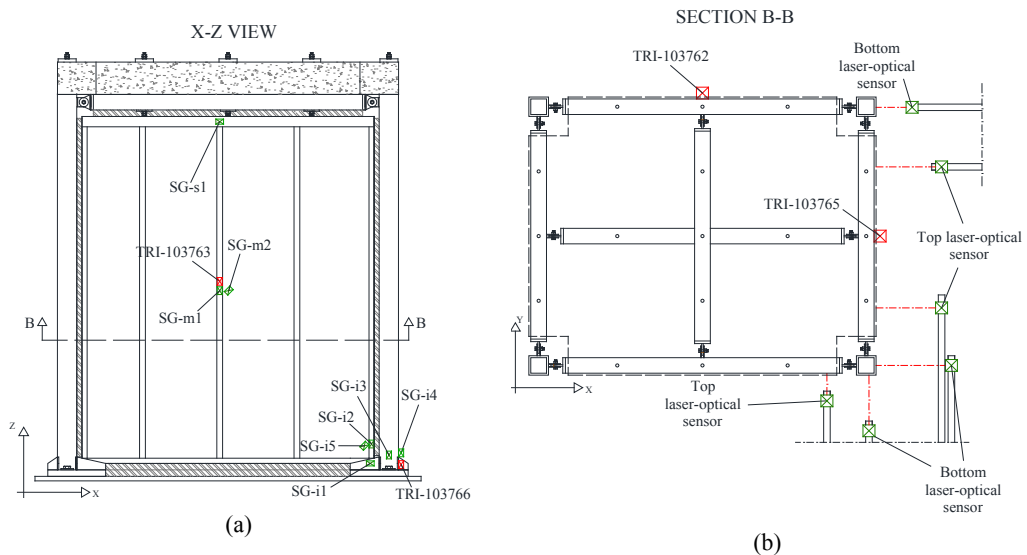


Figure 10. Scheme of test instrumentation: (a) lateral view; (b) horizontal cross section.

2.1.2.4 INPUT AND TESTING PROTOCOL

The table input is provided through acceleration time histories representative of expected/target ground motion and acting simultaneously along the two horizontal directions; the time histories are artificially defined in order to match the Required Response Spectrum (RRS), provided by the ICBO-AC156 code “Acceptance criteria for seismic qualification testing of nonstructural components” (International Conference of Building Officials (ICBO), 2000).

According to ICBO, the RRS is obtained as a function of the spectral acceleration at 0.2 seconds, S_{DS} , which is the parameter characterizing the ground motion. For horizontal design-basis earthquake shaking, the International Building Code (International Code Council (ICC), 2000) defines the design spectral response acceleration at short periods S_{DS} as:

$$S_{DS} = \frac{2}{3} \cdot F_A \cdot S_S$$

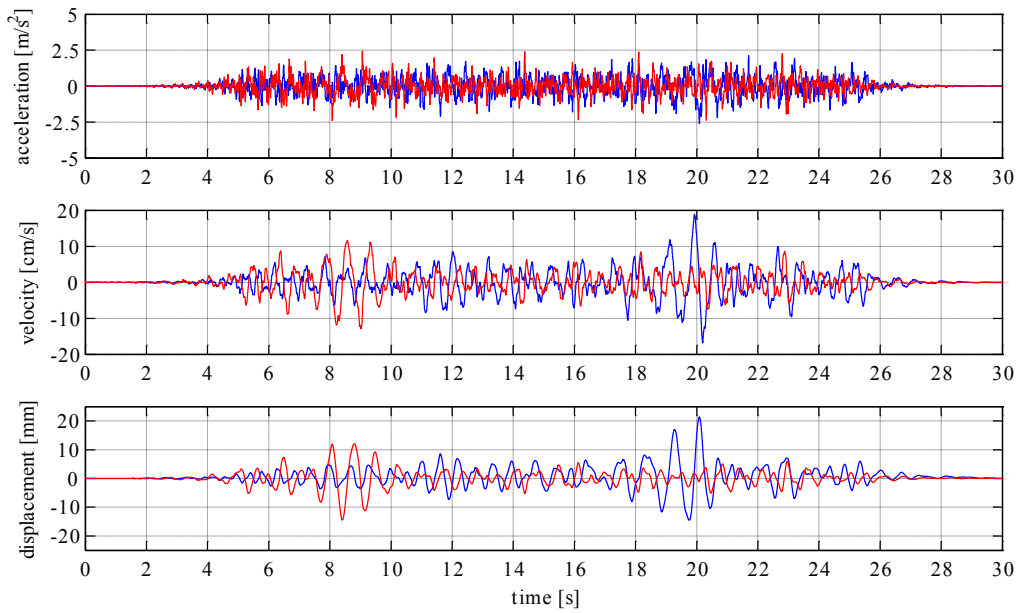
where F_A is a site soil coefficient, set equal to 1 in this study, and S_S is the mapped Maximum Considered Earthquake (MCE) spectral acceleration at short periods.

The selection procedure is performed for a RRS corresponding to S_{DS} equal to 1.50 g; the records (in X and Y direction) are then scaled in order to match other levels of the target spectrum.

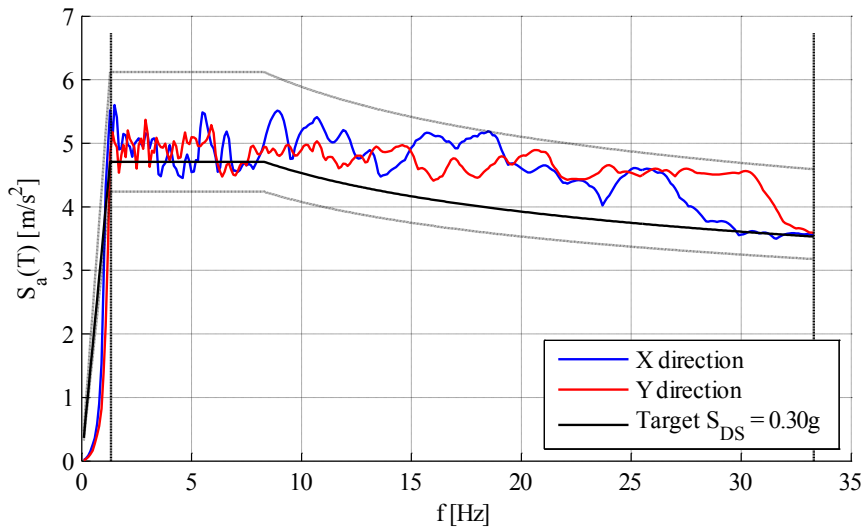
The earthquake histories used to test the partitions are generated according AC156 code procedure. In details, a baseline signal is defined starting from nonstationary broadband random excitations with energy content from 1.3 to 33.3 Hz and one-sixth-octave bandwidth resolution. The selected baseline earthquake has a total length equal to 30 seconds and presents a rise time, a steady state and a decline time of the resultant acceleration record. Then, the signal is enhanced by introducing wavelets using the spectrum-matching procedure of RSP Match program (Hancock et al., 2006) in order to make it compatible with RSS. The matching procedure is ensured over the frequency range from 1.3 to 33.3 Hz; the elastic response spectrum ordinates shall not be lower than 0.9 times RRS and larger than 1.3 times RRS. In order to obtain a drive motion compatible with the shaking table acceleration, velocity and displacement limits, the so obtained matched record is band passed filtered over the same range frequency. Two different time histories are defined for the two horizontal directions.

Figure 11 shows the obtained time histories for the X (blue line) and Y (red line) directions in terms of acceleration, velocity and displacement, their elastic response acceleration spectra, the RRS corresponding to S_{DS} equal to 0.30 g and the RRS scaled to 90% and 130%.

2.1 Shake table test on innovative plasterboard partitions



(a)



(b)

Figure 11. Input time histories and spectra for S_{DS} equal to 0.30 g: (a) acceleration, velocity and displacement time-history - X direction (blue) and Y direction (red); (b) input accelerogram spectra, RRS (bold line), upper and lower limits (dashed line), matching frequency range (vertical dashed line).

The input levels range are chosen from $S_{DS} = 0.10$ g to $S_{DS} = 1.50$ g in order to generalize the execution of the test, being representative of a large range of real earthquakes. Such acceleration range implies that the partition is subjected to interstory drifts larger than the limit, i.e. 0.5%, required by Eurocode for standard partitions and infill. Indeed, the test frame is designed in order to exhibit a 0.5% interstory drift for an earthquake characterized by S_{DS} equal to 0.60 g, representative of an earthquake with $a_g = S_{DS} / 2.5 = 0.24g$, i.e. an intensity level of earthquake with 50 years return period in a high seismicity zone according to Paulay and Priestley (1992).

In particular, 8 bidirectional (B) and 3 unidirectional (U) tests, with different intensity values, are chosen, as shown in the Table 1.

Test ID	1	2	3	4	5	6	7	8	9	10	11
Test typology	B	B	B	B	B	B	B	B	U	U	U
S_{DS} [g]	0.10	0.15	0.22	0.30	0.45	0.60	0.90	1.05	1.20	1.35	1.50

Table 1. Test ID, typology and S_{DS} values for the different input test levels.

Even if AC156 is implicitly intended for acceleration-sensitive components, such as ceilings, the input motion is defined according to such a procedure for the following reasons:

- internal partitions are mainly displacement sensitive components; however, out of plane acceleration can cause the damage/collapse of such components;
- the use of a flexible test frame, subjected to the defined input motions, allows investigating the behavior of the tested component at different levels of relative displacement demands.

2.1.3 TEST RESULTS AND OBSERVATIONS

2.1.3.1 DYNAMIC IDENTIFICATION

Different procedures are used to evaluate the fundamental period and the damping ratio of the test setup. In order to evaluate the influence of the plasterboard partitions, the procedure is applied both on the bare steel frame and on the infilled structure.

Three methods are illustrated in the following. For each method, the results concerning the bare steel test frame are presented; the method no. 1 is also applied on the infilled frame.

Method no. 1: Transmissibility curve

This method consists of applying to the base of the test frame a harmonic drive motion with predefined amplitudes and frequency f . The maximum acceleration at the roof of the bare test frame $\ddot{u}_{\max, \text{top}}$ and the harmonic base amplitude $\ddot{u}_{\max, \text{base}}$ are recorded for

each frequency f . The transmissibility ratios $TR = \ddot{u}_{\max, \text{top}} / \ddot{u}_{\max, \text{base}}$ are then evaluated (blue dots in Figure 12). The peak of the curve gives the natural frequency f_n , while the damping ratio is evaluated applying the half-bandwidth method.

The procedure points out a fundamental frequency f_n of 3.81Hz and a 0.92% damping ratio.

In Figure 12 the experimental points are also fitted with the theoretical curve (blue line), using the following relationship (Chopra, 1995):

$$TR = \left\{ \frac{1 + [2 \cdot \zeta \cdot (f/f_n)]^2}{[1 - (f/f_n)^2]^2 + [2 \cdot \zeta \cdot (f/f_n)]^2} \right\}^{1/2} \quad (1)$$

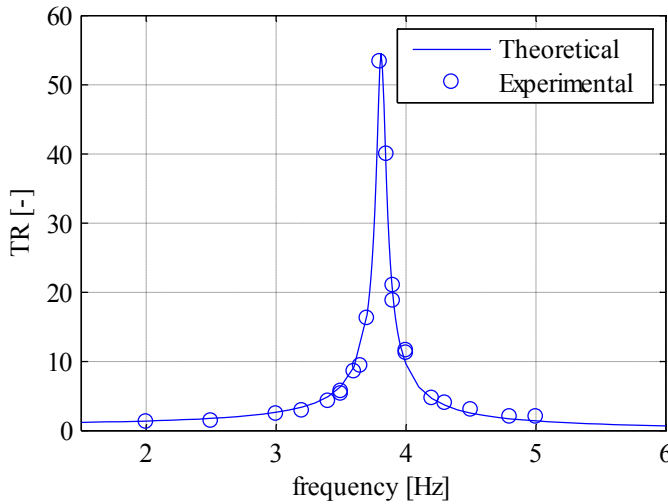


Figure 12. Transmissibility ratios curve for the bare steel frame.

The very low damping generates a very high amplification close to the resonance frequency, causing very high accelerations and inertial forces on the test frame roof; in order to avoid the test frame going into the inelastic range, limited points are evaluated in this region.

Note that the half-bandwidth method is theoretically valid for a displacement response factor R_d - frequency curve (Chopra, 1995). Nevertheless, this method is applicable still in the case of TR - frequency curve since they are very close one another around the peak (Chopra, 1995). Indeed, the ratio TR/R_d is theoretically evaluated as:

$$\frac{TR}{R_d} = \sqrt{1 + (2 \cdot \zeta \cdot f/f_n)^2} \quad (2)$$

resulting in ratio very close to 1 for the typical values of damping and for frequency not so far from the resonance (see Figure 13).

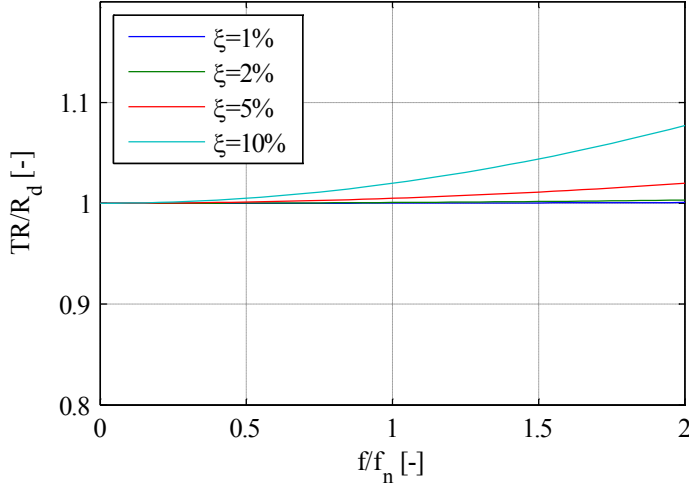


Figure 13. Ratio between theoretical Transmissibility ratio TR and Displacement response factor R_d for different damping values.

As clearly shown in Figure 13, the value of TR for $f=f_n$ is very close to the value of R_d. This implies that the damping ratio can be also evaluated as:

$$\zeta = \frac{1}{2 \cdot R_{d,f=f_n}} \cong \frac{1}{2 \cdot TR_{f=f_n}} \quad (3)$$

The formula yields a 0.94% damping ratio. However, this value can be considered as an upper bound of the damping ratio, due to the lack of experimental points close to the resonance, as highlighted above.

The procedure is also applied on the infilled frame in order to evaluate the influence of the partitions on the dynamic parameters of the test setup. A 8.33% damping value is evaluated upon the transmissibility curve peak (Figure 14); the peak occurs at 4.02Hz, defining a very light increase of the natural frequency and a significant influence of the partitions on the damping ratio. The half bandwidth method, instead, gives out a 5.42% damping ratio.

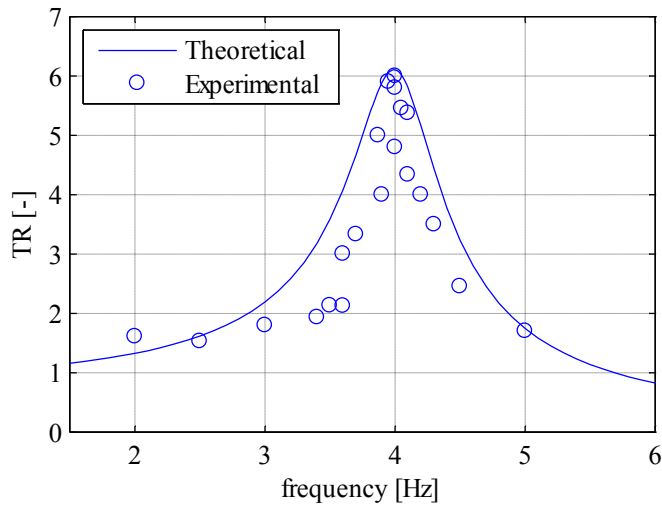


Figure 14. Transmissibility ratios curve for the infilled structure.

Method no. 2: Transfer curve

The transfer curve method is also used to evaluate the natural frequency and the damping ratio of the bare test frame. The transfer function is defined, in this case, as the ratio of the roof acceleration response to the input base motion, i.e. a white noise time history, in the frequency domain (Bracci et al., 1992).

The half-bandwidth method is used for the damping ratio evaluation, while the peak denotes the natural frequency of the system.

A 3.86Hz natural frequency and 1.63% damping ratio are evaluated for a white noise input motion (Figure 15).

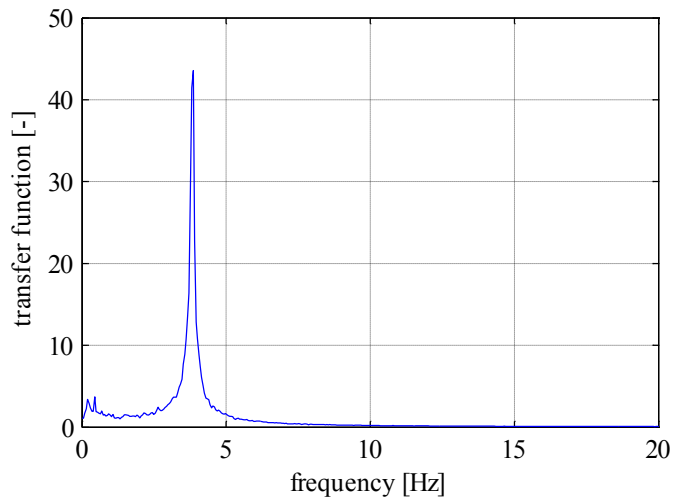


Figure 15. Transfer function generated by a white noise input on the bare structure.

Method no. 3: free vibration decay

This method allows the evaluation of the damping ratio value in free vibration conditions upon the ratio of two peak displacements measured over m consecutive cycles (Clough and Penzien, 1995).

$$\zeta = \frac{1}{2 \cdot \pi \cdot m} \ln \frac{u_i}{u_{i+m}} \quad (4)$$

In case of lightly damped systems this procedure can be adopted in term of accelerations that usually are easily recorded:

$$\zeta = \frac{1}{2 \cdot \pi \cdot m} \ln \frac{\ddot{u}_i}{\ddot{u}_{i+m}} \quad (5)$$

This procedure is applied referring to the acceleration time history recorded after a quite intense shaking ($\ddot{u}_{roof} > 1.5g$). Due to the very low level of damping recorded, the test frame continues vibrating significantly for many cycles (black box in Figure 16).

In order to apply such procedure, the signal was band-pass filtered in a frequency range close to the natural frequency, obtaining the green curve in Figure 16.

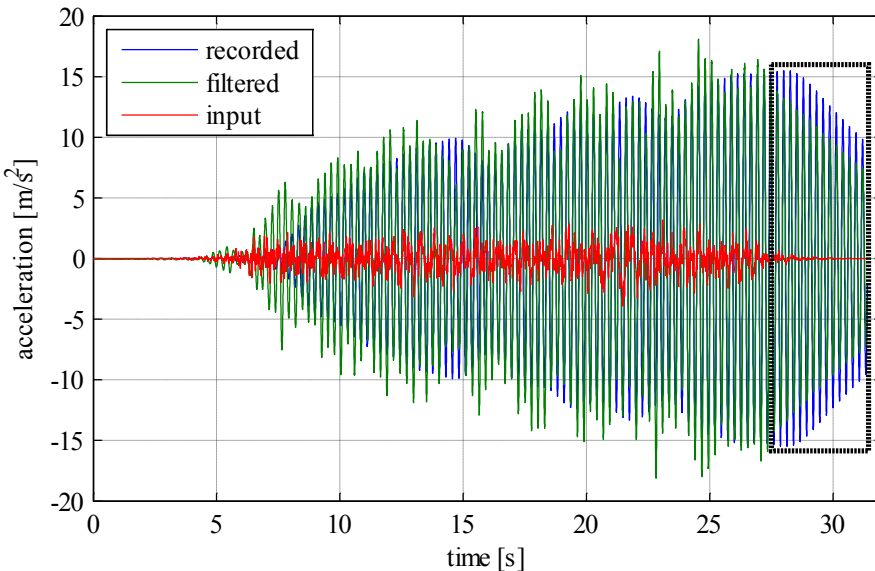


Figure 16. Acceleration time history recorded at the base of the test frame, Filtered and recorded acceleration time histories at the top of the test frame. The black box indicates the region in which the free vibration decay method is applied.

The procedure is applied with respect to all the possible peaks couple combinations. In the following tables the damping ratio is evaluated and listed referring to the peak

2.1 Shake table test on innovative plasterboard partitions

decay from the i^{th} cycle (rows) to the $i+m^{\text{th}}$ cycle (columns). Averaging the results, the damping ratio value is estimated to be $\zeta = 0.649\% \pm 0.162\%$.

ζ [%]		$i+m^{\text{th}}$ cycle											
		2	3	4	5	6	7	8	9	10	11	12	13
i^{th} cycle	1	0.05	0.13	0.22	0.30	0.37	0.42	0.47	0.50	0.53	0.56	0.58	0.60
	2		0.21	0.30	0.38	0.45	0.50	0.54	0.57	0.59	0.62	0.64	0.66
	3			0.39	0.46	0.52	0.57	0.61	0.63	0.65	0.67	0.68	0.70
	4				0.53	0.59	0.63	0.66	0.68	0.69	0.71	0.72	0.73
	5					0.65	0.68	0.70	0.71	0.72	0.73	0.75	0.76
	6						0.71	0.73	0.74	0.74	0.75	0.76	0.77
	7							0.74	0.75	0.75	0.76	0.77	0.78
	8								0.75	0.76	0.77	0.78	0.79
	9									0.76	0.78	0.79	0.80
	10										0.79	0.80	0.82
	11											0.82	0.83
	12												0.84

Table 2. Damping evaluation according to free vibration decay method – positive cycles.

ζ [%]		$i+m^{\text{th}}$ cycle											
		2	3	4	5	6	7	8	9	10	11	12	13
i^{th} cycle	1	0.12	0.21	0.30	0.37	0.43	0.48	0.52	0.55	0.58	0.60	0.62	0.64
	2		0.30	0.38	0.46	0.51	0.56	0.59	0.61	0.63	0.65	0.67	0.69
	3			0.46	0.53	0.58	0.62	0.64	0.66	0.68	0.69	0.71	0.73
	4				0.60	0.64	0.67	0.69	0.70	0.72	0.73	0.74	0.75
	5					0.68	0.70	0.72	0.73	0.74	0.75	0.76	0.77
	6						0.73	0.74	0.75	0.75	0.76	0.77	0.79
	7							0.75	0.75	0.76	0.77	0.78	0.80
	8								0.76	0.77	0.78	0.79	0.81
	9									0.78	0.79	0.80	0.82
	10										0.80	0.82	0.83
	11											0.84	0.85
	12												0.86

Table 3. Damping evaluation according to free vibration decay method – negative cycles.

The results of the dynamic identification procedures are summarized in the Table 4.

Considering these results, it can be concluded that:

- The natural frequency matches the analytical one: the assumed restraints and constraints well model the behavior of the bare test frame.
- The innovative plasterboard partitions do not significantly influence the natural frequency of the test frame. The goal of not interfering with the hosting structure is achieved.
- The damping ratio of the test setup significantly increases with the insertion of the partition within the test frame, causing a beneficial effect in the dynamic response.

Method	Transmissibility curve		Transfer curve		Free-vibration decay
Structure	f_n [Hz]	ζ [%]	f_n [Hz]	ζ [%]	ζ [%]
Bare frame	3.81	0.94%	3.86	1.63%	0.65%
Infilled frame	4.02	8.33%	-	-	-

Table 4. Outcomes of the dynamic identification procedures performed on bare and infilled frame in terms of natural frequency f_n and damping ratio ξ (Magliulo et al., 2012).

2.1.3.2 RESULTS SUMMARY

Using the selected drive motions, eight bidirectional and three unidirectional shaking tests along X direction (see Figure 5b) are performed.

After each test the compatibility of the spectrum of the recorded acceleration time-history with the required target response spectrum according to AC156 is verified. The compatibility is almost ensured in the frequency range between 1.3 Hz and 33.3 Hz (Figure 18 and Figure 20). In Figure 17 and Figure 19 the time-histories in terms of acceleration, velocity and displacement at the shake table level are shown (in blue). The velocity and displacement time-histories are evaluated from the integrals of the acceleration and the velocity time-histories, respectively. Before the evaluation of the integrals, an acausal Butterworth filter is applied and zero pads are added before the start and after the end of the record (Boore and Bommer, 2005). In particular, a band-pass filter is applied in the frequency range between 0.7 Hz and 50 Hz with an order equal to 4. The application of a filter is required in order to remove the long-period noise that cause permanent velocity and, especially, displacements. The application of an acausal filter is preferred with respect to a causal filter in order to reduce phase shift in the record. The zero pads addition is required to avoid offsets and trends in the baselines of the velocity and displacements obtained by integration.

The so-obtained time-histories are compared to the input time histories (red dotted lines) and to the recorded displacement at the shake-table level (green line). A good agreement of the compared time-histories is evidenced.

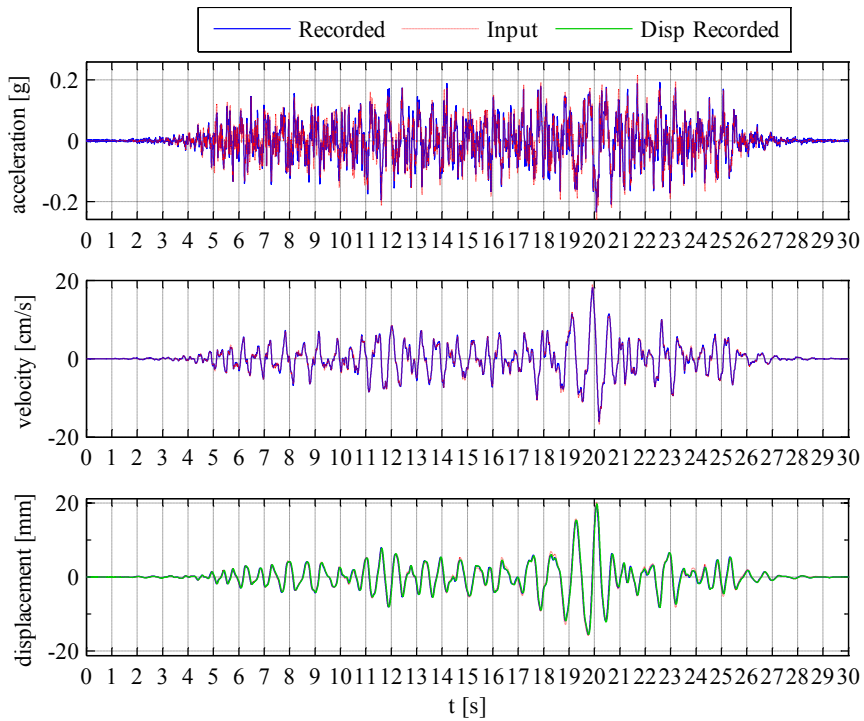


Figure 17. Input vs recorded time-histories in X-direction – test no. 4.

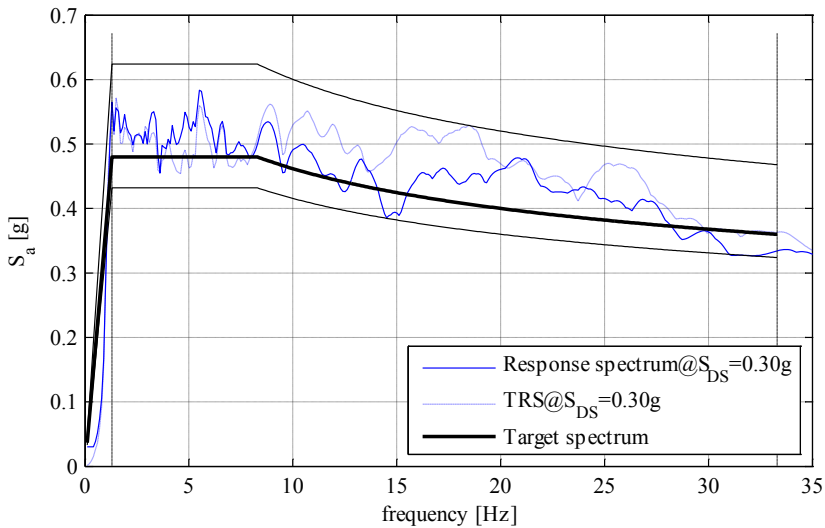


Figure 18. Recorded response spectra vs the Test Response Spectrum (TRS) and the Required Response Spectrum (Target Spectrum) in X-direction – test no. 4.

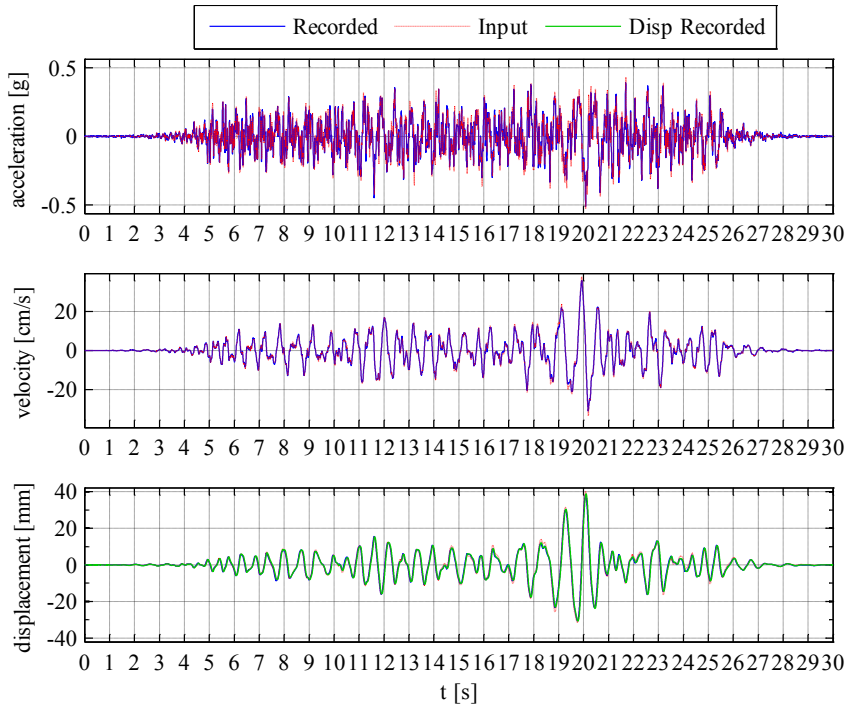


Figure 19. Input vs recorded time-histories in X-direction – test no. 6.

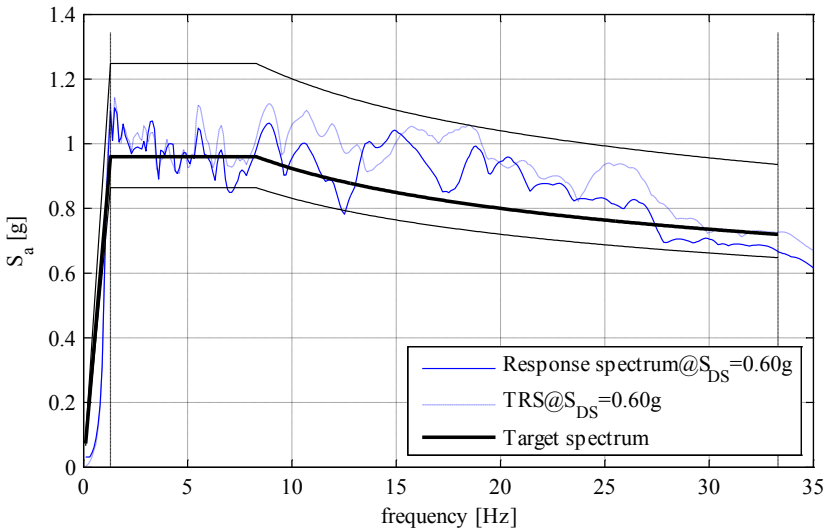


Figure 20. Recorded response spectra vs the Test Response Spectrum (TRS) and the Required Response spectrum (Target Spectrum) in X-direction – test no. 6.

In Table 5 the maximum recorded values of acceleration at the base and on the roof of the test frame are listed; the maximum accelerations on the partition, both in plane

2.1 Shake table test on innovative plasterboard partitions

(i.p.) and out of plane (o.o.p.), are then compared to those values. As visible, due to dynamic amplification, the maximum value of acceleration recorded at the base of the table is completely different from the ones recorded on the roof and on the partitions. This aspect may be crucial for experimental tests on shaking table. For this reason, the procedure described in Maddaloni et al. (2011), concerning the optimization of the drive motion to predict the signal recorded at desired locations, i.e. on the partitions, using a compensation procedure, will be taken into account in the next experimental testing program.

It should be noted that during test no. 9, 10 and 11 some problems have occurred in acquiring accelerograms data.

Position Accelerometer	Base		Roof				Partition	
	Table		103762		103765		103763	
Direction	X	Y	X	Y	X	Y	i.p.	o.o.p.
test no. 1	0.10 g	0.17 g	0.09 g	0.20 g	0.08 g	0.19 g	0.08 g	0.26 g
test no. 2	0.13 g	0.22 g	0.13 g	0.32 g	0.13 g	0.31 g	0.13 g	0.38 g
test no. 3	0.19 g	0.27 g	0.19 g	0.43 g	0.19 g	0.42 g	0.19 g	0.45 g
test no. 4	0.23 g	0.35 g	0.27 g	0.54 g	0.26 g	0.56 g	0.24 g	0.54 g
test no. 5	0.35 g	0.47 g	0.47 g	0.76 g	0.50 g	0.80 g	0.35 g	0.73 g
test no. 6	0.50 g	0.57 g	0.81 g	0.97 g	0.82 g	0.97 g	0.46 g	0.95 g
test no. 7	0.81 g	0.90 g	1.66 g	1.32 g	1.69 g	1.32 g	1.30 g	1.34 g
test no. 8	0.95 g	1.03 g	2.22 g	1.54 g	2.20 g	1.53 g	1.82 g	1.81 g
test no. 9	1.12 g	-	N/A	-	N/A	-	N/A	N/A
test no. 10	1.43 g	-	3.84 g	-	N/A	-	N/A	N/A
test no. 11	1.85 g	-	4.14 g	-	N/A	-	N/A	N/A

Table 5. Maximum recorded accelerations at the test frame base and roof in X and Y directions and at the partition center both in plane (i.p.) and out of plane (o.o.p.) for the different test intensities.

Relative displacements are also evaluated using the laser sensors records. In Table 6 the maximum recorded relative displacements in X and Y directions are listed and the maximum interstory drifts are evaluated. Values up to 1.08% drift are recorded, representative of a moderate earthquake intensity level.

Direction	Relative displacement		Interstory drift	
	X	Y	X	Y
test no. 1	0.9 mm	3.2 mm	0.03%	0.12%
test no. 2	1.1 mm	5.3 mm	0.04%	0.19%
test no. 3	1.3 mm	8.1 mm	0.05%	0.29%
test no. 4	2.4 mm	9.8 mm	0.09%	0.36%
test no. 5	4.9 mm	12.7 mm	0.18%	0.46%
test no. 6	8.5 mm	15.0 mm	0.31%	0.55%
test no. 7	15.9 mm	19.6 mm	0.58%	0.71%
test no. 8	20.1 mm	22.7 mm	0.73%	0.83%
test no. 9	25.4 mm	-	0.93%	-
test no. 10	26.9 mm	-	0.98%	-
test no. 11	29.5 mm	-	1.08%	-

Table 6. Maximum recorded relative displacements and interstory drifts in X and Y directions for the different test intensities.

2.1.3.3 DAMAGE DESCRIPTION

In this study three limit states are considered for the seismic response definition of the plasterboard partitions. In particular:

- OLS → Operational limit state (damage state 1 limit);
- DLS → Damage limit state (damage state 2 limit);
- LSLs → Life safety limit state (damage state 3 limit).

Operational limit state achievement implies the need of repairing the damaged element, in order to restore the original condition; damage limit state achievement, instead, implies that the component is damaged so that it must be partially removed and replaced; finally life safety limit state implies that the damage level is such that life safety is not ensured and the partition needs to be totally replaced.

After each test, damage is observed inspecting the specimen components. The recorded damage in each component is then correlated to one of the three limit states defined above. The level of damage required to reach a limit state is defined for each damage typology of each system component (i.e. plasterboards, studs, runners and screws). This damage is defined quantitatively, if possible; in the opposite case a qualitative definition of the level of damage is defined. Obviously, the damage state is the maximum between the different damage states recorded in each component.

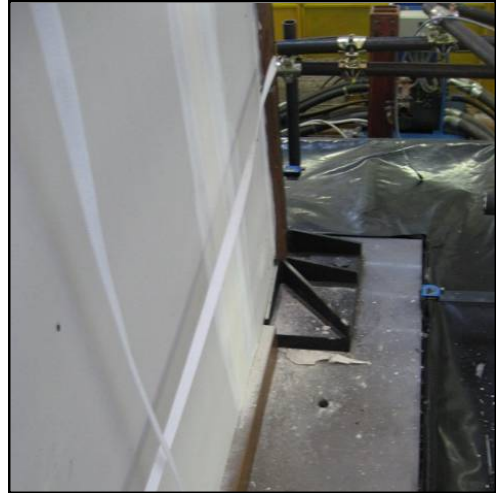
Both bidirectional and unidirectional tests show a limited damage up to 1.08% drift, including:

2.1 Shake table test on innovative plasterboard partitions

- acrylic silicone, inserted in the separation between partition and wooden vertical support, detachment (Figure 21a) in test no. 6 (partially) and in test no. 7 (complete);
- gypsum dust fall from test no. 7 with increasing intensity as the demand increases (Figure 21b);
- cracking of the vertical joints between plasterboards in test no. 10 (Figure 21c);
- crushing of the corners of the plasterboards in test no. 10 (Figure 21d).



(a)



(b)



(c)



(d)

Figure 21. Recorded damage after different shaking tests: (a) acrylic silicone detachment; (b) gypsum dust fall; (c) cracking of the vertical joints between plasterboards; (d) crushing of the corners of the plasterboards.

The recorded damage yields that damage state 1 is attained at 0.58% drift level, due to the need of restoring the acrylic silicone, and damage state 2 is attained at 0.98% drift level, due to the need of partially replacing the plasterboards. The correlation between the damage states and the engineering demand parameters is based upon the assumption that the damage occurs at the maximum engineering demand parameter that the specimen experiences during a single test.

The tested partition systems exhibit a good behavior under seismic actions. Particular attention, however, should be paid towards the definition of a large enough separation joint between partition and structure. This joint must be ensured both with the vertical structure (columns or partitions) and horizontal structure (slab). A smaller joint might compromise the system seismic performance.

Due to the particular construction technology, the partition behaves like a rigid block with three unrestrained degrees of freedom, i.e. horizontal translation and vertical translation in the partition plan and rotation around the orthogonal axis to the partition; when the structure exhibits displacements larger than the separation joint, the partition rigidly translates and rotates around a point at the base corner of the partition (Figure 22). For larger displacements the partition is stressed, stiffening the structure. This mechanism is widely supported by the analysis of tests video.

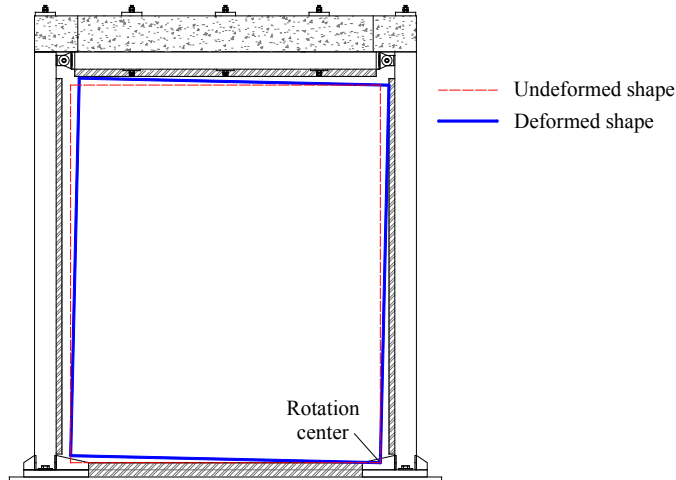


Figure 22. Partition rigid-body mechanism for moderate displacement demand level.

2.1.3.4 ANALYTICAL RESULTS

In order to analyze the test frame–partition interaction, the top acceleration, representative of the total inertia force, is plotted versus the relative displacement for different intensity levels (Figure 23).

From the hysteretic curve in X direction (Figure 23a) some comments can be stated:

- the trend of the hysteretic curve is linear until a 0.5% drift (14 mm) is reached, denoting no interaction between the partitions and the hosting structure; the slope of the initial linear envelope confirms the numerical model of the bare test frame: the linear trend slope, i.e. $(2\pi f)^2$, is equal to 705 (rad/sec)², corresponding to 4.23 Hz natural frequency;
- the contribution of the partitions is initially frictional, resulting in an increase of damping; for displacement close to twice the clearance between the partitions and the test frame, the energy dissipated increases due to the damage recorded within the partitions.
- the hysteretic behavior of the partitions can be consistently assumed to be a relationship with initial gap; a significant increase of stiffness is recorded for large relative displacement.

The hysteretic curve in Y direction (Figure 23b), i.e. partition out of plane direction, clearly shows that the partitions do not contribute to the lateral stiffness and strength in this direction, since the linear slope of the hysteresis loops corresponds to the bare test frame natural frequency.

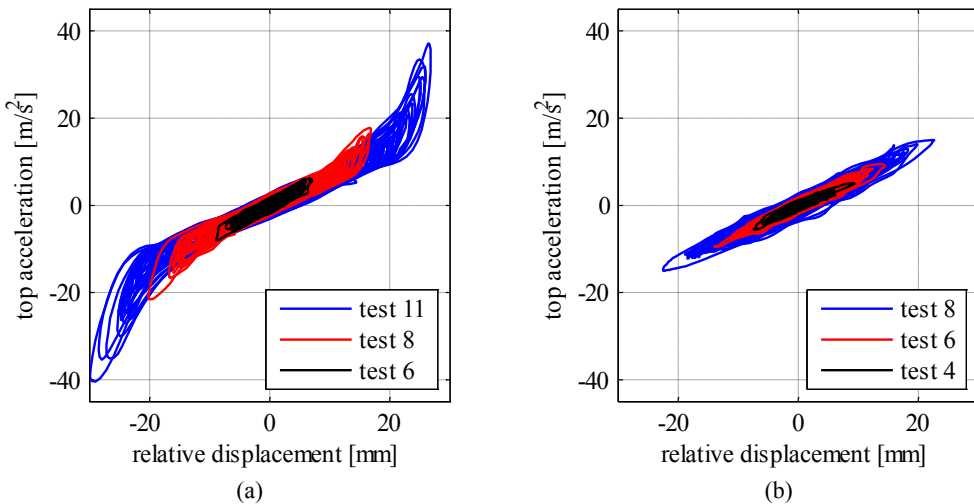


Figure 23. Top acceleration vs relative displacement plot for the different seismic tests in (a) X direction (b) Y direction.

2.1.3.5 FREQUENCY AND DAMPING EVALUATION

Standard techniques for the evaluation of the natural frequency of the test setup allowed comparing the influence of the partitions on the natural frequency of the

system (see Dynamic Identification Section). In the following paragraph the change in the natural frequency during the seismic tests is investigated in order to correlate the damages to the dynamic characteristics of the setup.

The transfer function, estimated as the ratio between the top and the base acceleration in the frequency domain, is applied with respect to the time histories recorded during the different seismic tests. This method allows following the change of the natural frequency during the tests, as shown in Figure 24a.

The procedure proposed by Hashemi and Mosalam (2006), which allows evaluating the average values of stiffness k and damping coefficient b from the dynamic equilibrium, is also implemented. This method consists in evaluating the values of stiffness k and damping coefficient b of an equivalent single degree of freedom system that minimize the error in evaluating the dynamic equilibrium equation for each time instant. Based on the “average” stiffness, the natural frequency is evaluated and plotted in Figure 24a for the different tests.

Assuming an exclusively viscous dissipation, the damping ratio ξ is proportional to the ratio between the dissipated energy per cycle, W_D (area enclosed within each hysteresis cycle), and the elastic energy E (Chopra, 1995) as follows:

$$\xi = \frac{W_D}{4\pi E} \quad (6)$$

Each hysteresis cycle of a single test is isolated to calculate its area, i.e. the dissipated energy W_D , and the associated elastic energy E . This procedure provides as much damping values as the number of hysteresis cycles in each test. In Figure 24b the median value of damping coefficient is plotted for each test.

The damping ratio ξ is also evaluated from the procedure proposed by Hashemi and Mosalam (2006) using the theoretical expression:

$$\xi = \frac{b}{2\sqrt{k \cdot m}} \quad (7)$$

where k is the lateral stiffness mentioned above and m is the mass of the equivalent single degree of freedom system. In Figure 24b the damping ratio, evaluated according to the latter procedure, is compared to the equivalent viscous damping computed according to the energetic method.

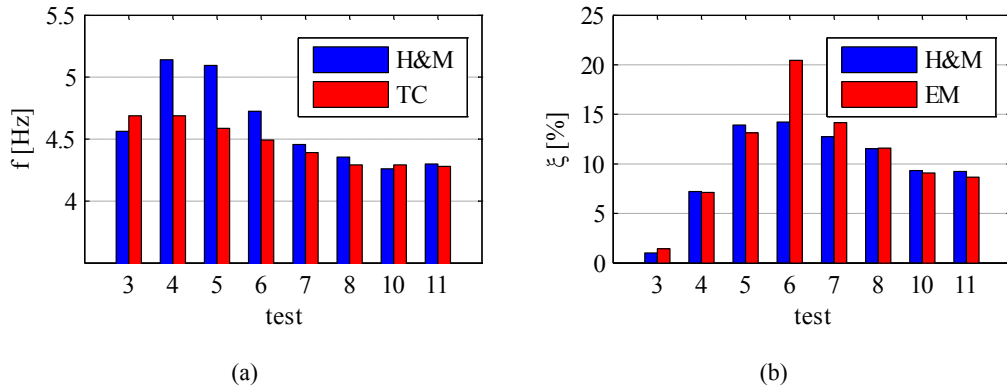


Figure 24. (a) Natural frequency evaluation according to Hashemi and Mosalam (2006) (H&M) procedure and transfer curve method (TC) for the different seismic tests; (b) damping ratio evaluation according to Hashemi and Mosalam (2006) (H&M) procedure and the energetic method (EM) for the different seismic tests.

The trend of both the natural frequency and the damping ratio confirms the recorded damage.

The presence of the acrylic silicone in the clearance between the test frame and the partition lightly contributes to the lateral stiffness in the first tests (small displacement demand), increasing the natural frequency. The decrease of the frequency in tests 6 and 7 denotes the failure of the acrylic silicone. Consequently the natural frequency tends to a lightly larger frequency than the bare test frame one. This is due to the fact that for large displacements, i.e. interstorey drifts larger than 0.5%, the partitions collaborate with the test frame, stiffening the setup (Figure 23a).

Similarly, from test no. 3 to test no. 6 an increase in the damping ratio and then a following decrease is exhibited, essentially due to the silicone progressive damaging. In test 6 a very high value of damping is recorded, mainly owed to two factors: the presence of the acrylic silicone which is a material characterized by high damping and the friction developed by the plasterboards that slide with respect to the top runner. Once the silicone is detached, the damping ratio decreases, since the damping due to the silicone vanishes.

2.1.3.6 BASE SHEAR REPARTITION

Through the analysis of the hysteretic curves (Figure 23) the base shear repartition between the partitions and the test frame is evaluated. The force adsorbed by the partitions is simply evaluated as the difference between the maximum inertia force and the force acting on the test frame; the latter force is calculated upon the natural frequency of the test frame and the attained displacement. The result is also validated using the strain gauge placed at the column base of the test frame.

In Figure 25 the base shear distribution between partitions and test frames in every test is shown. It can be seen that the contribution of the partitions is initially negligible. Partitions start collaborating after test 7, when the acrylic silicone is detached. The quantity absorbed by partitions passes from a value of approximately 20% (test 6) to 50% of the total base shear (tests 10-11).

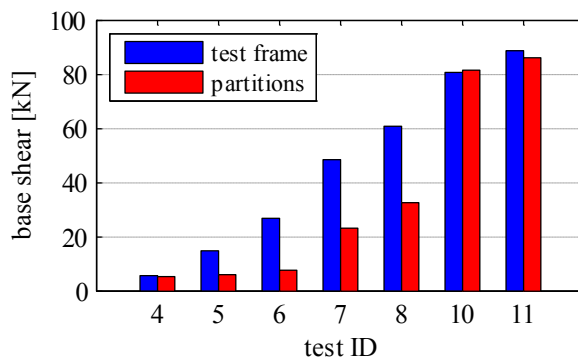


Figure 25. Base shear repartition between test frame and partition systems for the different seismic tests.

2.1.3.7 EVALUATION OF THE FREQUENCY OF THE COMPONENT

In order to evaluate the natural frequency in the out of plane direction, the transfer curve method is applied considering the base acceleration and the partition out of plane acceleration recorded by accelerogram no. 103763 (Figure 10). The method is applied for the eight bidirectional tests, in which the partition is subjected to acceleration in the out of plane direction.

The transfer function in Figure 26 yields two peaks: one with lower frequency, denoting the natural frequency in Y direction of the test frame that is constant for the different tests; the latter is related to the natural frequency of the nonstructural component in the out of plane direction. It should be noted that the frequency of the component decreases from a value of 16.8 Hz for test 1 to 11.5 Hz for test 8, being representative of the damage progression in the partition systems. The irregular trend of the transfer functions in Figure 26 is due to the fact that the input accelerogram is not intended for dynamic identification purposes, i.e. it is not a random/white noise excitation. However, the peaks are clearly evidenced also in case an AC156 accelerogram is adopted; indeed, such an accelerogram has a significant energy content from 1.3 to 33.3 Hz with one-sixth-octave bandwidth resolution.

The results confirm that the frequencies of the partitions are much larger than the typical structural fundamental frequencies. Hence, the ratio between the period of the nonstructural component (T_a) and the period of the building (T_1), considered in

Eurocode 8 (CEN, 2004b) for the evaluation of the seismic demand on the component, could be accordingly assumed equal to zero.

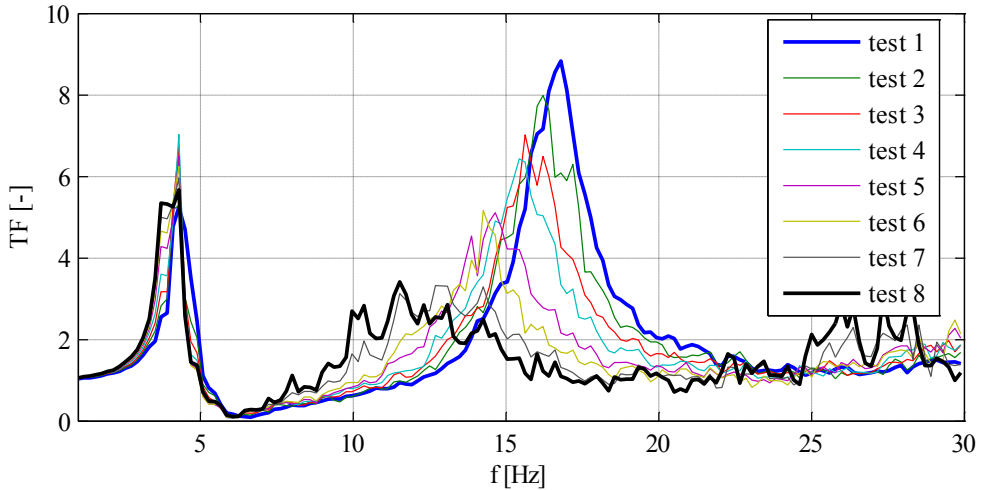


Figure 26. Transfer function from the base to the partition center in the out of plane direction for the bidirectional tests.

2.1.4 ANALYTICAL MODELLING: POST-TEST DYNAMIC ANALYSES

A numerical model of the test setup, i.e. the test frame and the partitions, is defined and subjected to the recorded base acceleration time-histories through OpenSees program (McKenna and Fenves, 2013). The test frame is modelled as a single degree of freedom system with a 4.33 t equivalent mass and a lateral stiffness evaluated upon the outcomes of the dynamic identification procedures above mentioned.

The tested partitions are included into the model through the insertion of two translational springs in parallel:

- a brittle-elastic translational spring with stiffness equal to k_{sil} that represents the contribution of the acrylic silicone to the lateral behavior; based on the recorded damage, the contribution of the spring vanishes once a displacement larger than 10 mm is attained;
- an elastic with gap translational spring, defined upon the parameters δ_{GAP} and k_{par} , that represent the width of the gap and the contribution of the partition system to the stiffness once the silicone fails, respectively.

The unknown parameters of the model are:

- the gap dimension δ_{GAP} ;
- the stiffness of the acrylic silicone k_{sil} ;

- the stiffness of the partition system k_{par} ;
- the damping ratio ξ_i , assumed to be different for each test.

The parameters of the model are set (Table 7) in order to minimize the difference between experimental and numerical results in terms of both maximum displacement/acceleration and dissipated energy.

δ_{GAP} [mm]	k_{sil} [kN/m]	k_{par} [kN/m]
21.5	1260	14000

Table 7. Gap dimension, stiffness of the acrylic silicone spring and of the partition system adopted in the model.

The damping ratios necessary for the experimental-numerical matching for the different tests confirm the outcomes of the procedures summarized in Figure 24b, passing from a value of $\xi=30\%$ in test 6 to $\xi=5.5\%$ in test 11.

The results of the analyses (blue line) for tests 6 ($\xi=30\%$) and 11 ($\xi=5.5\%$) are compared in Figure 27 and Figure 28 with the experimental outcomes (red line) in terms of hysteresis loops and displacement time histories.

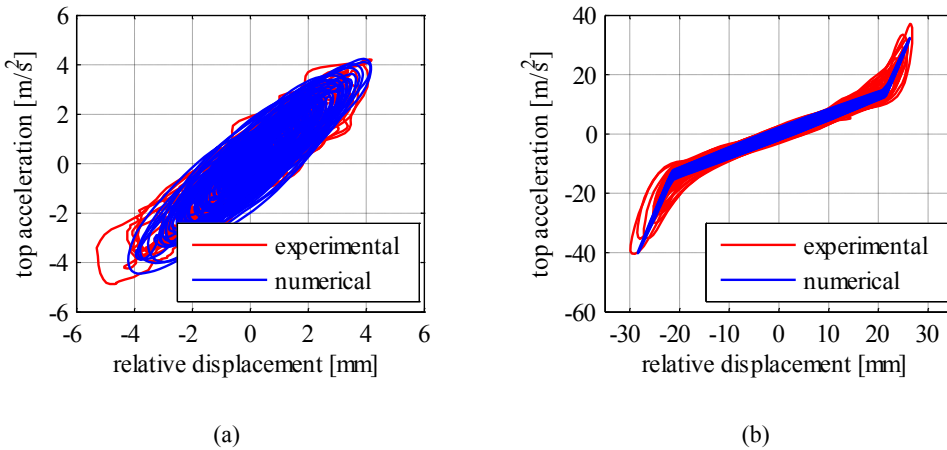


Figure 27. Comparison between experimental and numerical hysteresis loop: (a) test 6; (b) test 11.

The hysteretic curve comparison shows the good matching in terms of dissipated energy both for test 6, in which the silicone exhibits significant damage yielding a large damping ratio, and for test 11, in which the silicone is failed and the partitions collaborate for large displacement. The comparison between displacement time histories shows the excellent matching between experimental and numerical results.

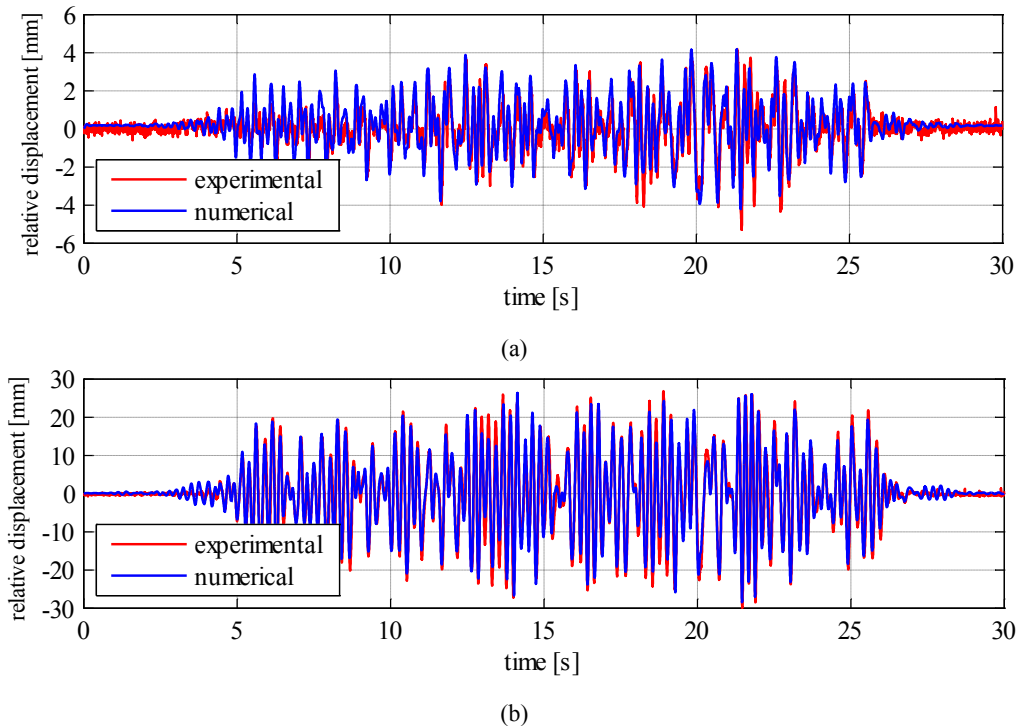


Figure 28. Comparison between experimental and numerical time histories: (a) test 6; (b) test 11.

2.1.5 CONCLUSIONS

In order to investigate the seismic behavior of plasterboard internal partitions, shaking table tests are carried out by the earthquake simulator system available at the laboratory of the Department of Structures for Engineering and Architecture at the University of Naples Federico II.

A steel test frame is properly designed in order to simulate the seismic effects at a generic building story. The tests are performed shaking the table simultaneously in both horizontal directions. To investigate a wide range of interstory drift demand and seismic damage, the shakes are performed scaling the accelerograms at eleven different intensity levels.

Relative displacements are evaluated using laser sensors records. Values up to 1.1% drift are recorded, representative of a moderate earthquake intensity level. The tested partition systems exhibit a good seismic behavior: a minor damage state is attained for 0.58% drift level, while a moderate damage state is attained for 0.98% drift level.

Standard methods for the dynamic identification of the test setup, both bare and infilled, are used in order to evaluate the influence of the plasterboard partitions on the

steel test frame. The change in the natural frequency and the damping ratio during the different seismic tests is correlated to the recorded damages.

Finally, a numerical model of the test setup, i.e. the test frame and the partitions, is defined and subjected to the recorded base acceleration time-histories through the OpenSees program. The test frame is modelled as a single degree of freedom system. The hysteretic curve comparison shows a good matching in terms of dissipated energy, while the comparison of displacement time histories shows the excellent matching between experimental and numerical results.

It should be underlined that the above presented conclusions and results are related and limited to the tested innovative partition typology; the use of acrylic silicone, as well as the non-connection of the boards to the guides along the perimeter, substantially influences the overall behavior of the panel.

2.1.6 REFERENCES

- Adham SA, Avanesian V, Hart GC, Anderson RW, Elmlinger J, Gregory J (1990) Shear Wall Resistance of Lightgauge Steel Stud Wall Systems. *Earthquake Spectra* 6 (1):1-14. doi:10.1193/1.1585555
- Anderson RW (1981) Investigation of the seismic resistance of interior building partitions. Agbabian Associates, El Segubehaviourndo, California, USA
- Boore DM, Bommer JJ (2005) Processing of strong-motion accelerograms: needs, options and consequences. *Soil Dynamics and Earthquake Engineering* 25 (2):93-115. doi:10.1016/j.soildyn.2004.10.007
- Bracci JM, Reinhorn AM, Mander JB (1992) Seismic resistance of Reinforced Concrete Frame Structures Designed Only for Gravity Loads: Part I - Design and Properties of a One-Third Scale Model Structure. Technical Report NCEER-92-0027. State University of New York at Buffalo, NY, US
- CEN (2004a) Eurocode 3: design of steel structures - Part 1-3: Supplementary rules for cold-formed members and sheeting. EN 1993-1-3. Brussels, Belgium
- CEN (2004b) Eurocode 8: design of structures for earthquake resistance - Part 1: general rules, seismic actions and rules for buildings. EN 1998-1. Brussels, Belgium.
- CEN (2005a) Eurocode 3: design of steel structures - Part 1-1: General rules and rules for buildings. EN 1993-1-1. Brussels, Belgium
- CEN (2005b) Eurocode 3: design of steel structures - Part 1-8: design of joints. EN 1993-1-8. Brussels, Belgium
- Chopra AK (1995) Dynamics of structures: Theory and Applications to Earthquake Engineering. Prentice Hall, Englewood Cliffs, New Jersey, USA
- Clough RW, Penzien J (1995) Dynamics of structures. Third edition. Computer & Structures, Inc., Berkeley, CA, US

- CSI Computer & Structures Inc. (2004) SAP2000. Linear and Nonlinear Static and Dynamic Analysis of Three-Dimensional Structures, Computer & Structures, Inc. Berkeley, California
- Filiatrault A, Mosqueda G, Retamales R, Davies R, Tian Y, Fuchs J (2010) Experimental Seismic Fragility of Steel Studded Gypsum Partition Walls and Fire Sprinkler Piping Subsystems. In: Structures Congress 2010. pp 2633-2644. doi:doi:10.1061/41130(369)237
- Fülöp LA, Dubina D (2004a) Performance of wall-stud cold-formed shear panels under monotonic and cyclic loading: Part I: Experimental research. *Thin-Walled Structures* 42 (2):321-338. doi:10.1016/S0263-8231(03)00063-6
- Fülöp LA, Dubina D (2004b) Performance of wall-stud cold-formed shear panels under monotonic and cyclic loading: Part II: Numerical modelling and performance analysis. *Thin-Walled Structures* 42 (2):339-349. doi:10.1016/S0263-8231(03)00064-8
- Hancock J, Watson-Lamprey J, Abrahamson NA, Bommer JJ, Markatis A, McCoyh E, Mendis R (2006) An improved method of matching response spectra of recorded earthquake ground motion using wavelets. *Journal of Earthquake Engineering* 10 (sup001):67-89. doi:10.1080/13632460609350629
- Hashemi A, Mosalam KM (2006) Shake-table experiment on reinforced concrete structure containing masonry infill wall. *Earthquake Engineering & Structural Dynamics* 35 (14):1827-1852. doi:10.1002/Eqe.612
- International Code Council (ICC) (2000) International Building Code, 2000 Edition (IBC 2000). Falls Church, Virginia, USA.
- International Conference of Building Officials (ICBO) (2000) AC 156 Acceptance Criteria for the Seismic Qualification of Nonstructural Components. ICBO Evaluation Service, Inc., Whittier, California, USA
- Kanvinde AM, Deierlein GG (2006) Analytical models for the seismic performance of gypsum drywall partitions. *Earthquake Spectra* 22 (2):391-411. doi:Doi 10.1193/1.2191927
- Landolfo R, Fiorino L, Della Corte G (2006) Seismic behavior of sheathed cold-formed structures: Physical tests. *Journal of Structural Engineering-Asce* 132 (4):570-581. doi:Doi 10.1061/(Asce_0733-9445(2006)132:4(570)
- Lee TH, Kato M, Matsumiya T, Suita K, Nakashima M (2007) Seismic performance evaluation of non-structural components: Drywall partitions. *Earthquake Engineering & Structural Dynamics* 36 (3):367-382. doi:10.1002/Eqe.638
- Maddaloni G, Ryu KP, Reinhorn AM (2011) Simulation of floor response spectra in shake table experiments. *Earthquake Engineering & Structural Dynamics* 40 (6):591-604. doi:10.1002/Eqe.1035
- Magliulo G, Petrone C, Capozzi V, Maddaloni G, Lopez P, Manfredi G (2014) Seismic performance evaluation of plasterboard partitions via shake table tests. *Bulletin of Earthquake Engineering*:(online first). doi:10.1007/s10518-013-9567-8
- Magliulo G, Petrone C, Capozzi V, Maddaloni G, Lopez P, Talamonti R, Manfredi G (2012) Shake Table Tests on Infill Plasterboard Partitions. *The Open*

- Construction and Building Technology Journal 6 (Suppl 1-M10):155-163. doi:10.2174/1874836801206010155
- McCormick J, Matsuoka Y, Pan P, Nakashima M (2008) Evaluation of Non-Structural Partition Walls and Suspended Ceiling Systems through a Shake Table Study. In: Structures Congress 2008. pp 1-10. doi:doi:10.1061/41016(314)223
- McKenna F, Fenves GL (2013) OpenSees Manual <http://opensees.berkeley.edu>. Pacific Earthquake Engineering Research Center, Berkeley, California.,
- Mosqueda G, Retamales R, Filiatrault A, Reinhorn A (2009) Testing Facility for Experimental Evaluation of Non-Structural Components under Full-Scale Floor Motions. Structural Design of Tall and Special Buildings 18 (4):387-404. doi:10.1002/Tal.441
- Paulay T, Priestley M (1992) Seismic design of reinforced concrete and masonry buildings. Wiley, New York, US
- Restrepo JI, Bersofsky AM (2011) Performance characteristics of light gage steel stud partition walls. Thin-Walled Structures 49 (2):317-324. doi:10.1016/j.tws.2010.10.001
- Restrepo JI, Lang AF (2011) Study of Loading Protocols in Light-Gauge Stud Partition Walls. Earthquake Spectra 27 (4):1169-1185. doi:10.1193/1.3651608
- Retamales R, Davies R, Mosqueda G, Filiatrault A (2013) Experimental Seismic Fragility of Cold-Formed Steel Framed Gypsum Partition Walls. Journal of Structural Engineering 139 (8):1285-1293. doi:10.1061/(ASCE)ST.1943-541X.0000657

2.2 SHAKE TABLE TEST ON HOLLOW BRICK PARTITIONS

The collapse of hollow brick internal partitions is one of the most widely reported nonstructural damage after an earthquake, especially in the European area. Full-scale experimental tests on standard hollow brick partitions are described in this Section (Petrone et al., 2013). In particular, bidirectional shaking table tests are performed in order to investigate the seismic performance of hollow brick partitions, subjecting the partition simultaneously to interstory relative displacements in their own plane and accelerations in the out of plane direction. A steel test frame is properly defined in order to simulate the seismic effects at a generic building story. A set of five couples of accelerograms are selected matching the target response spectrum provided by the U.S. code for nonstructural components in order to investigate a wide range of seismic input. Three damage states are considered in this study and correlated to an engineering demand parameter, i.e. the interstory drift ratio, through the use of a damage scheme. The tested specimen exhibits significant damage for 0.3% interstory drift and extensive damage for drift close to 1%. The correlation between the dynamic characteristics of the test setup, in terms of damping ratio and natural frequency, and the recorded damage is evidenced.

2.2.1 INTRODUCTION

Few studies were conducted in the past on nonstructural components performance evaluation, particularly referring to suspended ceiling systems (Magliulo et al., 2012c; Badillo-Almaraz et al., 2007; Gilani et al., 2010) and plasterboard partitions (Magliulo et al., 2013; Magliulo et al., 2012d; Mosqueda et al., 2010; Lee et al., 2007). Very limited studies were conducted in the past on the seismic behavior of hollow brick internal partitions, even though they are very common in the European area both in residential and industrial buildings (Magliulo et al., 2008; Magliulo et al., 2011). Furthermore, recent earthquakes evidenced that brick partitions usually exhibit extensive damage that jeopardizes the practicability of the whole building.

In this study the seismic performance of hollow brick partitions is investigated. Such partitions are built in order to be representative of the “classical” existing partitions, widespread in the European area. The seismic performance evaluation is pursued via shake table tests with increasing intensity. The shake table tests allow subjecting the partition simultaneously to interstory relative displacements in their own plane and accelerations in the out of plane direction.

The recorded damage states are correlated to an engineering demand parameter through the use of a damage scheme; some considerations on the hysteretic curve, the

natural frequency, the damping ratio and the partition base shear are made through a complete analysis of the recorded quantities.

2.2.2 EXPERIMENTAL FACILITIES AND TEST SET UP, SPECIMENS AND INPUT

The shake table tests are performed in the laboratory of the Department of Structures for Engineering and Architecture of the University of Naples Federico II. The tests aim to investigate the seismic behavior of hollow brick partitions.

As shown in Figure 29, the test setup consists of: (a) a shake table simulator; (b) an existing 3D steel test frame (see Section 2.1), used in a test campaign on plasterboard partitions (Magliulo et al., 2012d; Magliulo et al., 2012c), able to transfer the seismic input to the partitions; (c) the specimen, i.e. hollow brick partitions.

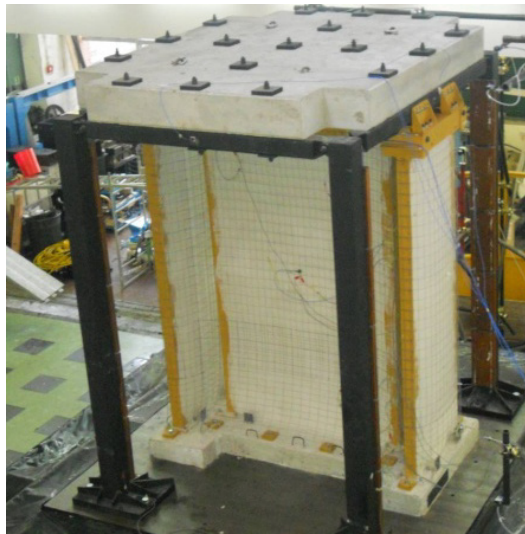


Figure 29. Global view of the test setup.

The seismic qualification of hollow brick partitions is carried out by the earthquake simulator system available at the laboratory of the Department of Structures for Engineering and Architecture at the University of Naples Federico II. The system consists of two 3 m x 3 m square shake tables. Each table is characterized by two degrees of freedom in the two horizontal directions. The maximum payload of each shake table is 200 kN with a frequency range of 0 - 50 Hz, peak acceleration, associated to the maximum payload, equal to 1.0 g, peak velocity equal 1 m/sec and total displacement equal to 500 mm (± 250 mm). Only one shake table is used in this experimental campaign.

The function of the existing test frame is to dynamically excite the specimen, subjecting the partitions to a wide range of interstory drifts and accelerations. Indeed, internal partitions are architectural nonstructural components that are displacement-sensitive in their own plane and acceleration-sensitive in their out of plane direction. A steel test frame is therefore designed in order to simulate the seismic behavior of a generic story of a structure located in a high seismicity area (Magliulo et al., 2013). In particular, it is characterized by:

- a realistic value of mass, i.e. specific mass ratio equal to 1.0 t/m^2 ;
- a realistic stiffness: the interstory displacement d_r is assumed to be equal to 0.005 times the interstory height, for a “frequent” (i.e. 50 years return period) earthquake typical of high seismicity areas. Indeed, the test frame is designed in order to exhibit a 0.5% interstorey drift for an earthquake characterized by S_{DS} equal to 0.60 g. Such an intensity level is representative of an earthquake with 0.24 g peak ground acceleration, i.e. an intensity level of earthquake with 50 years return period in a high seismicity zone according to the indications included in Paulay and Priestley (1992).

The columns of the test frame are 150x150x15 mm box sections; each column is 2.9 m high. Steel horizontal beams, consisting of 120x120x15 mm cross section profiles, are connected to the columns through pin connections. At the top of the structure a reinforced concrete slab is placed; its plan dimensions are 2,15 m x 2,65 m and its thickness is 250 mm. The total mass of the test frame (excluding partitions) is 5.215 t. The test frame is designed according to the Eurocodes 3 and 8 (CEN, 2005a, b, 2004) by modal response spectrum analysis. It is considered one load combination, the seismic one, with the two orthogonal horizontal components acting simultaneously. The behavior factor is assumed to be equal to 1, since the test frame is designed to remain in the elastic range even if subjected to the most intense input acceleration time history. Further details on the definition of the test frame are indicated in (Magliulo et al., 2013).

The specimen consists of three partitions and as many steel frames surrounding them placed on an “I” shape RC slab (Figure 30): the steel frames and the slab connect the specimen with the existing test frame and the shake table. The partitions are constituted by hollow bricks jointed and plastered with mortar; the vertical joints among the bricks are staggered.

2.2.2.1 TEST SETUP AND SPECIMEN

The design and the geometry of the setup are defined to simulate the realistic conditions to which a standard hollow brick partition is typically subjected.

The specimen is doubly symmetric and presents a 150 cm wide partition and two smaller 80 cm wide partitions in the orthogonal direction. The partitions are 2.6 m high; the connection between the specimen and the shake table is ensured by an “I” shape RC slab (Figure 30a).

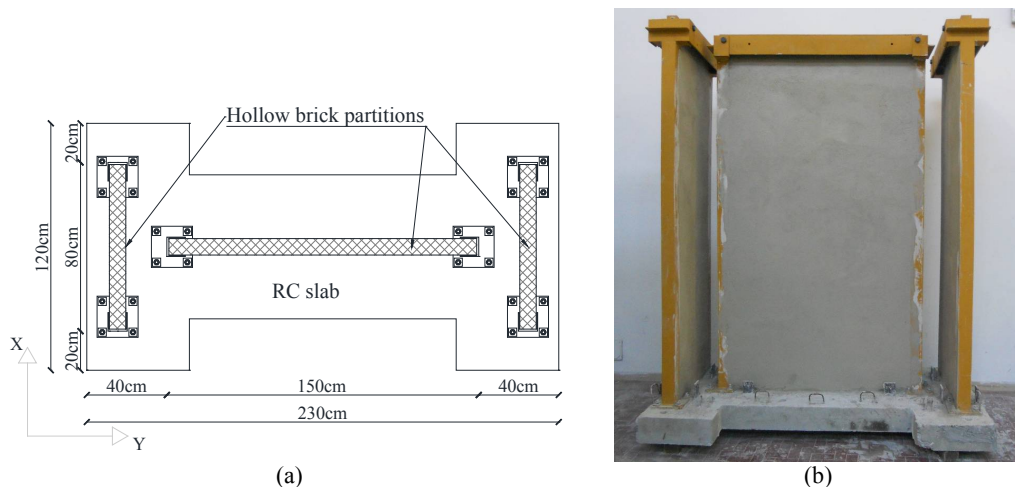


Figure 30. Specimen: (a) plan view; (b) general view.

The walls are made with hollow bricks 250x250x80 mm connected together and plastered with mortar. A steel frame is defined around the partition (Figure 30b) in order to connect the specimen to the existing test frame and to reproduce the partition typical conditions, in which it is disposed between two restraining orthogonal panels. The columns of the steel frame, i.e. welded 90x90x5mm “C” profiles, are hinged to the top horizontal beams. Indeed a hollow brick partition is typically placed between other two orthogonal partitions that restrain it, introducing alternatively the bricks in the orthogonal partitions. The gaps along the vertical edges of the partition, which result from this schematization, are filled with mortar to reproduce the bricks of the ideal orthogonal partitions (Figure 31).

Due to their low lateral stiffness, it can be assumed that the steel profiles do not interfere with the partitions in resisting to the horizontal actions. The total mass of the specimen, i.e. RC slab, partitions and surrounding steel frame, is 2.24 t.

The plan layout of the panels ensures the global system to have a comparable stiffness in both the orthogonal directions; indeed, two 80 cm wide walls are arranged orthogonally with respect to the larger, 150 cm wide, partition (Figure 30a).

The width of the larger partition is determined by making a compromise between two different requirements. In particular, the width should be:

- sufficiently large, i.e. a width larger than 1.00 m, in order to test a realistic partition;

- sufficiently narrow to allow the investigation of the whole damage states range of the nonstructural component up to the failure of the component (see Section 2.2.2.4).

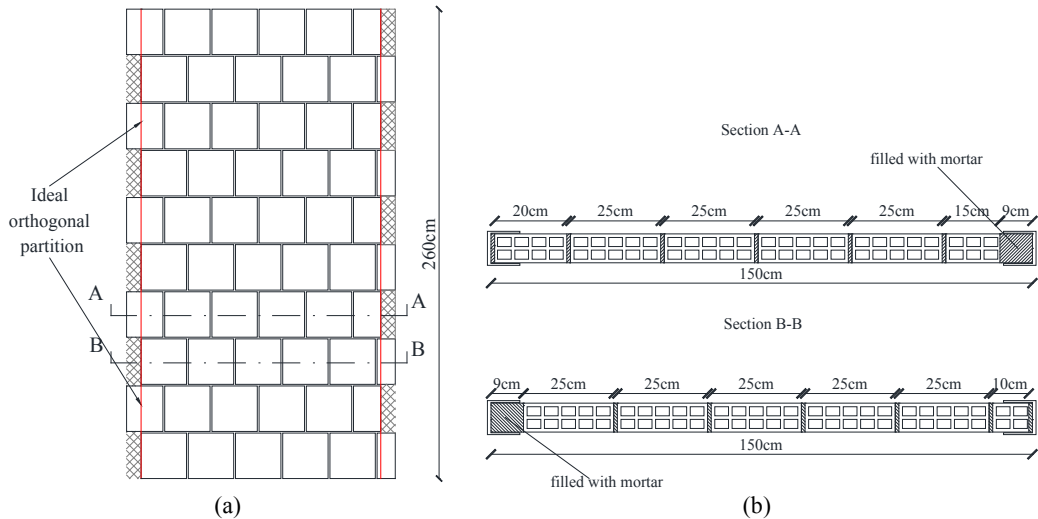


Figure 31. Cross sections of the specimen: (a) front view of the larger partition; (b) cross sections of the larger partition: gaps filled with mortar to reproduce the presence of the orthogonal partitions.

2.2.2.2 INSTRUMENTATION

Accelerometers, strain gauges and displacement laser sensors are used to monitor the response of both the test frame and the specimen.

One accelerometer, placed inside the shake table, measures the input accelerations in both the directions. Seven accelerometers are also arranged in order to monitor different points of the setup, as shown in Figure 32b.

The accelerometers 1, 2, 4 and 5 are installed on the top of the setup (Figure 32a); in particular, the accelerometers 1 and 2 are placed at half height of a test frame beam oriented in Y and X direction, respectively; the accelerometers 4 and 5 are located on the beam of the frame surrounding the largest partition, in order to verify the acceleration to which the specimen is subjected; the accelerometers 3 and 7 are positioned at the base of the column of the test frame and at the base of the frame surrounding one of the small partitions, respectively; accelerometer 6 is placed in the centroid of the main partition, in order to monitor the acceleration on the partition in the out of plane direction.

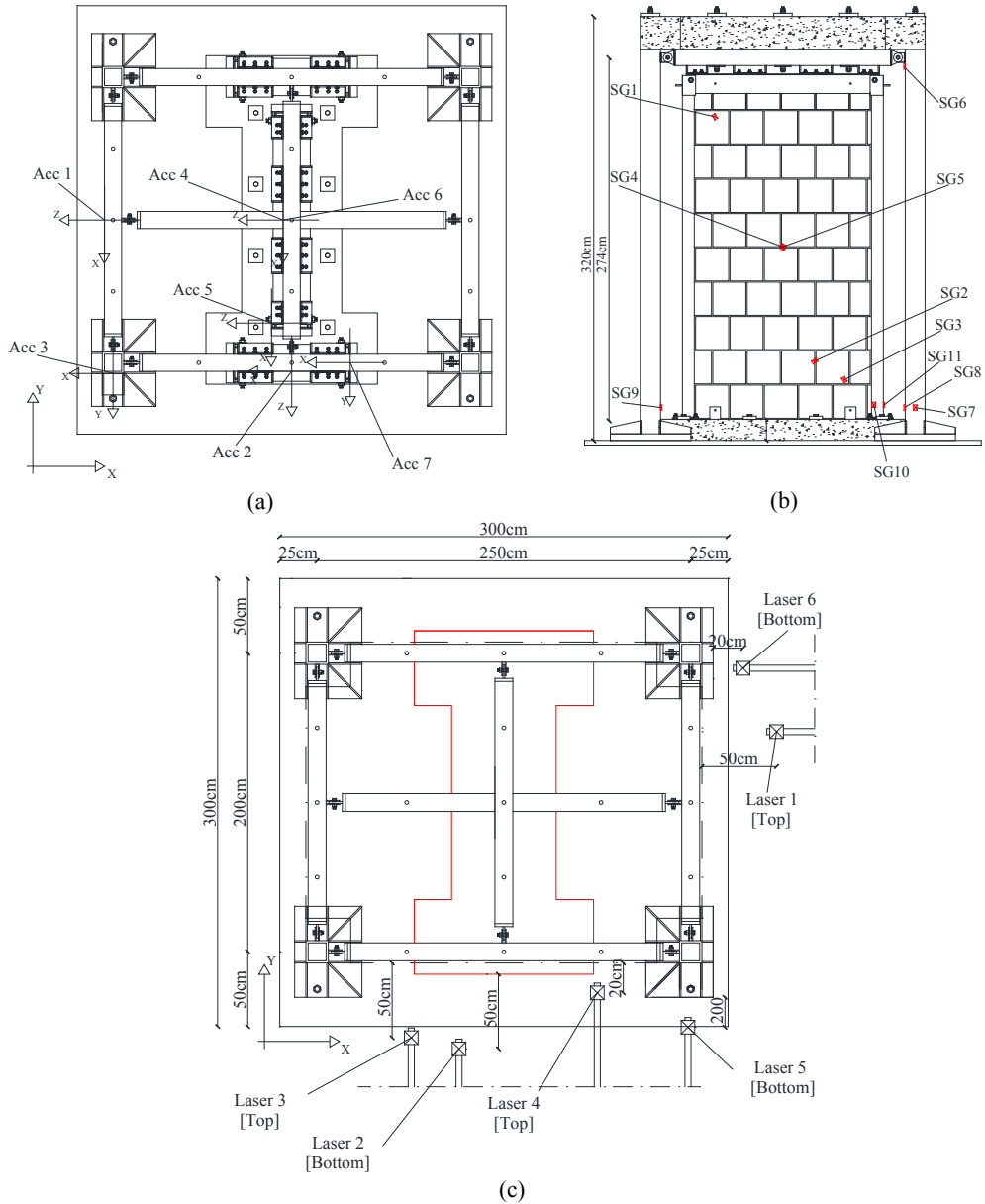


Figure 32. Instrumentation arrangement: (a) accelerometers position; (b) strain gauges arrangement; (c) displacement laser sensors layout.

Eleven strain gauges are adopted and indicated in Figure 32b: four strain gauges placed on the column of the test frame (SG6, SG7, SG8 and SG9); two strain gauges placed at the base of the column of the steel frame (SG10 and SG11); three diagonal strain gauges placed on the partition (SG1, SG2 and SG3), and a double strain gauge in the middle of the wall (SG4 and SG5).

Six laser-optical sensors are used to monitor the displacements in specific points of the test setup. Three lasers are placed at steel base plate mid-height (base plate that connects column to shaking table); the other three ones are placed halfway on the concrete slab (Figure 32c shows the laser arrangement).

2.2.2.3 INPUT AND TESTING PROTOCOL

The input to the table is obtained from time histories representative of a target ground motion and acting simultaneously along the two horizontal directions; the time histories are artificially defined to match the required response spectrum (RRS) provided by the AC156 code “Acceptance criteria for seismic qualification testing of non-structural components” (International Conference of Building Officials (ICBO), 2000). The testing protocols included in FEMA 461 (Federal Emergency Management Agency (FEMA), 2007) and in Retamales et al. (2011) are also considered. The AC156 protocol is preferred since the accelerogram provided by AC156 is better reproduced by the shake table facility used in this study. Moreover, this choice allows a straightforward comparison with previous studies that adopted the same testing protocol (Magliulo et al., 2014).

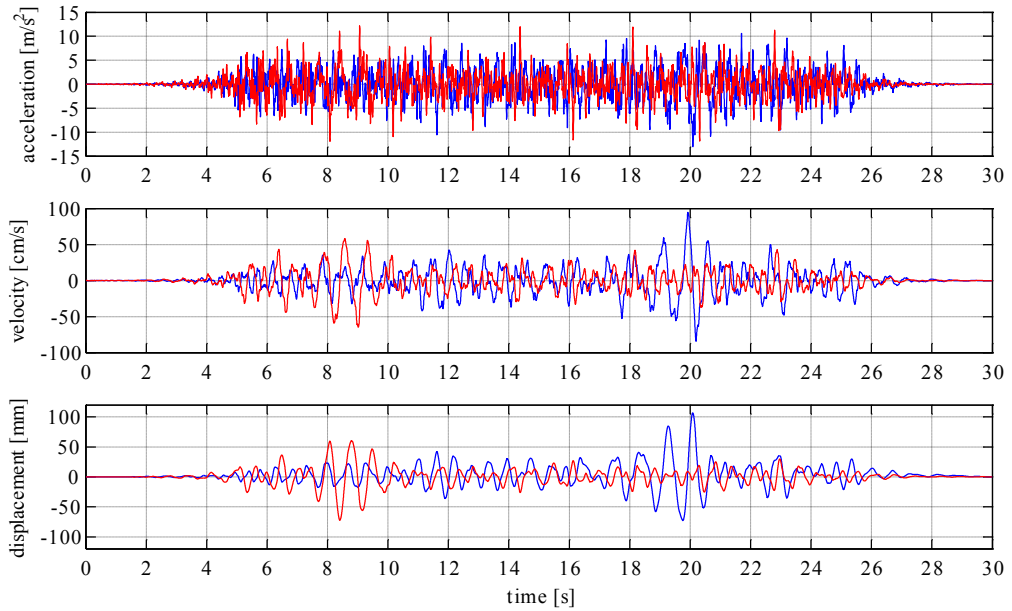
According to AC156, the RRS is obtained as a function of the spectral acceleration at short periods, i.e. S_{DS} . S_{DS} is the parameter characterizing the ground motion. For horizontal design-basis earthquake shaking, the International Building Code (International Code Council (ICC), 2000) defines the short period design-basis earthquake acceleration as follows:

$$S_{DS} = \frac{2}{3} \cdot F_A \cdot S_S \quad (8)$$

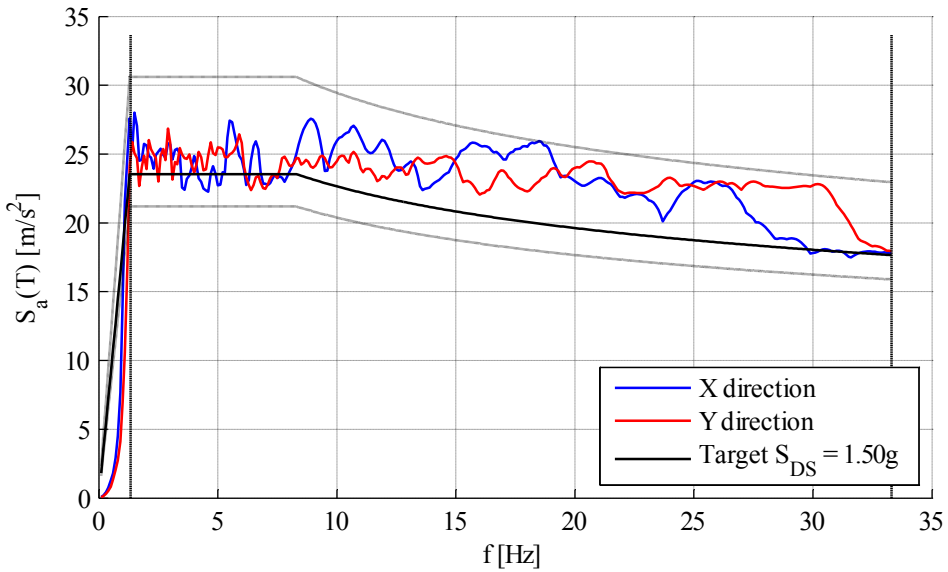
where F_A is a site soil coefficient and S_S is the mapped maximum considered earthquake (MCE) spectral acceleration at short periods.

Two artificial acceleration time histories are defined so as their response spectra, i.e. test response spectra, envelope the target spectrum over the frequency range from 1.3 to 33.3 Hz. The test response spectrum ordinates do not have to be lower than 0.9 times RRS and larger than 1.3 times RRS. The low frequency content is removed from the accelerograms in order to not exceed the displacement and velocity limitations of the earthquake simulator. The damping ratio for the evaluation of the response spectra is set equal to 5%. Further details are given by Magliulo et al. (2012c).

In Figure 11 the obtained time histories for the X and Y directions in terms of acceleration, velocity and displacement, their elastic response acceleration spectra, the RRS corresponding to S_{DS} equal to 1.50g and the RRS scaled to 90% and 130% are shown.



(a)



(b)

Figure 33. Input time histories and spectra for S_{DS} equal to 1.50 g: (a) acceleration, velocity and displacement time-history - X direction (blue) and Y direction (red); (b) input accelerogram spectra, RRS (bold line), upper and lower limits (dashed line), matching frequency range (vertical dashed line).

The input levels for the test campaign range from $S_{DS} = 0.30g$ to $S_{DS} = 1.50g$ in order to generalize the execution of the test and to make it representative of a large range of real earthquakes. Five bidirectional tests with different intensity values are defined (Table 8).

Test no.	S_{DS}
[-]	[g]
1	0.30
2	0.60
3	0.90
4	1.20
5	1.50

Table 8. S_{DS} values for five input test levels.

2.2.2.4 DEFINITION OF THE PARTITION DIMENSIONS

As explained in Section 2.2.2.1, the dimensions of the largest partition are defined in order to accomplish two main goals: to test a realistic partition and to investigate all the different damage states, i.e. from minor damage to collapse, of the specimen during the different tests. For the latter motivation partition sizes are chosen so as to activate failure mechanisms during the programmed tests.

The partition width should be less than one meter according to the typical amount of partitions contained in the floor area of the test setup. However, a 1.50m wide partition is chosen in order to test a more realistic specimen.

Preliminary analyses are conducted to evaluate the capacity of the chosen partition, in order to define the partition as large as possible and, simultaneously, bring the partition to collapse at least at the highest intensity level.

The in plane capacity is estimated making a non-linear dynamic analysis, using the acceleration time-histories defined in Section 2.2.2.3, through the OpenSees program (McKenna and Fenves, 2013). In particular, the system is modelled as a SDOF system with a force-displacement relationship obtained considering a linear elastic behavior for the steel elements whereas the partition in-plane behavior is reproduced by the nonlinear model proposed by Panagiotakos and Fardis (Panagiotakos and Fardis, 1996). The $F-\delta$ relationship presents a capping point defined by a displacement equal to 6.5 mm and a force equal to 95.5 kN. Non-linear dynamic analyses (omitted for the sake of brevity) show the collapse of the partition in Y-direction at the test no. 5.

Concerning the out of plane behavior of masonry walls, different research studies were conducted in the past years, both on unreinforced masonry (Komaraneni et al., 2011) and on FRP strengthened walls (Tumialan et al., 2003). The out of plane capacity is

evaluated in terms of the average acceleration ($a_{collapse}$) in the out of plane direction that causes the collapse of the specimen. The collapse acceleration, evaluated upon the out of plane load that causes the failure according to different formulations available in literature, is reported in Table 9.

Method	$a_{collapse}$ [g]
Angel et al. (1994)	1.89
Cohen and Liang (1956)	4.86
Dawe and Seah (1989)	4.80
Eurocode 6 (CEN, 2001)	3.38
Flanagan and Bennett (1999)	4.35
Garbin et al. (2005)	1.96
Moghaddam and Goudarzi (2010)	2.74

Table 9. Average acceleration ($a_{collapse}$) in the out of plane direction that causes the collapse of the specimen according to different formulations.

The formulations suggested by Dawe and Seah (Dawe and Seah, 1989) and Flanagan and Bennett (Flanagan and Bennett, 1999) consider that the partition is able to arch itself along both vertical and horizontal directions, depending on its boundary conditions. According to the limited width of the tested specimen, they are considered to be the most reliable. Comparing the collapse acceleration in the out-of-plane direction with the highest spectral acceleration for the test highest intensity level, i.e. 2.4 g, the collapse due to an out of plane action is not expected during the tests.

2.2.3 RESULTS AND DISCUSSION

2.2.3.1 DYNAMIC IDENTIFICATION

Before the execution of the test campaign, low-intensity random excitations are selected as input motions for the bare test frame in order to evaluate the natural frequency of the test frame in both the horizontal directions. The transfer curve method is applied between the base and the top acceleration time histories (Figure 34). The bare frame natural frequencies, denoted by the peak in the transfer curves, in X and Y directions (see Figure 32) are 3.83 Hz and 4.04 Hz, respectively. After the specimen is installed within the test frame and before executing the five shake table shakings, a random vibration is also applied in both the horizontal directions in order to measure the influence of the specimen on the natural frequency of the test setup. As shown in Figure 34, the “infilled” natural frequencies of the test setup significantly increase up

to 8.01 Hz and 7.62 Hz in X and Y directions. This confirms the large in plane stiffness of the specimen that significantly influences the dynamic properties of the test setup.

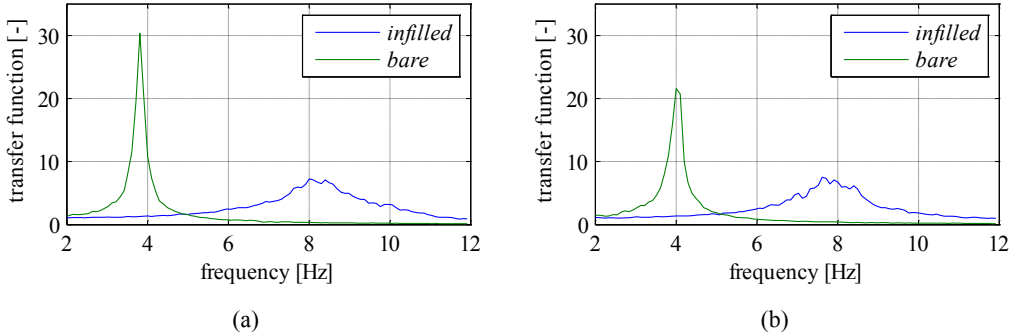


Figure 34. Transfer functions between base and top acceleration time histories for a low-intensity random vibration applied to both bare and infilled test setups (a) in X direction and (b) in Y direction.

2.2.3.2 RESULTS SUMMARY

Using the selected drive motions, five bidirectional shaking tests are performed. After each test the compatibility of the spectrum of the recorded acceleration time-history with the required target response spectrum according to AC156 is verified. The compatibility is almost ensured in the frequency range between 1.3 Hz and 33.3 Hz (Figure 36 and Figure 38).

In Figure 35 and Figure 37 the time-histories in terms of acceleration, velocity and displacement at the shake table level are shown (in blue). The velocity and displacement time-histories are evaluated from the integrals of the acceleration and the velocity time-histories, respectively. Before the evaluation of the integrals, an acausal Butterworth filter is applied and zero pads are added before the start and after the end of the record (Boore and Bommer, 2005). In particular, a band-pass filter is applied in the frequency range between 0.7 Hz and 50 Hz with an order equal to 4. The application of a filter is required in order to remove the long-period noise that cause permanent velocity and, especially, displacements. The application of an acausal filter is preferred with respect to a causal filter in order to reduce phase shift in the record. The zero pads addition is required to avoid offsets and trends in the baselines of the velocity and displacements obtained by integration.

The so-obtained time-histories are compared to the input time histories (red dotted lines) and to the recorded displacement at the shake-table level (green line). A good agreement of the compared time-histories is evidenced.

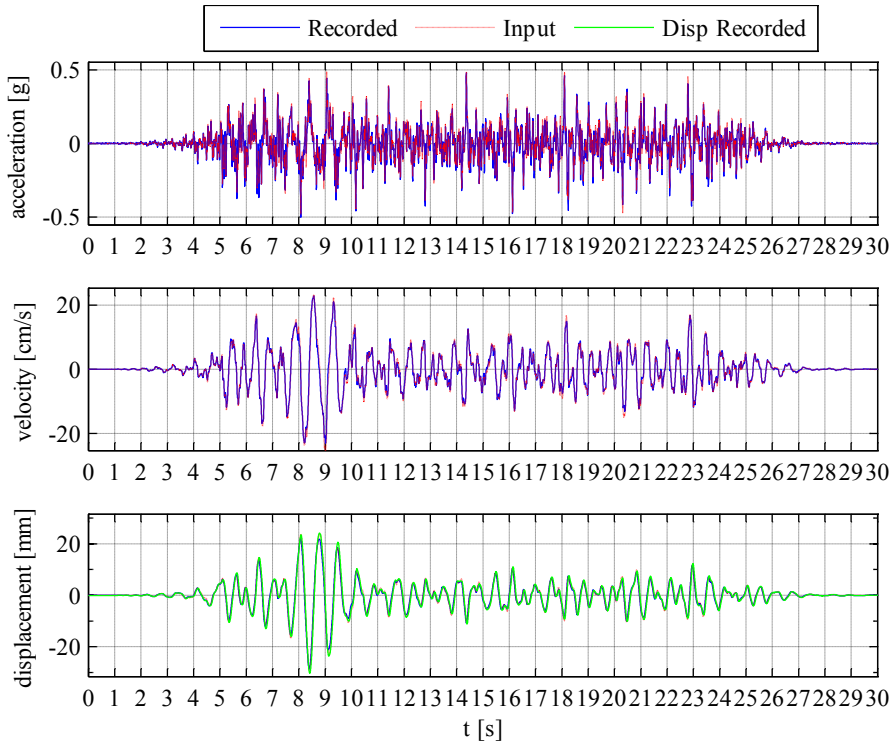


Figure 35. Input vs recorded time-histories in Y-direction – test no. 2.

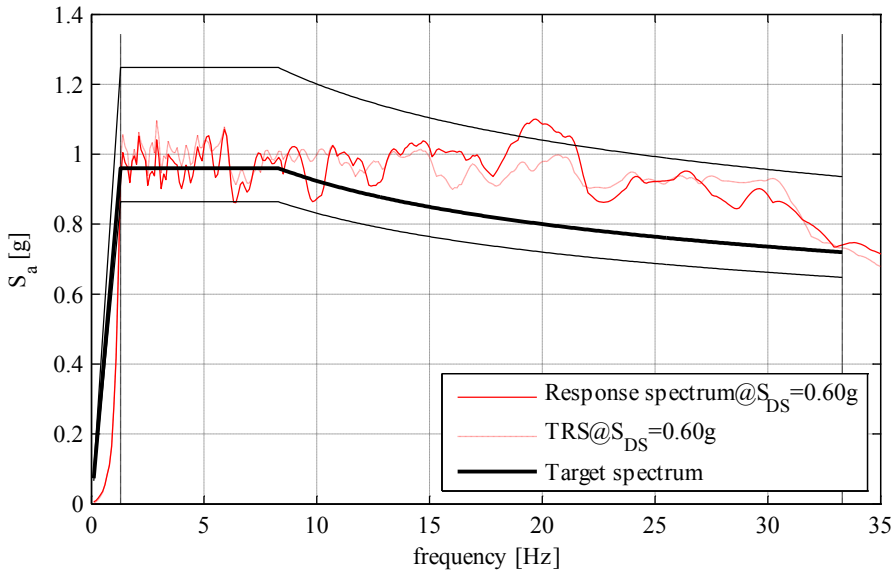


Figure 36. Recorded response spectra vs the Test Response Spectrum (TRS) and the Required Response spectrum (Target Spectrum) in Y-direction – test no. 2.

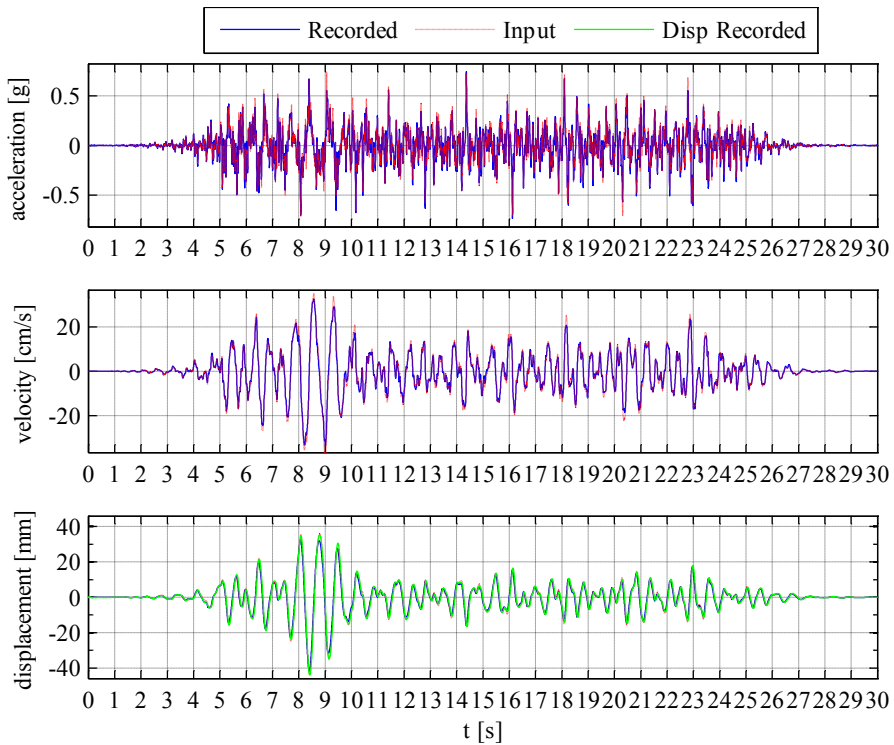


Figure 37. Input vs recorded time-histories in Y-direction – test no. 3.

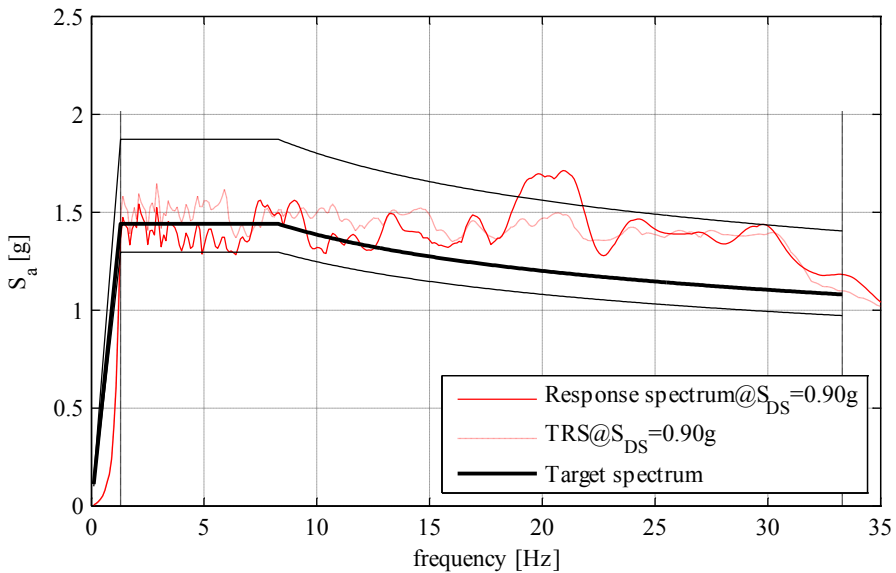


Figure 38. Recorded response spectra vs the Test Response Spectrum (TRS) and the Required Response Spectrum (Target Spectrum) in Y-direction – test no. 3.

In Table 10 the maximum recorded values of acceleration on the roof of the test frame and the maximum recorded relative displacement values are listed. The relative displacement is evaluated using the laser recordings at the top and at the base of the test frame. The acceleration values are measured by the accelerometers placed on the test frame top horizontal beams. Dynamic amplifications in the test setup lead to acceleration values larger than 2.0g on the roof in both X and Y directions. Due to a limitation imposed by the shake table facility, in the test no. 5 the input acceleration intensity value in the X direction is the same as in the test no. 4. This issue has not affected the Y direction, i.e. the largest partition direction, where the system reached higher accelerations in the last test shaking.

In order to analyze the partition behavior and its contribution to the global behavior of the test setup, the top acceleration, representative of the total inertia force, is plotted versus the relative displacement for different intensity levels (Figure 39). A dotted line denotes the behavior of the bare test frame based on its natural frequency and assuming to be in absence of damping.

test no.	Direction	1	2	3	4	5
top acceleration [g]	X	0.58	1.11	1.52	2.10	1.99
relative displacement [mm]		3.67	9.71	18.22	27.05	27.51
top acceleration [g]	Y	0.67	1.14	1.52	1.95	2.39
relative displacement [mm]		3.39	6.14	11.40	18.08	26.54

Table 10. Maximum recorded accelerations at the test frame roof and maximum recorded relative displacements in X and Y directions for the different test runs.

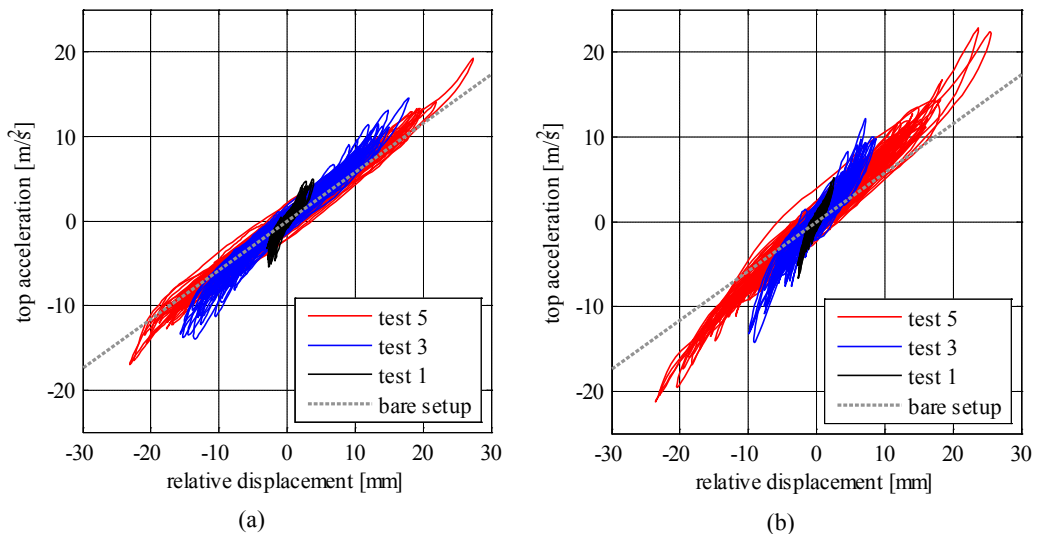


Figure 39. Top acceleration vs relative displacement plot for different seismic tests in (a) X direction and (b) Y direction.

From the analysis of the so-obtained hysteretic curves it can be noted that:

- a significant interaction between the partitions and the hosting structure is exhibited during the first test; during the fifth test, the hysteretic behavior is very close to the bare frame response;
- the secant stiffness, evaluated at the maximum displacement of each test, decreases as the relative displacement increases;
- the negligible influence of the partitions during the fifth test denotes the collapse of the specimen.

2.2.3.3 DAMAGE DESCRIPTION

In this study three damage states are considered for the seismic response definition of the partitions and in particular:

- DS1 - Minor damage state;
- DS2 - Moderate damage state;
- DS3 - Major damage state.

Minor damage state achievement implies the need of repairing the specimen, in order to restore its original condition, e.g. plaster replacing. Moderate damage state achievement, instead, implies that the nonstructural component is damaged so that it must be partially removed and replaced. Major damage state implies that the damage level is such that the partition needs to be totally replaced or the life safety is not ensured. The damage state definitions and their repercussions are indicated in Table 11, based upon the damage state definition given by Taghavi and Miranda (2003). In particular the correlation between each damage state and the loss is given in terms of (Federal Emergency Management Agency (FEMA), 2007): (a) life loss (deaths), (b) direct economic loss due to the repair or replacement of the NSC (damage) and (c) occupancy or service loss (downtime). Furthermore after each test, damage is observed inspecting the specimen components and consequently an appropriate damage table is compiled (Table 11). The level of damage required to overcome a limit state for each damage typology is defined. This process is very useful in order to define the fragility curves for this nonstructural component typology.

Bidirectional tests show a slight damage already up to 0.35% drift in X direction and 0.20% in Y direction. The damage level increases according to the shaking test intensity and the following damages are noticed:

- cracks along the perimeter of the specimen due to the partitions slip from the surrounding frame in test no. 2;

- fall of plaster and pieces of brick from the top of the specimen from test no. 3 with increasing intensity as the demand increases;
- horizontal cracks, wider than 0.3 mm, in the lower part of the walls in test no. 3 (Figure 40a);
- wide sliding cracks in mortar, crushing of mortar at the corner of the specimen and collapse of a brick in the top of the partition in test no. 4 (Figure 40b and Figure 40c);
- deep extended horizontal cracks in the mortar in the lower part of the walls, that let the part above the crack moves as a rigid block with a rocking behavior with respect to the surrounding frame in test no. 5 (Figure 40d and Figure 41a). At this damage level, the specimen does not offer any resistance against lateral displacements since it rigidly moves and rotates within the surrounding frame that restrains it in the out of plane direction.

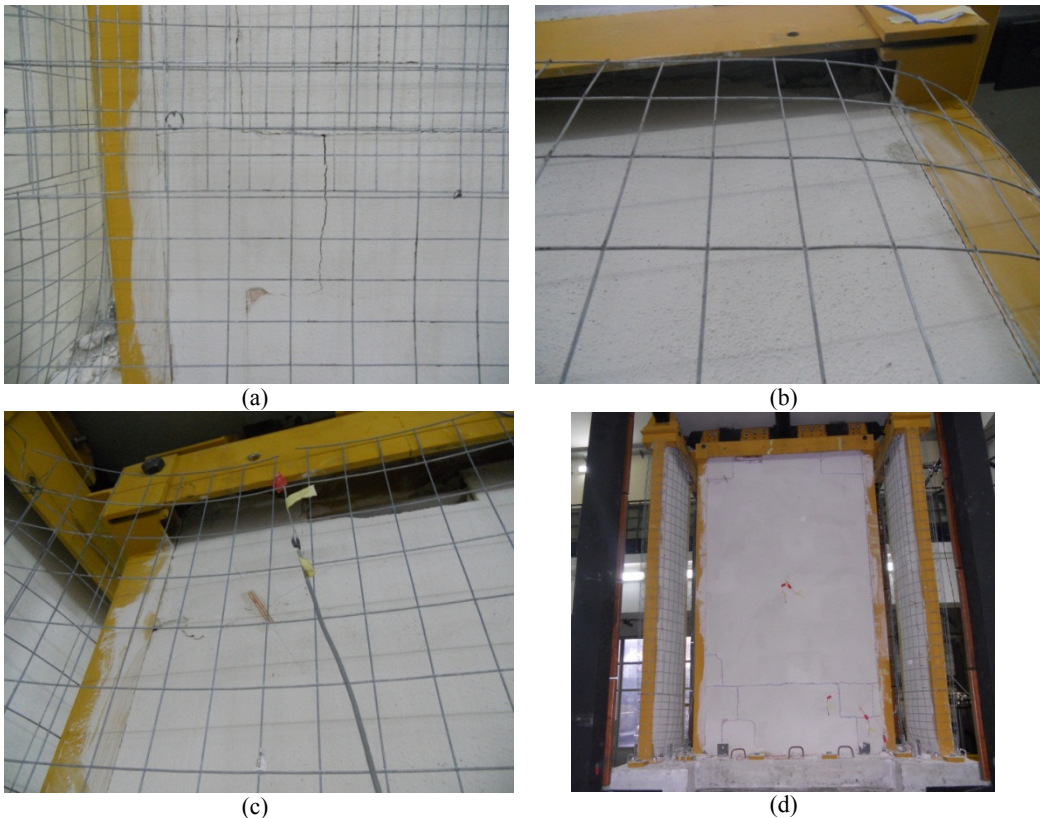


Figure 40. Recorded damage after different shaking tests: (a) wide sliding cracks in mortar in the joints between the bricks; (b) crushing of mortar at the corner; (c) collapse of a brick in the top of the partition; (d) deep extended horizontal cracks in mortar in the lower part of the wall.

2.2 Shake table test on hollow brick partitions

It should be noted that during the tests the specimen is wrapped with a metallic grid without any connection, only for safety purposes. The grid does not give any contribution to the specimen in resisting to the lateral forces.

Test ID: ____	ASSESSMENT	<input type="checkbox"/> DS0 <input type="checkbox"/> DS1 <input type="checkbox"/> DS2 <input type="checkbox"/> DS3
DAMAGE STATE	TYPE OF CONSEQUENCE	INFORMATION
Damage state 1: hairline cracks (width<0.3cm) in mortar and wall finishes	Repair actions	The wall needs some minor repairs of exterior finishes
	Damage consequences	It has no effect on the performance of other components and the building can be used immediately
	Functionality of bldg.	Fully functional
	Life hazard	None
	Component loss of function	None
Damage state 2: severe cracks (width>0.3mm) in wall and spalling of pieces of brick	Repair actions	Depending on the damage extent, some parts of the wall may need demolition and reconstruction. Also the damaged area needs repair of the exterior plaster and painting
	Damage consequences	The functionality of the rooms adjacent to the damaged wall may be interrupted until the wall gets repaired. If there are some small sensitive electrical and mechanical devices on the wall, they may not function and need repair
	Functionality of bldg.	Partially functional
	Life hazard	Small
	Component loss of function	Moderate
Damage state 3: total failure of the wall	Repair actions	The damaged area must be completely demolished and a new wall must be reconstructed.
	Damage consequences	The damaged wall must be demolished and reconstructed before the adjacent rooms can regularly function. Electrical systems, such as plugs and wiring, and mechanical systems, such as piping, may break or not work.
	Functionality of bldg.	Partially functional
	Life hazard	High
	Component loss of function	High

Table 11. Damage state definitions and their repercussions for hollow brick partitions.

The occurred damage is mostly related to the in-plane behaviour of the partition. Failure in the out of plane direction is not observed throughout the different performed tests, confirming the outcome of the blind prediction described in Section 2.2.2.4. However, it should be noted that the specimen is tested assuming a perfect restraint, given by vertical steel C elements, along the vertical edges in the out-plane direction;

such a restraint simulates an excellent connection of the partition with the orthogonal walls.

In Figure 41 the recorded damages after the last test are shown, both in the “large” partition and in the “small” one. The behavior of the specimen is investigated considering that the elements that restrain it along the vertical edges remain undamaged during the shakings, in order to assess the fragility of the component without considering any interaction with the boundary elements. Indeed the steel surrounding frame remains undamaged during the different shakings. Obviously, in case the interaction between the partitions and the restraining elements had been considered, a larger fragility of the component would have been recorded.

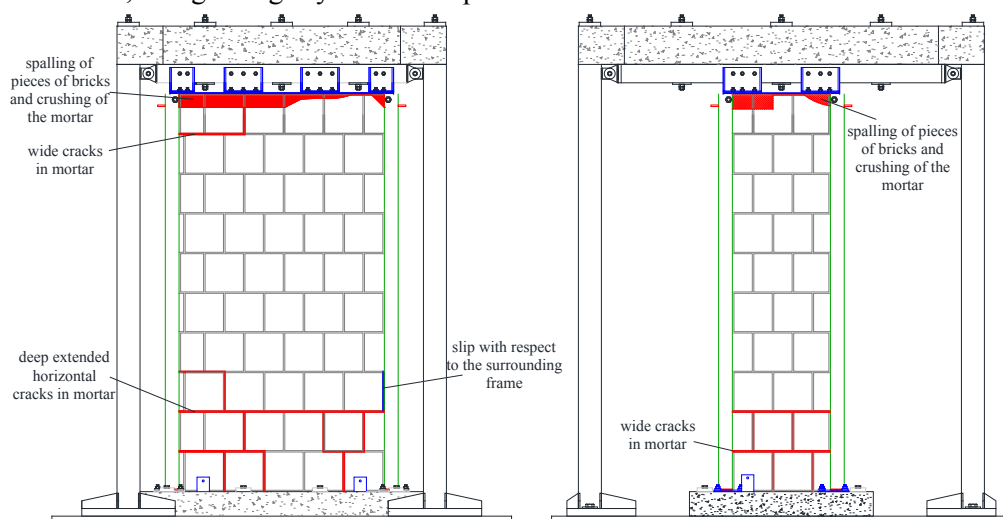


Figure 41. Final damage state at the end of the seismic tests in the largest partition and in the smallest partitions.

A correlation between EDP (Engineering Demand Parameter), i.e. interstory drift, and the DS (Damage State) is also defined (Table 12). Damage State 1 is attained in test 2 due to the need of restoring the cracked plaster along the perimeter of the wall; Damage State 2 is attained in test 3, due to the formation of cracks wider than 0.3 mm and the need of partially replacing the partition; finally Damage State 3 is attained for an interstory drift close to 1% in the three specimens, due to the significant damage and the consequent need of replacing the whole partition. The correlation between the damage states and the engineering demand parameters is based upon the assumption that the damage occurs at the maximum engineering demand parameter that the specimen experiences during a single test.

test no.	Direction	1	2	3	4	5
drift [%]	X	0.13	0.36	0.67	0.99	1.01
Damage State		DS0	DS1	DS2	DS3	DS3
drift [%]	Y	0.12	0.21	0.34	0.66	0.97
Damage State		DS0	DS1	DS2	DS2	DS3

Table 12. Interstory drifts and damage states in X and Y directions for the different tests.

This research study is mostly related to the experimental investigation of the seismic behaviour of brick internal partitions. Further studies will be conducted on numerical simulations, considering different refined models, such as (Dolatshahi and Aref, 2011; Oliveira and Lourenço, 2004; Lourenço, 1996).

2.2.3.4 FREQUENCY AND DAMPING EVALUATION

The presence of infill systems strongly influences the lateral stiffness of the portion of the structure in which they are inserted (Panagiotakos and Fardis, 1996), and may also affect the regularity of the structural system (Magliulo et al., 2012a; Magliulo et al., 2012b; Magliulo and Ramasco, 2007; D'Ambrisi et al., 2009). In Section 2.2.3.1 a standard technique for the evaluation of the natural frequency of the test setup allows estimating the influence of the partitions on the natural frequency of the system. In the following, instead, the change of the natural frequency during the seismic tests is investigated in order to correlate the damage to the dynamic characteristics of the specimen.

The transfer function, estimated as the ratio between the top and the base acceleration in the frequency domain, is evaluated with respect to the time histories recorded during the different seismic tests. This method allows following the change of the natural frequency during the tests, as shown (TC values) in Figure 42a (setup X direction) and Figure 42b (setup Y direction).

The procedure proposed by Hashemi and Mosalam (Hashemi and Mosalam, 2006), which allows evaluating the average values of stiffness k and damping coefficient b from the dynamic equilibrium, is also implemented. This procedure consists in evaluating the values of stiffness k and damping coefficient b of an equivalent single degree of freedom system that minimize the error in evaluating the dynamic equilibrium equation for each time instant. Based on the “average” stiffness, the natural frequencies are evaluated and plotted (H&M values) in Figure 42a (setup X direction) and Figure 42b (setup Y direction) for the different tests.

Assuming dissipation exclusively viscous, the damping ratio ξ is proportional to the ratio between the dissipated energy per cycle, W_D (area enclosed within each hysteresis cycle), and the elastic energy E (Chopra, 1995) as follows:

$$\xi = \frac{W_D}{4\pi E} \quad (9)$$

Each hysteresis cycle of a single test is isolated to calculate its area, i.e. the dissipated energy W_D . This procedure provides as much damping values as the number of hysteresis cycles in each test. In Figure 42c (setup X direction) and Figure 42d (setup Y direction) the median value of damping coefficient is plotted for each test.

The trend of both the natural frequency and the damping ratio confirms the recorded damage.

The natural frequency shows a great reduction during the first three tests due to the damage sustained by the specimen during the first tests and the consequent decrease of the lateral stiffness. Subsequently natural frequency values tends to the bare frame natural frequency.

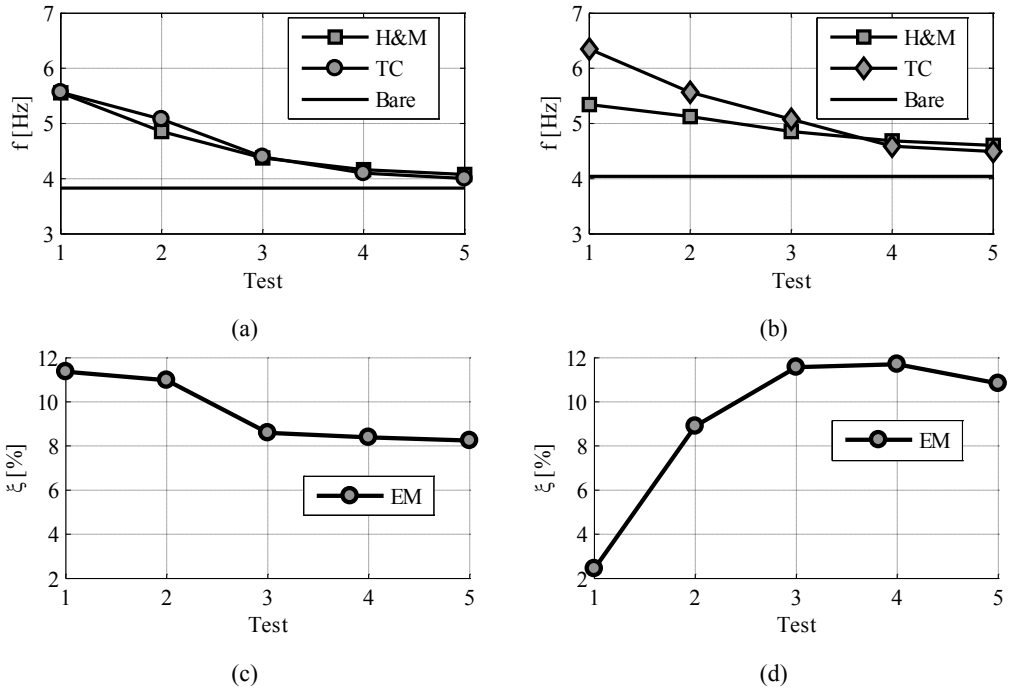


Figure 42. Test frame natural frequency evaluation according to the Transfer Curve method (TC) and to the Hashemi and Mosalam (H&M) procedure (Hashemi and Mosalam, 2006) and compared to the bare frame natural frequency (Bare) for the different seismic tests in (a) X and (b) Y directions; damping ratio evaluation according to the Energetic Method (EM) for the different seismic tests in (c) X and (d) Y directions.

Similarly, from test 1 to test 3, in the Y direction, an increase in the damping ratio is exhibited, essentially due to the wall progressive damaging, while in the X direction the damping is almost constant for the different tests. The damping trends confirm that

the two walls in the X direction start damaging before the one in the Y direction, since they are subjected to larger interstory drifts (Table 10).

In order to evaluate the natural frequency change during each single test the short time Fourier transform method (Gabor, 1946) is implemented. In particular, for every 1 second spaced time step t , a 7 seconds time window centered in t is considered. The transfer curve method is applied for each of the time windows, defining a transfer function for each t . In Figure 43 for each considered time t , the transfer function is plotted in the frequency domain, defining a 3D plot. The change in the peak of the transfer function over the time allows following the reduction of the natural frequency of the setup.

In both X and Y directions the natural frequency reduction is visible, especially for the first tests. For instance, in test no. 2 in Y direction the natural frequency passes from about 6.5 Hz at the beginning of the test to about 5.5 Hz at the end of the test (Figure 43). These diagrams confirm the results reported in Figure 42.

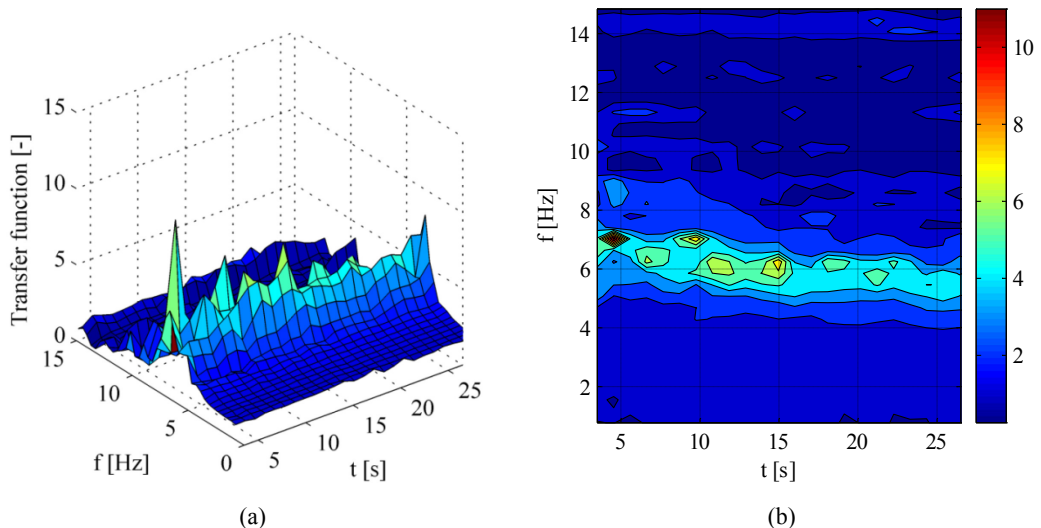


Figure 43. Transfer function for 7 seconds time windows for different time instants corresponding to test n. 2 in Y direction: (a) 3D view; (b) contour view.

2.2.3.5 BASE SHEAR DISTRIBUTION

Through the analysis of the hysteretic curves (Figure 39) the base shear repartition between the partitions and the test frame is evaluated. The force adsorbed by the partitions is simply evaluated as the difference between the maximum inertia force and the force acting on the test frame; the latter force is calculated upon the natural frequency of the test frame and the recorded displacement. The result is also validated using the strain gauge placed at the column base of the test frame.

In Figure 44 the base shear distribution between partitions and test frames in every test, in X (a) and Y (b) directions, is shown. It can be seen that the test frame adsorbs an increasing shear ratio with respect to the partitions, due to the progressive damage in the specimen. After test 4, just a minimum residual contribution of the partitions is exhibited. The shear demand on the partitions passes from a value of approximately 60% (test 1) to the 15% of the total base shear (test 5).

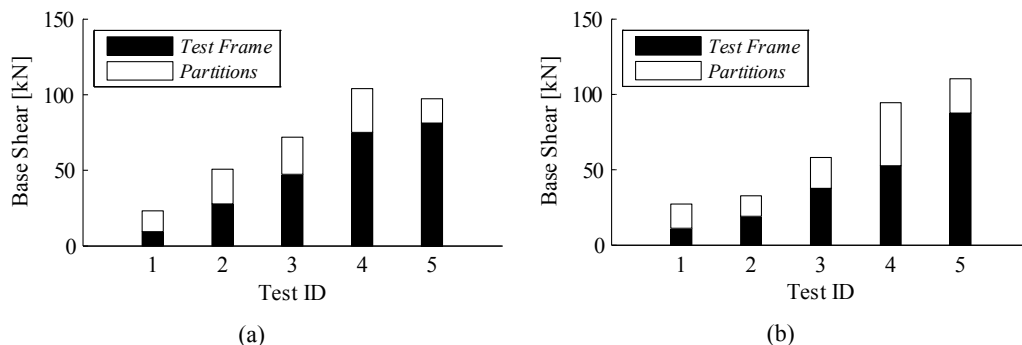


Figure 44. Base shear distribution between test frame and partition systems for the different seismic tests in (a) X and (b) Y directions.

2.2.3.6 EVALUATION OF THE NATURAL FREQUENCY OF THE COMPONENT

In order to evaluate the natural frequency in the out of plane direction, the transfer curve method is applied considering the base acceleration and the partition out of plane acceleration recorded by accelerogram no. 6 (Figure 32). The method is applied for the three random vibration tests in which the partition is subjected to acceleration in the out of plane direction.

The transfer function in Figure 45 yields two peaks: one with lower frequency, denoting the natural frequency in X direction of the test frame; the latter is related to the natural frequency of the nonstructural component in the out of plane direction. It should be noted that the three random vibration tests cause a minor decrease of the natural frequency of the test setup. The frequency of the component also exhibit a minor reduction from a value slightly larger than 30 Hz for test no. 1 to almost 30 Hz for test no. 3.

The results confirm that the frequencies of the partitions are much larger than the typical structural fundamental frequencies. Hence, the ratio between the period of the nonstructural component (T_a) and the period of the building (T_1), considered in Eurocode 8 (CEN, 2004) for the evaluation of the seismic demand on the component, could be accordingly assumed equal to zero.

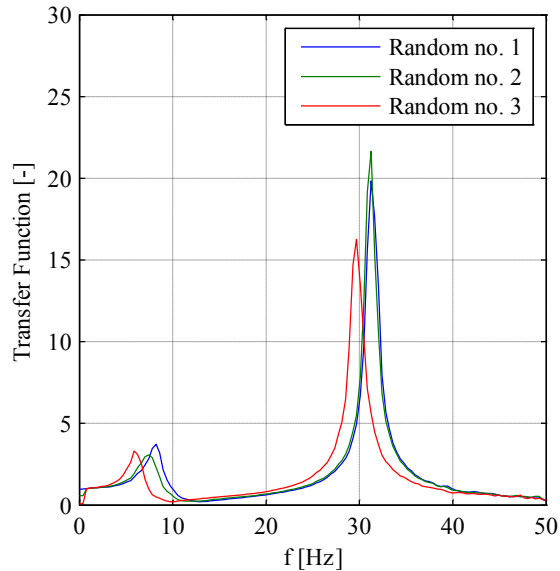


Figure 45. Transfer function from the base to the partition center in the out of plane direction for random vibration tests.

2.2.4 CONCLUSIONS

Shaking table tests are carried out by the earthquake simulator facility available at the Department of Structures for Engineering and Architecture at the University of Naples Federico II in order to investigate the seismic behavior of hollow brick internal partitions. The tested nonstructural component is widespread in the European area.

A steel test frame is adopted in order to simulate the seismic action acting at a generic building story and the specimen boundary conditions. The tests are performed shaking the table simultaneously in both the horizontal directions in order to subject the partition simultaneously to interstory relative displacements in its own plane and accelerations in the out of plane direction. A set of five couples of accelerograms are selected matching the target response spectrum provided by the U.S. code for nonstructural components to investigate a wide range of interstory drift demand and damage. Three damage states are considered in this study in order to characterize the seismic behavior of the specimen. The dimensions of the specimen are adequately chosen in order to (a) test a realistic partition and (b) allow the investigation of the whole damage states range.

The hollow brick partitions are subjected to interstory drift up to 1.0%. It exhibits minor damage for 0.2% interstory drift, moderate damage for 0.34% interstory drift and major damage for 0.97% interstory drift.

Standard methods for the dynamic identification of the test setup are used in order to evaluate the influence of the hollow brick partitions on the steel test frame. The change in the natural frequency and the damping ratio during the different seismic tests clearly evidence the damage recorded in the specimen.

2.2.5 REFERENCES

- Angel R, Abrams DP, Shapiro D, Uzarski J, Webster M (1994) "Behavior of Reinforced Concrete Frames with Masonry Infills," Structural Research Series 589, PhD thesis. Department of Civil Engineering, University of Illinois-Urbana, Urbana, IL.
- Badillo-Almaraz H, Whittaker AS, Reinhorn AM (2007) Seismic fragility of suspended ceiling systems. *Earthquake Spectra* 23 (1):21-40. doi:10.1193/1.2357626
- Boore DM, Bommer JJ (2005) Processing of strong-motion accelerograms: needs, options and consequences. *Soil Dynamics and Earthquake Engineering* 25 (2):93-115. doi:10.1016/j.soildyn.2004.10.007
- CEN (2001) Eurocode 6: design of masonry structures - Part 1.3: general rules for buildings, detailed rules on lateral loading. ENV 1996-1-3. Brussels, Belgium.
- CEN (2004) Eurocode 8: design of structures for earthquake resistance - Part 1: general rules, seismic actions and rules for buildings. EN 1998-1. Brussels, Belgium.
- CEN (2005a) Eurocode 3: design of steel structures - Part 1-1: General rules and rules for buildings. EN 1993-1-1. Brussels, Belgium
- CEN (2005b) Eurocode 3: design of steel structures - Part 1-8: design of joints. EN 1993-1-8. Brussels, Belgium
- Chopra AK (1995) *Dynamics of structures: Theory and Applications to Earthquake Engineering*. Prentice Hall, Englewood Cliffs, New Jersey, USA
- Cohen E, Liang E (1956) Discussion of "Arching theory of masonry Walls," by E. L. McDowell, K. E. McKee, and E. Sevin. *Journal of the Structural Division (ASCE)* 82 (1067):28-40
- D'Ambrisi A, De Stefano M, Tanganelli M (2009) Use of pushover analysis for predicting seismic response of irregular buildings: A case study. *Journal of Earthquake Engineering* 13 (8):1089-1100
- Dawe JL, Seah CK (1989) Out-of-Plane Resistance of Concrete Masonry Infilled Panels. *Canadian Journal of Civil Engineering* 16 (6):854-864
- Dolatshahi KM, Aref AJ (2011) Two-dimensional computational framework of meso-scale rigid and line interface elements for masonry structures. *Engineering Structures* 33 (12):3657-3667. doi:10.1016/j.engstruct.2011.07.030
- Federal Emergency Management Agency (FEMA) (2007) Interim protocols for determining seismic performance characteristics of structural and nonstructural components through laboratory testing. Report No. FEMA 461. Washington DC, US

- Flanagan RD, Bennett RM (1999) Bidirectional behavior of structural clay tile infilled frames. *Journal of Structural Engineering-Asce* 125 (3):236-244. doi:10.1061/(Asce)0733-9445(1999)125:3(236)
- Gabor D (1946) Theory of communications. *Journal of the Institution of Electrical Engineers* 93:429-457
- Garbin E, Galati N, Nanni A (2005) Design Guidelines for the Strengthening of Unreinforced Masonry Structures Using Glass Grid Reinforced Polymers (GGRP) Systems. Technical Report Prepared for Bondo Inc. & TechFab LLC., University of Missouri-Rolla, Rolla, Missouri,
- Gilani A, Reinhorn A, Glasgow B, Lavan O, Miyamoto H (2010) Earthquake Simulator Testing and Seismic Evaluation of Suspended Ceilings. *Journal of Architectural Engineering* 16 (2):63-73. doi:10.1061/(ASCE)1076-0431(2010)16:2(63)
- Hashemi A, Mosalam KM (2006) Shake-table experiment on reinforced concrete structure containing masonry infill wall. *Earthquake Engineering & Structural Dynamics* 35 (14):1827-1852. doi:10.1002/Eqe.612
- International Code Council (ICC) (2000) International Building Code, 2000 Edition (IBC 2000). Falls Church, Virginia, USA.
- International Conference of Building Officials (ICBO) (2000) AC 156 Acceptance Criteria for the Seismic Qualification of Nonstructural Components. ICBO Evaluation Service, Inc., Whittier, California, USA
- Komaraneni S, Durgesh CR, Vaibhav S (2011) Seismic Behavior of Framed Masonry Panels with Prior Damage When Subjected to Out-of-Plane Loading. *Earthquake Spectra* 27. doi:10.1193/1.3651624
- Lee TH, Kato M, Matsumiya T, Suita K, Nakashima M (2007) Seismic performance evaluation of non-structural components: Drywall partitions. *Earthquake Engineering & Structural Dynamics* 36 (3):367-382. doi:10.1002/Eqe.638
- Lourenço PB (1996) Computational strategies for masonry structures. PhD Thesis. Delft University Press, Netherlands
- Magliulo G, Capozzi V, Fabbrocino G, Manfredi G (2011) Neoprene-concrete friction relationships for seismic assessment of existing precast buildings. *Engineering Structures* 33 (2):535-538
- Magliulo G, Capozzi V, Ramasco R (2012a) Seismic performance of R/C frames with overstrength discontinuities in elevation. *Bulletin of Earthquake Engineering* 10 (2):679-694
- Magliulo G, Fabbrocino G, Manfredi G (2008) Seismic assessment of existing precast industrial buildings using static and dynamic nonlinear analyses. *Engineering Structures* 30 (9):2580-2588
- Magliulo G, Maddaloni G, Cosenza E (2012b) Extension of N2 method to plan irregular buildings considering accidental eccentricity. *Soil Dynamics and Earthquake Engineering* 43 (1):69-84. doi:10.1016/j.soildyn.2012.07.032
- Magliulo G, Pentangelo V, Maddaloni G, Capozzi V, Petrone C, Lopez P, Talamonti R, Manfredi G (2012c) Shake table tests for seismic assessment of suspended

- continuous ceilings. *Bulletin of Earthquake Engineering* 10 (6):1819-1832. doi:10.1007/s10518-012-9383-6
- Magliulo G, Petrone C, Capozzi V, Maddaloni G, Lopez P, Manfredi G (2013) Seismic performance evaluation of plasterboard partitions via shake table tests. *Bulletin of Earthquake Engineering*:(under review)
- Magliulo G, Petrone C, Capozzi V, Maddaloni G, Lopez P, Manfredi G (2014) Seismic performance evaluation of plasterboard partitions via shake table tests. *Bulletin of Earthquake Engineering*:(online first). doi:10.1007/s10518-013-9567-8
- Magliulo G, Petrone C, Capozzi V, Maddaloni G, Lopez P, Talamonti R, Manfredi G (2012d) Shake Table Tests on Infill Plasterboard Partitions. *The Open Construction and Building Technology Journal* 6 (Suppl 1-M10):155-163. doi:10.2174/1874836801206010155
- Magliulo G, Ramasco R (2007) Seismic response of three-dimensional r/c multi-storey frame building under uni- and bi-directional input ground motion. *Earthquake Engineering and Structural Dynamics* 36 (12):1641-1657
- McKenna F, Fenves GL (2013) OpenSees Manual <http://opensees.berkeley.edu>. Pacific Earthquake Engineering Research Center, Berkeley, California.,
- Moghaddam H, Goudarzi N (2010) Transverse Resistance of Masonry Infills. *ACI Structural Journal* 107 (4):461-467
- Mosqueda G, Filiatrault A, Retamales R, Davies R, Fuchs J, Tian Y (2010) Experimental Seismic Fragility of Steel Studded Gypsum Partition Walls and Fire Sprinkler Piping Subsystems. In: *Structures Congress 2010 (ASCE)*. pp 2633-2644. doi:doi:10.1061/41130(369)237
- Oliveira DV, Lourenço PB (2004) Implementation and validation of a constitutive model for the cyclic behaviour of interface elements. *Computers & Structures* 82 (17–19):1451-1461. doi:10.1016/j.compstruc.2004.03.041
- Panagiotakos TB, Fardis MN (1996) Seismic response of infilled RC frames structures. Paper presented at the Eleventh World Conference on Earthquake Engineering, Mexico. ,
- Paulay T, Priestley M (1992) *Seismic design of reinforced concrete and masonry buildings*. Wiley, New York, US
- Petrone C, Magliulo G, Manfredi G (2013) Shake table tests for the seismic assessment of hollow brick internal partitions. *Engineering Structures*:(under review)
- Retamales R, Mosqueda G, Filiatrault A, Reinhorn A (2011) Testing Protocol for Experimental Seismic Qualification of Distributed Nonstructural Systems. *Earthquake Spectra* 27 (3):835-856. doi:10.1193/1.3609868
- Taghavi S, Miranda E (2003) Response assessment of nonstructural building elements, PEER report 2003/05. College of Engineering, University of California Berkeley, USA
- Tumialan J, Galati N, Nanni A (2003) Field Assessment of Unreinforced Masonry Walls Strengthened with Fiber Reinforced Polymer Laminates. *Journal of Structural Engineering* 129 (8):1047-1056. doi:10.1061/(ASCE)0733-9445(2003)129:8(1047)

2.3 SHAKE TABLE TEST ON HOSPITAL BUILDING CONTENTS

Health care facilities may undergo severe and widespread damage that impairs the functionality of the system when it is stricken by an earthquake. Such detrimental response is emphasized either for the hospital buildings designed primarily for gravity loads or without employing base isolation/supplemental damping systems. Moreover these buildings need to warrant operability especially in the aftermath of moderate-to-severe earthquake ground motions.

The provisions implemented in the new seismic codes allow obtaining adequate seismic performance for the hospital structural components; nevertheless, they do not provide definite yet reliable rules to design and protect the building contents. To date, very few experimental tests have been carried out on hospital buildings equipped with nonstructural components as well as building contents.

The present study is aimed at establishing the limit states for a typical health care room and deriving empirical fragility curves by considering a systemic approach. Towards this aim, a full scale three-dimensional model of an examination (out patients consultation) room is constructed and tested dynamically by using the shaking table facility of the University of Naples, Italy. The sample room contains a number of typical medical components, which are either directly connected to the panel boards of the perimeter walls or behave as simple free-standing elements. The outcomes of the comprehensive shaking table tests carried out on the examination room have been utilized to derive fragility curves based on a systemic approach.

2.3.1 INTRODUCTION

The modern earthquake engineering has focused on the performance-based design of newly-built structures and the assessment of existing buildings and bridges (e.g. (Bozorgnia and Bertero, 2004)). Limit states (LSs), have thus been defined, either qualitatively or quantitatively, and evaluated through post-earthquake surveys, experimental tests and numerical simulations. In a broader socio-economic context, LSs may be related to repair costs (e.g., expressed as a percentage of replacement value) that are in excess of a desired amount, opportunity losses, morbidity and mortality. It applies to performance levels of structural, non-structural and contents (Miranda and Aslani, 2003; Taghavi and Miranda, 2003). The harmonization of the performance levels between structural and nonstructural systems is vital. The evaluation of the limit states and, in turn, the performance objectives of new and existing buildings depends on their use and occupancy. The seismic performance levels of critical facilities, such as hospital buildings and emergency units, are significantly

dependent on the functionality of the system. Thus, resilient health care facilities should prevent the disruption of their functionality during post-disaster emergency (e.g. (World Health Organization (WHO), 2007), among many others). It is estimated that 97% of earthquake related injuries occur within the first 30 minutes following the main shock (Gunn, 1995), thus it is of paramount importance that hospitals remain operational and continue providing fundamental health services following the disasters. A typical emergency response of hospitals in the aftermath of an extreme event, such as earthquakes, is pictorially displayed in Figure 46. The pre-accident capability is also shown in the figure as a benchmark for the needs of treatment demand caused by the occurrence of the seismic event.

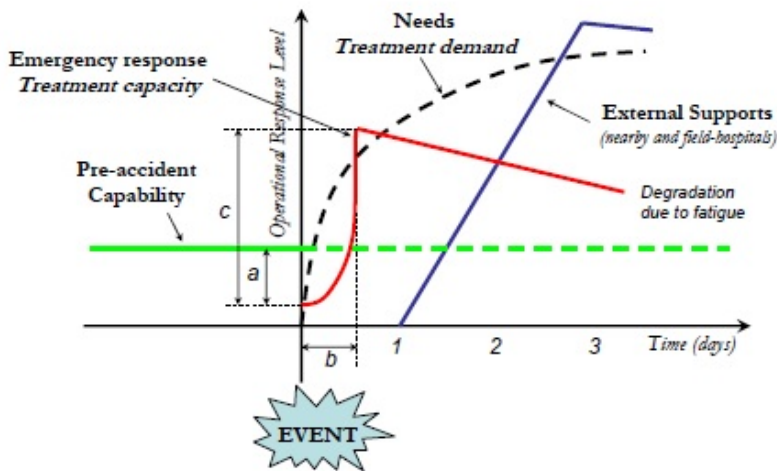


Figure 46. Typical emergency response of hospitals in the aftermath of an extreme event, such as an earthquake (Pinto et al., 2011).

Moreover, the occurrence of nonstructural damage, encompassing primarily failure of windows, doors, partition walls, suspended ceilings, lighting and floor coverings, should be inhibited as it may detrimentally affect the emergency response and, in turn, it may cause the medical evacuations (Federal Emergency Management Agency (FEMA), 2007a). Additionally, the architectural, mechanical and electrical components account for nearly 45% of the capital cost; thus their failure may cause massive losses for the social communities. Notwithstanding, surveys carried out in the aftermath of recent major earthquakes world-wide (Achour et al., 2011; Di Sarno et al., 2013; McIntosh et al., 2012), e.g. the 2008 Sichuan (China), the 2009 L’Aquila (Italy), the 2010-2011 Darfield-Christchurch (New Zealand), the 2011 Van (Turkey) and the 2012 Emilia-Romagna (Italy) earthquakes, have emphasized the inadequate performance of existing hospitals. Widespread nonstructural damage was detected primarily in

buildings that were not compliant with modern seismic codes. Nevertheless, the failure of services and building contents was surveyed both in newly built hospital and in structures designed only for gravity loads. Figure 47 displays the extensive damage to the building contents observed in the aftermath of the 2011 Van (Turkey) earthquake in the Yüzüncü Yil University – Faculty of Medicine Hospital. The losses of internal and external services as well as the damage to back-up systems were extensive, thus the nearly 500-beds hospital had to be completely closed and emergency response facilities relocated.



Figure 47. Damage to the building contents surveyed in the aftermath of the 2011 Van (Turkey) earthquake in the Yüzüncü Yil University – Faculty of Medicine Hospital.

In the last three decades thorough governmental actions, aiming at ensuring the life safety and collapse prevention of acute healthcare facilities, have been promoted. For example, in California, in addition to safety standards, over time, it is enforced that, by 2030, hospitals should also meet performance levels meant to ensure that they are capable of providing services to public after an earthquake or any other disaster. Numerous initiatives have also been promoted world-wide by the World Health Organization (WHO) and the United Nation International Strategy for Disaster Reduction (UNISDR), e.g. the global campaign “*Hospital Safe From Disasters*” (World Health Organization (WHO), 2008). However, designing for resilient hospitals still remains a challenging task; it needs an interdisciplinary approach encompassing the physical, namely structure, non-structural components and building contents, and non-physical components, i.e. procedures and organization, of a hospital system (Bruneau et al., 2003). Adequate performance criteria and robust but simple assessment methods should be implemented in seismic codes of practice and guidelines. There is a lack of comprehensive theoretical and experimental results dealing with the performance evaluation of the building contents for health care facilities. The earthquake response of such contents is not straightforward because of the complexity and variety, connections and functioning. Numerical simulation tools, albeit powerful,

are still not capable to predict reliably the seismic response of hospital building contents.

The above discussion demonstrates that there is still an urgent need to further investigate the earthquake performance of medical equipment and typical hospital components. The present paper illustrates the preliminary results of comprehensive shake table experimental tests carried out on a full-scale examination (out patients consultation) room unit equipped with typical architectural finishing, freestanding furniture items, desktop computer and medical equipment. The study aims at the seismic qualification of hospital building contents, such as free-standing cabinets, through the experimental method. Vulnerable freestanding components and medical appliances were identified on the basis of survey questionnaires and simplified evaluation forms compiled by hospital staff for numerous healthcare facilities worldwide (Achour et al., 2011; McIntosh et al., 2012; Aiello et al., 2012). Examination rooms are departments that are critical to their functioning in healthcare facilities (Myrtle et al., 2005; Office of Statewide Health Planning and Development (OSHPD), 2007). Thus, such rooms were selected as representative layouts for the experimental seismic performance assessment of the core units of hospital buildings. Different configurations were analyzed and relevant limit states identified for each component and the whole room unit. Acceleration time histories with increasing amplitudes were used to derive seismic fragility curves for the whole medical room, according to a systemic approach.

2.3.1.1 STATE OF THE ART RESEARCH

Recently, few studies have been initiated to analyze the seismic performance of a variety of furniture items, medical appliances and service utilities of typical hospital buildings and pharmacies. Full scale shake table tests were carried out on a base-isolated four story RC hospital structure (Sato et al., 2011; Furukawa et al., 2013). Recorded near-fault strong motions and artificial long-period, long duration records were used for the experimental tests. Significant reductions of the floor accelerations were observed for the base-isolated structure subjected to near-fault ground motions. Operational and functionality limit states of the healthcare buildings were significantly augmented if compared with the fixed-base case. The use of base-isolation was not sufficient to ensure the hospital service in case the long-period motions were employed. Under such loading conditions, significant motions of furniture items and medical appliances supported by casters were detected. Large sliding displacements and occasional collisions of furniture items and medical appliances with other furniture components or against the supports were observed at resonance. To ensure the functionality of the medical facility it was recommended to securely lock the casters of

furniture and medical appliances. Kuo et al. (2011) performed shake table tests on typical medicine shelves and contents placed in pharmacies, which are one of the critical departments for delivering post-earthquake emergency care. Using sinusoidal waveforms, it was found that the objects fell from the lower shelves of the stock and tablet medicine shelf units. Conversely, more objects fell from the upper shelves of the powder medicine shelf unit. Initiation of overturned shelves and fallen objects scattered on floors was caused by the peak acceleration of the input excitation. After the initiation, the response is influenced simultaneously by acceleration and velocity.

Experimental tests on composite hospital rooms have also been carried out at the Structural Engineering and Earthquake Simulation Laboratory (SEESL) at the University of Buffalo (UB) in the USA, using the Nonstructural Component Simulator (UB-NCS), which is a modular and versatile two-level structure for experimental seismic performance evaluation of full-scale acceleration and displacement sensitive nonstructural components under realistic floor motions expected within multi-story buildings (Mosqueda et al., 2009). The bi-directional shake table tests aimed at evaluating the earthquake effects on typical medical equipment and other nonstructural components in hospitals. The research focused primarily on steel-stud gypsum partition wall, lay-in suspended ceiling system, fire protection sprinkler piping systems. Similarly, the tests on the 5-story building, at the outdoor UCSD-NEES shake table facility in San Diego, California, deals with a broad array of nonstructural components, such as functioning passenger elevator, stairs, exterior walls, interior partition walls, piping, Heating, Ventilation and Air Conditioning (HVAC), ceiling, sprinklers, building contents, as well as passive and active fire systems (Chen et al., 2012). A number of experimental tests on the shake table dealing with medical laboratory components, such as low-temperature refrigerators, heavy incubators, freezers, microscopes and lighter computer equipment located on desks and shelves, were also carried out at the University of California, Berkeley (e.g. (Comerio, 2005; Konstantinidis and Makris, 2009)). Emphasis was on the derivation of fragility curves for earthquake loss estimation and formulation of retrofitting measures.

In Porter et al. (1993) the identification of the critical equipment component in critical facilities is discussed. The performance of different equipment during past earthquakes is also described, while in other studies (Johnson et al., 1999; Achour, 2007) methodologies for the evaluation of the seismic vulnerability of critical facilities are proposed. The results of the investigations are insightful although they do not encompass the specific components/equipment assessed herein and they are mainly based on past earthquake data.

In the last years, following the quoted experimental and numerical studies on nonstructural components, technical committees are developing standard provisions for nonstructural components.

The state of California is a reference on the topic (Tokas, 2007; California Building Standards Commission (CSBC), 2007). The Hospital Seismic Safety Act (HSSA), enacted following the 1971 San Fernando Earthquake, identified deficiencies in building codes and established new seismic safety standards, although it addressed merely new constructions. The 1994 Northridge (California) earthquake caused significant damage to pre-HSSA buildings and nonstructural damage to pre- and post-HSSA buildings. The latter earthquake initiated the SB1953 (Office of Statewide Health Planning and Development (OSHPD), 2007), the hospital seismic retrofit program, i.e. an amendment to the HSSA. The steps of the aforementioned program are: the evaluation of the hospital seismic retrofit issue, a database implementation of the hospital building stock, the retrofit to prevent collapse and loss of life and the retrofit to provide continued operation after an earthquake. The regulations developed as a result of SB1953 become effective upon approval by the California Building Standard Commission. According to the 2007 California Building Code (CBC), the requirements for nonstructural components in or attached to occupancy IV category structures are: seismic qualification of mechanical and electrical equipment (designed per chapter 13 of ASCE 7 (American Society of Civil Engineers, 2010) with importance factor $I_p > 1.0$); manufacturer's seismic certifications for architectural, mechanical and electrical components, supports and attachments. The seismic qualification can be attained by: test on a shake table (Magliulo et al., 2014; Petrone et al., 2013), analytical method using dynamic characteristics and forces, experience data (i.e. historical data demonstrating acceptable seismic performance), detailed analyses providing equivalent safety. The whole procedure concerning the design and the application of nonstructural components provides firstly that the engineer states the applicable requirements for the designated seismic system on construction documents, secondly the manufacturer provides the certificate of compliance, thirdly a California Structural Engineer reviews and accepts the certification and finally there is the approval of Building Official.

2.3.2 TEST SETUP, SPECIMEN, INSTRUMENTATION AND INPUT DEFINITION

2.3.2.1 TEST SETUP AND SPECIMENS

The seismic tests on hospital building contents are carried out by the earthquake simulator system available at the laboratory of Structures for Engineering and Architecture Department of University of Naples Federico II, Italy. The system

consists of two 3 m x 3 m square shake tables. Each table is characterized by two degrees of freedom along the two horizontal directions. The maximum payload of each shake table is 200 kN with a frequency ranging between 0 and 50 Hz, acceleration peak equal to 1 g, velocity peak equal 1 m/sec and total displacement equal to 500 mm (± 250 mm). A single shake table is utilized for the present experimental campaign.

A steel single-story framed system was designed (Figure 48) with the purpose of simulating the seismic effects on the medical contents of a typical hospital room. To simulate the effects of the earthquake at different floors on a hospital building, the geometry of the test frame was designed to prevent the onset of the resonance. As a result, the steel frame possesses a large lateral stiffness. The layout of the model consists of a 2.42 m x 2.71 m x 2.72 m test fixture of S275 steel material with concentric V-bracings (see Figure 48). The sample frame employs H-shaped columns (HE220A profile) and beams (HE180A profile); the connections are bolted. A horizontal double warping frame made of U-section steel profiles (UPN100) is bolted to the beams of the test frame (HE180A). Concentric V-bracing systems are also used to provide high lateral stiffness; bracing systems are made of steel U-section (UPN160). Further details on the steel test setup are included in (Magliulo et al., 2012a).

A finite element model (FEM) of the sample steel braced frame is implemented in the computer program SAP2000 (CSI Computer & Structures Inc., 2004). Elastic “beam” elements are used to simulate the response of the beams and the columns of the braced frames. The FEM model is employed to estimate the periods of vibration associated to the translational modes along the orthogonal directions; such period is about 0.02 s. The frame can thus be classified as rigid lateral resisting system. The total weight of the sample structure is 19.2 kN.

A typical hospital examination (out patients consultation) room background is reproduced within the sample steel frame. Plasterboard partitions and ceilings are mounted; linoleum sheets are also installed to cover both the floor and a large portion of the internal partitions. An overhead light and a ray film viewer are also installed in the room.

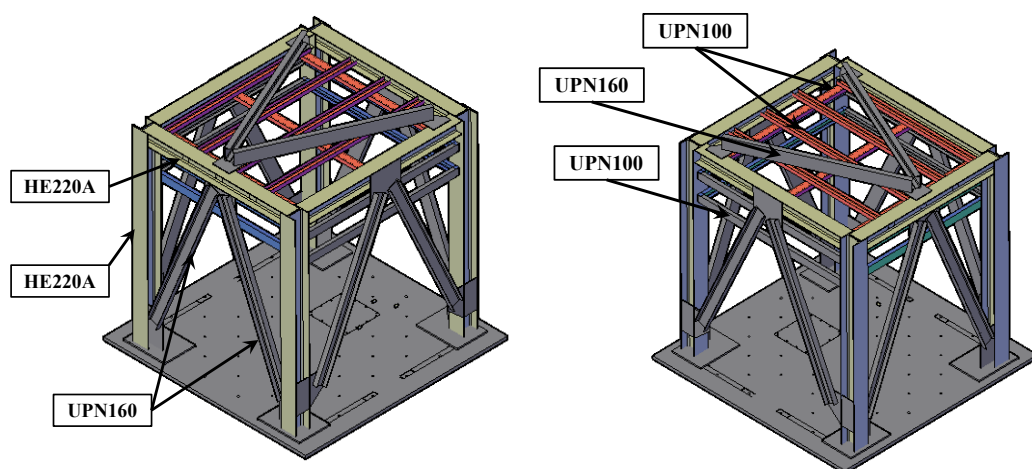


Figure 48. Global perspective of the test setup.

The building contents used for the examination room include: (a) a hospital medicine cabinet (Figure 49a), made of cold formed steel profiles, with dimension 75x38x165 cm, having double moving glass doors with locker and four mobile glass shelves; (b) a hospital medicine cabinet (Figure 49b) made of cold formed sheet with dimension 53x36x139 cm, having single moving glass door with locker and four mobile glass shelves; (c) a desktop computer (monitor, case, keyboard and mouse); (d) a desk made of a steel pipes frame and a wooden desktop and having two drawers with locker (Figure 49c). The mass of the two cabinets is 20 kg and 15 kg for the single-window and the double-windows cabinets, respectively; the mass of the desk is 31.6 kg. Cabinet contents with different slenderness as glass bottles, flasks and test tubes, are placed in the cabinets to simulate the actual conditions of a typical hospital room. Different mass distributions are also selected to distribute such contents in the single- and double-window cabinets (see Section 2.3.2.3).

High quality digital accelerometers are used to monitor the response of the hospital building contents. Four accelerometers are placed at the base, i.e. at the lowest shelf level, and at the top of the front side of each cabinet; one accelerometer is positioned at the top of the desk and at the top of the monitor; one accelerometer records the acceleration at the shake table level. The sampling frequency of the accelerometers is equal to 400 Hz.

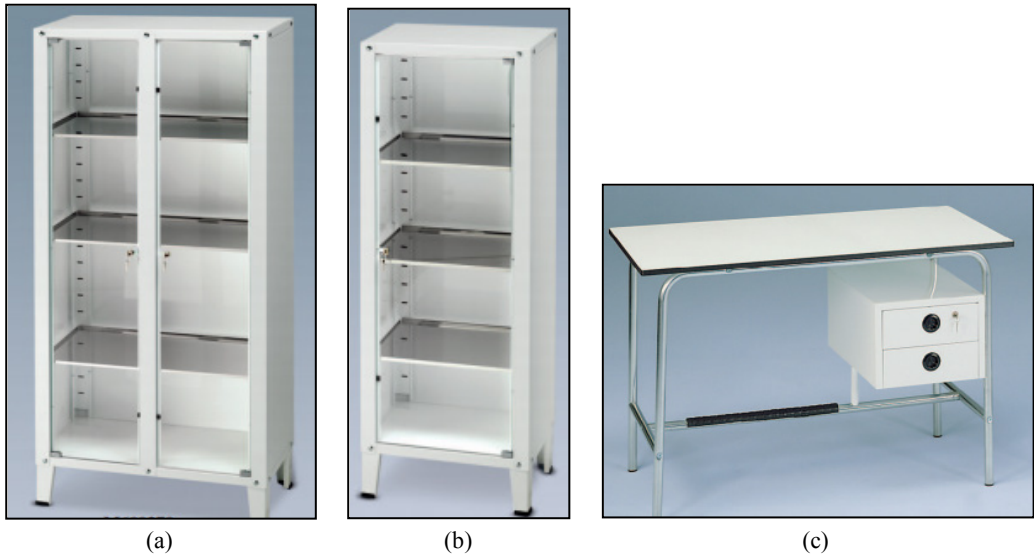


Figure 49. Tested hospital building contents: (a) double-windows cabinet, (b) single-window cabinet and (c) desk.

2.3.2.2 INPUT AND TESTING PROTOCOL

To investigate the seismic behavior of the hospital room, a suite of accelerograms, used as input for the unidirectional horizontal shakings (Figure 50), are adequately selected to match a target response spectrum, provided by the ICBO-AC156 code “Acceptance criteria for seismic qualification testing of nonstructural components” (International Conference of Building Officials (ICBO), 2000).

The first step consists in the definition of the target spectrum or required response spectrum (RRS). According to AC 156, the RRS is obtained as a function of the design spectral response acceleration at short periods, S_{DS} , depending on the site soil condition and the mapped maximum earthquake spectral acceleration at short periods (for more details see section 6.5 in ICBO-AC156). The procedure is performed for a Required Response Spectrum corresponding to S_{DS} equal to 1.50 g. As recommended by the AC156 code procedure, a baseline signal is defined starting from non-stationary broadband random excitations having an energy content ranging from 1.3 to 33.3 Hz and one-sixth-octave bandwidth resolution. The total length of the input motion is 30 seconds. Then, the signal is enhanced by introducing wavelets using the spectrum-matching procedure of the RSP Match program (Hancock et al., 2006). The acceleration response spectrum is shown in Figure 50b). The matching is approximately obtained over the frequency range from 1.3 to 33.3 Hz. To obtain a drive motion compatible with the shake table velocity and displacement limits, the so obtained matched record is high passed filtered for frequencies larger than 1.0 Hz.

Figure 50 shows the obtained time history acceleration, its elastic response spectra, the RRS corresponding to S_{DS} equal to 1.50g and the RRS scaled to 130%.

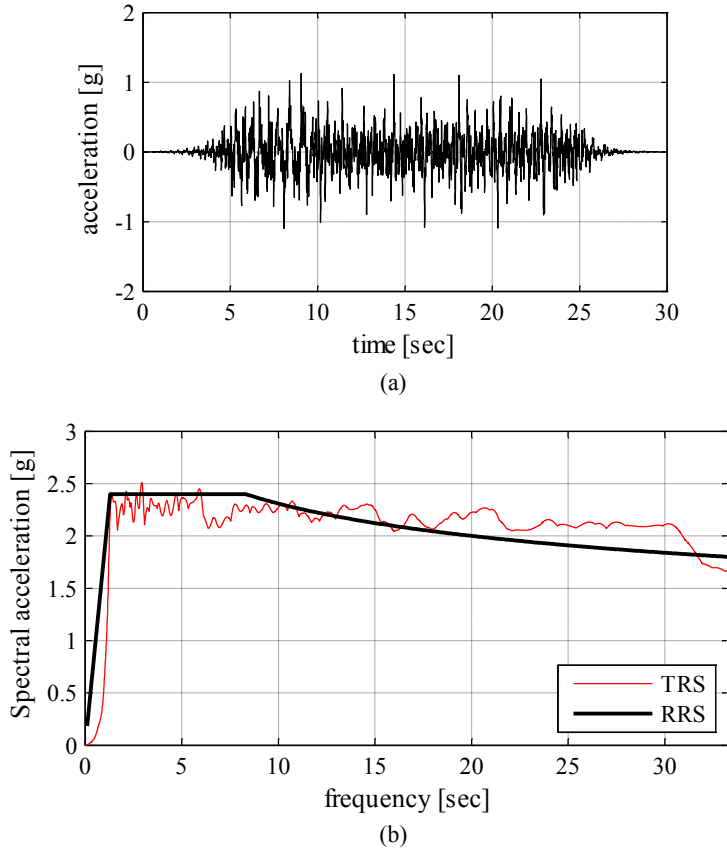


Figure 50. Earthquake time history and spectra for a level of shaking corresponding to S_{DS} equal to 1.50g: (a) acceleration time-history; (b) input accelerogram spectrum (TRS) and RRS (bold line).

The procedure is performed as mentioned for a RRS corresponding to $S_{DS}=1.50$ g; the so obtained record is then scaled to match different intensity levels. S_{DS} ranges between 0.15 g and 1.80 g in the different tests of the test campaign described in Section 2.3.2.3. Additional information on testing input and testing protocol is present in (Magliulo et al., 2012a; Magliulo et al., 2012b).

Preliminarily, system identification tests were also carried out using two single-axis loading protocols: low-amplitude sine-sweep and white noise with low-acceleration, i.e. with root-mean-square intensity limited to 0.05 ± 0.01 g, in compliance with the provisions included in Federal Emergency Management Agency (FEMA) (2007b).

2.3.2.3 TEST PROGRAM

The definition of a typical condition for the sample cabinets is a crucial issue of the research study. Different variables, related to the arrangement of the contents on the different shelves and to the position of the cabinets with respect to the wall behind, are considered. A few variables are investigated in the six test groups of the undertaken test campaign (Table 13).

Test group 100 assesses the behavior of the cabinet with an equivalent mass, i.e. sand inserted in boxes, at each shelf of the cabinets. 6 kg mass and 4 kg mass is added for each shelf of the double-window cabinet (Figure 51a) and single-window cabinet, respectively; the mass amount is representative of the mass of typical contents inserted in such a cabinet. The use of the equivalent mass is required in order to investigate the behavior of the cabinets with different contents on their shelves; the contents are simulated through the use of sand boxes in order to avoid damaging and replacing the contents after each shaking.

Test group 200 investigates the behavior of the cabinets with a decreasing mass distribution along the height. From the base to the top, on the four shelves of the double-window cabinet, 6 kg, 4 kg, 4 kg and 2 kg masses are placed (Figure 51b). Instead, on the four shelves of the single-window cabinet 4 kg, 2 kg, 2 kg and 0 kg masses are placed. The aim is to investigate the behavior of cabinets in which, as typically suggested, the heaviest contents are placed at the lowest shelves.

Typical glass contents are tested in test group 300, as shown in Figure 51c. The contents are equally placed on the different shelves of each cabinet. Glass bottles with different dimensions, i.e. 100 ml, 250 ml and 500 ml, are placed in the double-window cabinet whereas 250 ml and 100 ml flasks, test tubes and glass beaker are placed in the one-window cabinet. They are filled with colored sand, that simulates the presence of water. In this test group the behavior of real contents is also investigated



Figure 51. Double-window cabinet in (a) test groups 100 and 400, (b) test groups 200 and 500 and in (c) test groups 300 and 600.

In Figure 52a the plan configuration of the different components in test groups 100, 200 and 300 is shown. A different plan configuration is defined in test groups 400, 500 and 600 (Figure 52b). The different components are arranged in such a way that the different components are shaken along the orthogonal direction, given the unidirectional input motion. In test groups 400, 500 and 600 the same content mass configurations of test groups 100, 200 and 300, respectively, are chosen.

This work will focus primarily on the results carried out by applying the unidirectional loading component. Nevertheless, further investigation is ongoing and bidirectional input motion has been considered. This issue does not seem to be of significant detriment to the results presented herein.

Two test groups, i.e. 110 and 120, investigate the influence of the distance between the cabinets and the wall behind on the seismic response of the cabinets. The other parameters, e.g. contents mass, are the same as the ones adopted in test group 100. A 10 cm and a 15 cm cabinet-to-wall gap is defined in test groups 110 and 120, while in test group 100 the gap is 2 cm.

2.3 Shake table test on hospital building contents

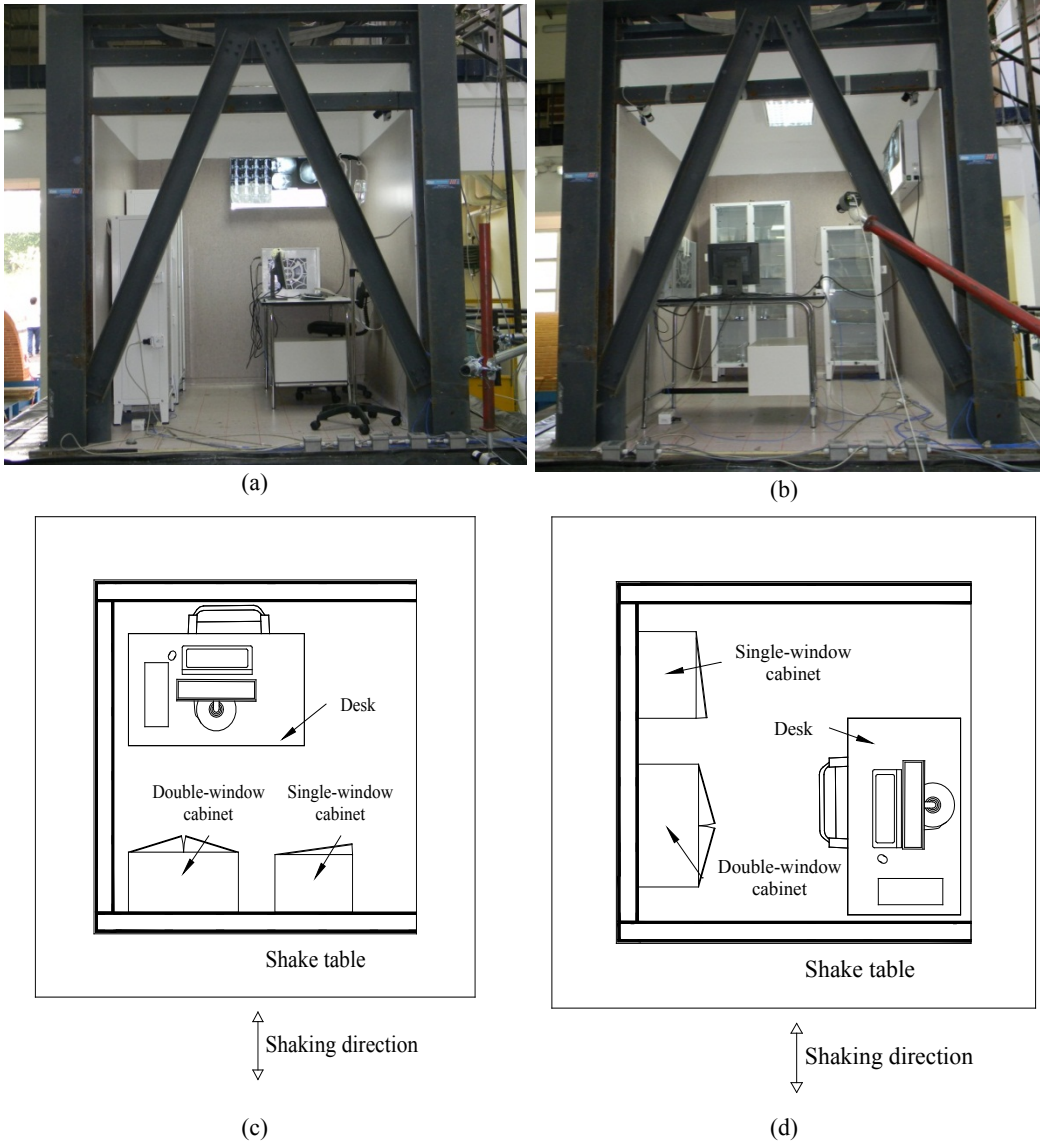


Figure 52. Photo and plan view of the test setup: (a) and (c) configuration 1, adopted in test groups 100, 200 and 300 and (b) and (d) configuration 2, adopted in test groups 400, 500 and 600.

For the whole test campaign it is chosen to lock the cabinet windows and do not to restrain the cabinet to the wall behind, which is representative of the typical conditions in European hospitals. Each test group provides a set of shakings with increasing intensity, according to Section 2.3.2.2. A total number of 63 shakings are performed during the whole test campaign. After each shaking the different components are relocated in their original condition.

Test group	Plan configuration	Cabinets contents	Cabinet-to-wall distance [cm]
100	1	Equivalent mass uniformly distributed along the height	2
110	1	Equivalent mass uniformly distributed along the height	10
120	1	Equivalent mass uniformly distributed along the height	15
200	1	Equivalent mass non uniformly distributed along the height	2
300	1	Typical glass contents uniformly distributed along the height	2
400	2	Equivalent mass uniformly distributed along the height	2
500	2	Equivalent mass non uniformly distributed along the height	2
600	2	Typical glass contents uniformly distributed along the height	2

Table 13. Test program definition.

2.3.3 RESULTS AND DISCUSSION

2.3.3.1 DYNAMIC IDENTIFICATION

Random vibration excitations are performed in order to dynamically identify the different tested components. In particular, before the execution of each of the test group campaigns, different random excitations at different intensity levels are executed (Table 14). Test 1001-1004 are performed before test group 100, test 2001-2002 before test group 200, and so forth.

	Test ID	Typology	Amplitude [g]	Root mean square [g]
1000	1001	Random	0.06	0.02
	1002	Random	0.11	0.03
	1003	Random	0.22	0.05
	1004	Random	0.27	0.06
2000	2001	Random	0.10	0.03
	2002	Random	0.20	0.05
3000	3000	Random	0.07	0.03
	3001	Random	0.11	0.02
	3002	Random	0.26	0.06
4000	4001	Random	0.10	0.03
	4002	Random	0.21	0.05
5000	5001	Random	0.10	0.03
	5002	Random	0.21	0.05
6000	6001	Random	0.11	0.03
	6002	Random	0.19	0.05

Table 14. Random vibration tests ID, amplitude and root mean square.

These low amplitude shakings allow evaluating the influence of the different parameters on the dynamic properties of the nonstructural components in terms of natural frequency. The root mean square of the performed tests are compliant with the value suggested by FEMA 461 (Federal Emergency Management Agency (FEMA), 2007b), i.e. $0.05g \pm 0.01g$.

Sine-sweep tests are also carried out; the outcome of such tests, which match the results of random vibration tests, are omitted in this study for the sake of brevity.

The transfer curve method (e.g. (Bracci et al., 1992)) is adopted to evaluate the natural frequency of the different components. Block averaging and Hanning windowing techniques (e.g. (Proakis and Monalakis, 2007), among many others) are also adopted. The length of each block, i.e. N_{FFT} , defines the resolution of the transfer curve. Moreover, a 50% block overlap is also selected. The length of each block is adequately selected in order to define a fairly regular transfer curve. The method is applied for the sample two cabinets and for the desk.

Typical transfer curves are plotted in Figure 53. The N_{FFT} is selected equal to 1024 and to 4096 for the transfer curves of the cabinets and the desk, respectively. Considering that the sampling frequency of the accelerometers is equal to 400 Hz, the frequency resolution of the transfer curve is 0.391 Hz for the cabinets and 0.098 Hz for the desk.

An average transfer curve is evaluated for each test group from the gray curves corresponding to each single test. The peak in the mean transfer curve denotes the natural frequency associated to one of the vibrational modes.

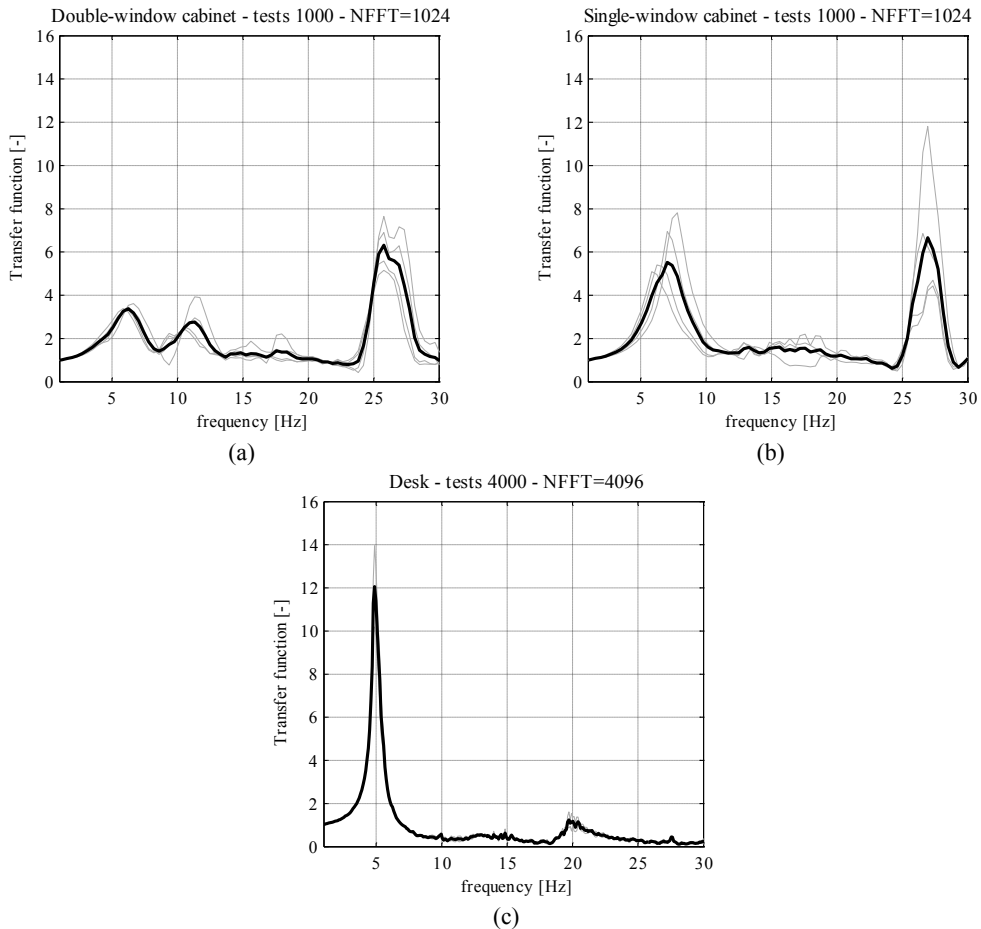


Figure 53. Transfer curves for (a) double-window cabinet – tests 1000, (b) single-window cabinet – tests 1000, (c) desk – tests 4000

The transfer curves in Figure 53 emphasizes the presence of multiple modes of vibration. In the case of the cabinets, the high frequency peaks seem to be related to modes that involve only a limited portion of the component, e.g. window natural mode, as discussed in Section 2.3.3.2.

The fundamental frequencies for the different random tests are summarized in Table 15. The results related to the first three test groups should be investigated separately from the results related to the last three test groups, due to the different input motion direction.

Test group ID	Double-window	Single-window	Desk
1000	6.25 Hz	7.03 Hz	20.31 Hz
2000	5.08 Hz	6.64 Hz	20.31 Hz
3000	6.25 Hz	7.03 Hz	20.70 Hz
4000	4.68 Hz	7.03 Hz	5.08 Hz
5000	5.08 Hz	8.20 Hz	5.08 Hz
6000	4.30 Hz	7.81 Hz	5.08 Hz

Table 15. Natural frequency of the tested components for the different random test groups.

The short time Fourier transform method (Gabor, 1946) is also implemented in order to evaluate the natural frequency variation during each single test. In particular, for every 1 second spaced time step t , a 7 seconds time window centered in t is considered. The transfer curve method is applied for each of the time window, defining a transfer function for each time step t . In Figure 54 for each considered time step t , the transfer functions of the tests on 2 widows cabinet are plotted in the time domain, defining a 3D plot, i.e. a spectrogram. The peaks in the transfer function identifies the natural frequency of the examined component. The change of the natural frequency can be thus easily detected through this methodology.

Both the 3D and the contour plots of the spectrogram recorded during test no. 1001 on the 2-window cabinet are shown in Figure 54. The spectrograms recorded on the 1-window cabinet and the desk during test no. 4001 and 4002 are depicted in Figure 55.

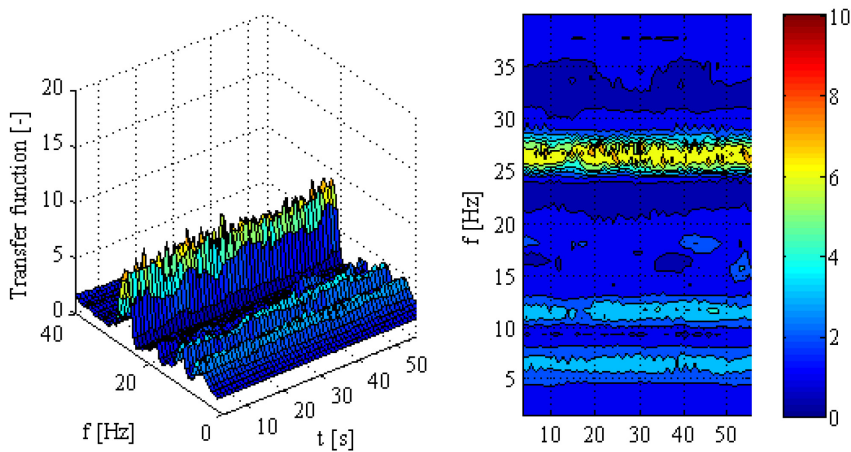


Figure 54. 3D and contour plots of the spectrograms recorded on the double-window cabinet during test no. 1001.

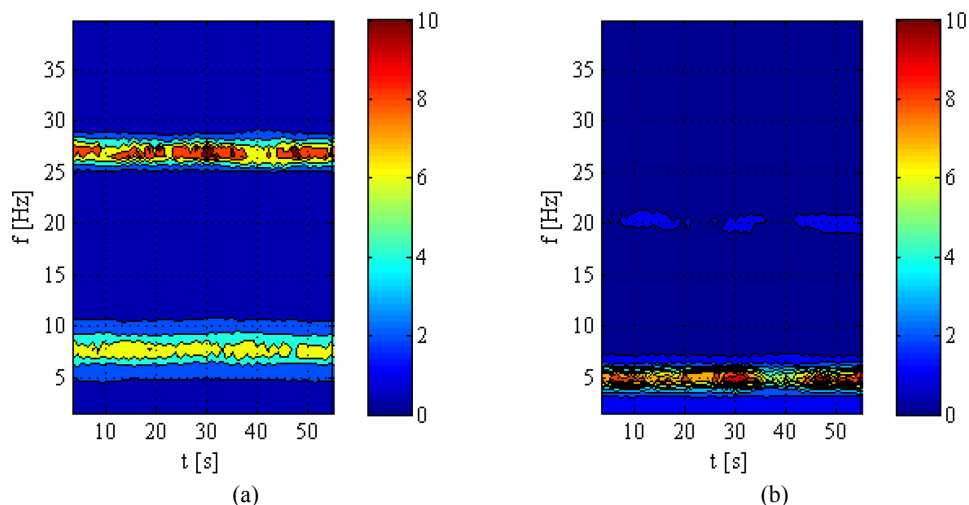


Figure 55. Contour plots of the spectrogram (a) on the single-window cabinet during test no. 1001 (b) on the desk during test no. 4001.

The components are characterized by different natural frequencies along the two horizontal directions. Three natural modes are detected in the double-window cabinet, in case it is shaken along its transversal direction, whereas the single-window cabinet exhibits two natural modes. The results related to the desk, which is not influenced by the different mass arrangement in the cabinets, evidence a single natural frequency; the natural frequency is slightly larger than 20 Hz in the transversal direction and about 5 Hz in the longitudinal direction. The peak recorded in the desk is narrower than the peaks recorded in the cabinets, thus denoting a less damped natural mode.

In case the cabinets are excited along the longitudinal direction, it is demonstrated that the reduction of the mass has an higher influence than the vertical arrangement of the mass. However, especially for the double-window cabinet, the natural frequency is not significantly affected by the mass amount and arrangement. It should be noted that the results and comparison among successive test groups may be affected by the progressive damage of the components during the shakings (Cosenza et al., 2014); the components are replaced only before test group 4000.

The spectrogram diagrams show that negligible variations of the natural frequencies are recorded during the random vibration tests.

These experimental results will be used as benchmarks for the calibration of the numerical models of the components, reported in Section 2.3.3.2.

The damping ratio associated to the first mode of the two cabinets and the desk is experimentally evaluated based on the dynamic identification tests. The half-power bandwidth (Bracci et al., 1992) method is applied on the transfer curves evaluated in Figure 53. In particular, this method estimates the damping ratio from the frequencies

f_a and f_b at which the maximum transfer function amplitude, that occurs at the natural frequency f_n , is reduced by the square root of 2. The evaluation of the damping ratio is conducted according to the following formula:

$$\xi = \frac{f_b - f_a}{2 \cdot f_n}$$

The transfer curves are enveloped by a spline curve, in order to increase the frequency resolution of the curve and, therefore, to have an accurate estimation of the f_a and f_b frequencies.

Figure 56 shows the mean transfer curves reported in Figure 53 (in blue) and their spline envelope of (in green); f_a and f_b frequencies are also included along with the estimated damping ratio. The estimation is reported for a single test group for the double-window cabinet, single-window cabinet and the desk.

The damping ratio values for the three considered components are indicated for the different test groups in Table 16. It can be noted that the damping ratio of the desk, which varies between 5.0% and 7.7%, is significantly smaller than the damping ratio of the two tested cabinets, which ranges between 13.4% and 26.9%. The maximum transfer function values, that occur at the natural frequency f_n , also confirm the above outcome. The direction of the seismic input on the components does not significantly influence the damping ratio values.

The estimation of the damping ratio with the half-power bandwidth method is remarkably affected by the resolution of the transfer curve, that is in turn related to the N_{FFT} value.

Test group ID	2 windows	1 window	Desk
1000	18.2%	17.3%	7.7%
2000	19.4%	18.0%	5.4%
3000	22.6%	13.4%	5.0%
4000	26.9%	25.0%	5.2%
5000	18.2%	17.3%	7.7%
6000	19.4%	18.0%	5.4%

Table 16. Damping of the tested components for the different random test groups.

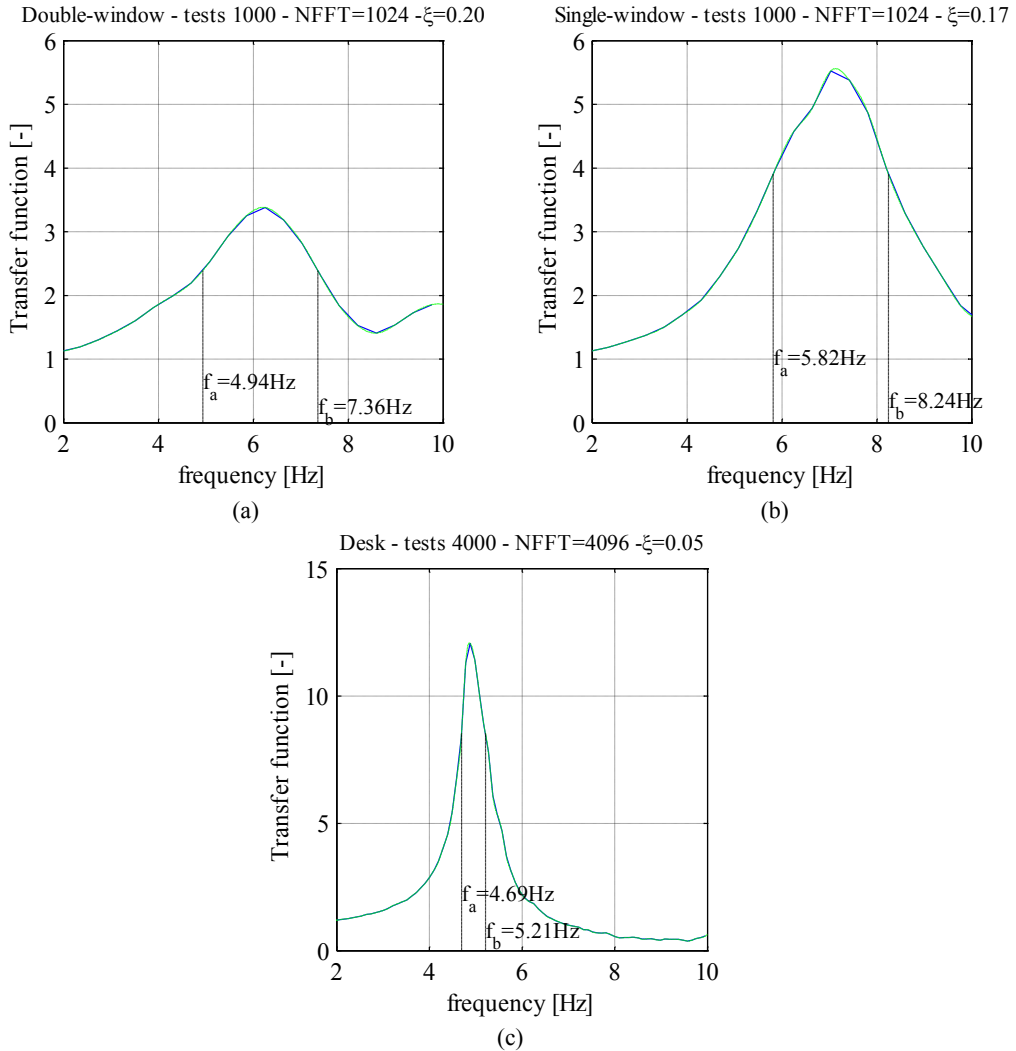


Figure 56. Half power bandwidth method applied at the spline envelopes (in green) of the original transfer curves (in blue) for (a) double-window cabinet – tests 1000, (b) single-windows cabinet – tests 1000 and (c) desk – tests 4000.

2.3.3.2 NUMERICAL MODELLING OF THE COMPONENTS

Desk

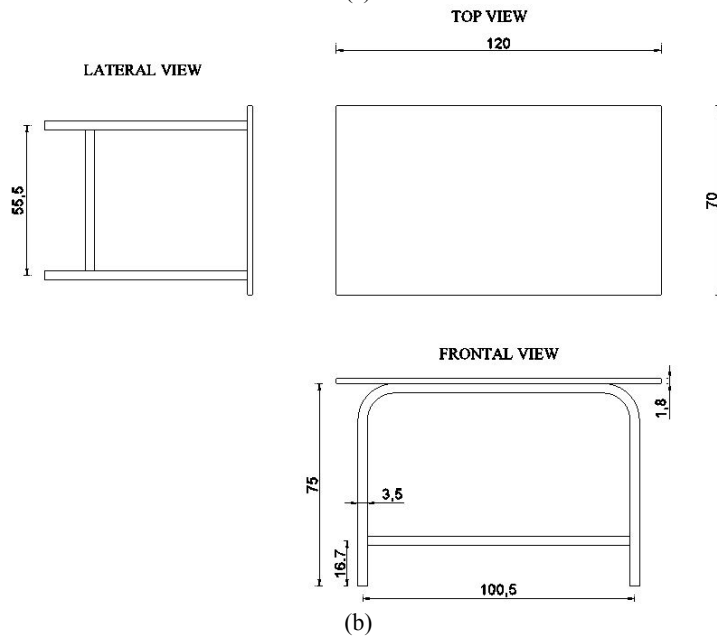
The tested components are also modelled through the Sap 2000 program (CSI Computer & Structures Inc., 2004). The results of the finite element models are compared to experimental outcomes. An accurate survey of the different components is required in order to increase the accuracy of the numerical models.

2.3 Shake table test on hospital building contents

The desk is composed of two tubular steel frames along its longitudinal side connected one another by four steel horizontal elements, a tubular footrest and a plywood top (Figure 57a). Moreover, a chest of drawers is screwed on the left vertical “columns” of the frames. The geometry is briefly represented in Figure 57b.



(a)



(b)

Figure 57. Desk (a) 3D view and (b) geometry (measures are in cm).

The plywood top is 120 cm x 170 cm x 1.8 cm and it is positioned at the top of the longitudinal frame at 75 cm height. The bay of the longitudinal frames is 100.5 cm wide and the distance between the frames is 55.5 cm. The longitudinal frame is composed of three different steel elements, i.e. two vertical and one horizontal elements, connected one another.

The tubular steel is characterized by a hollow circular cross section, whose diameter is 3.5 cm while the thickness is 0.18 cm. The longitudinal frames are connected each other through 4 steel elements: two 2.0 cm x 0.2 cm rectangular steel elements placed at the top of the frames and two 3.5 cm x 0.18 cm hollow circular steel element at 16.7 cm height. The footrest is connected to the frame through a single-bolted connection. The chest of drawers is connected to the vertical elements of the frames through a bolt at 4 different positions, i.e. two connections are located at 21 cm from the floor and the other two at 46 cm from the floor; the chest of drawers dimensions are 58 cm x 37 cm x 29 cm (height). The mass of the steel elements is 12.2 kg, while the mass of the drawers is 11.4 kg and the mass of the plywood top is 8.0 kg. A finite element model of the desk is defined through the Sap 2000 software (Figure 58).

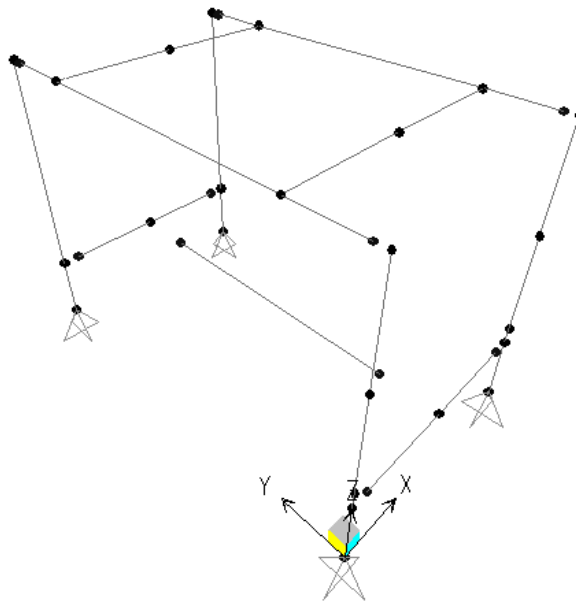


Figure 58. Finite element model of the desk created through Sap 2000.

The desk is fixed at the base through four hinges. Footrest have rotation releases that simulate the single-bolt connection. The connection between the vertical and horizontal elements of the longitudinal frames is characterized by a rotational stiffness equal to 2.2 kNm/rad. Such a stiffness models the partial constraint given by the tube-to-tube connection depicted in Figure 59. The stiffness value is calibrated in order to have a

good experimental-to-numerical matching. Indeed, in case such a connection is modelled through a fixed restraint, the natural frequency can increase up to 3 times, i.e. from 4.90 Hz to 13.58 Hz. The accurate estimation of the stiffness of tube-to-tube connection assumes therefore a key role in the evaluation of the dynamic properties of the tested desk.



Figure 59. Tube-to-tube connection between the steel elements of the desk.

The presence of the plywood top is modelled through the addition of four 2 kg masses applied at the top of the desk. The point of the longitudinal frame to which the desk is screwed are constrained with body constraints.

The chest drawers is modelled with four 2.85 kg masses applied at the connection points between the chest and the longitudinal frame. A different body constraint is imposed among these four points. Finally, the steel elements are modeled with a distributed mass and are characterized by a 210 GPa elastic modulus.

Modal analyses show a first mode frequency equal to 4.9 Hz and a second mode frequency equal to 22.6 Hz (Figure 60). The first mode shape denotes a pure translation in the longitudinal direction of the desk, while the second mode shape evidences a coupled motion in the transversal direction, due to the presence of the chest drawers.

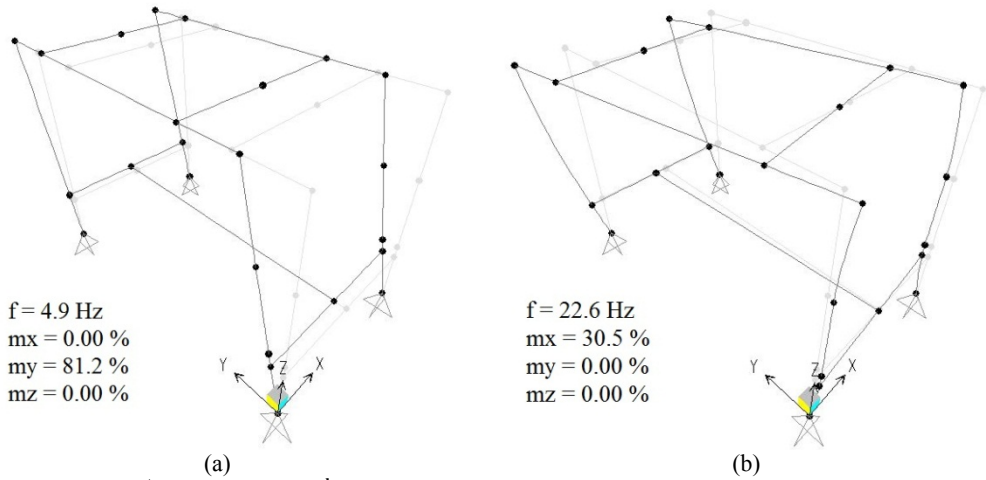


Figure 60. (a) 1st mode and (b) 2nd mode shapes, natural frequencies and participating mass ratios.

FEM results give a good matching with the experimental results (Table 15). In particular, the experimental tests evidences a significant differences in terms of natural frequency in case the component is shaken along the two horizontal directions. The comparison is clearly evidenced in Table 17.

Shaking Direction	Longitudinal	Transversal
FEM	4.9 Hz	22.6 Hz
Transfer curve	5.1 Hz	20.7 Hz

Table 17. Comparison between the natural frequencies resulting from modal applied to FEM and transfer curve.

Cabinets

The cabinets are composed of four steel vertical columns connected each other through steel elements. The global dimensions of both the investigated cabinets are summarized in Table 18.

	height [cm]	width [cm]	depth [cm]
Double-window cabinet	165	74.5	38
Single-window cabinet	139	53	36

Table 18. Dimensions of the investigated cabinets.

The vertical steel elements are characterized by an angular 55 cm x 50 cm “L” section with 0.1 cm thickness, with the 55 mm wide flange parallel to the transversal side of the cabinet. They are connected by two steel horizontal plates with side vertical flanges elements through bolted connections at the top of the cabinet and at 17 cm height (Figure 61). The steel plates and its flanges are characterized by 1 mm thickness, whereas the flanges are 3.0 cm high. Three of the four vertical bays are infilled with 1

mm thick steel plates, whereas glass windows are installed in the fourth bay. The double-window cabinet is also characterized by a 5 cm x 0.1 cm rectangular vertical steel element that separates the two glass windows.



Figure 61. Global view of the considered cabinets.

The vertical steel columns of the single-window cabinet are modelled according to their actual geometry. The presence of the steel elements that connect the four columns is modelled through four horizontal steel elements characterized by a 0.1 cm (width) x 3 cm (height) rectangular cross section both at the top and at 17 cm height of the cabinet. These horizontal elements are characterized by a large out-of-plane stiffness, i.e. large moment of inertia about the vertical axis, to simulate the presence of steel horizontal plate element. Furthermore, two diaphragm constraints are imposed between the 4 points at the top and the 4 points at 17 cm height. Vertical panels are not included in the model, since they are connected so as to not to increase the lateral stiffness of the cabinet. The glass window is modelled with a properly meshed shell element, assuming a 80 GPa elastic modulus. Hence, the adopted model is able to capture both the global modes in the two horizontal directions, that involve the whole cabinet, and local ones, that involve a portion of the cabinet. Rigid elements in the out-of-plane direction are included between the steel elements and the glass window in order to model the restraint given by their connection (Figure 62), whereas the glass window does not contribute to the in-plane stiffness; indeed, the glass window is connected to the

cabinet only along one of the two vertical sides. A rigid element in the out of plane direction is also included to model the lock of the glass window.



Figure 62. Connection between the steel elements and the glass window of the single-window cabinet.

The single-window cabinet mass is 15 kg, excluding the window mass; for the sake of simplicity, the mass is equally divided between the top and the base of the cabinet. The steel elements are characterized by no mass, whereas the mass is included in the glass window in order to correctly estimate the local vibrational modes of the glass window. Different mass amounts are inserted at the shelves height, according to the actual mass adopted in the experimental phase for the different test groups.

In Figure 63 the modal shape of the single-window cabinet for the test group 1000 are depicted. In Figure 63a the first vibrational mode, in Figure 63b the second vibrational mode, whose frequencies are 6.18 Hz and 7.38 Hz, are respectively represented. In Figure 63c a local mode that involves the glass window are represented.

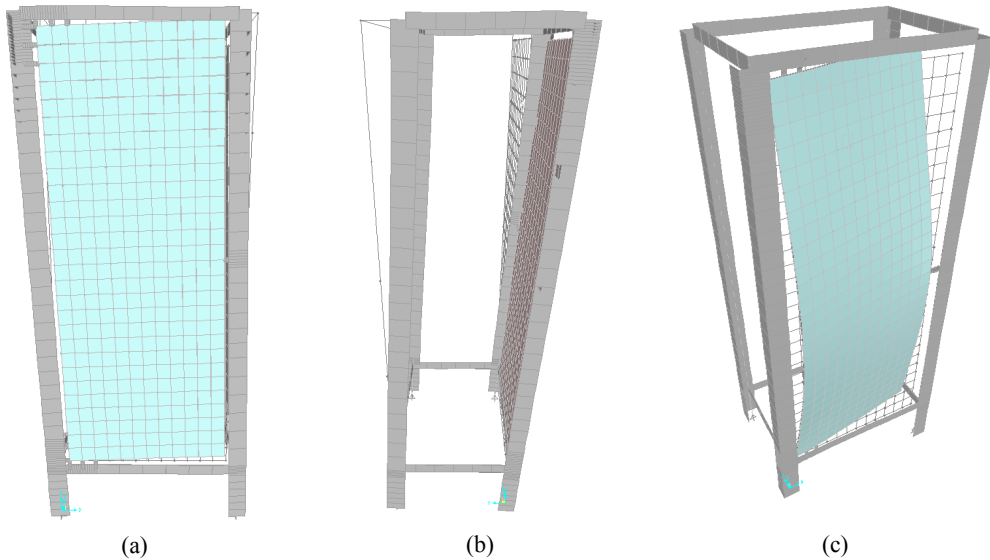


Figure 63. Single-window cabinet modal shapes in tests 1000: (a) I vibration mode which frequency is 6.18 Hz, (b) II vibration mode which frequency is 7.38 Hz, (c) III vibration mode which frequency is 23.12 Hz.

FEM results match very well the result of transfer curve represented in Figure 53b. The peak represented in the transfer curve that occurs at 26 Hz is compatible with the frequency of the local mode in the FEM model.

The comparison between the numerical and the experimental natural frequencies for the different test groups is summarized in Table 19.

Test group	FEM model	Experiment	Δ [%]
1000	7.38 Hz	7.03 Hz	+5.0
2000	8.84Hz	6.64 Hz	+33.1
3000	6.88 Hz	7.03 Hz	-2.1
4000	6.18 Hz	7.03 Hz	-12.1
5000	7.64 Hz	8.20 Hz	-6.8
6000	5.92Hz	7.81 Hz	-24.2

Table 19. Comparison between the frequency results from modal applied to FEM and transfer curve.

The numerical and the experimental frequencies of the tested cabinet are in similar ranges. Considering the low level of accuracy of the model with respect to the complexity of the geometry and the mechanical connection between the elements, the outcomes of the numerical analyses give a good approximation of the experimental ones. It is therefore demonstrated that simple models are able to catch the dynamic properties of the tested cabinet.

The modelling approach of the double-window cabinet is very similar to the one provided for the single-window cabinet. However, the dimension and the mass, i.e. 20 kg, is slightly different than the corresponding values in the single-window cabinet. The vertical steel element between the two windows is properly modelled according to its own geometry; such an element is hinged to the cabinet, in order to model the single-bolt connection. The connection between the cabinet and glass window is modelled through rigid elements in the out of plane direction, similarly to the single-window cabinet, that simulate the actual restraint given to the glass window by a steel connector.

The different mass amounts corresponding to the different performed test groups are inserted at the shelves height.

In Figure 64 the modal shape of the double-window cabinet for the test group 1000 are shown. The first four natural modes are included: the first two modes involve the whole cabinet, the third one is a local mode that involves the vertical element between the two glass windows and the fourth mode involves the glass windows.

FEM results match very well the result of transform curve represented in Figure 53a. The three peaks represented in the transfer curve that occurs at about 6 Hz, 11 Hz and 25 Hz, respectively, are compatible with the frequencies of the first, third and fourth modes in the FEM model. In particular, the numerical model allows justifying the differences in the transfer curves among the single- and the double-window cabinets. Indeed, the double-window transfer curve denotes three evident peaks, whereas the single-window one exhibits only two peaks.

The comparison between the numerical and the experimental natural frequencies for the different test groups is summarized in Table 20.

Test group	FEM model	Experiment	Δ [%]
1000	5.08 Hz	6.25 Hz	-18.7
2000	5.57 Hz	5.08 Hz	+9.6
3000	5.30 Hz	6.25 Hz	-15.2
4000	4.74 Hz	4.68 Hz	+1.3
5000	5.40 Hz	5.08 Hz	+6.3
6000	5.04 Hz	4.30 Hz	+17.2

Table 20. Comparison between the frequency results from modal applied to FEM and transfer curve.

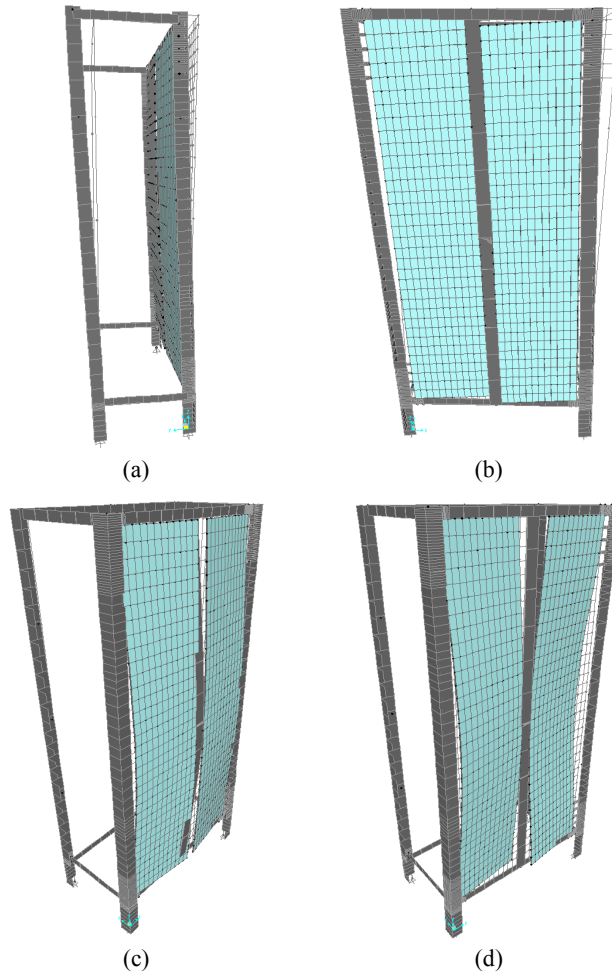


Figure 64. Double-window cabinet modal shapes in tests 1000: (a) I vibration mode which frequency is 4.74 Hz, (b) II vibration mode which frequency is 5.08 Hz, (c) III vibration mode whose frequency is 10.35 Hz, (d) IV vibration mode which frequency is 19.90 Hz.

Also for the double-window cabinet, the numerical and the experimental frequencies of the tested cabinet are in similar ranges. It can be concluded that simple models are able to catch the dynamic properties of the cabinets.

2.3.3.3 DAMAGE SCHEME DEFINITION

A damage scheme is defined in order to correlate the visual damage to the achievement of a given damage state. Three damage states are defined, i.e. Damage State 1 (DS1), Damage State 2 (DS2) and Damage State 3 (DS3). The damage state definitions are strictly related to the loss that a given damage state would cause. In particular the correlation between each damage state and the loss should take into account of

(Federal Emergency Management Agency (FEMA), 2007b): (a) the life loss (Deaths), (b) the direct economic loss due to the repair or replacement of the components (Damage) and (c) the occupancy or the service loss (Downtime). The onset of DS1 implies the need of repairing/repositioning the damaged component in its original condition; DS2 means that part of the component is damaged and it must be removed and replaced; DS3 implies that the life safety is threatened and the component needs to be totally replaced. Damage is observed after each test inspecting the tested specimen. The recorded damage in each component is then correlated to one of the three damage states defined above through the use of a damage scheme (Table 21). The level of damage required to reach a limit state is defined for each damage typology of each system component (i.e. cabinet, desk and contents). If possible, the damage type is defined quantitatively. The damage state achieved by the whole specimen is the maximum damage state recorded among the different components. After each test, damage is observed inspecting the specimen components and consequently an appropriate damage table is compiled (see Table 22) by visual inspectors.

		Damage state 1	Damage state 2	Damage state 3
	Damage typology	<i>Operational interruption</i>	<i>Need to replace damaged part of the components</i>	<i>Need to replace the whole component and/or threat for life safety</i>
	Residual displacement	Displacement larger than 2cm	-	-
Cabinet	Collapse	Screw loosening	Collapse of one support	Collapse of more than one support
		Residual displacement in shelves less than L/500	Permanent displacement in shelves larger than L/500	Shelves collapse
		Window opening	Window locking	Window collapse
		Overturning	Rocking	Hammering (with damage)
	Residual displacement	Displacement larger than 4cm	-	-
Desk	Collapse	Screw loosening	Collapse of one support	Collapse of more than one support
		Drawer opening	Drawer slipping out of rail	Desk collapse or overturning
Content	-	Displacement	Collapse (less than 10%)	Collapse (more than 10%)

Table 21. Damage scheme for the correlation of the visual damage to the damage state.

2.3 Shake table test on hospital building contents

This Section reports the damage table that the inspector compiles after each shake table test. The table collects the main experimental outcomes. The occurrence of different damage to the different components is reported. The permanent displacement along the two horizontal directions (graphically defined on the ground floor) of two edges of the cabinets and of the desk are also measured. The portion of glass contents that exhibit a certain type of damage is also described. In Table 22 the damage table compiled after test no. 308, corresponding to a 1.20 g S_{DS} value, is reported. The data collected in the damage table are then compared to the damage scheme (Table 21) for the evaluation of the occurred Damage State, i.e. DS1, DS2 or DS3, in the tested specimen.

TEST IDENTIFICATION		I - CABINETS						
Test group	300			2 Windows	1 Window			
ID Test	308	Displacement (P1) X [cm]		0	2.5			
Date	15 July	Displacement (P1) Y [cm]		-1	-0.3			
Time	17:51	Displacement (P2) X [cm]		0	2.5			
		Displacement (P2) Y [cm]		-1	-0.3			
		Window damage		no	no			
		Rocking		yes	yes			
		Overturning		no	no			
II – DRIP-FEED SUPPORT		III - MONITOR						
Sliding		yes		Sliding		no		
Overturning		no		Overturning		yes		
Collapse		no		Switch off		no		
IV - DESK		V - NEGATIVOSCOPE						
Sliding		yes		Damage		no		
Drawer opened		yes		Collapse		no		
Displacement (P1) X [cm]		6		Switch off		no		
Displacement (P1) Y [cm]		-10						
Displacement (P2) X [cm]		4						
Displacement (P2) Y [cm]		8						
VI – GLASS CONTENTS								
Double-window cabinet			Single-window cabinet					
Bottle	Bottle	Bottle	Flask	Flask	Test tube	Beaker	Beaker	
500ml	250 ml	100 ml	250 ml	100 ml	dock	250 ml	100 ml	
Sliding	12/12	8/8	8/8	8/8	4/4	4/4	4/4	
Overturning	1/12	3/8	5/8	0/8	0/8	2/4	0/4	0/4
Damage	0/12	0/8	0/8	0/8	0/4	0/4	0/4	0/4

Table 22. Damage table compiled after test no. 308.

2.3.3.4 TEST RESULTS

Earthquake shakings are performed according to the test program described in Section 2.3.2.3. After each test the compatibility of the spectrum of the recorded acceleration time-history with the required target response spectrum according to AC156 is verified. The compatibility is ensured in the frequency range between 1.3 Hz and 33.3 Hz. In Figure 65 the spectrum compatibility check is shown for test 101, corresponding to a S_{DS} value equal to 0.15 g.

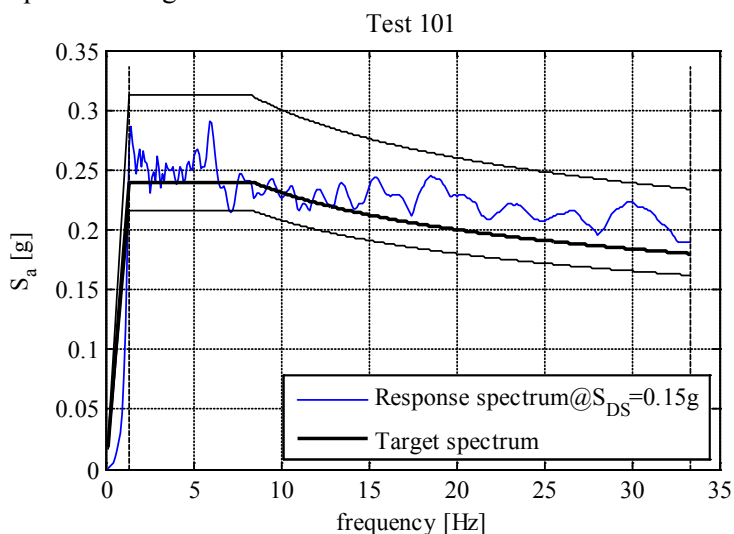


Figure 65. Spectrum compatibility between the spectrum of the recorded acceleration time-history and the target spectrum for test 101, corresponding to a S_{DS} value equal to 0.15 g.

In Table 23 and Table 24 the peak shake table acceleration (or peak floor acceleration, PFA) that causes the rocking mechanism initiation and the overturning, respectively, in both the cabinets is reported. The video recordings confirm the results of the “visual” damage detection. As expected, in test groups 400 – 500 – 600, in which the cabinets are shaken along their longitudinal direction, a larger peak floor acceleration is required in order to let the rocking mechanism develop in the single-window cabinet; the double-windows cabinet, instead, does not exhibit the rocking behavior at all, exhibiting a sliding-dominated motion in the same test groups. Moreover, the overturning of the cabinet is recorded only in case the cabinets are shaken along their transversal direction.

2.3 Shake table test on hospital building contents

Rocking	<i>single-window cabinet</i>	<i>double-windows cabinet</i>
<u>Test group</u>	<u>PFA [g]</u>	<u>PFA [g]</u>
100	0.37	0.48
200	0.49	0.49
300	0.49	0.61
400	0.74	-
500	0.95	-
600	0.84	-

Table 23. Peak floor acceleration (PFA) that causes the rocking mechanism initiation for the different test groups and for the two tested cabinets.

Overturning	<i>single-window cabinet</i>	<i>double-windows cabinet</i>
<u>Test group</u>	<u>PFA [g]</u>	<u>PFA [g]</u>
100	1.10	1.24
200	1.24	0.97
300	1.10	-
400	-	-
500	-	-
600	-	-

Table 24. Peak floor acceleration (PFA) that causes the cabinet overturning for the different test groups and for the two tested cabinets.

Recorded maximum acceleration on the components is also correlated to the peak shake table acceleration. In Figure 66 the ratio between the peak component acceleration and the peak shake table acceleration, i.e. the component amplification, is plotted versus the peak shake table acceleration. It can thus be argued that:

- The component amplification is in the range between 2 and 3 for low intensity shakings, i.e. peak shake table acceleration less than 0.3 g.
- As the shake table input intensity increases, several spikes are recorded in the component acceleration time histories and, consequently, the component amplification increases; the spikes are caused by the rocking behavior of the component; obviously, the spikes are larger for larger amplitude rocking mechanism.
- In test groups 100 – 200 – 300 the rocking amplitude is large enough to induce spikes in the acceleration time histories for a peak shake table acceleration equal to 0.5 g; this phenomenon is clearly visible for the single-window cabinet (Figure 66b).
- The cabinets low component amplification values, detected in test groups 400 – 500 – 600, denote the small amplitude of the rocking behavior in the cases in

which the cabinets are shaken along their longitudinal direction. Indeed, the component amplification values is below 4 for the different shakings.

- The desk component amplification is larger for low-to-moderate intensity shakings; as the peak floor acceleration exceeds the 0.5g value, the desk slides on the floor reducing the component acceleration; in the last tests of 200 and 300 test groups, the hammering of the desk with the cabinet is clearly recorded in the acceleration time history with a large amplitude spike.

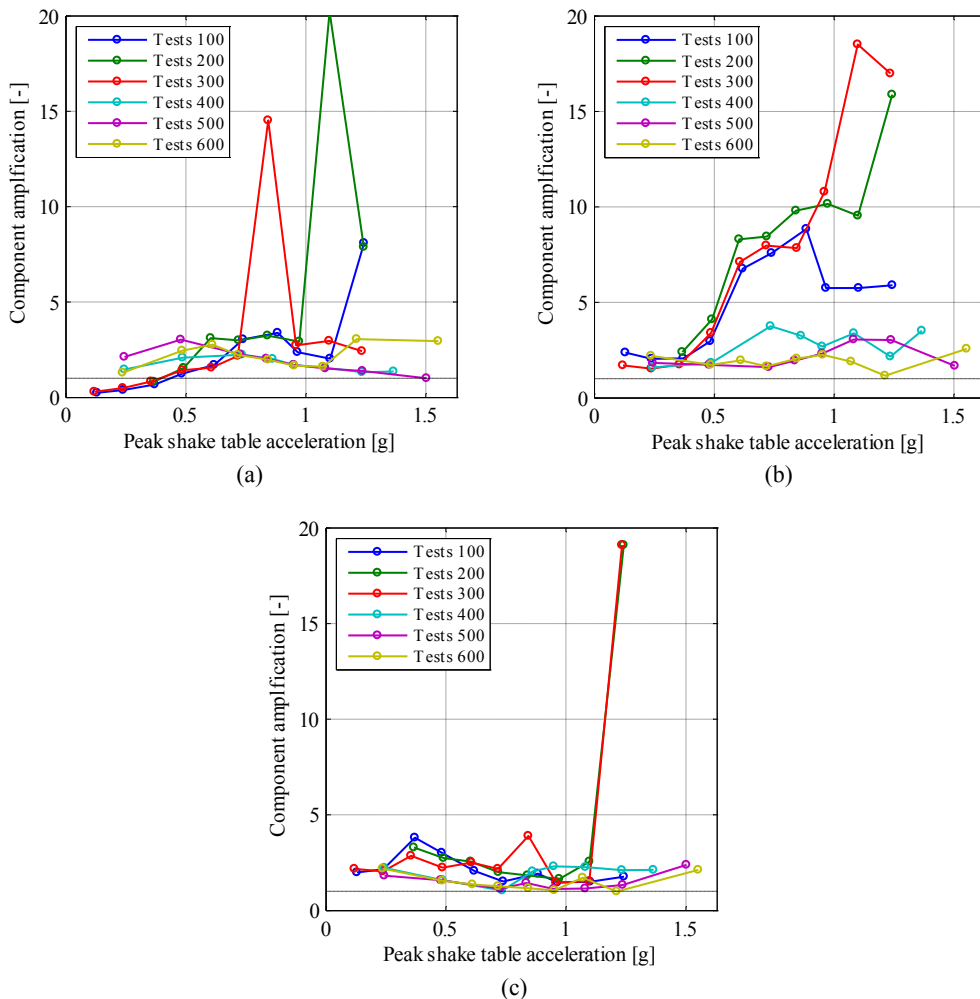


Figure 66. Ratio between peak component acceleration and peak shake table acceleration in (a) large cabinet, (b) small cabinet and (c) desk.

The rocking mechanism of the cabinets can be caught in vertical acceleration time-histories recorded in the different components. For instance, in Figure 67 the vertical

acceleration time history at the base of the single-window cabinet is recorded for the different tests of the test group 100. The rocking initiation in test 103 can be easily correlated to the record of few spikes. The spike amplitude becomes larger when the intensity of the input motion increases.

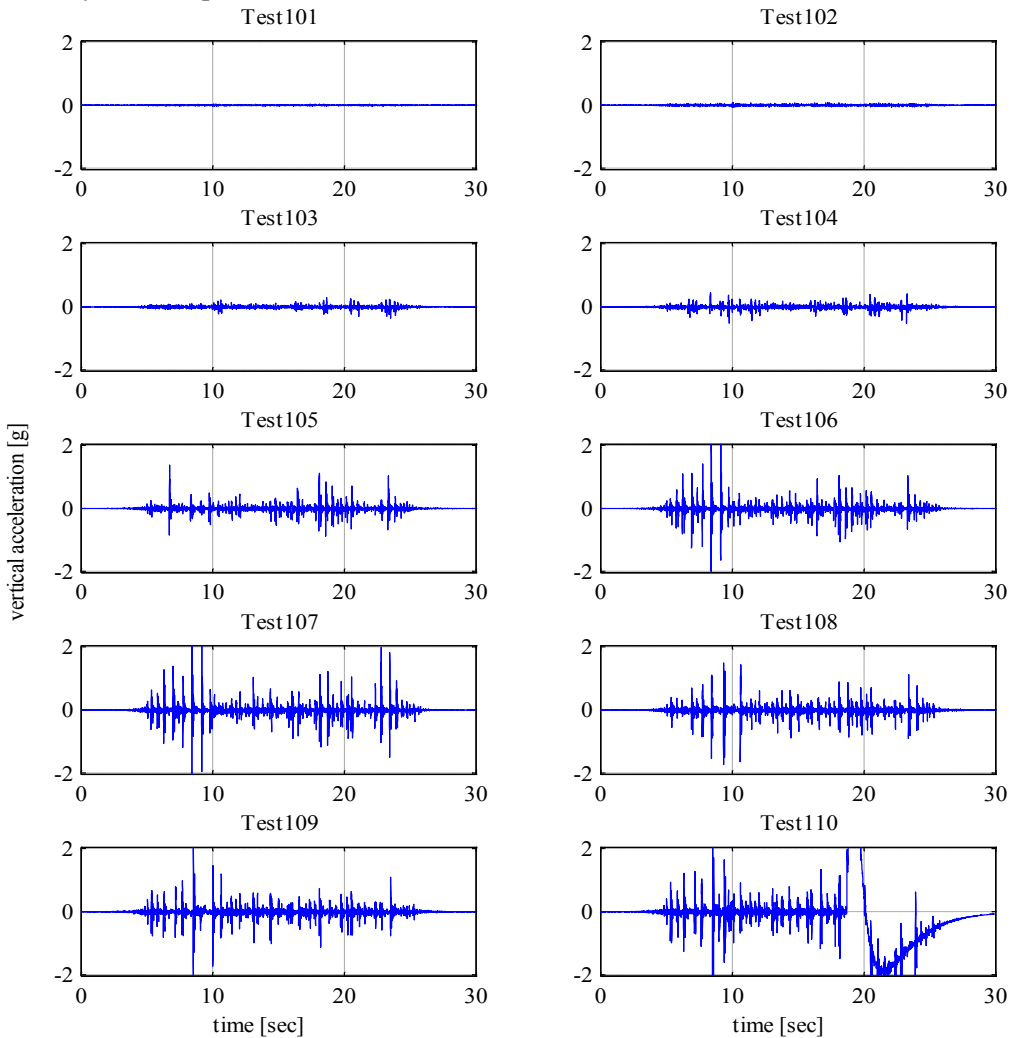


Figure 67. Vertical acceleration time history recorded at the base of the single-window cabinet for the different tests of the test group 100.

The effects of the vertical component of the ground motion have been ignored in this study. Notwithstanding, it is expected that such an effect does not remarkably influence the dynamic response of the components, e.g. the cabinets, due to their slenderness.

2.3.3.5 FRAGILITY CURVE EVALUATION

As shown in Section 2.3.2.2, the input motion is unidirectional. In order to correlate the chosen engineering demand parameter, i.e. peak floor acceleration (PFA), to the three defined damage states, the results of the test groups 100, 200 and 300 are combined with the results of the test groups 400, 500 and 600. For instance, the PFA that causes the DS1 threshold is the minimum between the PFA that induces DS1 in test groups 100 and the PFA that induces DS1 in test groups 400. It is assumed that the simultaneous combined effects of the two orthogonal motions are negligible.

Given this assumption in Table 25 the PFA values that trigger the different damage states for the different test groups are reported. It should be noted that DS2 PFA values are omitted. This is due to the fact that DS2 is recorded only in tests 300-600 for the overturning of some contents that are inserted in the cabinets, corresponding to a PFA equal to 0.486 g. In tests 100-400 and 200-500, in which sand equivalent masses are inserted in the cabinets, damage state 2 is not recorded at all, i.e. the specimen directly moves from DS1 to DS3. Hence, experimental data are not sufficient to evaluate the DS2 fragility curve.

Test group	DS1	DS3
100-400	0.371 g	1.103 g
200-500	0.491 g	0.974 g
300-600	0.486 g	1.099 g

Table 25. Peak floor accelerations that induces damage state 1 (DS1) and damage state 3 (DS3) for the different test groups.

Based upon the data in Table 25, the fragility curve is evaluated according to Porter et al. (2007). According to this procedure, the fragility parameters are computed as:

$$x_m = \exp\left(\frac{1}{M} \cdot \sum_{i=1}^M \ln r_i\right) \quad (10)$$

$$\beta_{\text{mod}} = \sqrt{\frac{1}{M-1} \sum_{i=1}^M (\ln(r_i/x_m))^2 + \beta_u^2} = \sqrt{\beta_{\text{fit}}^2 + \beta_u^2} \quad (11)$$

where M is the number of the tested specimen, r_i is the peak floor acceleration (PFA) at which a given damage state occurs in the i -th specimen and β_u , equal to 0.25, takes into account that the specimens are subjected to the same loading history and the number of the tested specimen is less than 5 (Porter et al., 2006). The fragility curves that fit the experimental data (dotted thick lines in Figure 68) are clearly evidenced with respect to the ones with the larger dispersion (solid thick lines in Figure 68). The latter also take into account the logarithmic standard deviation β_u . As expected, β_{fit} is very small, since it includes only the variability due to the different mass configuration.

In order to evaluate the influence that the distance between the cabinet and the wall has on the seismic response of the cabinet, the fragility curve is evaluated considering the data related to test groups 110 and 120. PFA values that cause DS3 are 0.738 g and 0.851 g for test groups 110 and 120, respectively. Considering a group that includes the DS3 PFA values for test groups 100, 110 and 120, a fragility curve that takes into account the randomness due to different wall-to-cabinets distances can be evaluated (gray lines in Figure 69).

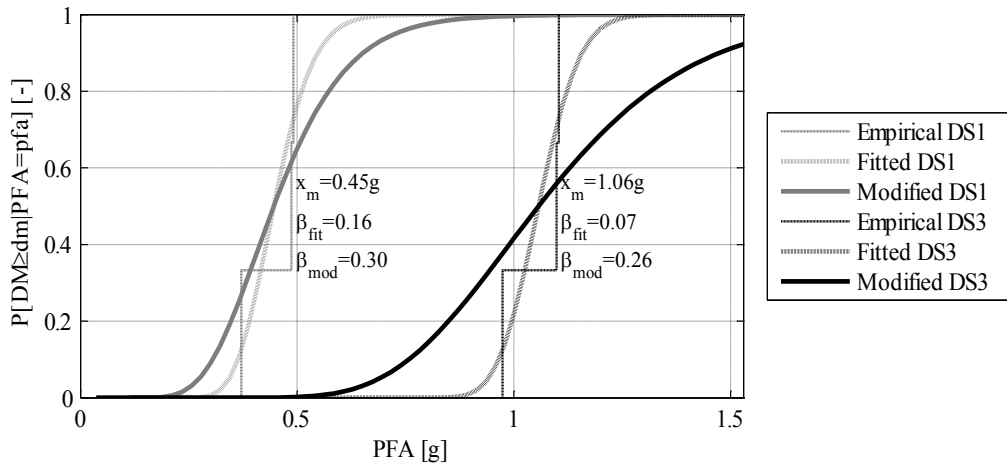


Figure 68. Fragility curves for the damage states 1 and 3 considering mass variability.

In Figure 69 this fragility curve is compared to the one that takes into account the mass variability (Figure 68). It can be observed that the gap variability significantly decreases the DS3 median value that moves from 1.06 g to 0.89 g. This confirms the observation included in (Filiatrault et al., 2004) that the larger the wall-to-cabinets/bookcase distance, the higher the probability that it would overturn.

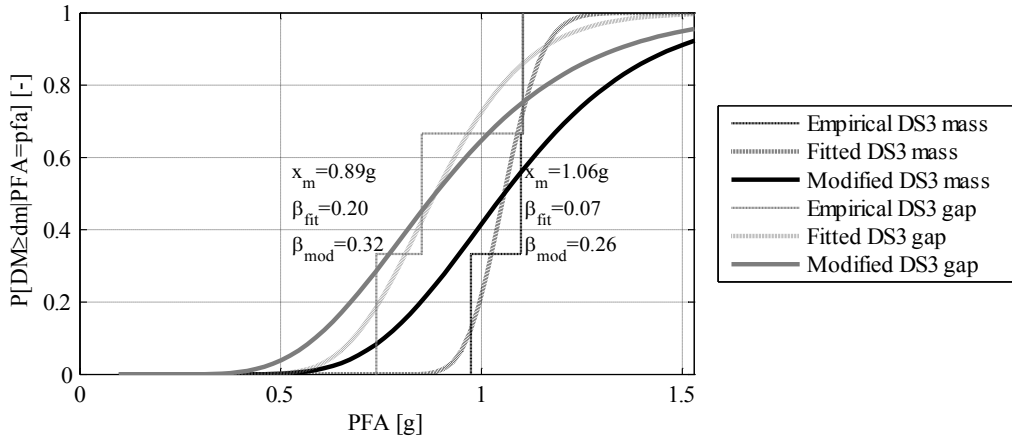


Figure 69. Fragility curves evaluated considering gap and mass variability for the damage state 3.

Finally, considering the five experimental DS3 data, related to test groups 100-400, 110, 120, 200-500 and 300-600, a fragility curve (dotted thick line in Figure 70) that takes into account both mass and gap variability can be evaluated. The DS3 fragility curve that includes also the β_u standard deviation is then evaluated (solid thick line in Figure 70). This fragility curve satisfies the Lilliefors goodness-of-fit test (Lilliefors, 1967); a 5% confidence level is adopted.

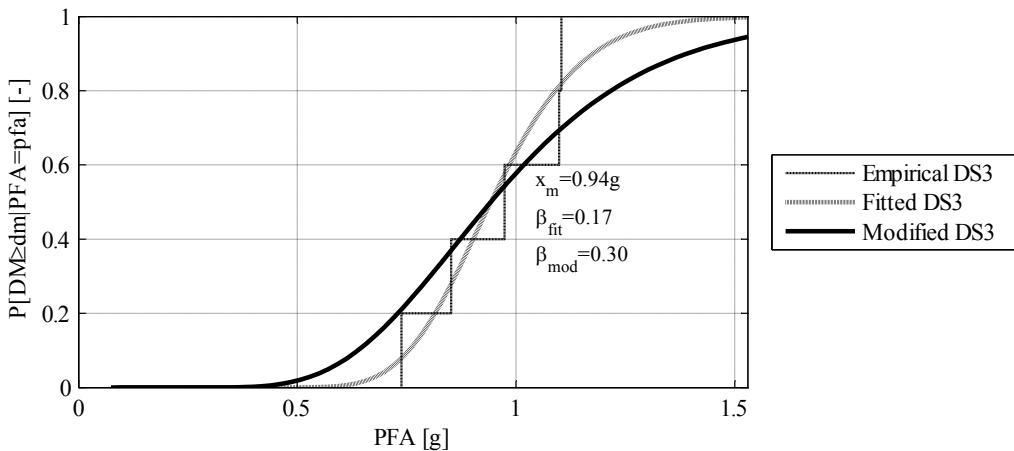


Figure 70. Fragility curves evaluated considering both gap and mass variability in the same experimental data for the damage state 3.

2.3.3.6 HORIZONTAL ACCELERATION PATTERN ON CABINET

The evaluation of the seismic acceleration distribution along the height of the cabinets is one of the goals of this study. At this purpose, few low-intensity unidirectional

shakings are performed along the transversal direction of both the cabinets. The input is defined according to AC 156 (International Conference of Building Officials (ICBO), 2000) and scaled at different S_{DS} , i.e. the spectral acceleration at short periods, levels. The intensity of the shakings is low in order to avoid any rocking mechanism of the cabinets that would induce spikes in the accelerograms.

Horizontal accelerations are recorded at four different levels of the cabinets in order to analyze the distribution of seismic demand along the height of the tested components. In Figure 71 and Figure 72 the arrangement and the ID of the accelerometers on the cabinets is shown.

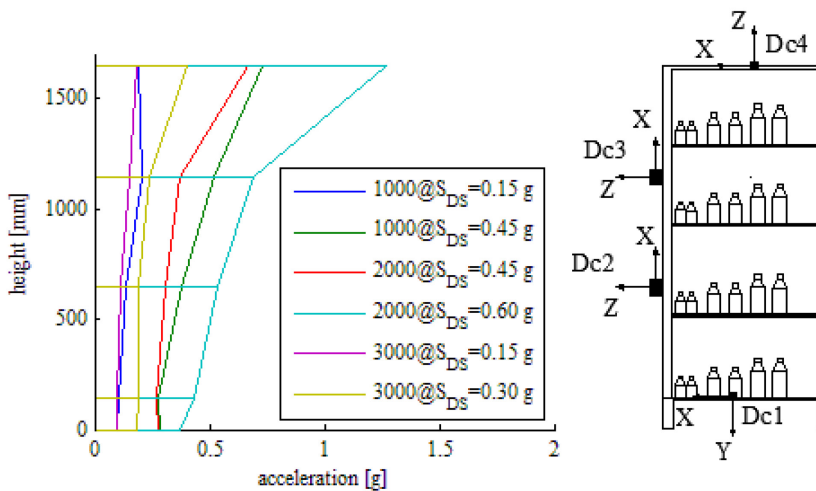


Figure 71. Horizontal acceleration distribution on the double-window cabinet at different intensity levels for the different mass distribution.

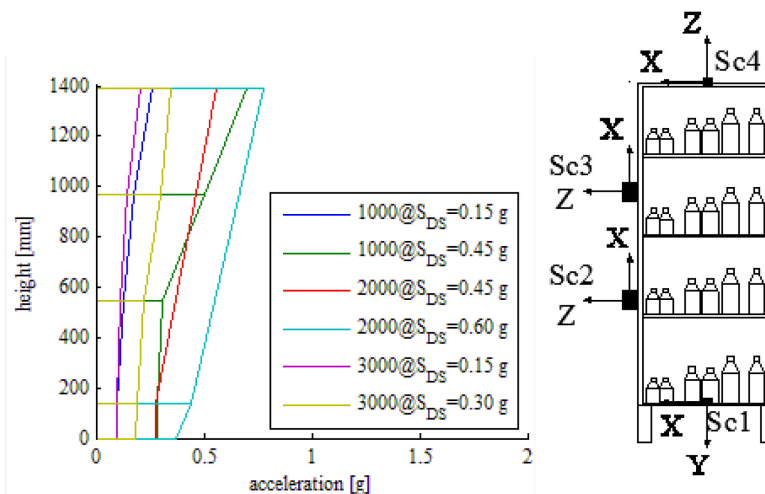


Figure 72. Horizontal acceleration distribution on the single-window cabinet at different intensity levels for the different mass distribution.

The acceleration recorded during the test group 1000 corresponding to a 0.45 g S_{DS} value at the base of the double-window and the single-window cabinet and along their height are shown in Figure 73 and in Figure 74, respectively. The filtering and amplification effects of the two tested cabinets are clearly visible in the recorded accelerograms.

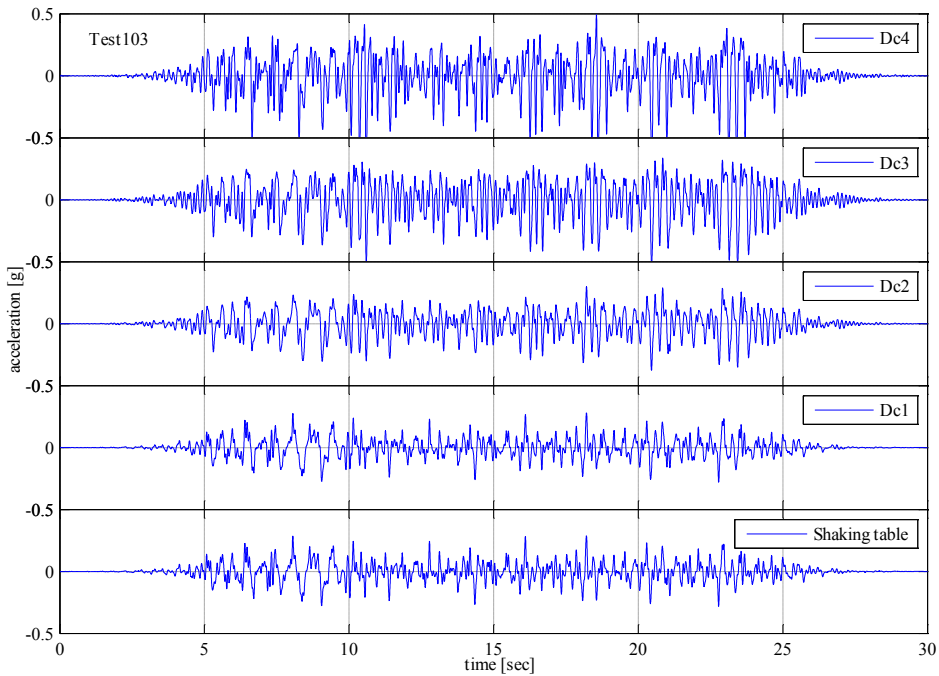


Figure 73. Horizontal accelerograms recorded during the test group 1000 corresponding to a 0.45 g S_{DS} value on the double-window cabinet.

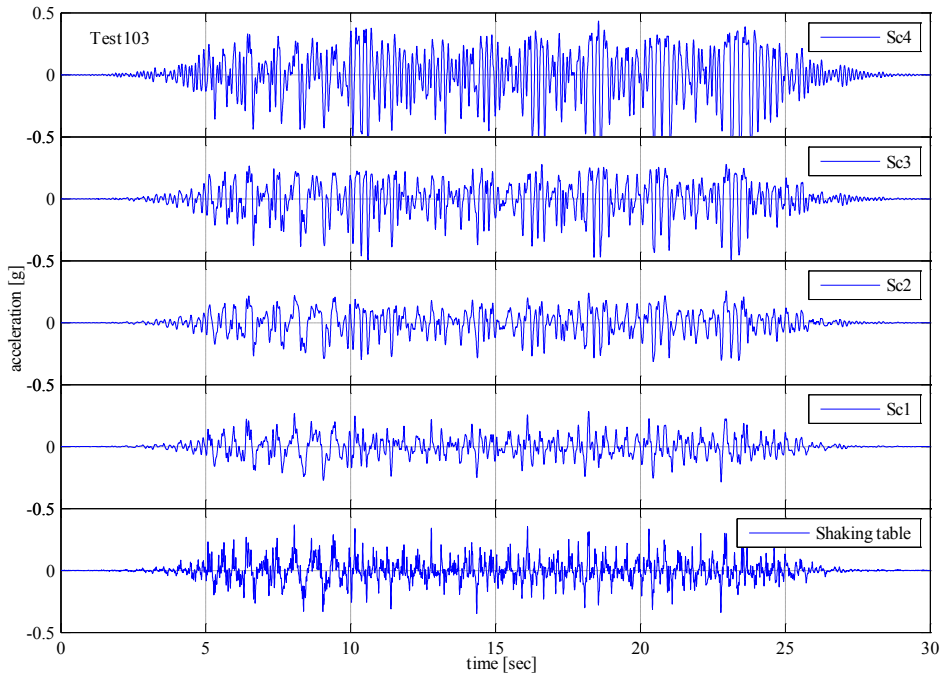
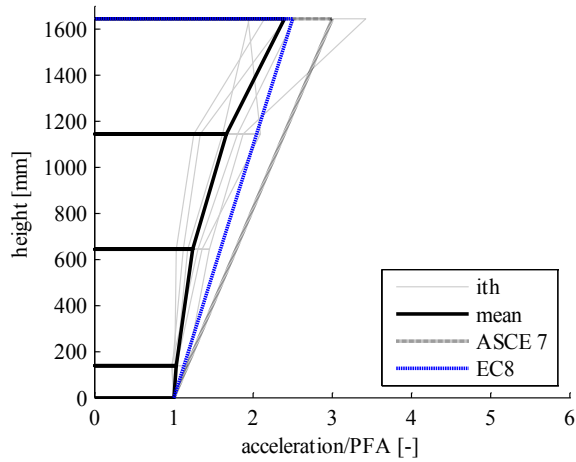


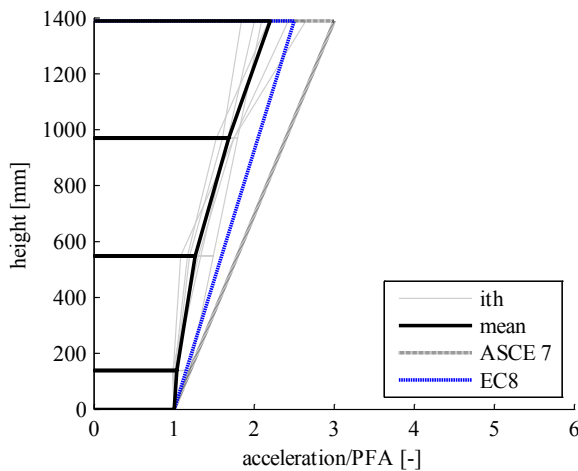
Figure 74. Horizontal accelerograms recorded during the test group 1000 corresponding to a 0.45 g S_{DS} value on the single-window cabinet.

The acceleration distribution along the height for the considered tests (Figure 71 and Figure 72) is similar to the shape of the first mode of vibration of the cabinets.

The recorded accelerations on the cabinets are normalized to the maximum acceleration at their base, i.e. the Peak Floor Acceleration (PFA), in order to generalize the results. The accelerations recorded on cabinets during each test (in gray), normalized with respect to the PFA, and their mean (in black), are represented in Figure 75 for both the double- and the single-window cabinets. These diagrams are compared with the trend of the horizontal floor accelerations in buildings, provided by ASCE 7 (American Society of Civil Engineers, 2010) and Eurocode 8 (CEN, 2004). The acceleration provided by ASCE 7 is linearly distributed from PGA at the base to a tripled value at the top. The Eurocode 8 provides a similar criteria, assuming a top acceleration value equal to 2.5 times the peak ground acceleration.



(a)



(b)

Figure 75. Trend of the horizontal accelerations along the height for the different performed tests (gray and black lines) compared to the structural floor acceleration trend provisions included in ASCE 7 and EC8 (dotted lines) for (a) the double-window and (b) the single-window cabinets.

The structural horizontal acceleration trend along the building height provided by Eurocode 8 provides a good fit of the horizontal acceleration trend on the tested freestanding cabinets, while ASCE 7 trend lightly overestimates the experimental results.

The experimental acceleration trend on the cabinets are compared in Figure 76 to the acceleration trend on nonstructural components assumed by Eurocode 8 (EC8); indeed, Eurocode 8 implicitly assumes that the horizontal acceleration is uniformly distributed along the height of the component. It is concluded that for the tested components the acceleration trend suggested by EC8 for the floor structural acceleration can be also

adopted to evaluate the acceleration trend on nonstructural elements, such as freestanding cabinets.

It is evident that the seismic force resulting from the distribution of accelerations currently considered by EC8 on nonstructural component is safe-sided. The overturning moment produced by EC8 distribution is 20% higher than the moment induced by the proposed distribution (dotted blue line in Figure 76), while the shear overestimation is larger than 30%.

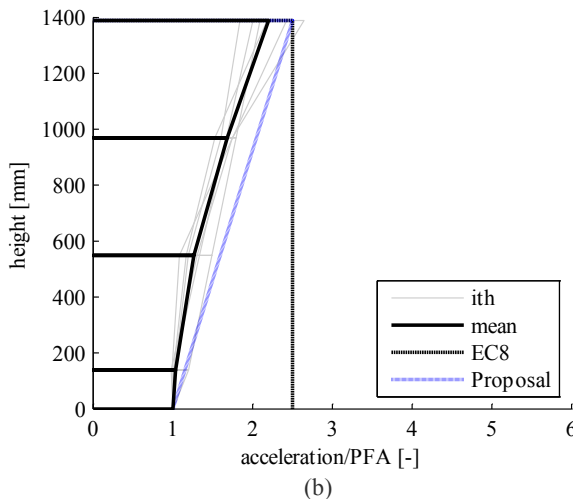
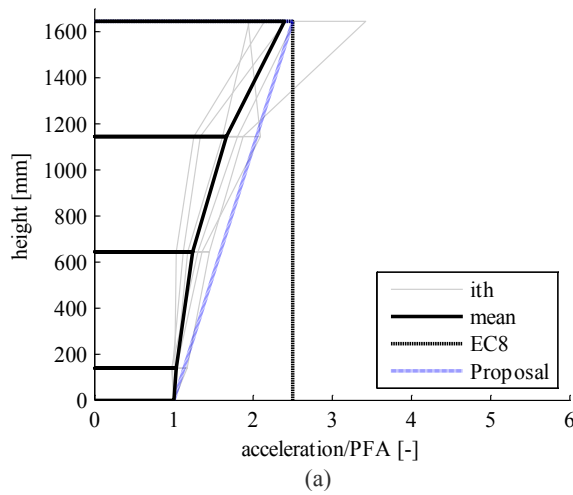


Figure 76. Comparison between the horizontal acceleration trend recorded during the tests (gray and black lines) compared to the current Eurocode 8 (EC8) provision for nonstructural components and to the proposed trend for (a) the double-window and (b) the single-window cabinets.

2.3.4 CONCLUSIONS

The research study is motivated by the urgent needs to further investigate the seismic performance of medical equipment and typical hospital components. The preliminary results of shake table tests on a full-scale laboratory room unit equipped with typical architectural finishing, freestanding furniture items, desktop computer and medical equipment are discussed.

An examination (out patients consultation) room is selected as representative layout for the experimental seismic performance assessment of the core units of hospital buildings. The building contents utilized for the examination room include two cabinets, a desktop computer and a desk; different glass contents are also included in the cabinets in some tests. Different mass distributions are selected to distribute such contents in the single- and double-window cabinets. 63 shakings are performed during the whole test campaign.

- The natural frequency of the different components is estimated. It is found that the distribution of the mass along the height assumes a key role to evaluate the natural frequency of the cabinets in case they are shaken along their transversal direction.
- The tested components are modelled through a finite element approach. It is demonstrated that simple models are able to catch the dynamic properties of the tested cabinets.
- The peak shake table acceleration (PFA) that causes the rocking mechanism initiation and the overturning, respectively, in both the cabinets are analyzed. In particular, the rocking mechanism in the two tested specimen initiates for a PFA that ranges between 0.37 g and 0.61 g; instead the overturning of the cabinets occurs for PFA slightly larger than 1.00 g.
- The accelerations recorded at the top of the different components are strictly related to rocking phenomenon, that induces spikes in the recorded time-histories. It is noted that as the peak floor acceleration exceeds the 0.5g value, the desk slides on the floor reducing the acceleration recorded on the component.
- By investigating the vertical acceleration time histories recorded on the cabinets, it is concluded that the rocking mechanism of the cabinets can be easily caught in these time histories.
- A damage scheme is defined in order to correlate the visual damage to the onset of the selected three-stage damage states in the hospital examination room. Fragility curves are defined for damage state 1 and damage state 3. Such fragility curves are derived based on a systemic approach, i.e. encompassing

the performance levels of the components within the sample examination rooms. Different groups of specimens are considered in the evaluation of the fragility curves in order to investigate the mass variability, cabinet-to-wall distance variability and both mass and cabinet-to-wall distance variability. It is emphasized that the cabinet-to-wall distance increase can significantly reduce the seismic performance of the cabinets. This confirms that the higher the wall-to-cabinets/bookcase distance, the higher the probability of the overturn of the component.

- The seismic acceleration distribution along the height of the cabinets is investigated and compared to the EC8 provision for nonstructural component. It is concluded that for the tested components the acceleration trend suggested by EC8 overestimates the seismic demand. Moreover, the shape of the peak floor structural acceleration can be also adopted to evaluate the acceleration trend on nonstructural elements, such as freestanding cabinets.

2.3.5 REFERENCES

- Achour N (2007) Estimation of malfunction of a healthcare facility in case of earthquake. PhD Thesis. Kanazawa University, Kanazawa, Japan
- Achour N, Miyajima M, Kitaura M, Price A (2011) Earthquake-Induced Structural and Nonstructural Damage in Hospitals. *Earthquake Spectra* 27 (3):617-634. doi:10.1193/1.3604815
- Aiello A, Pece M, Di Sarno L, Perrone D, Rossi F (2012) A safety index for hospital buildings. *Disaster Advances* 5 (4):270-277
- American Society of Civil Engineers (2010) ASCE/SEI 7-10: Minimum Design Loads for Buildings and Other Structures. Reston, Virginia, US
- Bozorgnia Y, Bertero VV (2004) *Earthquake Engineering From Engineering Seismology to Performance-Based Engineering*. CRC PRESS, Boca Raton, Florida, USA
- Bracci JM, Reinhorn AM, Mander JB (1992) Seismic resistance of Reinforced Concrete Frame Structures Designed Only for Gravity Loads: Part I - Design and Properties of a One-Third Scale Model Structure. Technical Report NCEER-92-0027. State University of New York at Buffalo, NY, US
- Bruneau M, Chang SE, Eguchi RT, Lee GC, O'Rourke TD, Reinhorn AM, Shinozuka M, Tierney K, Wallace WA, von Winterfeldt D (2003) A framework to quantitatively assess and enhance the seismic resilience of communities. *Earthquake Spectra* 19 (4):733-752. doi:10.1193/1.1623497
- California Building Standards Commission (CSBC) (2007) California Building Code. Sacramento. CA, US
- CEN (2004) Eurocode 8: design of structures for earthquake resistance - Part 1: general rules, seismic actions and rules for buildings. EN 1998-1. Brussels, Belgium.

- Chen M, Pantoli E, Wang X, Espino E, Mintz S, Conte J, Hutchinson T, Marin C, Meacham B, Restrepo J, Walsh K, Englekirk R, Faghihi M, Hoehler M (2012) Design and Construction of a Full-Scale 5-Story Base Isolated Building Outfitted with Nonstructural Components for Earthquake Testing at the UCSD-NEES Facility. ASCE Structures Congress 2012, Chicago, IL, US. doi:DOI: 10.1061/9780784412367.121
- Comerio M (2005) PEER Testbed Study on a Laboratory Building: Exercising Seismic Performance Assessment. PEER Report No. 2005/12. Pacific Earthquake Engineering Research Center, College of Engineering, University of California, Berkeley, California, USA
- Cosenza E, Di Sarno L, Maddaloni G, Magliulo G, Petrone C, Prota A (2014) Shake table tests for the seismic fragility evaluation of hospital rooms. *Earthquake Engineering and Structural Dynamics* (submitted for publication)
- CSI Computer & Structures Inc. (2004) SAP2000. Linear and Nonlinear Static and Dynamic Analysis of Three-Dimensional Structures, Computer & Structures, Inc. Berkeley, California
- Di Sarno L, Yenidogan C, Erdik M (2013) Field evidence and numerical investigation of the Mw= 7.1 October 23 Van, Tabanlı and the Mw> 5.7 November earthquakes of 2011. *Bulletin of Earthquake Engineering* 11 (1):313-346. doi:10.1007/s10518-012-9417-0
- Federal Emergency Management Agency (FEMA) (2007a) Design Guide for Improving Hospital Safety in Earthquakes, Floods and High Winds. Report No. FEMA 577. Washington D.C., USA
- Federal Emergency Management Agency (FEMA) (2007b) Interim protocols for determining seismic performance characteristics of structural and nonstructural components through laboratory testing. Report No. FEMA 461. Washington DC, US
- Filiatrault A, Kuan S, Tremblay R (2004) Shake table testing of bookcase – partition wall systems. *Canadian Journal of Civil Engineering* 31 (4):664-676. doi:10.1139/104-031
- Furukawa S, Sato E, Shi Y, Becker T, Nakashima M (2013) Full-scale shaking table test of a base-isolated medical facility subjected to vertical motions. *Earthquake Engineering & Structural Dynamics* 42 (13):1931-1949. doi:10.1002/eqe.2305
- Gabor D (1946) Theory of communications. *Journal of the Institution of Electrical Engineers* 93:429-457
- Gunn SWA (1995) Health effects of earthquakes. *Disaster Prevention and Management* 4 (5):6-10
- Hancock J, Watson-Lamprey J, Abrahamson NA, Bommer JJ, Markatis A, McCoyh E, Mendis R (2006) An improved method of matching response spectra of recorded earthquake ground motion using wavelets. *Journal of Earthquake Engineering* 10 (sup001):67-89. doi:10.1080/13632460609350629

- International Conference of Building Officials (ICBO) (2000) AC 156 Acceptance Criteria for the Seismic Qualification of Nonstructural Components. ICBO Evaluation Service, Inc., Whittier, California, USA
- Johnson GS, Sheppard RE, Quilici MD, Eder JE, Scawthorn CR (1999) Seismic Reliability Assessment of Critical Facilities: A Handbook, Supporting Documentation, and Model Code Provisions. Technical Report MCEER-99-0008. University at Buffalo, NY, US
- Konstantinidis D, Makris N (2009) Experimental and analytical studies on the response of freestanding laboratory equipment to earthquake shaking. *Earthquake Engineering & Structural Dynamics* 38 (6):827-848. doi:10.1002/Eqe.871
- Kuo K-C, Suzuki Y, Katsuragi S, Yao GC (2011) Shake table tests on clutter levels of typical medicine shelves and contents subjected to earthquakes. *Earthquake Engineering & Structural Dynamics* 40 (12):1367-1386. doi:10.1002/eqe.1094
- Lilliefors HW (1967) On the Kolmogorov-Smirnov Test for Normality with Mean and Variance Unknown. *Journal of the American Statistical Association* 62 (318):399-402. doi:10.2307/2283970
- Magliulo G, Pentangelo V, Maddaloni G, Capozzi V, Petrone C, Lopez P, Talamonti R, Manfredi G (2012a) Shake table tests for seismic assessment of suspended continuous ceilings. *Bulletin of Earthquake Engineering* 10 (6):1819-1832. doi:10.1007/s10518-012-9383-6
- Magliulo G, Petrone C, Capozzi V, Maddaloni G, Lopez P, Manfredi G (2014) Seismic performance evaluation of plasterboard partitions via shake table tests. *Bulletin of Earthquake Engineering*:(online first). doi:10.1007/s10518-013-9567-8
- Magliulo G, Petrone C, Capozzi V, Maddaloni G, Lopez P, Talamonti R, Manfredi G (2012b) Shake Table Tests on Infill Plasterboard Partitions. *The Open Construction and Building Technology Journal* 6 (Suppl 1-M10):155-163. doi:10.2174/1874836801206010155
- McIntosh JK, Jacques C, Mitrani-Reiser J, Kirsch TD, Giovinazzi S, Wilson TM (2012) The Impact of the 22nd February 2011 Earthquake on Christchurch Hospital. Paper presented at the New Zealand Society for Earthquake Engineering conference, 13-15 April 2012, Christchurch, New Zealand,
- Miranda E, Aslani H (2003) Building-specific loss estimation methodology. PEER Report No.2003-03. Pacific Earthquake Engineering Research Center, University of California at Berkeley, Berkeley, California
- Mosqueda G, Retamales R, Filiatrault A, Reinhorn A (2009) Testing Facility for Experimental Evaluation of Non-Structural Components under Full-Scale Floor Motions. *Structural Design of Tall and Special Buildings* 18 (4):387-404. doi:10.1002/Tal.441
- Myrtle RC, Masri SE, Nigbor RL, Caffrey JP (2005) Classification and prioritization of essential systems in hospitals under extreme events. *Earthquake Spectra* 21 (3):779-802. doi:10.1193/1.1988338
- Office of Statewide Health Planning and Development (OSHPD) (2007) SB 1953 Regulations (2007), Title 24, Part 1, California Building Standards Administrative Code. OSHPD, State of California, US

- Petrone C, Magliulo G, Manfredi G (2013) Shake table tests for the seismic assessment of hollow brick internal partitions. *Engineering Structures*:(under review)
- Pinto PE, Lupoi A, Franchin P (2011) Deliverable D.2.8 – Definition of system components and the formulation of system function to evaluate the performance of critical facilities. SYNER-G project: Systemic Seismic Vulnerability and Risk Analysis for Buildings, Lifeline Networks and Infrastructures Safety Gain, University of Rome “La Sapienza”, Rome, Italy
- Porter K, Johnson G, Zadeh M, Scawthorn C, Eder S (1993) Seismic Vulnerability of Equipment in Critical Facilities: Life-Safety and Operational Consequences. Technical Report NCEER-93-0022. State University of New York at Buffalo, NY, US
- Porter K, Kennedy R, Bachman R (2006) Developing Fragility Functions for Building Components for ATC-58. A Report to ATC-58. Applied Technology Council, Redwood City, CA, US
- Porter K, Kennedy R, Bachman R (2007) Creating Fragility Functions for Performance-Based Earthquake Engineering. *Earthquake Spectra* 23 (2):471-489. doi:10.1193/1.2720892
- Proakis JG, Monalakis DG (2007) *Digital Signal Processing: Principles, Algorithms and Applications*. Pearson Prentice Hall, New Jersey, NY
- Sato E, Furukawa S, Kakehi A, Nakashima M (2011) Full-scale shaking table test for examination of safety and functionality of base-isolated medical facilities. *Earthquake Engineering & Structural Dynamics* 40 (13):1435-1453. doi:10.1002/Eqe.1097
- Taghavi S, Miranda E (2003) Response assessment of nonstructural building elements, PEER report 2003/05. College of Engineering, University of California Berkeley, USA
- Tokas C (2007) California’s Hospital Seismic Retrofit Program. Symposium on Seismic Regulations and Challenges for Protecting Building Equipment, Components and Regulations, University at Buffalo, Buffalo, US
- World Health Organization (WHO) (2007) Risk reduction in the Health Sector and Status of Progress. Proceedings of the Disaster Risk Reduction in the Healthcare Sector – Thematic Workshop, Geneva, Switzerland
- World Health Organization (WHO) (2008) WHO/UNISDR World Disaster Reduction Campaign. <http://www.safehospitals.info/>.

2.4 IN-PLANE TEST ON HIGH PLASTERBOARD PARTITIONS

Quasi-static tests are performed on six 5 m high plasterboard internal partitions, commercialized by Siniat company in industrial and commercial buildings in the European area. A steel test setup is designed in order to transfer the load, provided by the actuator, to the partition. The testing protocol provided by FEMA 461 is adopted for the quasi-static tests.

The specimens typical failure mode is the buckling of a steel stud, that involves the boards attached to the buckled stud. The buckling failure usually concentrates across plasterboard horizontal joints. The hysteresis loops evidence first a frictional behavior for low demand levels, and then a pinched behavior for moderate-to-high demand levels.

The interstory drift ratios (IDRs) required to reach a given damage limit state are evaluated through a predefined damage scheme. Based on the experimental data the fragility curves for three different damage states are estimated. The fragility curve yields median IDR values equal to 0.28%, 0.81% and 2.05% and logarithmic standard deviations equal to 0.39, 0.42 and 0.46 for DS1, DS2 and DS3, respectively.

2.4.1 INTRODUCTION

Many past research studies focused on the seismic performance assessment of nonstructural components and contents (Furukawa et al., 2013; Kuo et al., 2011; Magliulo et al., 2012b; Badillo-Almaraz et al., 2007). The seismic performance of plasterboard internal partitions characterized by cold-formed steel stud has been investigated in different past studies. Lee et al. (2007) tested different 2.8 m high drywall plasterboard partitions via quasi-static and dynamic tests; three different configurations, i.e. plain partition, partition with a door and partition with an intersecting wall, are considered. The loss related to the evidenced damage is also discussed, evidencing that the repair cost reaches almost the initial cost under 2% interstory drift ratio. Restrepo and Lang (2011) investigated the influence of two different loading protocols on the response of full-scale three-dimensional gypsum light gage metal-stud partition walls, representing a typical room in an office building. The specimens showed a small sensitivity to the two proposed quasi-static loading protocols. Restrepo and Bersofsky (2011) performed quasi-static tests on eight pairs of light gage steel stud partition walls, 2.44 m high, that were constructed following common United States practice. Three different damage limit states were identified and correlated to the interstory drift ratio. Tasligedik et al. (2012) performed experimental tests on two typical drywall partitions, whose internal structure is either steel or timber

framed, respectively. It was confirmed that the drywall systems adopted in current practice exhibit damage that would require repairing interventions for low drift levels. The differences between the two partition typologies are highlighted and some comments on the serviceability limit state criterion provided by New Zealand Code are provided. Magliulo et al. performed bidirectional shake table tests on innovative drywall internal partitions, in order to evaluate their seismic performance considering in-plane and out-of-plane interaction (Magliulo et al., 2014; Magliulo et al., 2012c). At this purpose a steel test frame is designed in order to simulate the seismic effects at a generic building story. The innovative partition systems exhibit a minor damage state for 0.58% drift and a moderate damage state for 0.98% drift. Retamales et al. (2013) performed an extensive campaign, i.e. 28 quasi-static tests, on common interior partition configurations used in residential, commercial, office, and institutional buildings. The failure mechanisms are reported and correlated to three damage states. Fragility curves are then provided for different partition groups.

In this research study, quasi-static tests are performed on 5 m tall plasterboard internal partitions. This partition typology is representative of typical partitions used in industrial and commercial buildings in the European countries. A proper steel test frame is defined in order to perform quasi-static tests on such components. Six different specimens, representative of typical partition typologies, are subjected to the quasi-static testing protocol provided by FEMA 461 (2007). Observed damage is briefly described and correlated to predefined damage states. Finally, the fragility curves for three different damage states are evaluated.

2.4.2 EXPERIMENTAL FACILITIES, TEST SETUP, SPECIMENS AND TESTING PROTOCOL

The quasi-static test campaign is conducted in the Laboratory of the Department of Structures for Engineering and Architecture at the University of Naples Federico II. The tests are aimed at assessing the seismic behavior of internal plasterboard partitions used in industrial buildings.

Figure 77 shows the test setup which is composed of a steel frame (see §2.4.2.1), the specimen, i.e. a plasterboard partition, a hydraulic actuator and a reaction wall.



Figure 77. Global view of test setup

The tested plasterboard partitions are 5.0 m high and 5.1 m wide. Generally they are constituted of perimeter guides, vertical studs, and plasterboards screwed in the studs and in the guides; no screwed connections between studs and guides are provided.

2.4.2.1 TEST SETUP: CONCEPT, DESIGN AND TEST ON BARE SETUP

The steel test frame is conceived so as to transfer the load provided by the hydraulic jack to the partition without absorbing lateral forces, hence a statically indeterminate scheme is developed (Figure 78a). Moreover, since the reaction wall cannot reach the height of the system, the actuator is placed at the middle height of the test setup. In this way, a given displacement produced by the actuator is doubled at the top of the setup, assuming a rigid loading column.

The actuator is connected to a loading column at its mid span, and the loading column is connected to the frame surrounding the partition through a horizontal pendulum. Consequently the column acts as a simply supported beam loaded by a force in the centerline; a half of the actuator force is transmitted at the top of the setup, and another half is transmitted at the base restraint.

The setup design is defined according to Eurocode 3 (CEN, 2005a, b). As shown in Figure 79, it is composed by:

- an I-shaped “HE 450B” vertical loading steel column 4.785 m long;
- two tubular 180x180x10 mm lateral steel columns 4.785 m long;
- an I-shaped “HE 280B” top horizontal steel beam 5.370 m long;

- an horizontal steel tubular profile 150x150x12.5 mm S355 placed between the loading column and the nearby lateral column;
- an I-shaped “HE 280B” base horizontal steel beam, 7.800 m long.

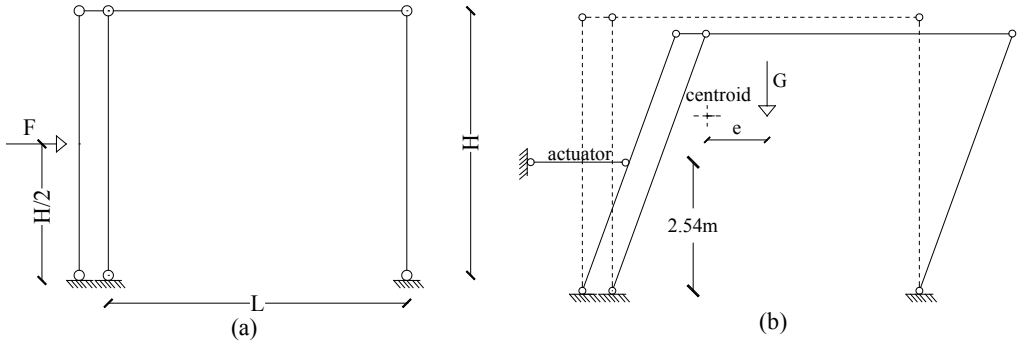


Figure 78. (a) Conception scheme of the test setup; (b) kinematic mechanism of the test frame without partition.

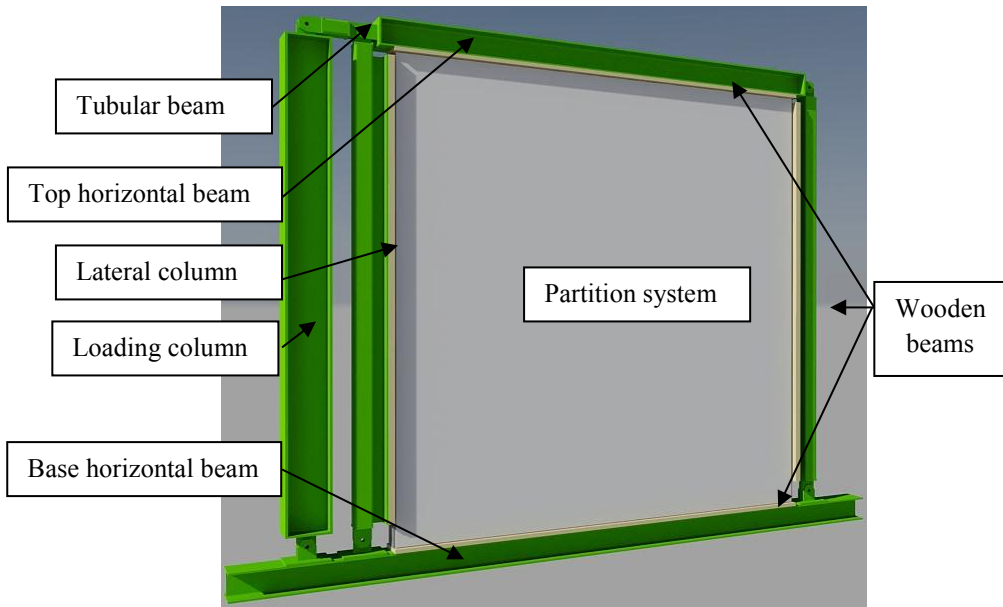


Figure 79. Test frame 3D view.

Wooden beams are both fixed to the vertical tubular columns and the horizontal beams. Their function is primarily technological, allowing the tightening of the partition steel guides without special equipment. The different elements are connected by pin connections; the base restraint is obtained through bolted connections between the columns and the base steel beam. Finally the base beam is connected to the floor through bolted anchoring systems.

An out-of-plane reaction system is defined (Figure 77) in order to avoid undesired out-of-plane displacements. It consists of two I-shaped “HE 140A” columns and two I-shaped “HE 160A” horizontal beams for each side of the test setup. Four steel rollers (Figure 80) facilitate the sliding of the specimen and avoid out-of-plane displacements that could occur during the test.



Figure 80. Lateral view on the rollers of the out-of-plane reaction system.

In addition, two diagonal stiffening inclined steel beams are provided in the out-of-plane direction (Figure 77). The weight of the whole steel test frame is about 80 kN.

A test on the test frame without plasterboard partition is performed before conducting the test campaign, in order to verify the kinematic mechanism of the test frame and the absence of friction mechanisms in the test setup. The test consists in pushing and pulling the test frame up to 10 cm at the actuator height. In addition, the inclination of the vertical elements is recorded via an inclinometer in order to verify that the vertical elements exhibit the same rotation throughout the test. The force-displacement relationship is recorded in Figure 81.

The hysteresis negative stiffness can be justified considering the scheme in Figure 78b. Indeed, when the test frame is loaded, the actuator represents a restraint for lateral column to which it is connected, i.e. it acts as a horizontal pendulum. The impressed displacement produces an eccentricity, i.e. e in Figure 78b; and the self-weight loads tend to increase the impressed displacement. The moment due to gravitational loads is balanced by the one produced by the actuator horizontal reaction, since the actuator represents a restraint for the test frame. Hence the steel frame lets the actuator be in tension during the pushing phase, and in compression, in case the test frame is pulling.

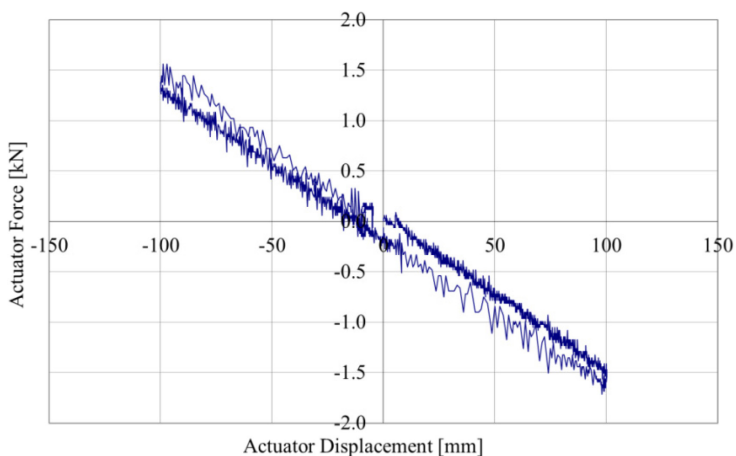


Figure 81. Test on bare test setup: force – displacement relationship.

The centroid of the bare test frame is at 3.24m from the base hinges and the weight of the portion of the test setup involved in the mechanism is 29.72kN, the force in the actuator for a displacement in the actuator equal to 100 mm is simply evaluated as follows:

$$G \cdot e = R_{actuator} \cdot H / 2 \Rightarrow R_{actuator} = G \cdot \frac{e}{H / 2} = \frac{29.72kN \cdot \left(0.10m \cdot \frac{3.24m}{2.54m} \right)}{2.54m} = 1.48kN \quad (12)$$

This result underlines that the force recorded in the actuator is related to the mechanism of the bare test frame. It can be neglected with respect to the force that the partition usually withstands, since this value is very small for the level of displacement expected during the test campaign. Finally, the force-displacement relationship denotes that the friction is negligible.

2.4.2.2 INSTRUMENTATION

Different instruments are used in order to monitor the specimens behavior during the cycling tests. The monitoring system consists of the following instrumentation typologies:

- two displacement laser sensors, placed at half the height of the column and at the top of the same column, respectively, in order to verify the rigid movement of the vertical column and to monitor top in-plane displacement;
- two wire potentiometers, placed in parallel with respect to the laser sensors;
- two displacement transducers placed at the two edges of the top horizontal beam, that measure out-of-plane displacements, in order to verify the planarity of the motion;

- twelve strain gauges (Figure 82), equally divided among the steel studs (sg1 – sg6) and the outer plasterboard layer (sg7 – sg12); in particular, sg7 corresponds to the same position of sg1, sg8 to sg2 and so forth.

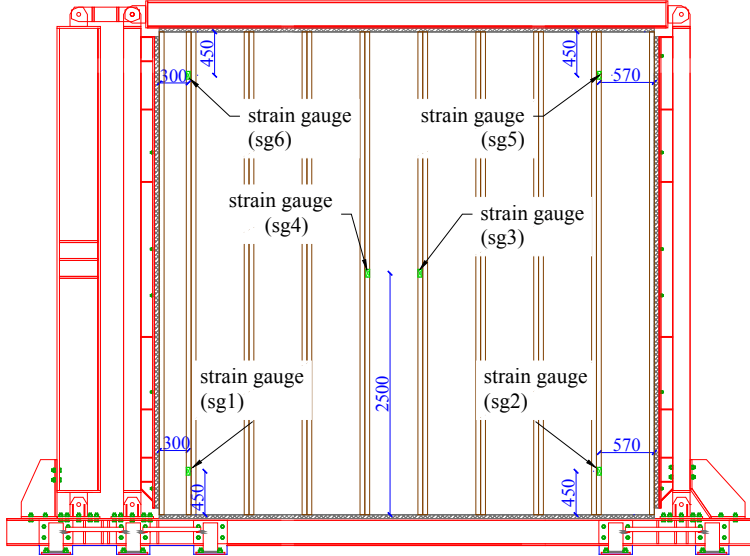


Figure 82. Strain gauge position on the steel vertical stud.

2.4.2.3 TESTING PROTOCOL

The protocol definition of the quasi-static test is based on the regulations given by F.E.M.A. 461 “Interim Testing Protocols for Determining the Seismic Performance Characteristics of Structural and Nonstructural Components” (FEMA 461, 2007). FEMA 461 proposes the loading history as numeric succession of two consecutive steps with amplitude a_i and a_{i+1} according to the following relationship:

$$a_{i+1} = c \cdot a_i \quad (13)$$

Two cycles at the same amplitude a_i are provided for each step. Equation (13) is calibrated in order to be representative of the response of SDOF systems subjected to a set of ground motions in ordinary conditions (not near fault) recorded in US area, adopted in (Krawinkler et al., 2001). The suggested value of the parameter c is 1.4.

A set of fourteen European records, taken from (Magliulo et al., 2012a), is also considered to estimate a value of the parameter conforming to European conditions. The set of accelerograms (Table 26) is compatible with Eurocode 8 design spectrum, soil B type and with a design ground acceleration on type A ground equal to 0.35 g.

Earthquake code	Earthquake name	Moment magnitude	Epicentral distance [km]	Site class	PGA_X [m/s ²]	PGA_Y [m/s ²]
000187	Tabas	7.3	57	B	9.08	10.81
000196	Montenegro	6.9	25	B	4.45	3.00
000199	Montenegro	6.9	16	B	3.68	3.56
000230	Montenegro (aftershock)	6.2	8	B	1.17	2.62
000291	Campano Lucano	6.9	16	B	1.53	1.72
006263	South Iceland	6.5	7	B	6.14	5.02
006334	South Iceland (aftershock)	6.4	11	B	4.12	7.07

Table 26. Set of European ordinary ground motions considered in the input definition study.

Linear dynamic analyses are performed on a simple degree of freedom (SDOF) system using as input the set of European records. The SDOF system is characterized by a period equal to 1.0 second, which averages typical fundamental periods of bare precast structures (Magliulo et al., 2013) in which the tested partitions are ideally installed. For each record the displacement response is rearranged using the rainflow cycle counting method (ASTM, 2003) and normalized with respect to the cycle largest amplitude. Only “pre-peak” excursions are considered, as indicated in FEMA 461 (2007).

The parameter c is calibrated in order to minimize the scatter between the amplitudes given by (13) and the mean normalized pre-peak displacement resulting from the analyses. A number of steps equal to 15 is considered. The minimum scatter is given by the following relationship:

$$a_{i+1} = 1.39 \cdot a_i \quad (14)$$

In Figure 83 the discrepancy between the analytical results and the protocol provided by equation (14) is evidenced. Even if the proposed loading protocol exhibits a moderate discrepancy with the target amplitudes, it is feasible for the investigation of intermediate damage states.

The chosen loading protocol is reported in Table 27 in terms of drifts and normalized amplitudes.

step ID	1	2	3	4	5	6	7	8	9	10	11	12	13	14	15
drift [%o]	0.3	0.4	0.6	0.8	1.1	1.5	2.2	3.0	4.2	5.2	8.0	11.2	15.5	21.6	30
a_i/a_{15} [%]	1.0	1.3	2.0	2.6	3.7	5.0	7.3	10	14	19	27	37	52	72	100

Table 27. Loading history protocol.

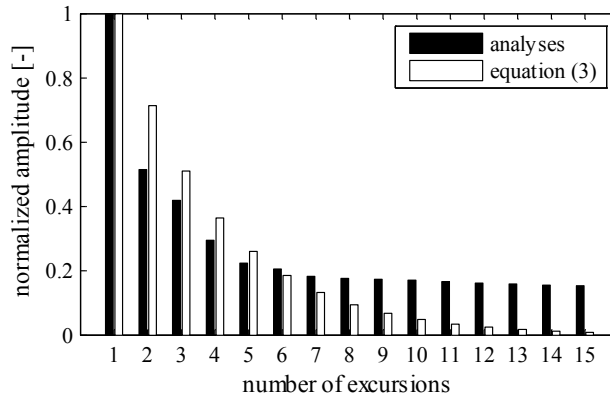


Figure 83. Comparison between the ordered normalized amplitudes resulting from the analyses and the amplitudes provided by equation (14).

2.4.2.4 SPECIMENS

The specimens reproduce plasterboard partitions, commercialized in Europe by Siniat company, installed in industrial buildings. They can be classified into two groups, based on the horizontal cross section of the partitions shown in Figure 84:

- Symmetric partitions, i.e. specimens no. 1 to no. 4.
- Staggered partitions, i.e. specimens no. 5 to no. 6.

The two groups present different typologies of horizontal and vertical tracks, in which single or back-to-back studs are placed. Indeed symmetric partitions have C-shaped tracks; instead staggered ones exhibit both C-shaped and L-shaped tracks. Both the typologies provide single or double layers of Siniat boards and in one case even three layers. Vertical and horizontal plasterboard joints are filled by paper and compound. It is avoided connecting with a single screw the plasterboard both to studs and horizontal guides: studs are just placed in the tracks, without any direct mechanical connection.

In Table 28, the components adopted for each specimen are described. A global view of the different specimen inserted in the test setup is presented in Figure 85.

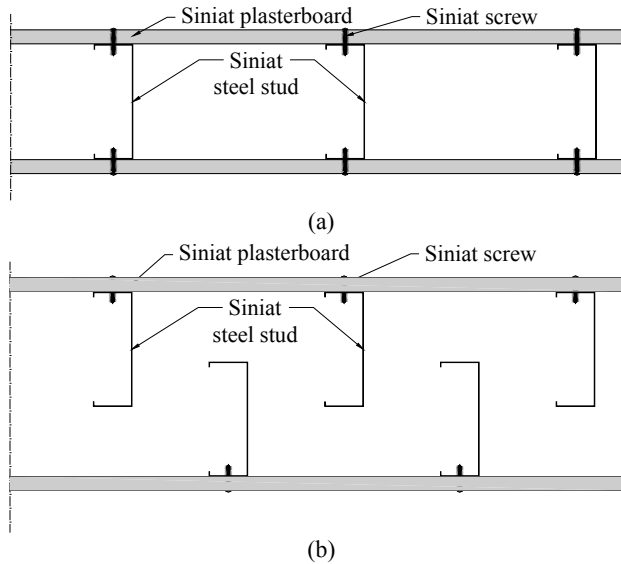


Figure 84. Symmetric (a) and staggered (b) partitions cross sections.

Components	Specimen no. 1	Specimen no. 2	Specimen no. 3
Siniat plasterboard panels	2 layers of Siniat standard boards 12.5mm thick	2 layers of Siniat standard boards 12.5mm thick	1 layer of Siniat standard boards 18mm thick
Siniat studs	50-150-50mm section, 0.6mm thick, back to back, 600mm spacing	50-150-50mm section, 0.6mm thick, single, 600mm spacing	50-100-50mm section, 0.6mm thick, single, 900mm spacing
Siniat tracks	50-150-50mm section, 0.6mm thick	50-150-50mm section, 0.6mm thick	30-100-30mm section, 0.6mm thick
Joints	Paper and Siniat compound	Paper and Siniat compound	Paper and Siniat compound

Components	Specimen no. 4	Specimen no. 5	Specimen no. 6
Siniat plasterboard panels	2 layers of Siniat standard boards 18mm thick	1 layer of Siniat standard boards 18mm thick	3 layers of Siniat standard boards 12.5mm thick
Siniat studs	50-100-50mm section, 0.6mm thick, back-to-back, 400mm spacing	50-150-50mm section, 0.6mm thick, single and staggered, 600mm spacing	50-100-50mm section, 0.6mm thick, back-to-back and staggered, 600mm spacing
Siniat tracks	30-100-30mm section, 0.6mm thick	50-150-50mm section, 0.6mm thick and 50-50mm "L" section, 0.6mm thick	30-100-30mm section, 0.6mm thick and 50-50mm "L" section, 0.6mm thick
Joints	Paper and Siniat compound	Paper and Siniat compound	Paper and Siniat compound

Table 28. Description of the different components used for each tested specimen.

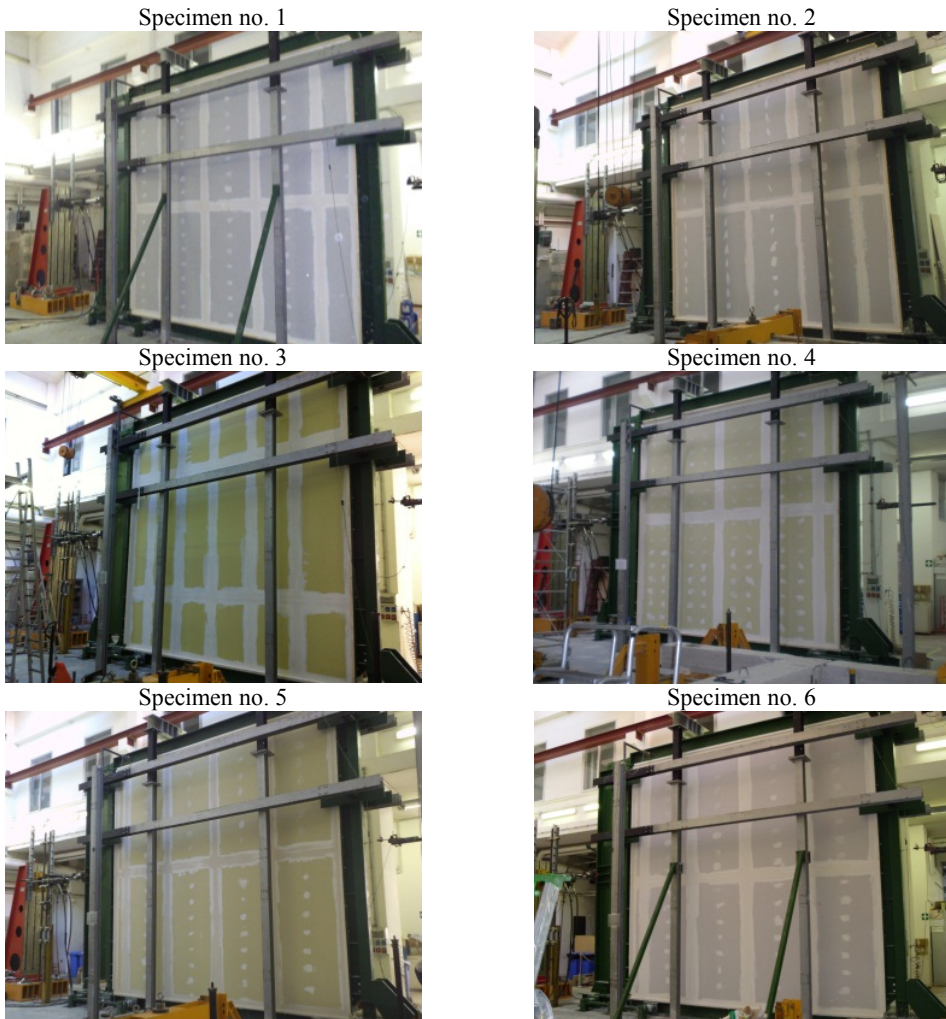


Figure 85. Global view of the specimens from no. 1 to no. 6 (from top-left to bottom-right).

2.4.3 RESULTS AND DISCUSSION

2.4.3.1 DAMAGE DESCRIPTION

Both the symmetric and staggered specimens show similar damage trend except the “seismic” partitions. The recorded damage can be summarized in the following phases:

- the first damage occurs along the perimeter: the paper starts cracking (Figure 86a), detaching the partition along the edges;
- further cracks also occur in the vertical and horizontal joints between the panels allowing adjacent panels to exhibit relative displacements for slightly

larger drift levels (Figure 86b). The damage is localized in correspondence of these joints. Panel corners cracks are evidenced and a significant creaking is heard from the partition: this sound is related to the bearing failure of the boards-to-steel screwed connections; this failure mode is clearly shown in the plasterboard inner layers during the dismantling phase (Figure 86c);

- for even larger top displacements, the specimen collapses in the out-of-plane direction due to the buckling of steel studs. The buckling mechanism usually involves a limited portion of the partition (Figure 86d). Only in test no. 3 a global buckling of the partition is evidenced (Figure 86e).

During the dismantling phase local buckling in studs is clearly evidenced. The stud buckling failure mainly concentrates across plasterboard horizontal joints (Figure 86f).

2.4.3.2 RESULTS SUMMARY

Quasi-static tests are performed on the six specimens using the defined testing protocol. Hysteretic curves are obtained by plotting the half of the force provided by the actuator (§2.4.2.1) versus the top displacement recorded by the wire potentiometer and the laser (Figure 87).

The following features can be noted observing the trend of the hysteretic curves:

- the high initial secant stiffness of the different specimens that decreases as the relative displacement increases;
- the degrading behavior, exhibited once the maximum force is reached, i.e. the post-capping negative stiffness;
- a significant degrading behavior between two cycles at the same displacements;
- the buckling-dominated failure modes of the different specimens, clearly visible in the sudden decrease of the recorded force once the specimen buckles;
- the frictional behavior in the first cycles and the strongly pinched behavior, exhibited as the screwed connections starts damaging.

2.4 In-plane test on high plasterboard partitions

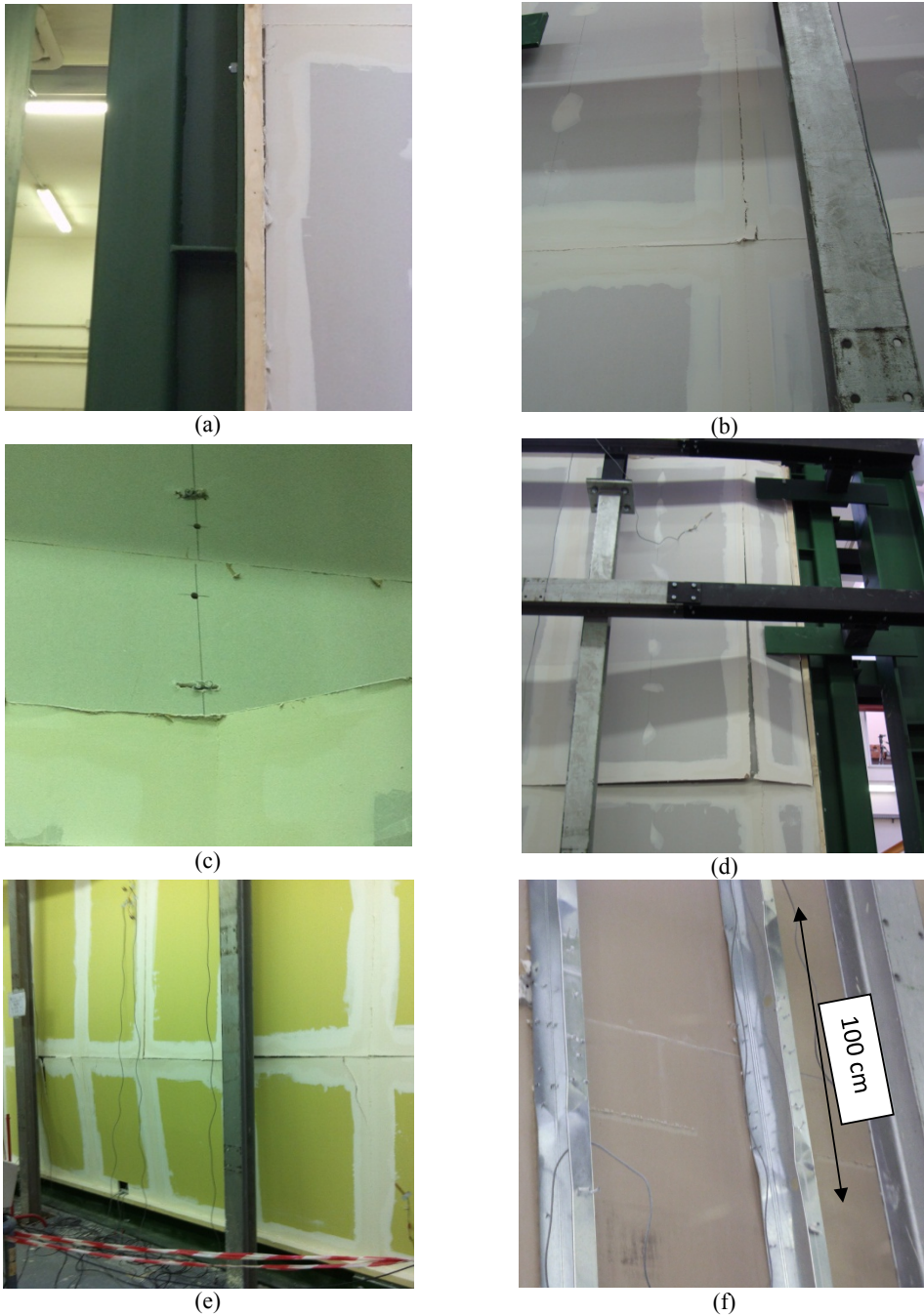


Figure 86. Damage in the specimen: (a) paper cracking along the perimeter (test no. 1); (b) paper cracking in the vertical and horizontal joints (test no. 6); (c) bearing failure of the boards-to-steel screwed connections (test no. 2); (d) local buckling of the partition (test no. 2); (e) global buckling of the partition (test no. 3); (f) buckling of the stud across plasterboard horizontal joints (test no. 2).

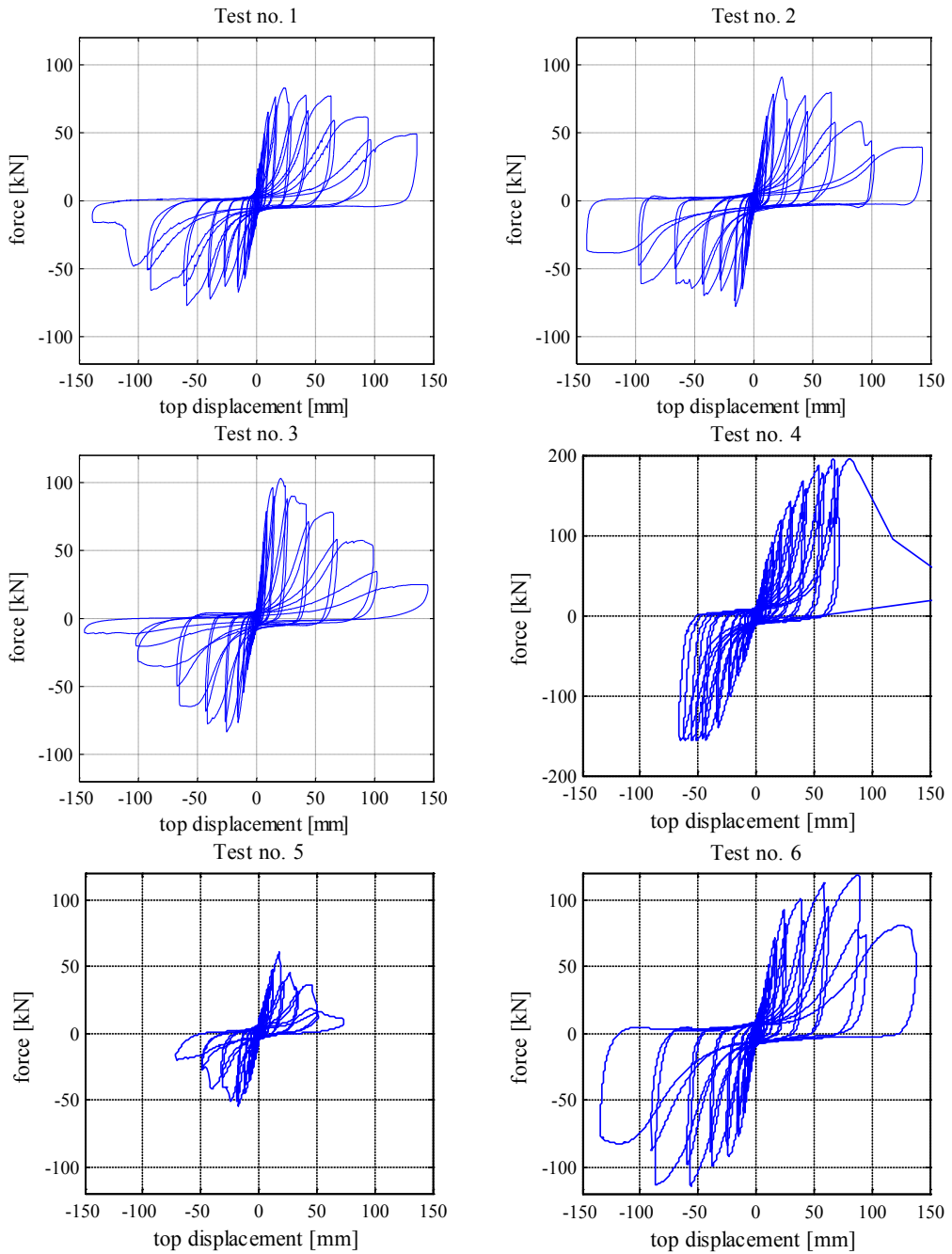


Figure 87. Hysteretic loops from test 1 to test 6.

Both symmetric and staggered partitions show similar backbone curves (Figure 88a). In particular, all symmetric partitions have very similar initial stiffness.

- Staggered partitions exhibit secant stiffness trend similar to the symmetric ones; however, they have slight lower collapse displacement values compared to the symmetric partitions.
- The use of back-to-back steel studs does not provide significant variations in the in-plane behavior, comparing test no. 1 and test no. 2 backbones.
- The use of a large amount of boards, instead, provides a significant increase in terms of strength with a reduction in terms of the collapse displacement, comparing test no. 3 and test no. 4.
- A significant different performance, both in terms of strength and collapse displacement, is evidenced between the staggered specimen no. 5 and specimen no. 6.

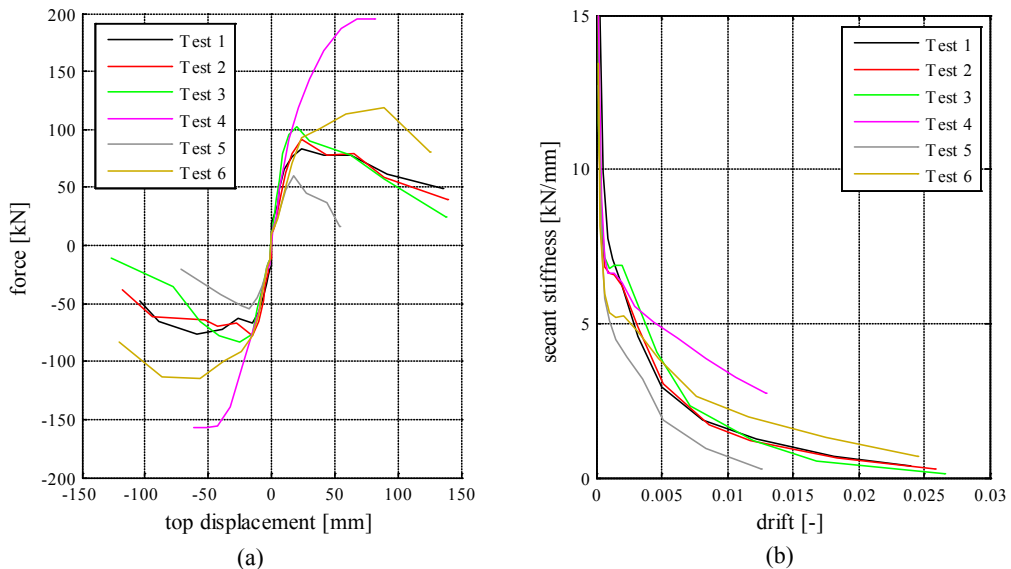


Figure 88. Comparison among (a) the backbones and the (b) secant stiffness recorded during the different tests

Both groups of specimens present the same trend of their secant stiffness (Figure 88b). Three phases can be identified:

- an initial friction-dominated phase in which high secant stiffness values are recorded until the paper and compound joints crack;
- a phase in which the secant stiffness exhibits a horizontal branch, as shown in Figure 88b for interstorey drifts between 0.10% and 0.25%; in this phase the

paper in the joints is cracked and adjacent panels come into contact one another;

- a final pinching-dominated phase in which the panels and studs experience damage, especially in their relative connections; the secant stiffness decreases up to the specimen failure.

Figure 89 shows the dissipated energy in test no. 1 for each cycle of the protocol and for each negative and positive semi-cycle. The strongly degrading behavior of the specimen is clearly evidenced:

- the testing protocol provides two consecutive cycles at the same displacement (see Section 2.4.2.3); the energy dissipated in the second cycle of the step is significantly smaller than the energy dissipated in the first cycle of the same step;
- the energy dissipated in the negative semi-cycle is smaller than the energy dissipated in the preceding positive semi-cycle.

The same conclusions can be drawn looking at the dissipated energy trends of the test no. 2 to test no. 6.

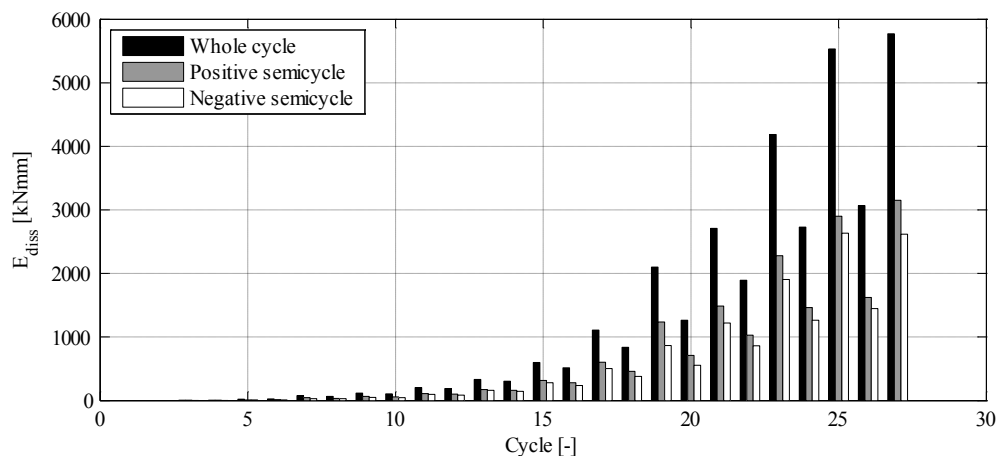


Figure 89. Energy dissipated in test no. 1 for each cycle of the protocol and for each negative and positive semi-cycle.

The strain gauge recordings on studs and plasterboards (Figure 90) lead to the following observations:

- the load is mainly carried by the plasterboards for low-to-moderate drift demands. Then the screwed connections start transferring load from the boards to the studs, and the steel strains increase until the steel stud buckling occurs;

- the steel strain trend underlines the stud buckling during the test, i.e. consequently to the buckling the strain gauges only record tensile strains (negative strains in Figure 90a);
- the large strains in sg3 and sg4 confirm that the demand in the steel stud is concentrated across the horizontal joints.

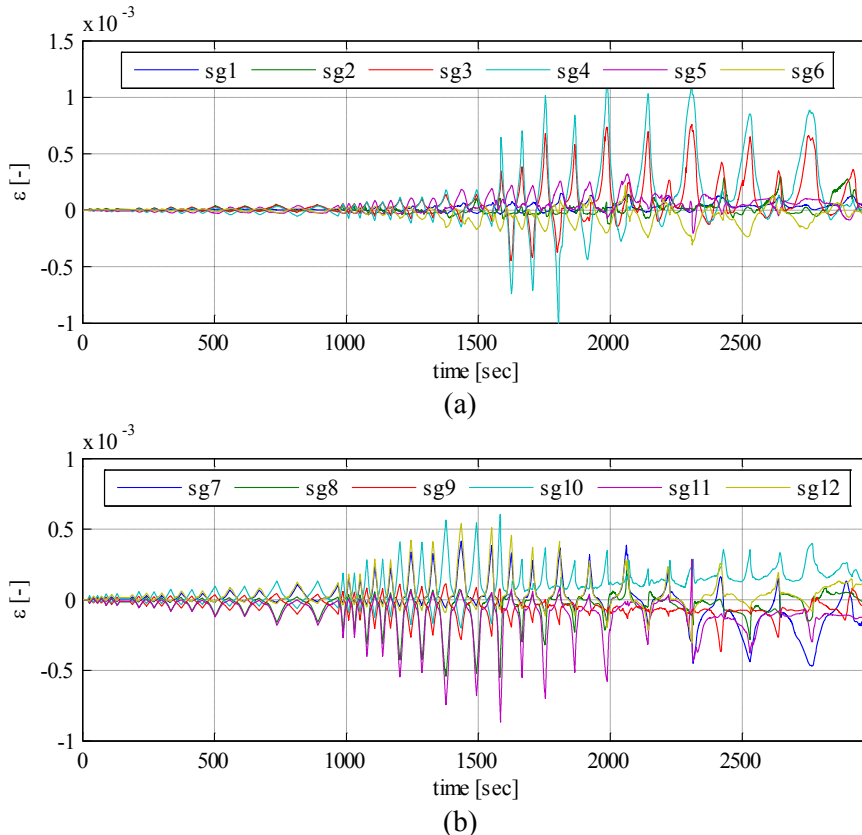


Figure 90. Strain gauge recording in (a) Siniat steel studs and in (b) Siniat plasterboards in test no. 2.

2.4.3.3 DS-EDP CORRELATION

The correlation between a set of damage states (DS) and the engineering demand parameter (EDP) assumes a key role in the definition of the fragility curve. In this study three damage states are considered for the seismic response definition of the plasterboard partitions, i.e. DS1, DS2 and DS3.

DS1 implies limited and minor damage in the component, that can be easily repaired in order to restore the original condition; instead DS2 achievement implies that the component exhibits such a damage level that it must be partially removed and

replaced; finally DS3 implies that either the produced damage level does not ensure life safety or the partition must be totally replaced.

In order to correlate the observed damage to a defined damage state, a “damage scheme” is defined (Table 29). In particular, the damage level required to reach a given damage state is indicated for each component of the partition. Obviously, the damage state of the studs, guides and part of the screws can be observed only at the end of test, after dismantling the plasterboards.

Component	Damage State 1 (DS1)	Damage State 2 (DS2)	Damage State 3 (DS3)
Siniat plasterboards	Drop of gypsum dust, small slip between adjacent panels (<2mm), minor detachment with respect to lateral borders (<5mm)	Out-of-plane rotation between adjacent panels, slight crack (≤ 0.3 mm wide) in the panel, panel portion failure	Expulsion of a partition portion, out-of-plane rotation between adjacent panel, large cracks on panels (> 0.3 mm wide)
Siniat metal studs	-	Local plastic deformations, small bump on the flanges, buckling deformations of the web	Buckling failure of a stud, large out-of-plane displacement ($d/h \geq 1/200$), diffused local plastic deformation on flanges or web, dislodgement from the top or base guide
Siniat guides	-	Localized plastic deformations	Permanent displacements, spread plastic deformations, buckling failure of the web or a flange
Siniat screws	-	Unscrewing of few screws ($\leq 5\%$), bearing mechanism of the screws connecting plasterboard panels to metal studs and guides	Unscrewing of several screws ($> 5\%$), bearing stress and expulsion of the screws connecting plasterboard panels to metal studs and guides ($> 5\%$)
Paper and compound	Visible opening in the joints paper on lateral borders or horizontal and vertical joints	-	-
Silicone	Detachment with respect to the perimeter. The silicone needs to be restored.	-	-

Table 29. Damage scheme for the correlation between the recorded damage in each component of the partition and the attained damage state.

The correlation between the damage state (DS) and the interstory drift ratio (IDR) is shown in Table 30 for each performed test through the use of the defined “damage scheme”.

IDR [%o]	<u>DS1</u>	<u>DS2</u>	<u>DS3</u>
<u>Test no. 1</u>	3.39	8.74	27.81
<u>Test no. 2</u>	1.56	9.12	29.20
<u>Test no. 3</u>	3.23	8.86	20.45
<u>Test no. 4</u>	3.23	11.55	16.14
<u>Test no. 5</u>	2.44	4.22	10.94
<u>Test no. 6</u>	3.42	8.30	25.46

Table 30. Interstory drift ratio (IDR) at which the considered damage states (DS) occur for the different performed tests.

The IDRs that cause the achievement of DS3 are larger than the limitation provided by current Italian and European Building codes, i.e. between 5‰ and 10‰ drift, for both symmetric and staggered specimens.

Staggered partitions exhibit a worse behavior than symmetric partitions due to their geometry; they are less stiff than symmetric ones in the out-of-plane direction; thus, they tend to buckle at lower drift levels.

2.4.3.4 FRAGILITY CURVE EVALUATION

Fragility curve evaluation is performed according to the data included in Table 30. Method A is adopted, according to Porter et al. (2007), in which the fragility parameters are computed as:

$$x_m = \exp\left(\frac{1}{M} \cdot \sum_{i=1}^M \ln r_i\right) \quad (15)$$

$$\beta_{mod} = \sqrt{\frac{1}{M-1} \sum_{i=1}^M (\ln(r_i/x_m))^2 + \beta_u^2} = \sqrt{\beta_{fit}^2 + \beta_u^2} \quad (16)$$

where M is the number of the tested specimen, r_i is the interstory drift ratio (IDR) at which a given damage state occurs in the i -th specimen and β_u is equal to 0.25 since all specimens are subjected to the same loading history (Porter et al., 2006). The fragility curves for the three considered damage states are plotted in Figure 91. The fragility curves that fit the experimental data (dashed thick lines in Figure 91) are clearly evidenced, like the ones with the larger dispersion β_{mod} (solid thick lines in Figure 91), that also takes into account the logarithmic standard deviation β_u . The fragility curves satisfy the Lilliefors goodness-of-fit test (Lilliefors, 1967) adopting a 5% confidence level.

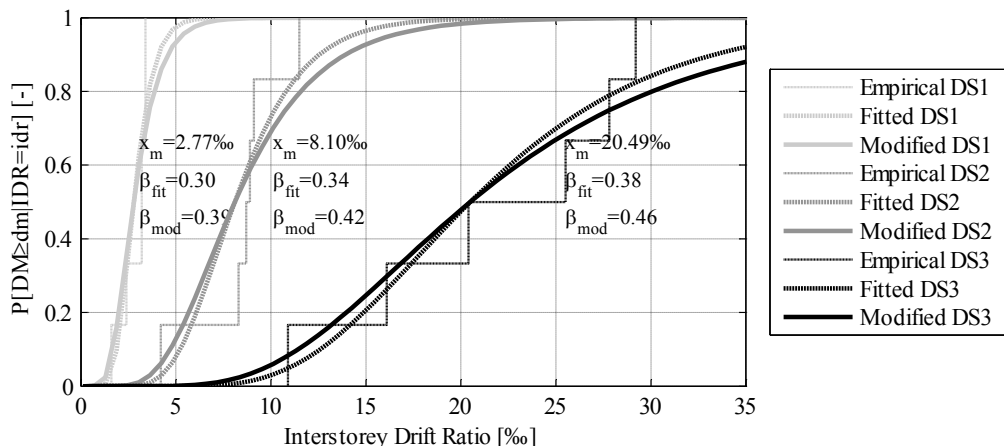


Figure 91. Fragility curves for the considered damage states for the tested specimens. The dashed thick lines are the fragility curve that fits the experimental data (dashed lines); the solid thick lines are the fragility curves that includes a larger standard deviation due to the use of the same loading protocol for the different specimen (Porter et al., 2006).

The median IDR values that cause DS2 and DS3 are slightly larger than the ones evaluated by Retamales et al. (2013), i.e. 6.7‰ and 10.5‰ for DS2 and DS3 respectively; instead, logarithmic standard deviations are in the same order of magnitude. The difference in the DS2 and DS3 median IDR values may be justified by the larger flexibility, by the larger number of plasterboards joints and by the non-connection of the studs to the tracks in the tested 5 m high partitions. Moreover, the construction details, typical of the US and European partitions, respectively, may have influenced the larger fragility of the US partitions.

2.4.4 CONCLUSIONS

Quasi-static tests are performed on 5 m high plasterboard internal partitions commercialized by Siniat company in industrial and commercial building in the European countries. A steel test setup is designed in order to transfer the load provided by the hydraulic jack to the partition without absorbing lateral forces. Six different specimens, representative of European typical partition typologies, are tested. The specimens are subjected to the quasi-static testing protocol provided by FEMA 461. The testing protocol, defined upon US ground motions, is adapted to a set of European ground motions; minor modification to the existing testing protocol is provided.

The specimens collapse in the out-of-plane direction because of the buckling of steel studs, that involves the boards attached to the buckled studs. The buckling failure concentrates across plasterboard horizontal joints.

The different specimen hysteretic loops evidence the frictional behavior in the first cycles, i.e. low drift demand levels, and the strongly pinched behavior exhibited when the screwed connections start damaging. Moreover, the degrading behavior of the specimen is clearly evidenced considering both two consecutive cycles at the same target displacement and positive and negative semi-cycles.

The correlation between a set of three damage states and the engineering demand parameter, i.e. the interstory drift ratio (IDR), is evaluated through the use of a predefined damage scheme. Based on the experimental data, evaluated upon the six performed tests, the fragility curves for three different damage states are evaluated. Their evaluation yields a median IDR value equal to 0.28%, 0.81% and 2.05% and a logarithmic standard deviation equal to 0.39, 0.42 and 0.46 for DS1, DS2 and DS3, respectively.

2.4.5 REFERENCES

- ASTM (2003) Standard Practices for Cycle Counting on Fatigue Analysis. ASTM-1049, American Society for Testing and Materials, West Conshohocken, PA, USA
- Badillo-Almaraz H, Whittaker AS, Reinhorn AM (2007) Seismic fragility of suspended ceiling systems. *Earthquake Spectra* 23 (1):21-40. doi:10.1193/1.2357626
- CEN (2005a) Eurocode 3: design of steel structures - Part 1-1: General rules and rules for buildings. EN 1993-1-1. Brussels, Belgium
- CEN (2005b) Eurocode 3: design of steel structures - Part 1-8: design of joints. EN 1993-1-8. Brussels, Belgium
- FEMA 461 (2007) Interim Testing Protocols for Determining the Seismic Performance Characteristics of Structural and Nonstructural Components. Redwood City, California, USA
- Furukawa S, Sato E, Shi Y, Becker T, Nakashima M (2013) Full-scale shaking table test of a base-isolated medical facility subjected to vertical motions. *Earthquake Engineering & Structural Dynamics* 42 (13):1931-1949. doi:10.1002/eqe.2305
- Krawinkler H, Parisi F, Ibarra L, Ayoub A, Medina R (2001) Development of a Testing Protocol for Wood Frame Structures. CUREE Publication No. W-02, Consortium of Universities for Research in Earthquake Engineering, Richmond, CA, USA
- Kuo K-C, Suzuki Y, Katsuragi S, Yao GC (2011) Shake table tests on clutter levels of typical medicine shelves and contents subjected to earthquakes. *Earthquake Engineering & Structural Dynamics* 40 (12):1367-1386. doi:10.1002/eqe.1094
- Lee TH, Kato M, Matsumiya T, Suita K, Nakashima M (2007) Seismic performance evaluation of non-structural components: Drywall partitions. *Earthquake Engineering & Structural Dynamics* 36 (3):367-382. doi:10.1002/eqe.638

- Lilliefors HW (1967) On the Kolmogorov-Smirnov Test for Normality with Mean and Variance Unknown. *Journal of the American Statistical Association* 62 (318):399-402. doi:10.2307/2283970
- Magliulo G, Ercolino M, Manfredi G (2013) Influence of cladding panels on the dynamic behavior of one-story precast buildings. *Earthquake Engineering & Structural Dynamics*:(under review)
- Magliulo G, Maddaloni G, Cosenza E (2012a) Extension of N2 method to plan irregular buildings considering accidental eccentricity. *Soil Dynamics and Earthquake Engineering* 43 (1):69-84. doi:10.1016/j.soildyn.2012.07.032
- Magliulo G, Pentangelo V, Maddaloni G, Capozzi V, Petrone C, Lopez P, Talamonti R, Manfredi G (2012b) Shake table tests for seismic assessment of suspended continuous ceilings. *Bulletin of Earthquake Engineering* 10 (6):1819-1832. doi:10.1007/s10518-012-9383-6
- Magliulo G, Petrone C, Capozzi V, Maddaloni G, Lopez P, Manfredi G (2014) Seismic performance evaluation of plasterboard partitions via shake table tests. *Bulletin of Earthquake Engineering*:(online first). doi:10.1007/s10518-013-9567-8
- Magliulo G, Petrone C, Capozzi V, Maddaloni G, Lopez P, Talamonti R, Manfredi G (2012c) Shake Table Tests on Infill Plasterboard Partitions. *The Open Construction and Building Technology Journal* 6 (Suppl 1-M10):155-163. doi:10.2174/1874836801206010155
- Porter K, Kennedy R, Bachman R (2006) Developing Fragility Functions for Building Components for ATC-58. A Report to ATC-58. Applied Technology Council, Redwood City, CA, US
- Porter K, Kennedy R, Bachman R (2007) Creating Fragility Functions for Performance-Based Earthquake Engineering. *Earthquake Spectra* 23 (2):471-489. doi:10.1193/1.2720892
- Restrepo JI, Bersofsky AM (2011) Performance characteristics of light gage steel stud partition walls. *Thin-Walled Structures* 49 (2):317-324. doi:10.1016/j.tws.2010.10.001
- Restrepo JI, Lang AF (2011) Study of Loading Protocols in Light-Gauge Stud Partition Walls. *Earthquake Spectra* 27 (4):1169-1185. doi:10.1193/1.3651608
- Retamales R, Davies R, Mosqueda G, Filiatrault A (2013) Experimental Seismic Fragility of Cold-Formed Steel Framed Gypsum Partition Walls. *Journal of Structural Engineering* 139 (8):1285-1293. doi:10.1061/(ASCE)ST.1943-541X.0000657
- Tasligedik AS, Pampanin S, Palermo A (2012) Damage states and cyclic behaviour of drywalls infilled within rc frames. *Bulletin of the New Zealand Society for Earthquake Engineering* 45 (2):84-94

2.5 SHAKE TABLE TEST ON PLASTERBOARD CONTINUOUS CEILINGS

After an earthquake, the failure of suspended ceiling systems is one of the most widely reported types of nonstructural damage in building structures. Since suspended ceiling systems are not amenable to traditional structural analysis, full-scale experimental testing is planned and executed. In particular, shaking table tests are performed in order to investigate the seismic behavior of plasterboard continuous suspended ceilings under strong earthquakes (Magliulo et al., 2012). Two kinds of ceiling systems, named single frame ceiling (SFC) and double frame ceiling (DFC), are tested. A steel test frame is properly designed in order to simulate the seismic effects at a generic building story. A set of five accelerograms, used as input for the shakings, are selected matching the target response spectrum provided by the U.S. code for nonstructural components. Three limit states (occupancy, damage and life safety limit state) are considered in this study in order to characterize the seismic response of suspended ceiling systems. The tested ceilings show no damage at all intensity levels, evidencing a low fragility. Three main aspects may be the cause of this low vulnerability: (a) the continuous nature of the tested ceilings; (b) the dense steel channel grid that supports the plasterboard panels; (c) the large number of hangers that connects the ceiling system to the roof, avoiding any vertical movement of the ceilings.

Finally, an interesting comparison is made with a previous vulnerability study on a different typical U.S. ceiling system.

2.5.1 INTRODUCTION

The failure of ceiling systems has been one of the most widely reported types of nonstructural damage in building structures during past earthquakes (Badillo-Almaraz et al., 2006; Gilani et al., 2010). The recent L'Aquila earthquake, occurred on April the 6th, 2009, in central Italy, has widely confirmed the last assertion: the majority of the evacuated buildings showed undamaged structural elements and moderate-to-heavy damaged nonstructural components, especially ceiling systems (Magliulo et al., 2009).

Limited studies were conducted in the past on the performance evaluation of ceiling systems. In particular since 1980s and 1990s few research studies were conducted on typical ceiling systems, dynamically excited with real and artificial strong-motion (ANCO Engineers Inc., 1983, 1993; Rihal and Granneman, 1984; Yao, 2000). An extensive study aiming at evaluating the fragility curve of a ceiling system composed of tiles supported by metallic grids was carried out in Buffalo via shaking table test (Badillo-Almaraz et al., 2007; Gilani et al., 2010). The influence of some innovative devices, such as the use of retainer clips and compression posts, on system fragility

was investigated; the difference between normal and undersized tiles was also addressed. A typical fragility curve for the ceiling systems is also reported in Miranda et al. (2004). The interaction between plasterboard partitions and continuous ceilings was studied in McCormick et al. (2008) via unidirectional horizontal shake table tests; this ceiling typology demonstrated an excellent performance up to very large interstory drifts (0.03rad) and accelerations (2.1g). In Maddaloni et al. (2011) ceiling tests are discussed, presenting a procedure for the best simulation of floor response spectra in shake table experiments.

In this study, the seismic behavior of plasterboard continuous suspended ceilings under strong earthquakes is investigated. The ceiling system differs from the systems of the most of the previous studies due to its “continuous” nature: it consists of a unique plasterboard panel obtained by connecting few boards to each other. The vulnerability evaluation of this particular plasterboard ceiling system is the main goal of the research. This aim is pursued via shake table tests: this experimental facility is particularly needed in this case. Indeed, since analytical methods are not easily applicable to nonstructural components, such as ceilings, and data from past earthquakes are not suitable for the characterization of the fragility, the most appropriate technique to evaluate the fragility of such systems is the experimental method. A comparison with tests on a U.S. common ceiling system is also presented.

2.5.2 EXPERIMENTAL FACILITIES AND TEST SET UP, SPECIMENS AND INPUT

The shaking table tests, performed in order to investigate the seismic behavior of plasterboard continuous suspended ceilings, are carried out at the laboratory of the Structural Engineering Department of the University of Naples Federico II.

Two typologies of plasterboard continuous suspended ceilings are tested: single frame ceiling (SFC) and double frame ceiling (DFC) systems. A schematic representation of the two systems is shown in Figure 92. The main components of tested suspended ceiling systems are: the “primary channel”, C steel section profiles spaced at 500 mm and 1000 mm for SFC and DFC systems, respectively; the “secondary channel”, C steel section profiles spaced at 500 mm for DFC system; the “perimetral channel”, U steel section profiles laterally restraining the ceiling (used for SFC and DFC systems); the “hangers”, pinned bars, spaced every 1000 mm (500 mm orthogonally to the primary channel direction in SFC), that links the steel grid (made of only primary channel (SFC) or primary and secondary channels (DFC)) with the roof, 200 mm or 500 mm long for SFC and DFC respectively; the “plasterboards”, gypsum panels properly sized and horizontally jointed, weighing 89 N/m².

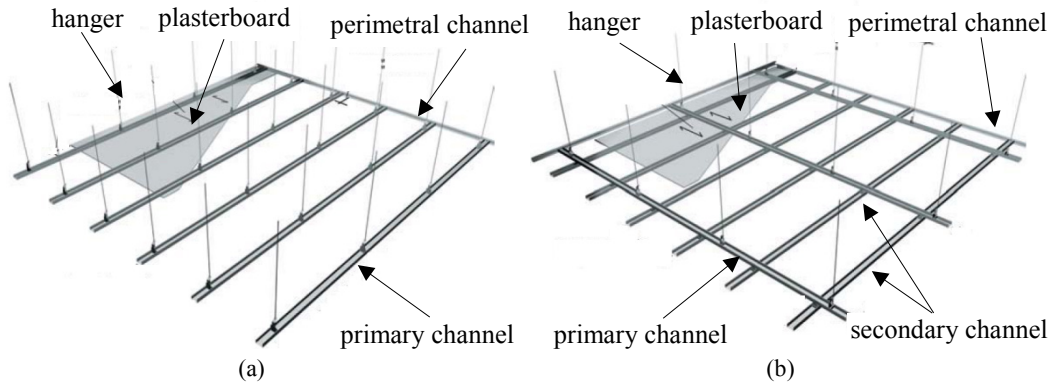


Figure 92. Suspended plasterboard continuous ceilings: (a) single frame ceiling (SFC); (b) double frame ceiling (DFC).

2.5.2.1 TEST SETUP AND SPECIMENS

The seismic qualification of a suspended ceiling is carried out by the earthquake simulator system available at the laboratory of Structural Engineering Department of University of Naples Federico II. The system consists of two 3 m x 3 m square shake tables. Each table is characterized by two degrees of freedom in the two horizontal directions. The maximum payload of each shake table is 200 kN with a frequency range of 0 - 50 Hz, acceleration peak equal to 1 g, velocity peak equal to 1 m/sec and total displacement equal to 500 mm (± 250 mm). Only one shake table is used in this experimental campaign.

A steel test frame is properly designed and built (Figure 93) with the purpose of simulating the seismic effects on the ceilings. The geometry of the test frame is defined taking into account two requirements: (a) a low fundamental period, outside of the range of frequencies of nonstructural components range (i.e. about 1 - 33 Hz, see ICBO, 2000) in order to avoid resonance problems: indeed, the tested ceiling system is excited by the acceleration time history that occurs on plasterboard perimeter, which can be strongly influenced by the flexibility of the test frame (Gilani et al., 2010); (b) height of the specimen sufficient in order to facilitate its assembly. The result is a 2.42 m (X dir.) x 2.71 m (Y dir.) x 2.72 (Z dir.) test structure of S275 steel material with concentric V-bracings (see Figure 93). The test frame presents rolled H-shaped columns (HE220A profile) and beams (HE180A profile); the connections are bolted. A horizontal frame made of U-section steel profiles (UPN100) is bolted to the beams of the test frame (HE180A), as shown in Figure 93a, in order to allow the anchorage of the ceiling system to the roof. As mentioned earlier, concentric V-bracing systems are placed as shown in Figure 93b and c, in order to strongly stiffen the structure; bracing systems are made of steel U-section (UPN160). Two U-section profiles (UPN100) are

welded around the perimeter of the test frame, at a distance of 20 cm and 50 cm from the roof; a 40 mm x 100 mm timber ledger is inserted in the U-section profile in order to easily laterally restrain the ceiling system. Indeed, the plasterboards of the ceiling are connected by a perimeter U-section runner to the timber ledger. Consequently, the light mass and the large stiffness of the timber-channel profiles system represent the typical boundary conditions of a ceiling on structural elements.

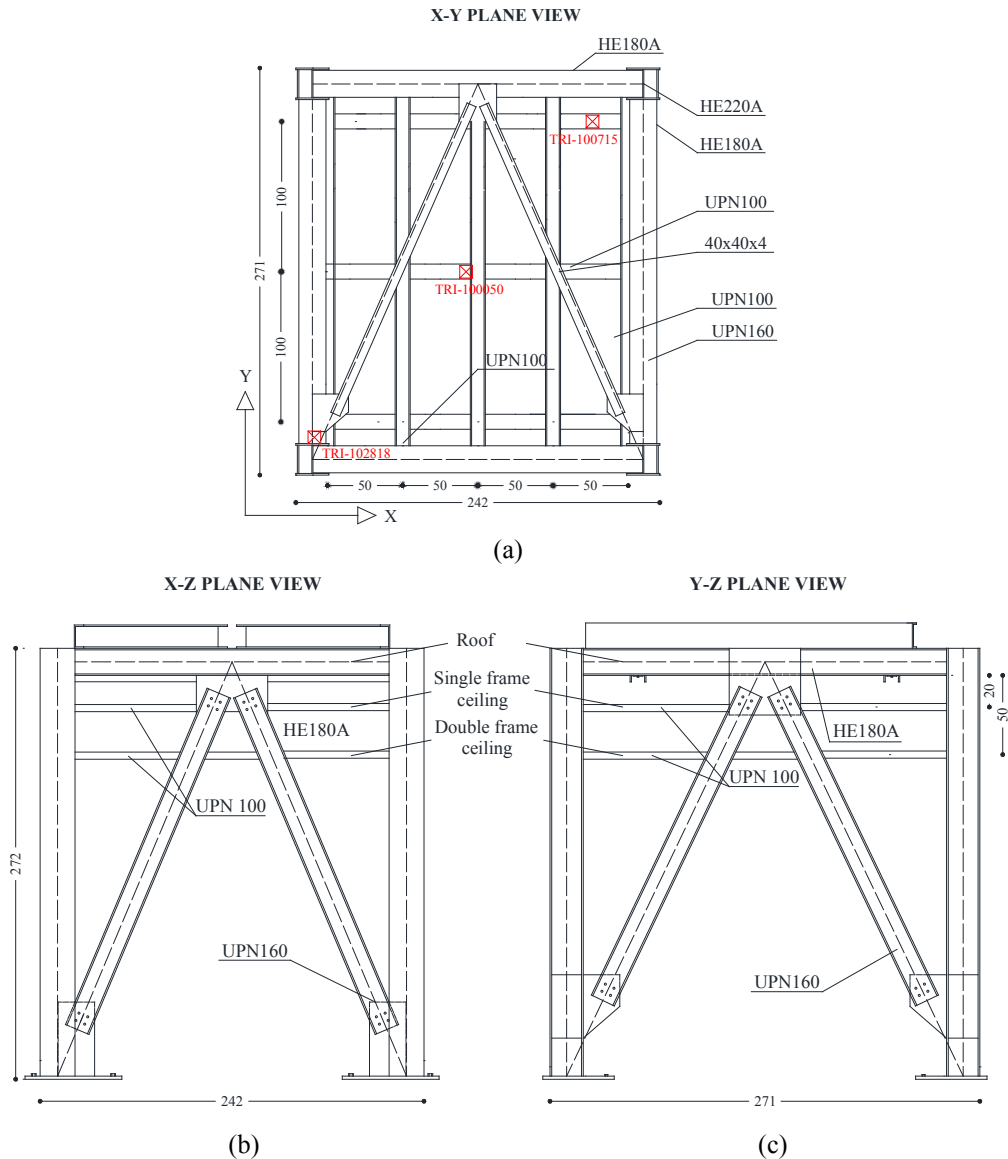


Figure 93. Technical scheme of the test setup: (a) plan view, (b) and (c) lateral views.

A FEM model of the test frame is assembled by means of the computer program SAP2000 (CSI Computer & Structures Inc., 2004). Each element of the test frame is implemented as elastic “beam” finite element. The FEM model is implemented in order to perform the analysis and to obtain an estimation of the first period along both orthogonal directions of the test frame: along X direction it is 0.02s, along Y direction it is 0.018s. The test frame is designed according to Eurocode 3 (CEN, 2005a, b) and Eurocode 8 (CEN, 2004) provisions by elastic modal response spectrum analysis. The total weight of the test frame is equal to 19.2 kN. In Figure 94 a picture of the installed final setup on the shake table is shown.

The tested specimen is composed by three plasterboards connected one another via stucco, both for SFC and DFC (see Figure 94b and Figure 95). The total dimension of the specimen is 2.20 m x 2.20 m.



Figure 94. (a) Test frame installed on the shake table; (b) SFC specimen detail.

2.5.2.2 INSTRUMENTATION

Accelerometers and strain gauges are used to monitor the response of the test frame and plasterboard ceilings in both ceiling system configurations.

Three strain gauges are installed in SFC tests in order to monitor deformations in the above mentioned perimetral channel (SG1) and in the plasterboard panels (SG2, SG3). Two additional strain gauges are adopted in DFC tests, in order to measure the primary (SG4) and secondary (SG5) channels stress level.

In order to adequately measure roof rigid rotation and unexpected relative displacements, three triaxial accelerometers (named TRI-100050, TRI-102818, TRI-100715) are installed at the center (TRI-100050) and at the edges of the roof (TRI-102818, TRI-100715).

In Figure 95 the position of other three accelerometers is indicated. In particular, for both tests performed on single and double frame ceiling systems, one accelerometer is

placed on the top side of the plasterboard (TRI-103765), one on the “primary channel” steel profile (TRI-103763) and one on the “perimetral channel” steel profile (TRI-103762). One triaxial accelerometer is also placed at the base of the frame, in order to verify the real input transmitted to the specimen from the shaking table.

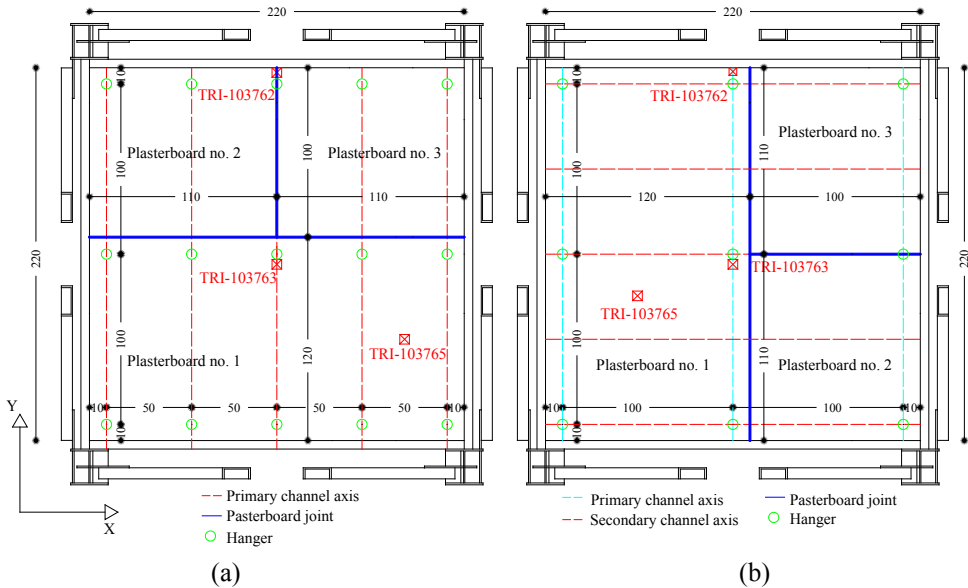


Figure 95. Triaxial accelerometers, plasterboard and hanger position in the case of single frame ceiling (a) and double frame ceiling (b) specimen.

2.5.2.3 INPUT AND TESTING PROTOCOL

In order to investigate the seismic behavior of plasterboard continuous suspended ceilings, a set of five accelerograms, used as input for the shakings in Y direction (see Figure 93), are specifically selected to match a target response spectrum, as provided by the ICBO-AC156 code “Acceptance criteria for seismic qualification testing of nonstructural components” (International Conference of Building Officials (ICBO), 2000).

The first step consists in the definition of the target spectrum or required response spectrum (RRS). According to ICBO, the RRS is obtained as a function of the design spectral response acceleration at short periods, S_{DS} , depending on the site soil condition and the mapped maximum earthquake spectral acceleration at short periods (for more details see section 6.5 in ICBO-AC156). The procedure is performed for a Required Response Spectrum corresponding to $S_{DS}=1.50g$. In details, as recommended by the AC156 code procedure, a baseline signal is defined starting from non-stationary broadband random excitations having an energy content ranging from 1.3 to 33.3 Hz and one-sixth-octave bandwidth resolution. The total length of the input motion is 30

seconds. Then, the signal is enhanced by introducing wavelets using the spectrum-matching procedure of the RSP Match program (Hancock et al., 2006). The matching is obtained when, over the frequency range from 1.3 to 33.3 Hz, the elastic response spectrum ordinates are not lower than the RRS ordinates by more than 10 percent and do not exceed the RRS ordinates by more than 30 percent. In order to obtain a drive motion compatible with the shaking table velocity and displacement limits, the so obtained matched record is driven through a high pass filter for frequencies larger than 1.0 Hz.

Figure 96 shows the obtained acceleration time history, its elastic response spectrum, namely the test response spectrum (TRS), the RRS corresponding to S_{DS} equal to 1.50g and the RRS scaled to 90% and 130%.

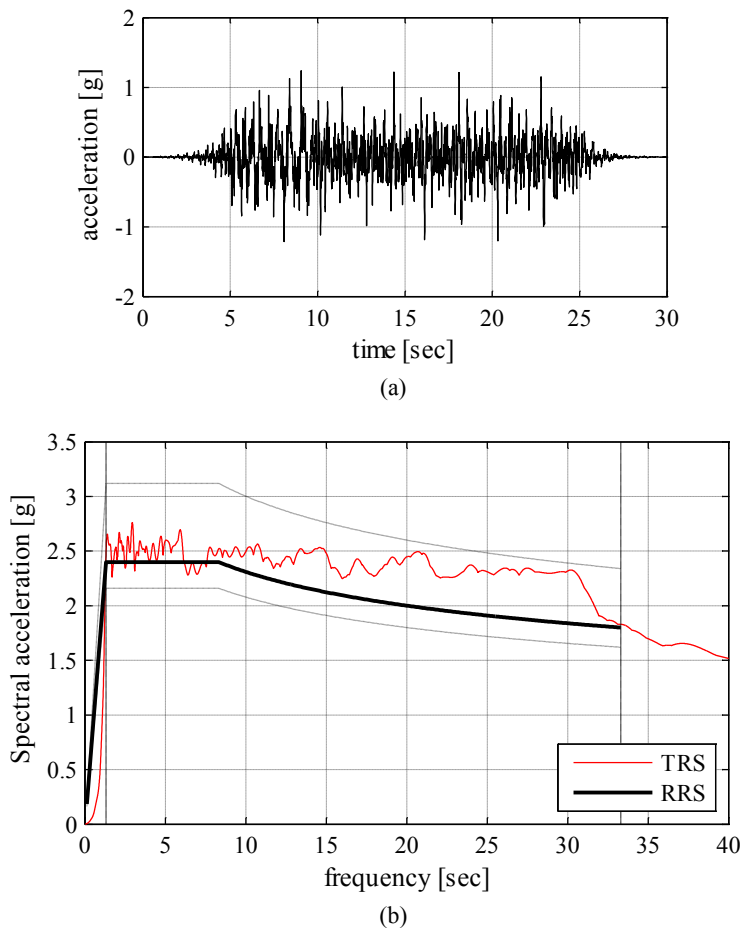


Figure 96. Earthquake time history and spectra for a level of shaking corresponding to S_{DS} equal to 1.50g: (a) acceleration time-history; (b) input accelerogram spectrum (TRS), RRS (bold line), upper and lower matching limits (dashed line).

The procedure is performed, as mentioned, for a RRS corresponding to $S_{DS}=1.50g$; the so obtained record is then scaled to match other four levels of the target spectrum (corresponding to S_{DS} 0.30g, 0.60g, 0.90g and 1.20g). The range of S_{DS} corresponds to peak ground accelerations from 0.12g to 0.60g on stiff soil, representative of low-to-high seismic zones.

2.5.3 RESULTS, COMPARISONS AND OBSERVATIONS

In order to define the experimental fundamental period in the Y direction of shaking, a dynamic identification procedure is performed using a white noise test. A frequency value of about 30 Hz, i.e. 0.03 s, is obtained; it is close to the numerical results and confirms the high stiffness of the test frame. This feature, in addition to the test frame-to-ceiling rigid connection and the ceiling in-plane stiffness, causes, as desired, an acceleration on the ceiling (Table 31 and Table 32) close to the horizontal spectral acceleration for rigid equipment, i.e. A_{RIG} in AC 156. Indeed, continuous ceiling systems can be classified as rigid nonstructural components ($16.7 \text{ Hz} < f < 33.3 \text{ Hz}$) in the horizontal direction.

Using the selected drive motions, five unidirectional shaking tests along Y direction (see Figure 93) are performed for both ceiling systems. In Table 31 and Table 32 the maximum recorded acceleration values on the ceilings and on the test frame roof are listed and compared to the maximum acceleration registered at the base of the shake table. This comparison is done both for single (Table 31) and for double frame ceiling (Table 32). Values greater than 2.0g, due to dynamic amplifications in the specimen, are recorded on the ceiling. As known, usually, the signal recorded at desired locations is completely different from the expected effect of shake table motion. The dynamic amplification aspect may be crucial when the build of a fragility curve is the main goal of the research since the values of acceleration recorded on the component can be not predict before the test is performed. For this reason, the procedure described in Maddaloni et al. (2011), concerning the optimization of the drive motion to predict the signal recorded at desired locations, i.e. on the ceilings, using a compensation procedure, will be taken into account in the next experimental campaigns.

2.5 Shake table test on plasterboard continuous ceilings

<u>Position</u>	<u>Ceiling</u>				<u>Roof</u>		<u>Base</u>
<u>Accel. No.</u>	<u>103763</u>	<u>103762</u>	<u>103765</u>	<u>100050</u>	<u>100715</u>	<u>102818</u>	<u>103766</u>
<u>test no. 1</u>	0.42g	0.40g	0.42g	0.45g	0.42g	0.41g	0.25g
<u>test no. 2</u>	0.78g	0.78g	0.75g	0.78g	0.74g	0.78g	0.50g
<u>test no. 3</u>	1.10g	1.04g	1.02g	1.15g	1.04g	1.18g	0.69g
<u>test no. 4</u>	1.75g	1.79g	1.66g	1.90g	1.70g	1.93g	1.04g
<u>test no. 5</u>	2.28g	2.28g	2.19g	2.51g	2.22g	2.48g	1.36g

Table 31. Maximum recorded accelerations on the specimen (*Ceiling*), test frame top (*Roof*) and at the shake table level (*Base*) as indicated in Figure 93: single frame ceiling test.

<u>Position</u>	<u>Ceiling</u>				<u>Roof</u>		<u>Base</u>
<u>Accel. No.</u>	<u>103763</u>	<u>103762</u>	<u>103765</u>	<u>100050</u>	<u>100715</u>	<u>102818</u>	<u>103766</u>
<u>test no. 1</u>	0.42g	0.42g	0.42g	0.46g	0.43g	0.42g	0.28g
<u>test no. 2</u>	0.68g	0.69g	0.69g	0.75g	0.68g	0.74g	0.52g
<u>test no. 3</u>	1.07g	1.06g	1.05g	1.17g	1.11g	1.18g	0.75g
<u>test no. 4</u>	1.84g	1.77g	1.85g	2.06g	1.81g	2.03g	1.06g
<u>test no. 5</u>	2.29g	2.36g	2.25g	2.58g	2.36g	2.52g	1.35g

Table 32. Maximum recorded accelerations on the specimen (*Ceiling*), test frame top (*Roof*) and at the shake table level (*Base*) as indicated in Figure 93: double frame ceiling test.

The compatibility of the achieved shaking table motions with the RRS is almost guaranteed for the frequency range 1.3 - 33.3 Hz. In Figure 97, the accelerogram spectra, recorded at the base of the test frame, for single and double frame ceiling tests are compared with the RRS corresponding to S_{DS} equal to 1.50g.

The acceleration amplification from the base to the roof of the test frame is within the expected behavior of the test, as it was predicted from the spectra in Figure 96 for the natural frequency of the test frame, i.e. the spectral acceleration around 30 Hz is very close to the maximum recorded acceleration. No amplification from the test frame roof to the ceiling system is recorded, as clearly shown in Table 31 and Table 32, denoting the large in-plane stiffness of the ceiling system and the substantial rigid behavior of the specimen.

In this study, three limit states are considered in order to characterize the seismic response of suspended ceiling systems: (a) occupancy limit state SLO; (b) damage limit state SLD; (c) life safety limit state SLV. The limit states are defined quantitatively by the number of damaged components (indicated as percentage of damage). From the first to the third considered limit states the damage in the ceiling increases (10%, 30% and 50% damage respectively).

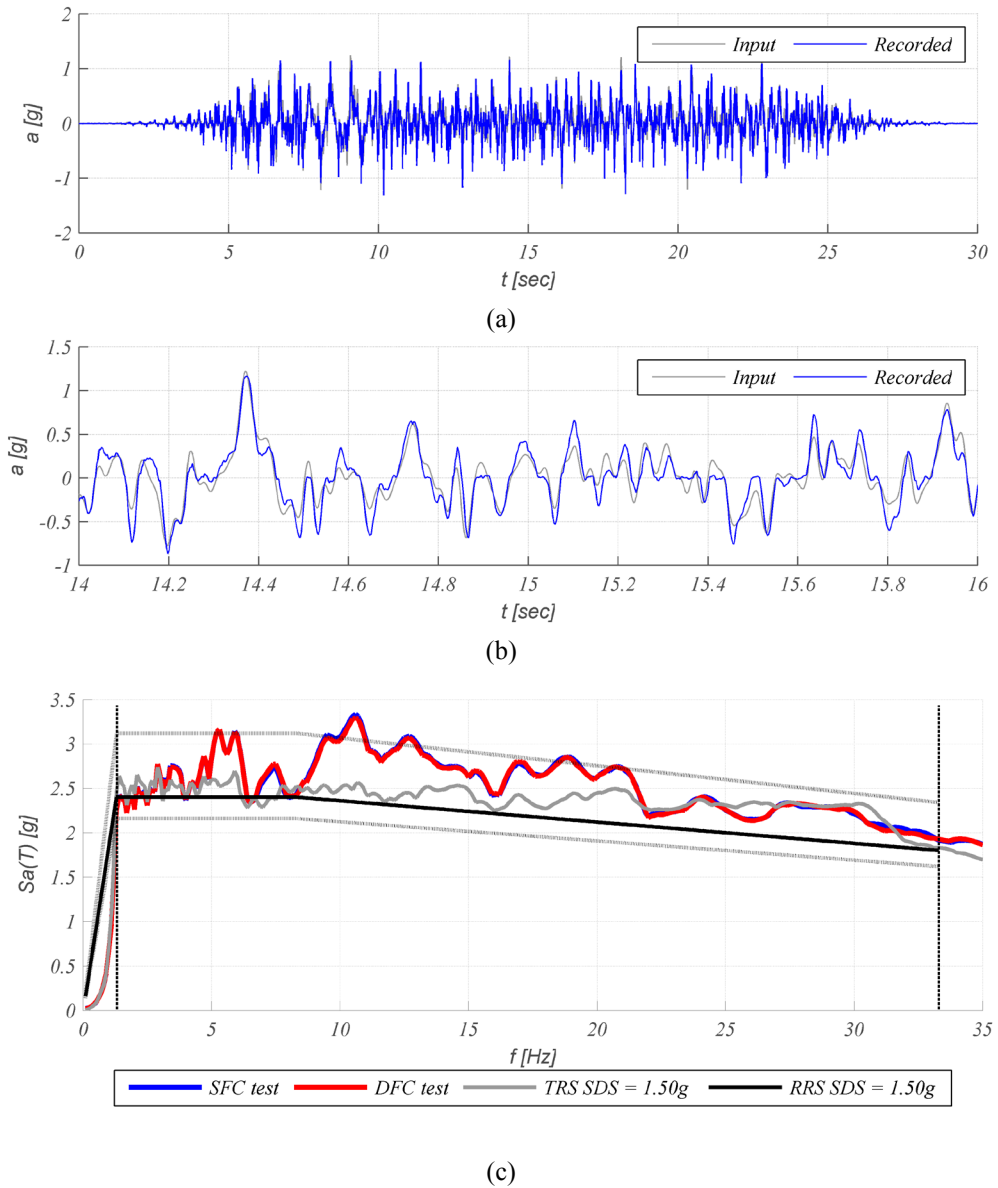


Figure 97. Tests corresponding to S_{DS} equal to 1.50g: shake table recorded acceleration time histories (a) zoomed in a 2 sec time range (b) for single frame ceiling tests compared to the shake table input; spectra for single frame (SFC) and double frame ceiling (DFC) compared to the RRS and the TRS (c).

After each shaking level, damage is observed by inspecting the physical conditions of the components. Concerning the main components of the SFC system (primary and perimetral channels, hangers, plasterboards panels and connections), the number of damaged elements observed during the test performed with intensity level S_{DS} equal to

1.50g, is indicated in Table 33. The table also reports for each component the total number of elements for the single frame ceiling system, the damage typology and the limit number of damaged elements required to reach a limit state.

As clearly shown in the Table 33, no damage is recorded, though the high level of horizontal accelerations experienced. The same result is obtained for double frame ceiling system. Strain gauges data confirm this statement: low strain/stress values are registered during the earthquake motion within the ceiling system (Figure 98).

Indeed, the strain gauges described in section 2.2 recorded deformations lower than 0.005% resulting in a undamaged state both in steel channels and in plasterboards; as expected, the demand in SFC plasterboards is larger than DFC ones (see SG3 in Figure 98 (b) and (c)) as well as the demand in the perimetral profile; this is due to the fact that SFC plasterboards are restrained by a less dense horizontal steel channel frame and that in DFC the stresses are better distributed along the perimetral channels, respectively. However both DFC and SFC exhibit an excellent seismic behavior.

Elements	Number	Damage	SLO (10%)	SLD (30%)	SLV (50%)	Damaged elements
Hangers	15		2	5	8	0
Primary channels	5	buckling	1	2	3	0
		bending				0
Perimetral channels	4	buckling	1	1	2	0
		bending				0
Plasterboard-channel connections (screws)	87	shear	9	26	43	0
		tension				0
		punching shear				0
Plasterboards	3	collapse	-	-	1	0

Table 33. Form for recording damage observed during the test performed on single frame ceiling with intensity level S_{DS} equal to 1.50g.

An interesting comparison with a previous vulnerability study performed by Badillo-Almaraz et al. (2006) on typical U.S. ceiling with tiles, shown in Figure 99, is made. The tests were performed at the Structural Engineering and Earthquake Simulation Laboratory (SEESL) at the University of Buffalo. A 4.88 m x 4.88 m (16 ft x 16 ft) square test fixture of ASTM Grade 50 steel was constructed in order to test the ceiling systems.

The test fixture was designed in order to simulate one story and one bay of a building with vertical floor frequencies in the range of 9 Hz to 12 Hz and horizontal frequencies in the range of 10 Hz to 16 Hz. Four limits states were defined in order to characterize the seismic response of ceiling systems: (1) minor damage, (2) moderate damage, (3) major damage, and (4) grid failure. Limit states from (1) to (3) are defined upon the

percentage of tiles that fell from the suspended grid; limit state (4) is associated with structural damage to the suspension grid.

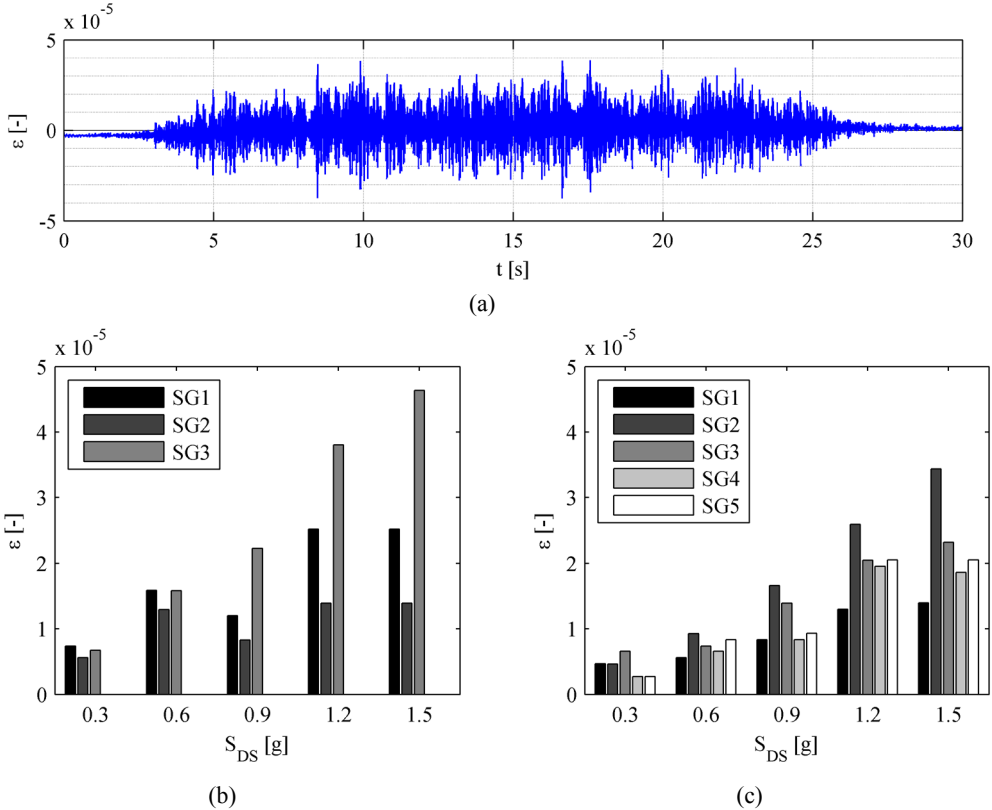


Figure 98. Tests corresponding to SDS equal to 1.50g: deformation time history recorded by SG3 in single frame ceiling test (a); maximum deformations recorded by strain gauges in (b) SFC tests and (c) DFC tests.

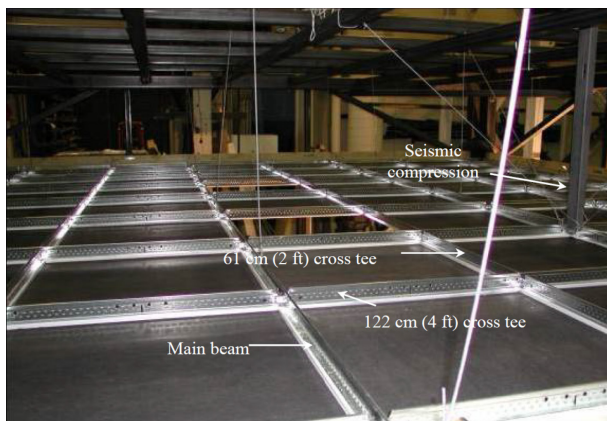


Figure 99. Ceiling with undersized tiles (Badillo-Almaraz et al., 2007).

In order to make a comparison, the fragility curve for ceilings with undersized tiles (Badillo-Almaraz et al., 2007) in terms of peak floor acceleration (PFA) is considered (Figure 100). This fragility curve, evaluated for the maximum acceleration induced by the shaking table in Naples, i.e. 1.35 g, gives almost 100% probability of exceeding minor and moderate damage state and 29% probability of exceeding major damage state.

As already reported, the ceilings tested in Naples, instead, show no damage at all intensity levels of the tests, resulting in a lower fragility with respect to the ceiling systems tested in Buffalo. Three main reasons may be the cause of this different vulnerability: (a) the continuous nature of the tested ceiling, that improves the seismic behavior with respect to the ceilings with tiles; (b) the dense steel channel grid (the “primary channel” span is 500 mm and 1000 mm for SFC and DFC systems respectively, the “secondary channel” span is 500 mm for DFC system), that connects one another the plasterboards in a unique horizontal element, ensuring high in-plane stiffness and strength; (c) the large number of hangers that connect the ceiling system to the roof, ensuring an adequate out of plane stiffness and strength, avoiding any ceiling vertical movement; (d) the smaller dimensions of the specimen tested in Naples with respect to the specimen tested in Buffalo (2.20m x 2.20m vs 4.88m x 4.88m), considering that very recent studies seem to show that specimen dimensions can affect the ceiling seismic response.

In test campaign developed in Naples, the issue of scaling is also considered; however this procedure is assessed to be inadequate for this research study, since the behavior of the specimen is very sensitive to details, such as the connections and the interactions between the different subcomponents.

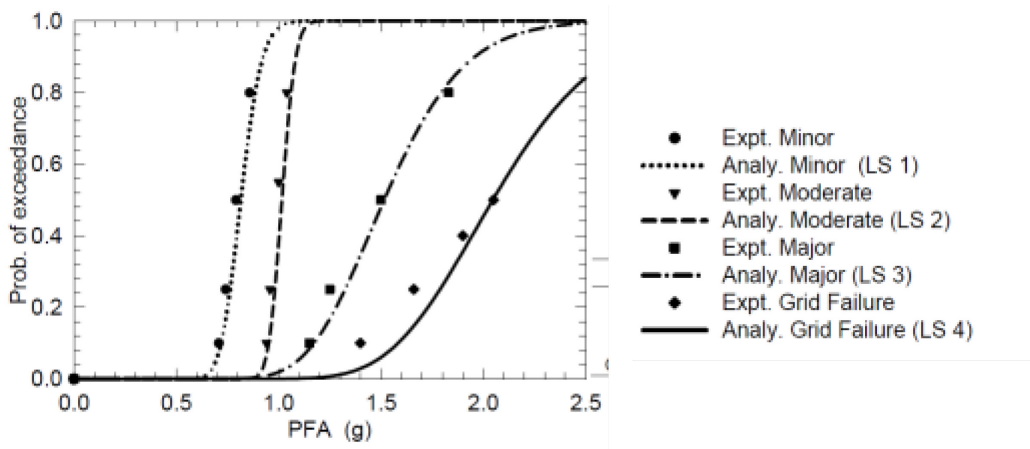


Figure 100. Ceiling fragility curve: ceiling with undersized tiles (Badillo-Almaraz et al. 2007).

The tests described in section 2.5.2 are performed shaking the table only in the horizontal Y direction. No vertical excitation is applied to the specimen. For the tested continuous ceiling systems, this component is not assumed as crucial. Indeed, the continuous plasterboard is connected to the roof with many vertical steel hangers (span is equal to 1 m along both the horizontal directions) with a sufficient axial stiffness (for steel hanger design, a safety factor larger than 3 is considered). Hence, no failure due to earthquake vertical component is expected.

The boundary conditions adopted in this test campaign may not be representative of a real case. The rigid restraint may not be representative if the partitions/infills, which the ceiling is connected to, overturn or deform differently one another, causing additional stresses within the ceiling. This problem is particularly emphasized when two different typologies of partition/infill restrain the ceiling: due to their different nature, they could deform asynchronously, producing large stresses within the ceiling. However, the boundary condition proposed in this research is realistic: it is representative of partitions/infills that do not exhibit significant relative displacements with respect to the structure they are installed in.

2.5.4 CONCLUSIONS

The tests performed on shaking table show, for both of the tested ceiling systems, no damage at all intensity levels, resulting in a low fragility. Three main reasons may be the cause of this low fragility: (a) the continuous nature of the tested ceilings; (b) the dense steel channel grid; (c) the large number of hangers that connects the ceiling system to the roof and provides a restraint in out-of-plane direction, avoiding any ceiling vertical movement.

This study on ceiling systems was carried out without considering any interaction with other components; further studies are needed to investigate this phenomenon, which represents the next step of this research.

Finally, an interesting comparison with a previous vulnerability study performed by Badillo-Almaraz et al. in 2007 on typical U.S. ceiling system with tiles was performed. The comparison points out the lower fragility of continuous plasterboard ceiling systems, tested in Naples, with respect to the ceiling with tiles systems, tested in the U.S.; however, this conclusion could be influenced by the smaller dimensions of the specimen tested in Naples with respect to the specimen tested in Buffalo.

2.5.5 REFERENCES

ANCO Engineers Inc. (1983) Seismic Hazard Assessment of Nonstructural Ceiling Components. NSF Rep. No. CEE-8114155. Culver City, CA, USA

- ANCO Engineers Inc. (1993) Earthquake testing of a suspended ceiling system. Culver City, CA, USA
- Badillo-Almaraz H, Whittaker AS, Reinhorn A, Cimellaro GP (2006) Seismic Fragility of Suspended Ceiling Systems, Report MCEER-06-0001. MCEER/SUNY/Buffalo
- Badillo-Almaraz H, Whittaker AS, Reinhorn AM (2007) Seismic fragility of suspended ceiling systems. *Earthquake Spectra* 23 (1):21-40. doi:10.1193/1.2357626
- CEN (2004) Eurocode 8: design of structures for earthquake resistance - Part 1: general rules, seismic actions and rules for buildings. EN 1998-1. Brussels, Belgium.
- CEN (2005a) Eurocode 3: design of steel structures - Part 1-1: General rules and rules for buildings. EN 1993-1-1. Brussels, Belgium
- CEN (2005b) Eurocode 3: design of steel structures - Part 1-8: design of joints. EN 1993-1-8. Brussels, Belgium
- CSI Computer & Structures Inc. (2004) SAP2000. Linear and Nonlinear Static and Dynamic Analysis of Three-Dimensional Structures, Computer & Structures, Inc. Berkeley, California
- Gilani A, Reinhorn A, Glasgow B, Lavan O, Miyamoto H (2010) Earthquake Simulator Testing and Seismic Evaluation of Suspended Ceilings. *Journal of Architectural Engineering* 16 (2):63-73. doi:10.1061/(ASCE)1076-0431(2010)16:2(63)
- Hancock J, Watson-Lamprey J, Abrahamson NA, Bommer JJ, Markatis A, McCoyh E, Mendis R (2006) An improved method of matching response spectra of recorded earthquake ground motion using wavelets. *Journal of Earthquake Engineering* 10 (sup001):67-89. doi:10.1080/13632460609350629
- International Conference of Building Officials (ICBO) (2000) AC 156 Acceptance Criteria for the Seismic Qualification of Nonstructural Components. ICBO Evaluation Service, Inc., Whittier, California, USA
- Maddaloni G, Ryu KP, Reinhorn AM (2011) Simulation of floor response spectra in shake table experiments. *Earthquake Engineering & Structural Dynamics* 40 (6):591-604. doi:10.1002/Eqe.1035
- Magliulo G, Pentangelo V, Maddaloni G, Capozzi V, Petrone C, Lopez P, Talamonti R, Manfredi G (2012) Shake table tests for seismic assessment of suspended continuous ceilings. *Bulletin of Earthquake Engineering* 10 (6):1819-1832. doi:10.1007/s10518-012-9383-6
- Magliulo G, Pentangelo V, Manfredi G (2009) Danneggiamento delle controsoffittature a seguito del terremoto dell'Aquila dell'aprile 2009 V1.00, available on <http://www.reluis.it> (in Italian).
- McCormick J, Matsuoka Y, Pan P, Nakashima M (2008) Evaluation of Non-Structural Partition Walls and Suspended Ceiling Systems through a Shake Table Study. In: Structures Congress 2008. pp 1-10. doi:doi:10.1061/41016(314)223
- Miranda E, Aslani H, Taghavi S Assessment of seismic performance in terms of economic losses. In: Bled '04 International workshop on performance-based seismic design, June 28–July 1, Bled, Slovenia, 2004.

- Rihal S, Granneman G (1984) Experimental Investigation of the Dynamic Behavior of Building Partitions and Suspended Ceilings During Earthquakes, Rep. No. ARCER84-1. California Polytechnic State University, Pomona, CA, USA
- Yao G (2000) Seismic Performance of Direct Hung Suspended Ceiling Systems. *Journal of Architectural Engineering* 6 (1):6-11. doi:doi:10.1061/(ASCE)1076-0431(2000)6:1(6)

Chapter 3 SEISMIC DEMAND ON NONSTRUCTURAL COMPONENTS

3.1 FLOOR RESPONSE SPECTRA IN RC FRAME STRUCTURES DESIGNED ACCORDING TO EUROCODE 8

A parametric study is conducted on five RC frame structures in order to evaluate the floor response spectra. The structures, designed according to Eurocode 8, are subjected to a set of earthquakes, compatible with the design response spectrum.

Time-history analyses are performed both on elastic and inelastic models of the considered structures. Eurocode formulation for the evaluation of the seismic demand on nonstructural components does not well fit the analytical results. Some comments on the target spectrum provided by AC 156 for the seismic qualification of nonstructural components are also included and a modification is proposed.

3.1.1 INTRODUCTION

Nonstructural components should be subjected to a careful and rational seismic design, in order to reduce the economic loss and to avoid threats to the life safety, as well as what concerns the structural elements. Nonstructural components are subjected to severe seismic actions due to the dynamic interaction with the primary system. The design of nonstructural components is based on the evaluation of the maximum inertia force, which is related to the floor spectral accelerations. Several research studies were conducted in the past concerning the evaluation of the floor acceleration and the floor response spectra.

Rodriguez et al. (2002) conducted an analytical investigation for the evaluation of the earthquake-induced floor horizontal accelerations in cantilever wall buildings built with rigid diaphragms. The following paragraph describes several methods prescribed by design standards and proposes a new method for deriving the design horizontal forces. Singh et al. (Singh et al., 2006b, a) proposed two methods for calculating the seismic design forces for flexible and rigid nonstructural components. The validity of

such methods was verified by comparing their floor response spectra with the ones obtained for an ensemble of earthquakes exciting several buildings with different numbers of stories. Sankaranarayanan and Medina (2007) evaluated the main factors that influence the variation of the floor response spectrum values caused by the inelasticity in the primary structure. Analyses were carried out on moment-resisting frame structures with 3, 6, 9, 12, 15, and 18 stories. It was found that the main factors that influence the “inelastic” floor response spectrum are the location of the NSC in the supporting structure, the periods of component and building, the damping ratio of the component, and the level of inelasticity of the supporting structure. The influence was evaluated through the assessment of an acceleration response modification factor, that addressed both the decrease and the increase in elastic floor response spectral values due to the yielding of the supporting structure. Wieser et al. (2013) analyzed a set of special moment resisting frame (SMRF) buildings using the incremental dynamic analysis procedure. They proposed an improved estimation for the PFA/PGA ratio by incorporating the elastic natural period of the structure and the expected level of ductility. Moreover, they debated the use of a constant component amplification factor and proposed an alternative design approach that directly amplifies the ground acceleration spectrum to achieve the desired floor acceleration spectrum.

Very limited studies were performed concerning the Eurocode 8 (CEN, 2004b) formulation for the evaluation of the floor spectral acceleration, according to which the seismic demand on a given nonstructural component is evaluated. Moreover, past studies were usually focused on steel buildings or wall structures. For this reason a set of benchmark RC frame structures are selected and designed according to Eurocode 8 (Petrone et al., 2014). Dynamic nonlinear analyses are performed on the benchmark structures in order to validate the Eurocode formulation; a set of accelerograms compatible with the Eurocode 8 design spectrum is defined. Dynamic analyses are performed both on elastic and inelastic models of the benchmark structures, in order to evaluate the influence of the inelasticity on the definition of the floor response spectrum. The floor response spectra are compared to Eurocode 8 formulation; some considerations on the peak floor acceleration and the maximum floor spectral acceleration are also given. Finally, some comments on the target spectrum provided by AC 156, for the seismic qualification of nonstructural components via shake table tests, are also performed and a modification is proposed.

3.1.2 METHODOLOGY

3.1.2.1 DESCRIPTION OF THE PARAMETRIC STUDY

A parametric study is conducted to investigate the seismic demand to which a light acceleration-sensitive nonstructural component may be subjected in multi-story RC frames. 2D frame structures are considered: they are representative of a tridimensional structure with a double symmetric plan and with three frames arranged in each direction (Figure 101 and Figure 102). Benchmark structures with different number of stories are considered: one-, two-, three-, five- and ten-story buildings, with a 3 m interstory height and two 5 m wide bays.

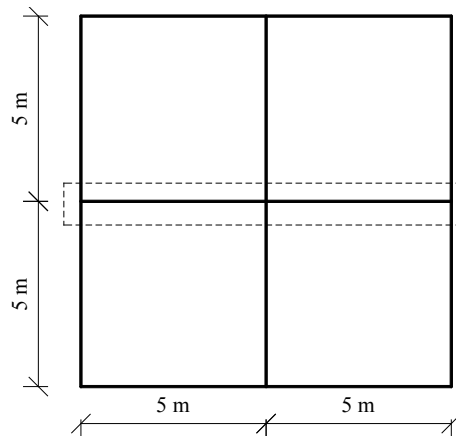


Figure 101. Plan view of the benchmark structures.

The benchmark structures are designed according to Eurocode 8 (EC8) (CEN, 2004b) provisions. A 0.25 g design ground acceleration a_g is considered. The horizontal elastic response spectrum is defined referring to a 5% damping ratio and to a 1.2 soil factor, i.e. soil type B.

The seismic design meets the ductility class “high” (DCH) requirements: the behavior factor is equal to 4.95 for one-story building and 5.85 for multi-story frames. The sizing of primary elements is strongly influenced, especially for tall structures, by the restricted value of normalized design axial force, i.e. the ratio between the average compressive stress and the concrete compression strength, which must not exceed 0.55. Moreover, the seismic detailing requirements in terms of longitudinal and transversal reinforcements provide an amount of reinforcement which is larger than the one strictly required by the design analysis. They produce high overstrength ratios which influence the structural response, as discussed in Section 3.1.2.4. A halved moment of inertia is considered for the primary elements during the design phase, according to EC8, in order to take into account the effect of cracking. The fundamental period of the

benchmark structures, evaluated according to such a “reduced” flexural stiffness, are listed in Figure 102.

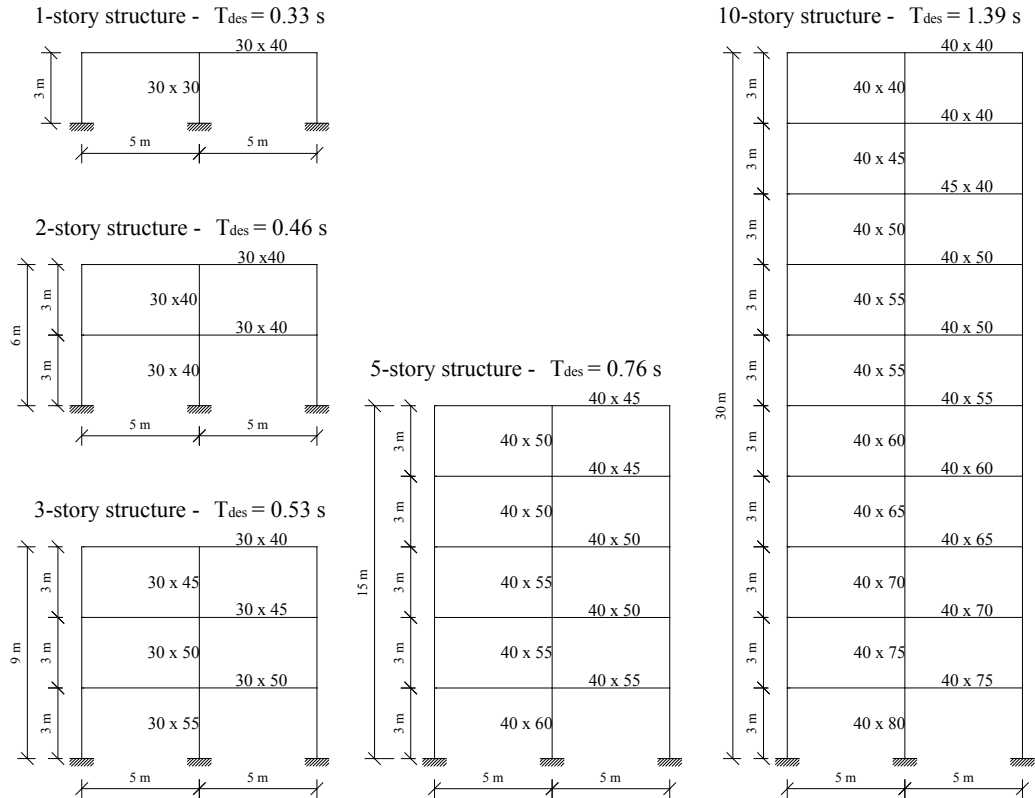


Figure 102. Lateral view of the considered building models and their design fundamental period (T_{des}). Dimensions of the cross sections are in [cm].

3.1.2.2 MODELING

Both elastic and inelastic structural responses are investigated. Dynamic analyses are carried out for a set of seven earthquake records, on both linear and nonlinear models. Rigid diaphragms are considered for each floor; a third of the seismic mass of the corresponding 3D building is assigned to a master joint at each floor. Analyses are performed using the OpenSees program (McKenna and Fenves, 2013).

The linear modeling provides that the primary elements are modeled as elastic beam-column elements with the gross moment of inertia. Concrete is modelled as an elastic material with a Modulus of Elasticity equal to 31476 MPa according to the C25/30 class concrete assumed during the design phase.

A lumped plasticity nonlinear approach is also considered: it is assumed that the primary elements have an elastic behavior and that any inelasticity source is lumped in

plastic hinges at their ends. Moment–rotation envelopes in the plastic hinges are defined according to the formulation suggested by Haselton (2006). The nonlinear behavior of the plastic hinges is defined by peak-oriented hysteretic rules, which simulate the modified Ibarra-Medina-Krawinkler (Ibarra et al., 2005) deterioration model. The cracking point is neglected, i.e. the initial stiffness is equal to the yielding secant stiffness. In order to determine the moment-curvature diagrams, appropriate cross sections are defined for each element considering the actual geometry and steel reinforcement. The cross section is divided into fibers and a stress-strain relationship is defined for each fiber. Different constitutive laws are applied to three different kinds of fibers: unconfined concrete law is associated to cover fibers, confined concrete law is associated to core fibers and steel law is associated to the longitudinal reinforcement fibers. The stress–strain relationship proposed by Mander et al. (1988) is used both for unconfined and confined concrete. The B450C steel class is adopted with a bilinear with hardening relationship. The steel mechanical characteristics are calculated according to Eurocode 2 (Table C.1, “Properties of reinforcement”) (CEN, 2004a). Table 34 shows the comparison between the first and second vibrational periods of each structure, which can be obtained with either the design-approximated stiffness assumption ($T_{i,des}$) or gross section elastic stiffness ($T_{i,el}$) or inelastic yielding secant stiffness ($T_{i,nl}$). The period range in Table 34 evidences the large uncertainty in the assessment of the structural period during the design phase. This range would have been even wider if the infill contribution to the lateral stiffness had been considered. It is especially valid in case of brick infills, widespread in the European area (Petrone et al., 2013).

No. story	$T_{i,des}$	$T_{i,el}$	$T_{i,nl}$	$T_{2,el}$	$T_{2,nl}$
[-]	[s]	[s]	[s]	[s]	[s]
1	0.33	0.23	0.42	-	-
2	0.46	0.32	0.64	0.11	0.22
3	0.53	0.37	0.78	0.14	0.26
5	0.76	0.52	1.11	0.18	0.37
10	1.39	0.95	2.12	0.36	0.78

Table 34. Comparison of the first and second vibrational periods evaluated according to different models of the considered structures.

3.1.2.3 GROUND MOTION RECORDS

The structural response is investigated through time history analyses. Therefore, a suitable set of 7 accelerograms (Table 35) is provided, matching the design spectrum at the life safety limit state, i.e. 475 years return period earthquake, according to the EC8 recommendations (Maddaloni et al., 2012):

- the mean of zero-period spectral response acceleration values, that is equal to 3.69 m/s^2 , is larger than the design value, i.e. $a_g \cdot S$;
- the mean elastic spectrum of the selected ground motions is larger than 90% of the design elastic response spectrum in the range of periods between $0.2T_{1,\min}$ and $2T_{1,\max}$, where $T_{1,\min}$ and $T_{1,\max}$ are, respectively, the minimum and the maximum fundamental period of the benchmark 2D structures (Figure 103).

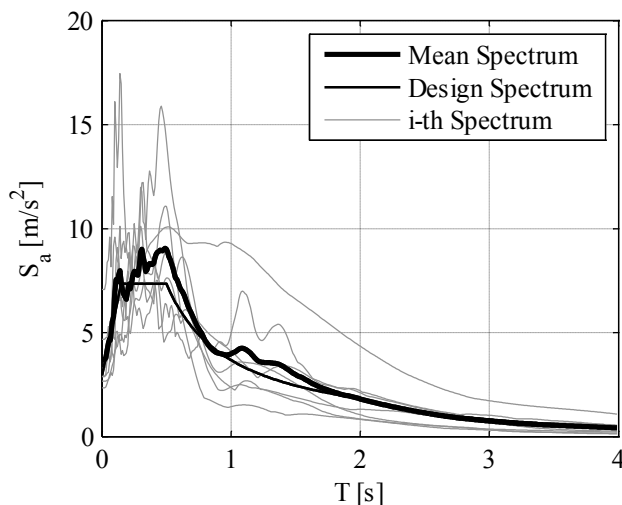


Figure 103. Comparison between the mean acceleration response spectrum of the adopted set of accelerograms and the design spectrum according to EC8.

Waveform	Eqk ID	Earthquake Name	Date	M_w [-]	R [km]	Dir.	PGA [m/s^2]
146	65	Friuli (aftershock)	15/09/1976	6.0	14	y	3.296
197	93	Montenegro	15/04/1979	6.9	24	x	2.880
413	192	Kalamata	13/09/1986	5.9	10	y	2.910
414	192	Kalamata	13/09/1986	5.9	11	x	2.354
414	192	Kalamata	13/09/1986	5.9	11	y	2.670
4673	1635	South Iceland	17/06/2000	6.5	15	y	4.677
6334	2142	South Iceland (aftershock)	21/06/2000	6.4	11	y	7.070

Table 35. Waveform ID, earthquake ID (Eqk ID) and name, date, moment magnitude (MW), epicentral distance (R), horizontal direction (Dir.) and peak ground acceleration (PGA) of the accelerograms selected for dynamic analyses (Ambraseys et al., 2002).

3.1.2.4 PRELIMINARY NONLINEAR STATIC ANALYSES

The acceleration demand on nonstructural components depends on both the dynamic interaction with the primary structure and the structural energy dissipation (Rodriguez et al., 2002; Politopoulos, 2010). The energy dissipation tends to reduce the intensity of the acceleration time history at a given floor. Structural overstrength, instead, makes the structure dissipate less energy and reduce the ductility demand compared to the ductility assumed during the design phase. The smaller the ductility demand is, the larger the floor accelerations are and they tend to be equal to the floor accelerations evaluated on the elastic structure (Medina et al., 2006).

In order to estimate the effective structural response and evaluate the overstrength ratios, nonlinear static analyses are performed applying a pattern of lateral forces proportional to the first mode displacement shape. For each structure, the relationship between the base shear force and the roof displacement is determined. The pushover curve, evaluated on the MDOF system, is converted in the capacity curve for the equivalent SDOF system; the idealized bilinear force–displacement relationships are obtained in accordance to the Italian Building Code (Consiglio Superiore dei Lavori Pubblici, 2009) (Figure 104): the ultimate displacement d_u is the SDOF displacement corresponding to a strength reduction equal to the 15%; the bilinear curve initial stiffness and yielding shear force are obtained imposing that the first branch intersects the capacity curve at $0.6 F_u$ and imposing the equality of the areas under the actual and the bilinear curves until the ultimate displacement d_u .

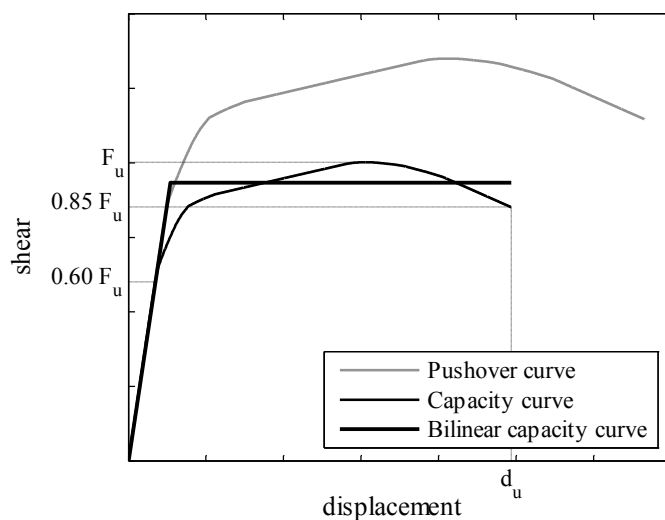


Figure 104. Evaluation of the bilinear capacity curve according to the Italian Building Code (Consiglio Superiore dei Lavori Pubblici, 2009).

The bilinear curve can be plotted in the ADRS (*Acceleration-Displacement Response Spectrum*) plane, where the design spectrum is plotted. In order to investigate the different sources of overstrength, the following ratios are evaluated for each structure (Figure 105):

- α , the ratio between the spectral acceleration evaluated for the equivalent SDOF structure with a linear behavior (S_{ae}) and the spectral acceleration corresponding to the yielding of the SDOF system (S_{ay}). This ratio represents the reduction of spectral acceleration demand due to the non-linear behavior of the structure and, therefore, provides an estimation of the global ductility demand;
- β , the ratio between the spectral acceleration value corresponding to the yielding of the SDOF system (S_{ay}) and the spectral acceleration that produces the first plastic hinge yielding (S_{ah}). This ratio takes into account the overstrength caused by the structural redundancy;
- γ , the ratio between the value of spectral acceleration corresponding to the first plastic hinge (S_{ah}) and the design spectral acceleration (S_{ad}). This ratio represents the overstrength due to materials and design or detailing of RC members;
- δ , the ratio between the spectral acceleration demand considered during the design phase ($S_{ae,des}$) and the spectral acceleration evaluated for the equivalent SDOF structure with a linear behavior (S_{ae}). This ratio takes into account the reduction of the stiffness in the nonlinear model.

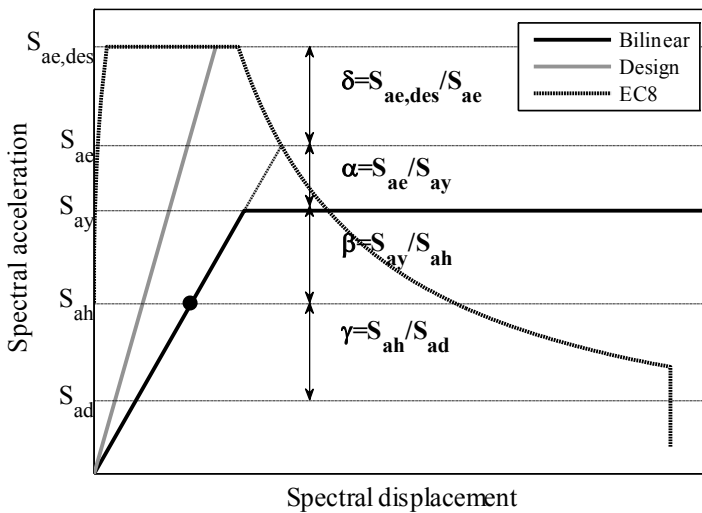


Figure 105. Overstrength ratios definition.

In Figure 106 the bi-linearized capacity curves of the different structures are plotted in the ADRS plane and compared to the EC8 design spectrum. The first plastic hinge yielding is pointed out by a circle. Table 36 shows the overstrength ratios for the different structures. It shows that RC frames, designed according to Eurocode 8 rules, are characterized by a high global overstrength. A low ductility demand is expected, which is very far from the assumed behavior factor q ; hence, the effective floor acceleration time histories are likely to be not significantly reduced with respect to the ones evaluated with the elastic model (Politopoulos, 2010).

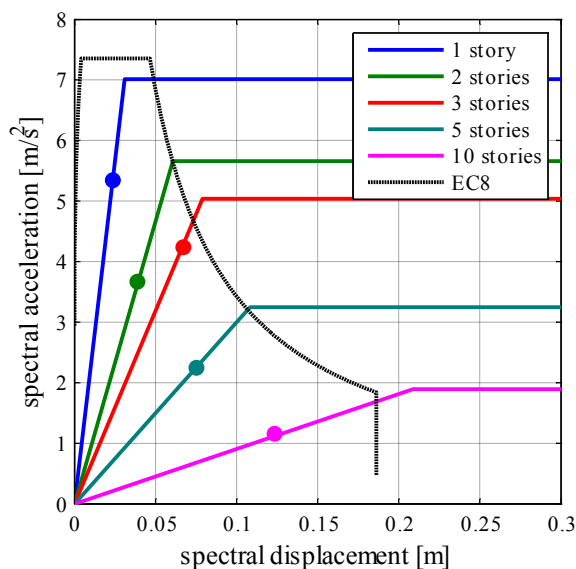


Figure 106. Capacity curves of the benchmark structures plotted in the Acceleration Displacement Response Spectrum plane.

No. story	α	β	γ	δ
1	1.05	1.31	3.59	1.00
2	1.00	1.55	2.91	1.30
3	0.92	1.19	3.50	1.52
5	1.03	1.45	2.67	1.47
10	0.88	1.66	2.46	1.63

Table 36. Overstrength ratios values for the analyzed structures.

Moreover, the safety assessment clearly shows that the displacement capacity is much larger than the demand in RC frame structures designed according to Eurocode 8; the displacement capacity values are omitted for the sake of brevity. Based on the conclusions included in (Magliulo et al., 2007), the safety assessment in the dynamic analysis could be even more conservative.

For all the structures, γ values are generally overestimated in this study, due to the adopted plastic hinge model with initial stiffness equal to the yielding secant stiffness. Indeed, the absence of the cracking point in the moment-rotation relationship reduces the bending moment at beam ends due to vertical loads. A larger base shear is then required to reach the yielding in the beam plastic hinges. It should be noted that the assessment of the total overstrength value, i.e. β times γ , is not much affected by such an approximation and can be considered correctly evaluated.

3.1.3 RESULTS AND DISCUSSION

3.1.3.1 ELASTIC AND INELASTIC FLOOR RESPONSE SPECTRA

Dynamic analyses on both elastic and inelastic models are performed and the horizontal acceleration time-histories at different levels are recorded for each selected accelerogram. A lumped plasticity approach is adopted in the inelastic models. Floor response spectra are obtained for each floor accelerogram with a 5% damping ratio and a mean response spectrum is plotted for each floor (Figure 107). These spectra provide the acceleration demand of nonstructural components that are connected to the floor and exhibit a fundamental period T . Figure 107 shows the mean floor response spectra, evaluated on both the elastic (dotted line) and inelastic (solid lines) models for the 5-story structure.

Due to the dynamic interaction, the primary structure modifies the frequency content of the earthquake so that the floor accelerogram, amplified with respect to the base accelerogram, has a large frequency content for periods close to the vibration periods of the elastic model. If the nonstructural component period corresponds to one of the vibration periods of the structure, a double-resonance phenomenon occurs; the floor response spectra exhibit peaks which may exceed five times the acceleration of gravity, i.e. about 20 times the base acceleration, at the top floor of the structure. Two main peaks are recorded corresponding to periods, i.e. $T_{1,el-eff}$ and $T_{2,el-eff}$, very close to the periods associated to the first and second vibration modes, i.e. $T_{1,el}$ and $T_{2,el}$ (Table 34). Table 37 shows the ratio between the two peak values obtained for the top floor of the different structures ($S_{Fa}(T_{1,el-eff})/S_{Fa}(T_{2,el-eff})$). For each floor, the acceleration which corresponds to the fundamental period ($T_{1,el-eff}$) is larger than the one associated to the period of second mode ($T_{2,el-eff}$), except for the 10-story structure. As expected, the higher modes influence on the definition of the floor spectra is predominant for such a tall building.

No. story	$S_{Fa}(T_{1,el-eff})/S_{Fa}(T_{2,el-eff})$	$S_{Fa}(T_{1,nl-eff})/S_{Fa}(T_{2,nl-eff})$	$S_{Fa,max\ el}/S_{Fa,max\ nl}$
[-]	[-]	[-]	[-]
1	-	-	1.11
2	3.79	1.52	2.43
3	1.90	0.94	1.90
5	2.18	0.58	2.42
10	0.68	0.39	1.17

Table 37. Ratio between the first two peak floor spectral accelerations obtained for the top floor of the different structures in both the elastic and inelastic models. Comparison between maximum floor spectrum acceleration in the elastic and inelastic models.

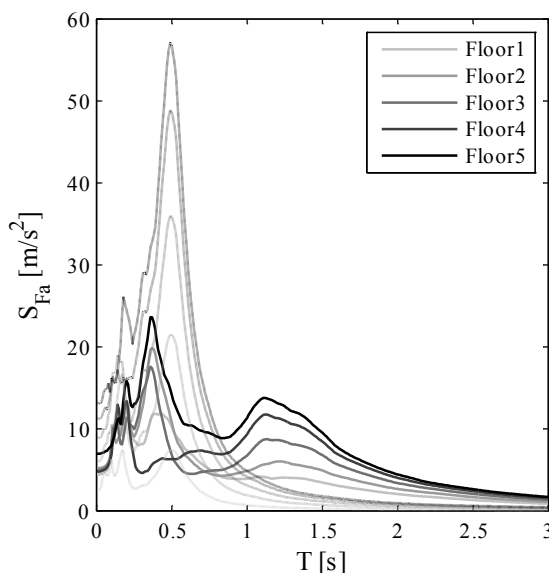


Figure 107. Floor response spectra of the 5-story structure evaluated on both the elastic (dotted line) and inelastic models (solid line).

The inelastic floor response spectra (solid lines in Figure 107), show that the curves exhibit peaks at periods, i.e. $T_{1,nl-eff}$ and $T_{2,nl-eff}$, much larger than the elastic ones, due to the different initial stiffness of the two models (see Section 3.1.2.2).

Figure 108 shows the comparison between elastic and inelastic floor response spectra for the remaining structures. The following comments can be drawn:

- a significant period elongation is exhibited, comparing the peak related to the first structural mode of the elastic model with the inelastic one;
- the comparison of the peak related to the first structural mode of the elastic model with the inelastic one also shows a substantial reduction of the peak spectral ordinate: the maximum spectral values of the inelastic model are less

than 3 g for the different structures. The reduction is caused by both the period elongation phenomenon and the ductility demand experienced by the structure. This phenomenon is not evidenced for the one-story structure, because the period elongation does not modify the base response spectral ordinate, as denoted by the δ factor in Table 36;

- higher modes effect is significant in the 10-story structure. Moreover, the peak spectral values associated with the higher modes are slightly reduced in the inelastic model. At lower stories, the spectral values associated with higher modes can be even larger than the elastic ones, as also pointed out by (Chaudhuri and Villaverde, 2008) in a research study on steel moment-resisting frames. This phenomenon confirms that the higher mode influence becomes more significant in the inelastic range (Fischinger et al., 2011; Rejec et al., 2012).

Table 37 shows the ratio between the two peak values obtained for the top floor of the different structures in the inelastic models ($S_{Fa}(T_{1,nl-eff})/S_{Fa}(T_{2,nl-eff})$); the ratio between the maximum elastic and inelastic spectral ordinate is also evidenced ($S_{Fa,max\ el}/S_{Fa,maxnl}$). It can be observed that the inelastic spectral acceleration demand reduction is significantly far from the assumed behavior factor, due to the large structural overstrength (see Section 3.1.2.4). It is also confirmed that the energy dissipation is mostly related to the first mode; indeed the peak value associated to $T_{2,nl-eff}$ may exceed the peak value associated to $T_{1,nl-eff}$. It can be concluded that in case inelastic models are considered, higher modes give a larger contribution to the definition of the floor spectral ordinates.

From these considerations it follows that three factors mainly influence the floor spectral acceleration caused by the earthquakes compatible with the design spectrum (Sankaranarayanan and Medina, 2007): (a) the structural ductility demand level, strongly related to the structural overstrength; (b) the relative structural height at which the component is installed; (c) the dynamic characteristics of nonstructural components in terms of natural period, normalized with respect to the structural period.

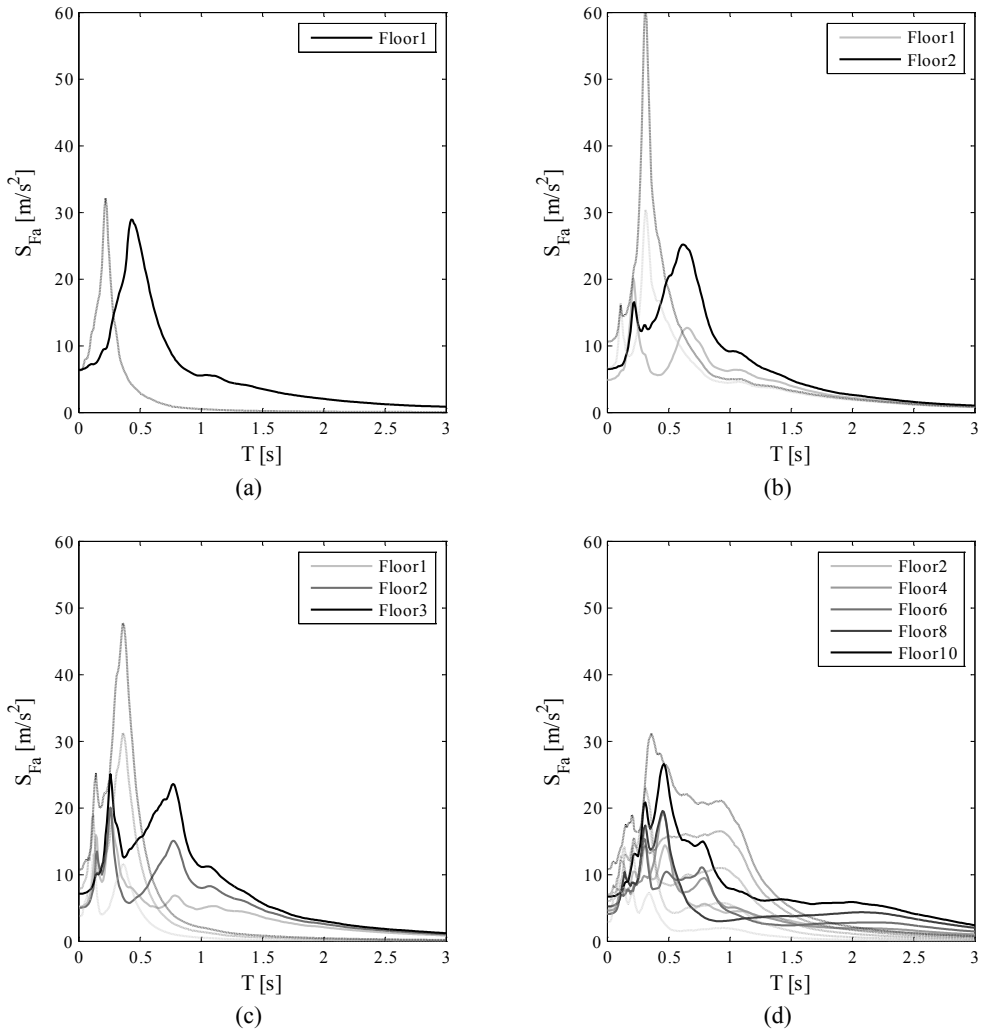


Figure 108. Floor response spectra of the (a) 1-story, (b) 2-story, (c) 3-story and (d) 10-story structures evaluated on both the elastic (dotted line) and inelastic models (solid line).

3.1.3.2 FLOOR AMPLIFICATION EVALUATION

The ratio between peak floor acceleration (PFA) and peak ground acceleration (PGA) is plotted versus the relative height in Figure 109 for the benchmark structures, in order to study the floor acceleration magnification with height. The PFA over PGA trend with the relative structural height is shown for both elastic and inelastic models.

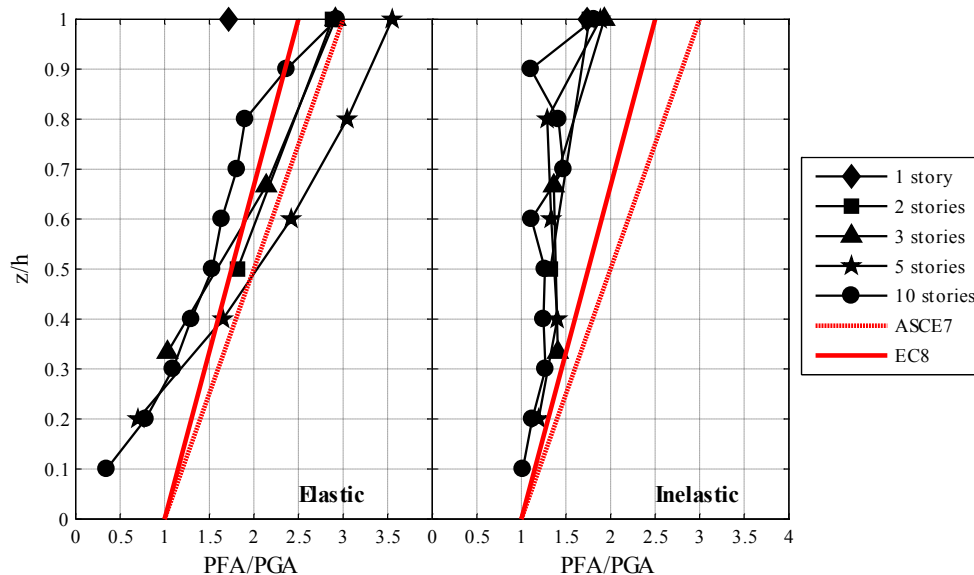


Figure 109. Ratio between peak floor acceleration and peak ground acceleration, versus the relative height (z/h) for the different considered structures compared to the provisions included in ASCE7 and EC8.

The elastic model diagrams, which represent the average response of each structure, show an almost linear trend and they reach values of PFA/PGA close to three at the top floor. At the same relative height, the values of the ratio PFA/PGA are larger for structures with a larger number of floors, except for the tallest structure. At the lower stories of tall structures, PFA values are smaller than PGA values.

The inelastic model diagrams also show a linear trend. In this case the amplification is smaller than the one of the elastic models: the PFA/PGA values are always greater than one and they reach the maximum value, close to 2, at the top story. As pointed out by Wieser et al. (2013) and Ray-Chaudhuri and Hutchinson (2011), the yielding of the structure and the period elongation cause a significant reduction of the peak floor accelerations.

Both the elastic and inelastic trends are compared to ASCE7 (American Society of Civil Engineers, 2010) and Eurocode 8 provisions (Figure 109). The ASCE7 and EC8 provisions are described respectively in Section 3.1.3.5 and 3.1.3.4. Such a comparison shows that both the ASCE7 and EC8 provisions are safe-sided for the inelastic diagrams, which are the most realistic ones. Finally, a linear trend that goes from 1 at the base to 2 at the top would better fit the outcomes of the nonlinear analyses.

3.1.3.3 COMPONENT AMPLIFICATION EVALUATION

The ratio between the maximum floor spectral acceleration and the PFA, i.e. a_p , is plotted versus the relative floor height for each floor of the analyzed structures in order to study the floor acceleration magnification on the component (Figure 110). This ratio represents the amplification of the floor acceleration demand for a nonstructural component that is in tune with the primary structure.

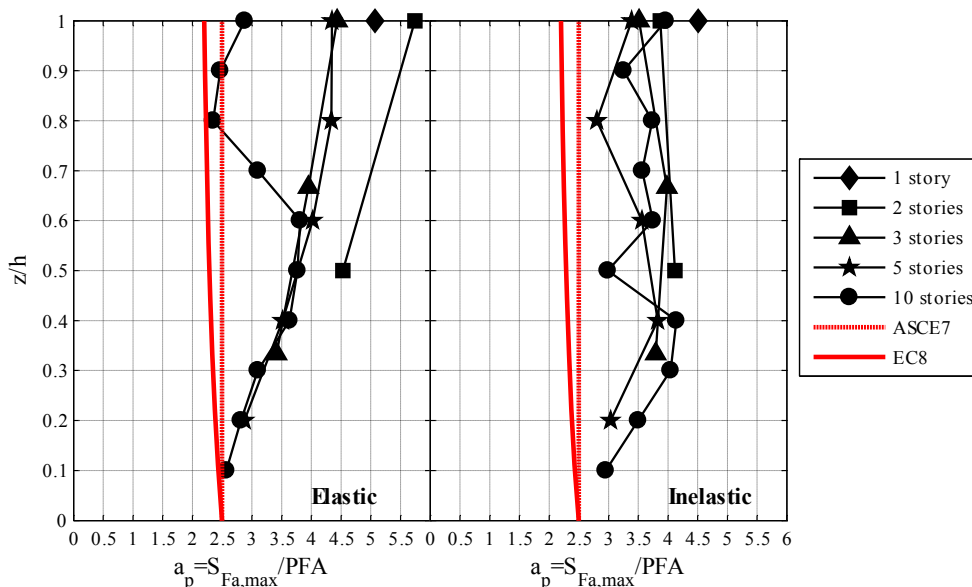


Figure 110. Floor acceleration magnification on nonstructural components.

The inelastic floor magnifications on nonstructural components are slightly smaller than the elastic ones. For the 10-story structure, the inelastic a_p values are larger than the elastic ones. This is due to the fact that the largest spectral ordinate value is given by higher modes, which are only slightly influenced by the nonlinearity experienced by the structure (Figure 108d) (Rejec et al., 2012); the PFA values, instead, are influenced by the first mode, and they significantly decrease in the inelastic model (Figure 109). Hence, the ratio between the maximum floor spectral acceleration and the PFA could be larger in inelastic models in tall structures.

Assuming both elastic and inelastic models, the trend is almost constant with the height and the a_p values are greater than 2.5, which is the value recommended by ASCE7 and EC8 (see Sections 3.1.3.5 and 3.1.3.4, respectively), and it is close to 4.5. A significant underestimation of the a_p values in the current building codes is clearly evidenced, confirming the results included in Medina et al. (2006).

3.1.3.4 COMPARISON WITH EC8 FORMULA AND LIMITATIONS

In order to take into account the realistic behavior of the primary structures, inelastic floor spectra should be considered. These curves are compared with the ones obtained by Eurocode 8 formulation (CEN, 2004b) for the evaluation of the floor response spectrum acceleration S_a acting on a nonstructural component:

$$S_a = \alpha \cdot S \cdot \left[\frac{3 \cdot (1 + z/H)}{1 + (1 - T_a/T_1)^2} - 0.5 \right] \cdot g \geq \alpha \cdot S \cdot g \quad (17)$$

where:

- α is the ratio between the ground acceleration and the gravity acceleration g ;
- S is a soil amplification factor;
- z/H is the relative structural height at which the component is installed;
- T_a is the nonstructural component period;
- T_1 is the fundamental period of the primary structure, assumed during the design phase.

The design floor response spectrum depends on the ratio between the nonstructural component period and the structural period, as well as by the level at which the nonstructural component is installed. The formulation does not identify separately the different factors that affect the floor spectral accelerations, as provided, instead, by ASCE7 formulation (American Society of Civil Engineers, 2010) (see Section 3.1.3.5). However, it implicitly assumes that the PFA linearly ranges from PGA at the base to 2.5 times PGA at the top of the structure, whereas a_p linearly ranges from 2.5 at the base to 2.2 at the top of the structure, as already mentioned in Section 3.1.3.2 and 3.1.3.3. Moreover, the maximum S_a value is equal to 5.5 times the PGA, i.e. the spectral acceleration acting on a component placed at the top floor which is in tune with the structure.

For different values of T_a and for each floor, the Eurocode formulation provides a curve that shows the maximum value for T_a equal to T_1 . In Figure 111 both inelastic floor spectra and design Eurocode 8 floor spectra are plotted for the benchmark structures. This comparison underlines that Eurocode formulation underestimates the maximum floor acceleration demand for a wide range of nonstructural component periods, whereas it may overestimate the acceleration demand on nonstructural components with a period close to the design period of the structure (T_{des} in Figure 102). Moreover the peak of the Eurocode curve is reached at the design period, which is lower than the effective one for all inelastic models (Table 1).

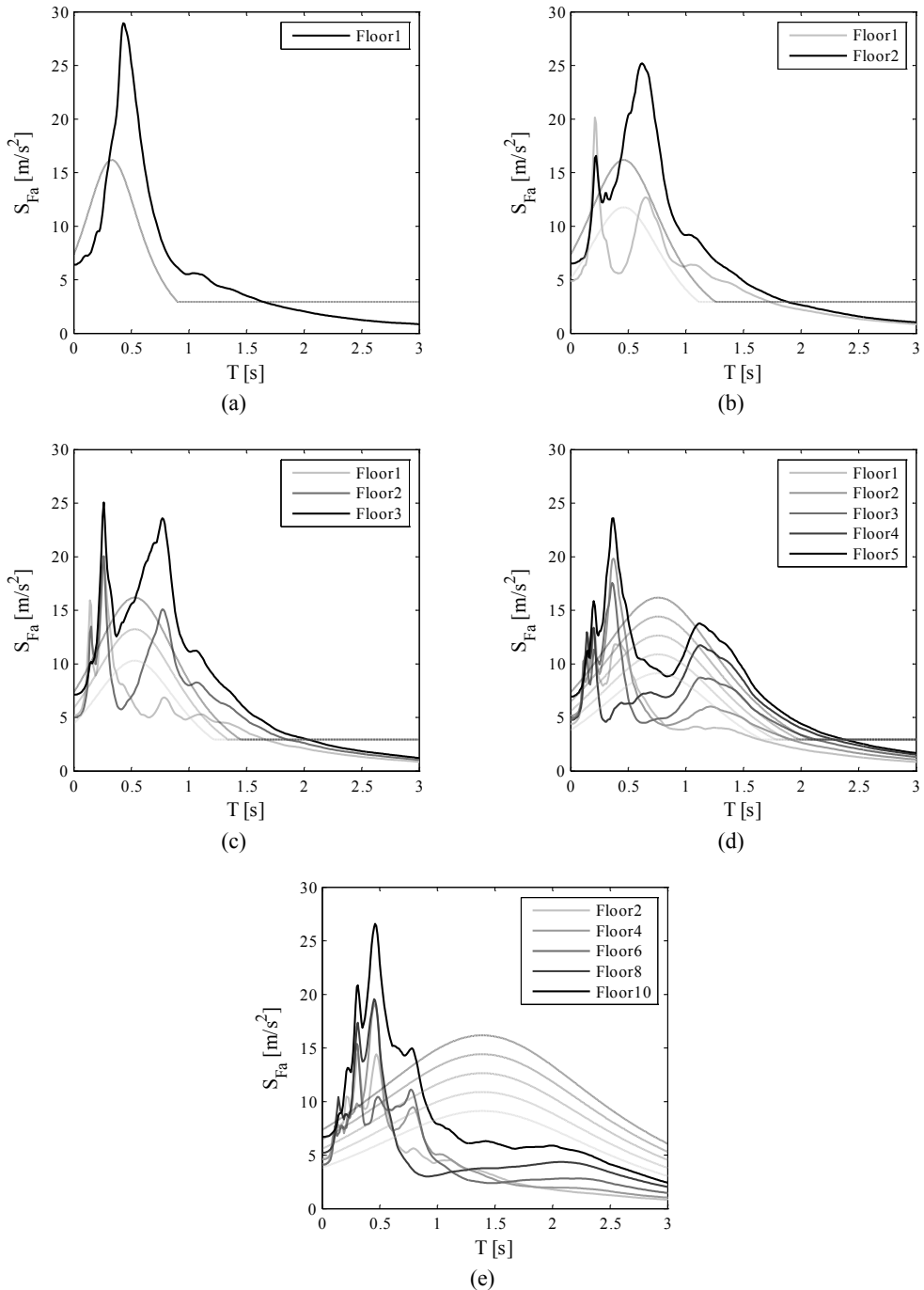


Figure 111. Comparison between effective inelastic floor response spectra (solid lines) and floor response spectra evaluated according to Eurocode 8 (dashed lines) for the (a) 1-story, (b) 2-story, (c) 3-story, (d) 5-story and (e) 10-story structures.

Eurocode formulation does not take into account higher modes: a significant underestimation is recorded in the range of periods close to the higher modes periods of vibration. The effective floor spectrum acceleration can be significantly underestimated, especially for tall structures, e.g. the 10-story structure in Figure 111e, in which higher modes are predominant.

The approach proposed by Fathali and Lizundia (2011), who considered a constant floor response spectral acceleration in a wide range of periods, could be adopted. It would allow removing both the issue related to the uncertainty in the definition of the structural fundamental period and the non-inclusion of the higher modes effects in the floor response spectra.

The effect of the higher modes in the floor response spectra is clearly influenced by the nonlinear excursion that the structure experiences during the earthquake motion (see Section 3.1.2.3). However, both European and US codes do not explicitly take into account the reduction of the floor response spectra due to the nonlinear behavior of structures, even though the adoption of a low a_p value, i.e. from 2.2 to 2.5, could include the reduction due to the nonlinear behavior of the main structure. Indeed, the a_p values recorded in structures that experience large ductility demand are typically smaller than the ones recorded in Figure 110, due to the low level of ductility demand experienced by the benchmark structures.

It would be better to explicitly include the ductility demand level in code formulas for the evaluation of floor spectra, as mentioned in Medina et al. (2006). The ductility level experienced by a structure, subjected to the design earthquake motion, is strongly influenced by the structural overstrength, which is in turn related to the prescriptions included in the code itself (see Section 3.1.2.1). Hence, the definition of a formula that includes the structural ductility demand level would certainly be code-dependent.

The structural overstrength of a given building cannot be easily assessed during the design phase. Moreover, it is related to many factors, e.g. the bay width, the presence of irregularities in plan or elevation and the design peak ground acceleration among others, that are not considered in this research study. Hence, a very wide parametric study is required to define a code formula that explicitly takes into account the ductility level that the structure experiences.

Alternatively, the code formulation for the evaluation of the nonstructural component demand could be referred to the elastic floor response spectrum. This approach would be too conservative, i.e. acceleration on components could be up to 20 times the acceleration at the base (see Section 3.1.3.1); moreover, it would not reflect the realistic behavior of the structure in terms of both the fundamental period and the ability of the structure to dissipate energy.

Finally, it is concluded that the Eurocode could not adequately address the design of acceleration-sensitive nonstructural components, as pointed out by Velasquez et al. (2012) who analyzed the floor time-history accelerations recorded during a shake-table test campaign.

3.1.3.5 COMPARISON WITH AC156 TARGET SPECTRUM

AC156 (International Conference of Building Officials (ICBO), 2000) provides a procedure for the seismic qualification of nonstructural components by shake table testing. The protocol provides that nonstructural components are shaken with a horizontal accelerogram whose response spectrum (Test Response Spectrum) is compatible with the Required Response Spectrum (RRS) shown in Figure 112.

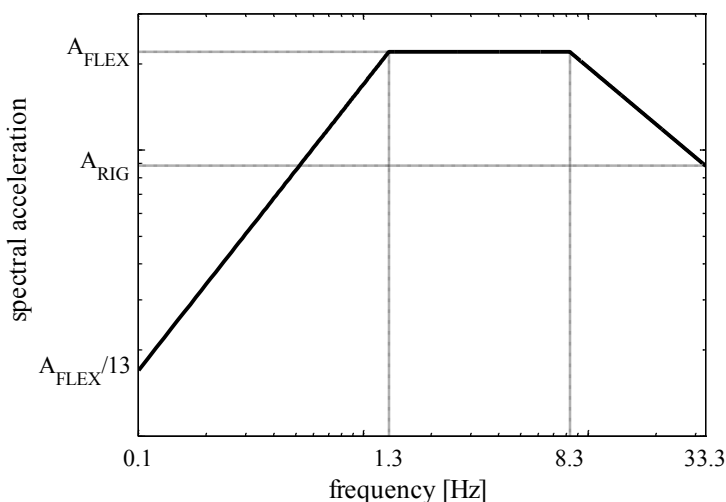


Figure 112. AC156 horizontal Required Response Spectrum (RRS) for qualification testing of nonstructural components.

The RRS reflects the provisions included in ASCE7 (American Society of Civil Engineers, 2010) for the seismic demand evaluation on nonstructural components. According to ASCE7, the nonstructural components are designed in order to withstand a force F_p acting in their centroid, evaluated as follows:

$$F_p = \frac{0.4 \cdot a_p \cdot S_{DS} \cdot W_p}{\left(\frac{R_p}{I_p} \right)} \cdot \left(1 + 2 \cdot \frac{z}{h} \right) \quad (18)$$

where a_p is the floor-to-component amplification factor, S_{DS} is the design spectral acceleration at short periods, W_p is the weight of the component, R_p is the component force reduction factor, I_p is the importance factor and z/h is the relative height ratio

where the component is installed. The force F_p is limited to be not larger than 1.6 times $S_{DS} \cdot I_p \cdot W_p$.

The AC156 RRS, which must be matched in the frequency range between 1.3 Hz and 33.3 Hz, is defined by the following values:

$$A_{FLEX} = S_{DS} \cdot \left(1 + 2 \cdot \frac{z}{h}\right) \quad (19)$$

$$A_{RIG} = 0.4 \cdot S_{DS} \cdot \left(1 + 2 \cdot \frac{z}{h}\right) \quad (20)$$

AC156 assumes that R_p/I_p is equal to 1, since during the seismic simulation test, the specimen “will respond to the excitation and inelastic behavior will naturally occur”; the factor a_p is set equal to 2.5 for flexible components ($1.3\text{Hz} < f < 8.3\text{Hz}$) and 1 for rigid components ($f > 8.3\text{Hz}$). A_{FLEX} is limited to a maximum value of 1.6 times S_{DS} .

For nonstructural components commonly installed at different stories of a structure, the ratio z/h is usually set equal to 1, i.e. considering the most intense condition. Many applications of the AC156 protocol can be found in the literature (Magliulo et al., 2012a; Magliulo et al., 2014; Magliulo et al., 2012b; Petrone et al., 2013; Badillo-Almaraz et al., 2007).

The spectrum provided by AC156 is aimed at inducing the maximum seismic demand acting on a given nonstructural component, whatever the structural typology could be. Therefore, it can be interpreted as an envelope of all the possible floor response spectra that are recorded at a given z/h ratio of a generic building typology. For this reason the AC156 RRS, evaluated for z/h ratio equal to 1, is compared to the floor response spectra recorded at the top story of the benchmark structures (Figure 113). The S_{DS} value is evaluated as 2.5 times the design peak ground acceleration of the analyzed structures, as reported in ASCE7. The comparison clearly evidences the significant underestimation of the floor spectrum ordinates in AC156 RRS. For low period components, instead, AC156 RRS gives larger accelerations, consequently to the comparison shown in Figure 109.

The above mentioned A_{FLEX} upper bound limitation, i.e. $1.6 \cdot S_{DS}$, reflects the similar limitation that ASCE7 defines on the force F_p acting on the component. However, the limitation on the force F_p should not be extended to the RRS, since the RRS does not include the reduction caused by the inelastic behavior of the tested nonstructural component, i.e. the R_p factor. In other words, the limitation on the force acting on the component implicitly assumes that a minimum R_p value is considered (ASCE7 provides R_p values larger than 1.5 for the different considered nonstructural components). Conversely, the seismic qualification testing does not include such a reduction. Medina (2013) also proposed to consider the removal of the upper limit of the force F_p , based on structural analyses on 3- 9- and 15-story structural wall systems.

If the limitation on A_{FLEX} is removed, the RRS well matches the floor response spectra resulting from the analyses (dotted line in Figure 113). In such a case, the RRS can be clearly interpreted as an envelope of all the possible floor response spectra that can be recorded at a given z/h ratio of a generic building.

It is underlined that the comparison refers to a limited number of RC frame structures. A larger set of buildings is required in order to generalize such a conclusion.

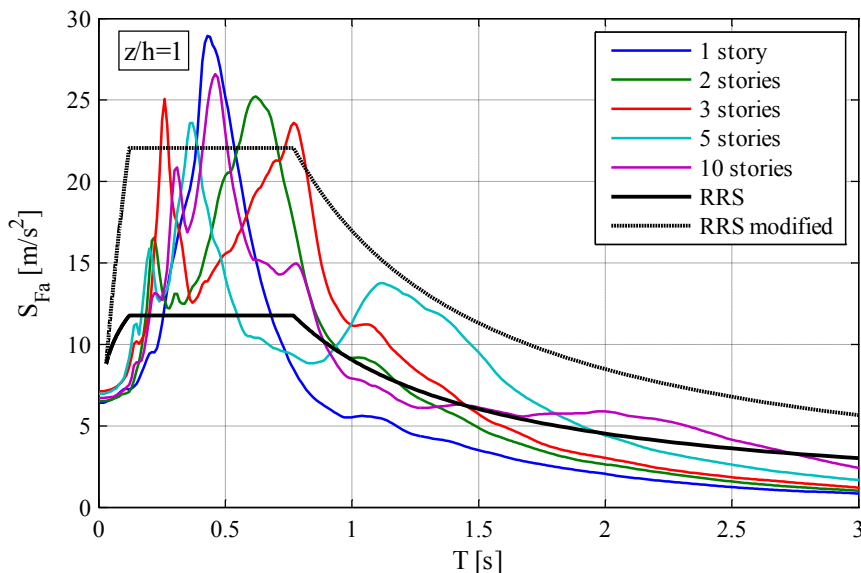


Figure 113. AC156 Required Response Spectrum (RRS), original and proposed, compared to the floor response spectrum at the top story of the different structures.

3.1.4 CONCLUSIONS

A parametric study for the evaluation of the floor response spectra in RC frame structures, i.e. 1- 2- 3- 5- and 10-story structures, is conducted. The structures, designed according to Eurocode 8, are subjected to a set of earthquakes that are compatible with the design response spectrum.

Preliminary nonlinear static analyses show that the benchmark structures are characterized by a significant overstrength, due to some geometric limitations included in the Eurocode 8.

Time-history analyses are performed both on elastic and inelastic models of the benchmark structures. The comparison between elastic and inelastic floor response spectra indicates a substantial reduction of the peak spectral ordinate associated to the first mode; moreover, the peak occurs at a longer period due to the period elongation phenomenon. The peak spectral values associated with the higher modes are only

slightly reduced in the inelastic model. At lower stories, the spectral values associated to higher modes can be even larger than the elastic ones.

The ratio between PFA and PGA trend with the relative structural height shows that both the ASCE7 and EC8 provisions are safe-sided. A linear trend that goes from 1 at the base of the structure to 2 at the top would better fit the outcomes of the analyses. The yielding of the structure gives a significant contribution to the peak floor acceleration reduction.

The component amplification, i.e. the ratio between the maximum floor spectral value and the PFA, is almost constant with the height for both elastic and inelastic models. An unsafe-sided estimation of the a_p values in the actual building codes is clearly evidenced: the component amplification a_p values are significantly greater than 2.5, which is the value recommended by ASCE7 and EC8, and close to 4.5.

It is found that Eurocode formulation for the evaluation of the seismic demand on nonstructural components does not fit well the results of the analyses. It underestimates the maximum floor acceleration demand for a wide range of nonstructural component periods, whereas it overestimates the acceleration demand on nonstructural components with a period close to the design period of the structure. The underestimation is significant for nonstructural component periods close to the higher modes structural periods, since the Eurocode formulation does not include higher modes effect.

The urgent need to include the structural ductility demand in code formulas for the evaluation of floor spectra is claimed. However, it is underlined that the ductility level is influenced by the structural overstrength, which is in turn related to the prescriptions included in the reference building code. Hence, the definition of a formula that includes the structural ductility demand level would certainly be code-dependent.

Some comments on the target spectrum provided by AC 156 for the seismic qualification of nonstructural component are included. In particular, it is shown that in case the upper bound limitation on the Required Response Spectrum (RRS) is removed, the RRS well matches the floor response spectra resulting from the analyses on the benchmark structures.

It should be underlined that the above presented results and conclusions are related and limited to a set of five RC “simple” structures designed according to Eurocode 8. A very wide parametric study is encouraged in order to define a code formula that explicitly takes into account the ductility level or the structural overstrength. A wide parametric study is needed in order to generalize the results and define a code formula since the structural overstrength of a building is related to many factors, e.g. the bay width, the presence of irregularities in plan or elevation and the design peak ground acceleration among others.

3.1.5 REFERENCES

- Ambraseys N, Smit P, Sigbjornsson R, Suhadolc P, Margaris B (2002) Internet-Site for European Strong-Motion Data. European Commission, Research-Directorate General, Environment and Climate Programme
- American Society of Civil Engineers (2010) ASCE/SEI 7-10: Minimum Design Loads for Buildings and Other Structures. Reston, Virginia, US
- Badillo-Almaraz H, Whittaker AS, Reinhorn AM (2007) Seismic fragility of suspended ceiling systems. *Earthquake Spectra* 23 (1):21-40. doi:10.1193/1.2357626
- CEN (2004a) Eurocode 2: Design of concrete structures - Part 1-1: General rules and rules for buildings. EN 1992-1-1. Brussels, Belgium
- CEN (2004b) Eurocode 8: design of structures for earthquake resistance - Part 1: general rules, seismic actions and rules for buildings. EN 1998-1. Brussels, Belgium.
- Chaudhuri S, Villaverde R (2008) Effect of Building Nonlinearity on Seismic Response of Nonstructural Components: A Parametric Study. *Journal of Structural Engineering* 134 (4):661-670. doi:doi:10.1061/(ASCE)0733-9445(2008)134:4(661)
- Consiglio Superiore dei Lavori Pubblici (2009) Circolare 2 febbraio 2009, n. 617, Istruzioni per l'applicazione delle «Nuove norme tecniche per le costruzioni». G.U. n. 27 del 26-2-2009 (in Italian)
- Fathali S, Lizundia B (2011) Evaluation of current seismic design equations for nonstructural components in tall buildings using strong motion records. *The Structural Design of Tall and Special Buildings* 20:30-46. doi:10.1002/tal.736
- Fischinger M, Ercolino M, Kramar M, Petrone C, Isakovic T Inelastic seismic shear in multi-storey cantilever columns. In: ECCOMAS Thematic Conference - COMPDYN 2011: 3rd International Conference on Computational Methods in Structural Dynamics and Earthquake Engineering: An IACM Special Interest Conference, Programme, 2011.
- Haselton CB (2006) Assessing seismic collapse safety of modern reinforced concrete moment frame buildings. Ph.D. thesis, Stanford University, California, US
- Ibarra LF, Medina RA, Krawinkler H (2005) Hysteretic models that incorporate strength and stiffness deterioration. *Earthquake Engineering & Structural Dynamics* 34 (12):1489-1511. doi:10.1002/eqe.495
- International Conference of Building Officials (ICBO) (2000) AC 156 Acceptance Criteria for the Seismic Qualification of Nonstructural Components. ICBO Evaluation Service, Inc., Whittier, California, USA
- Maddaloni G, Magliulo G, Cosenza E (2012) Effect of the seismic input on non-linear response of R/C building structures. *Advances in Structural Engineering* 15 (10):1861-1877
- Magliulo G, Maddaloni G, Cosenza E (2007) Comparison between non-linear dynamic analysis performed according to EC8 and elastic and non-linear static analyses.

- Engineering Structures 29 (11):2893-2900.
doi:10.1016/j.engstruct.2007.01.027
- Magliulo G, Pentangelo V, Maddaloni G, Capozzi V, Petrone C, Lopez P, Talamonti R, Manfredi G (2012a) Shake table tests for seismic assessment of suspended continuous ceilings. *Bulletin of Earthquake Engineering* 10 (6):1819-1832. doi:10.1007/s10518-012-9383-6
- Magliulo G, Petrone C, Capozzi V, Maddaloni G, Lopez P, Manfredi G (2014) Seismic performance evaluation of plasterboard partitions via shake table tests. *Bulletin of Earthquake Engineering*:(online first). doi:10.1007/s10518-013-9567-8
- Magliulo G, Petrone C, Capozzi V, Maddaloni G, Lopez P, Talamonti R, Manfredi G (2012b) Shake Table Tests on Infill Plasterboard Partitions. *The Open Construction and Building Technology Journal* 6 (Suppl 1-M10):155-163. doi:10.2174/1874836801206010155
- Mander J, Priestley M, Park R (1988) Theoretical Stress-Strain Model for Confined Concrete. *Journal of Structural Engineering* 114 (8):1804-1826. doi:10.1061/(ASCE)0733-9445(1988)114:8(1804)
- McKenna F, Fenves GL (2013) OpenSees Manual <http://opensees.berkeley.edu>. Pacific Earthquake Engineering Research Center, Berkeley, California.,
- Medina RA (2013) Seismic design horizontal accelerations for non-structural components. Paper presented at the Vienna Congress on Recent Advances in Earthquake Engineering and Structural Dynamics 2013 (VEESD 2013), 28-30 August 2013, Vienna, Austria,
- Medina RA, Sankaranarayanan R, Kingston KM (2006) Floor response spectra for light components mounted on regular moment-resisting frame structures. *Engineering Structures* 28 (14):1927-1940. doi:10.1016/j.engstruct.2006.03.022
- Petrone C, Magliulo G, Manfredi G (2013) Shake table tests for the seismic assessment of hollow brick internal partitions. *Engineering Structures*:(under review)
- Petrone C, Magliulo G, Manfredi G (2014) Floor response spectra in RC frame structures designed according to Eurocode 8. *Journal of Earthquake Engineering* (submitted for publication)
- Politopoulos I (2010) Floor Spectra of MDOF Nonlinear Structures. *Journal of Earthquake Engineering* 14 (5):726-742. doi:10.1080/13632460903427826
- Ray-Chaudhuri S, Hutchinson TC (2011) Effect of Nonlinearity of Frame Buildings on Peak Horizontal Floor Acceleration. *Journal of Earthquake Engineering* 15 (1):124-142. doi:10.1080/13632461003668046
- Rejec K, Isaković T, Fischinger M (2012) Seismic shear force magnification in RC cantilever structural walls, designed according to Eurocode 8. *Bulletin of Earthquake Engineering* 10 (2):567-586. doi:10.1007/s10518-011-9294-y
- Rodriguez ME, Restrepo JI, Carr AJ (2002) Earthquake-induced floor horizontal accelerations in buildings. *Earthquake Engineering and Structural Dynamics* 31 (3):693-718. doi:10.1002/eqe.149
- Sankaranarayanan R, Medina RA (2007) Acceleration response modification factors for nonstructural components attached to inelastic moment-resisting frame

- structures. *Earthquake Engineering and Structural Dynamics* 36 (14):2189-2210. doi:10.1002/eqe.724
- Singh M, Moreschi L, Suárez L, Matheu E (2006a) Seismic Design Forces. I: Rigid Nonstructural Components. *Journal of Structural Engineering* 132 (10):1524-1532. doi:10.1061/(ASCE)0733-9445(2006)132:10(1524)
- Singh M, Moreschi L, Suárez L, Matheu E (2006b) Seismic Design Forces. II: Flexible Nonstructural Components. *Journal of Structural Engineering* 132 (10):1533-1542. doi:10.1061/(ASCE)0733-9445(2006)132:10(1533)
- Velasquez JF, Restrepo J, Blandon CA (2012) Floor response spectra for the design of acceleration sensitive light nonstructural systems in buildings. Paper presented at the 15th World conference on earthquake engineering, 24-28 September 2013, Lisboa, Portugal,
- Wieser J, Pekcan G, Zaghi AE, Itani A, Maragakis M (2013) Floor Accelerations in Yielding Special Moment Resisting Frame Structures. *Earthquake Spectra* 29 (3):987-1002. doi:10.1193/1.4000167

3.2 CODE-ORIENTED EVALUATION OF THE SEISMIC DEMAND ON LIGHT ACCELERATION-SENSITIVE NONSTRUCTURAL COMPONENTS IN ORDINARY BUILDINGS

A parametric study is conducted in order to evaluate the seismic demand on light acceleration-sensitive nonstructural components caused by frequent earthquakes. The study is motivated by the counterintuitive approach of current building codes to the design of nonstructural components; moreover, the extensive nonstructural damage recorded after recent low intensity earthquakes also encouraged such a study.

A set of benchmark RC frame structures with different number of stories are selected and designed according to Eurocode 8. The structures are subjected to a set of frequent earthquakes. Dynamic nonlinear analyses are performed on the benchmark structures in order to assess the accuracy of Eurocode formulation. It is concluded that Eurocode underestimates the acceleration demand on nonstructural components for a wide range of periods, especially in the vicinity of the higher mode periods of vibration of the benchmark structures; for periods sufficiently larger than the fundamental period of the structure, instead, Eurocode formulation gives a good approximation, typically safe-sided, of the floor spectra. Finally, a novel formulation is proposed for an easy implementation in future building codes based on the actual Eurocode provisions. The proposed formulation gives a good estimation of the floor spectral accelerations and is able to envelope the floor spectral peaks due to the higher modes.

3.2.1 INTRODUCTION

Many research studies were conducted in the past with the purpose of assessing the seismic demand on nonstructural components, especially the acceleration-sensitive ones.

Rodriguez et al. (2002) evaluated the earthquake-induced floor horizontal accelerations in cantilever wall buildings built with rigid diaphragms. They described several methods prescribed by design standards and proposed a new method for the evaluation of the design horizontal forces. Singh et al. (Singh et al., 2006b, a) proposed two methods for calculating the seismic design forces for flexible and rigid nonstructural components. The methods exploited the dynamic characteristics of the component, expressed in terms of the fundamental periods and damping ratios, and the supporting structure to calculate the seismic demand on nonstructural components. The validity of such methods was verified by comparing their floor response spectra with the ones obtained for an ensemble of earthquakes exciting several buildings with different numbers of stories. Fathali and Lizundia (2011) analyzed the recorded ground and

floor motion data collected in the framework of the California Strong Motion Instrumentation Program (CSMIP). They proposed a nonlinear relationship between the peak floor acceleration (PFA) and the relative height of the component in the building. Moreover, they proposed a three-segment floor spectrum composed of a linear rise at short periods, a flat segment at medium-range periods and a nonlinear decaying segment at longer periods. Sullivan et al. (2013) addressed the shortcomings of Eurocode 8 formulation for the definition of floor response spectra both in an 8-story and a 20-story cantilever RC wall structure. They also proposed calibrated equations to predict floor spectra on single degree of freedom supporting structures. They finally encouraged further researches on multi-degree of freedom supporting structures.

A parametric study is conducted in order to evaluate the seismic demand on light acceleration-sensitive nonstructural components caused by frequent earthquakes. The study is motivated by the counterintuitive approach of current European and Italian Building Codes, as detailed in the Section 3.2.2. The above mentioned nonstructural damage exhibited after low intensity earthquakes also encouraged such a study. Moreover, very limited studies concerning the Eurocode 8 (CEN, 2004b) formulation for the evaluation of the floor spectral acceleration were performed, according to which the seismic demand on a given nonstructural component is evaluated. Past studies were usually focused either on simple structures, e.g. SDOF structures, or on steel and wall buildings.

A set of benchmark RC frame structures are selected and designed according to Eurocode 8. Dynamic nonlinear analyses are performed on the benchmark structures in order to validate the Eurocode formulation. The floor response spectra are compared to Eurocode 8 formulation; some considerations on the peak floor acceleration and the component amplification are also included. Finally, a novel formulation is proposed for an easy implementation in future building codes.

3.2.2 WHY TO INVESTIGATE FLOOR SPECTRA CAUSED BY FREQUENT EARTHQUAKES?

Current building codes, such as Eurocode 8 (EC8) (CEN, 2004b) and Italian Building Code (NTC 08) (Consiglio Superiore dei Lavori Pubblici, 2008), provide that ultimate limit states are not achieved for a rare earthquake, e.g. 475-year return period earthquakes for ordinary buildings, and damage/serviceability limit state are not overcome for a frequent earthquake, e.g. 50-year return period earthquakes for ordinary buildings, according to the approach included in (Structural Engineers Association of

California (SEAOC), 1995). Ultimate limit states concern the safety of the people and the structure whereas serviceability limit states concern the functioning of the structure. The Italian Building Code accurately defines the two limit states considered during the design phase. Ultimate limit state is reached in case nonstructural components are failed and structural components are damaged but the structure still has a safety margin with respect to the collapse. Damage limit state, instead, is reached in case structural components, nonstructural components and contents exhibit a minor damage level that does not threaten the life safety and reduce the safety of the building.

The “damage limitation requirement” is deemed to be satisfied by just limiting the structural interstory drifts for frequent earthquakes; the limitation implies that displacement-sensitive nonstructural components are not damaged in case a frequent earthquake occurs. Both EC8 and NTC 08 provide that acceleration-sensitive nonstructural components, instead, are designed in order to withstand the seismic demand caused by a rare earthquake, e.g. a 475-year return period event for ordinary buildings. This approach is counterintuitive: hence, while it is implicitly accepted that displacement-sensitive nonstructural components may collapse for a rare earthquake, acceleration-sensitive components should not collapse for such an intense motion.

It is definitely important to verify that nonstructural components do not exhibit major damage for a frequent earthquake, considering the limit state definitions mentioned above. Moreover, it is questionable to verify such components against a rare earthquake; it does not make sense to verify their safety while, according to the definition of the ultimate limit state, it is accepted that they can collapse for a rare earthquake. The verification for a rare earthquake could be conducted only for nonstructural components that can threaten the life safety in case of failure. Therefore it seems reasonable to design also acceleration-sensitive nonstructural components in ordinary buildings according to frequent earthquakes. For this reason, the research study aims at evaluating the seismic demand on acceleration-sensitive nonstructural components caused by frequent earthquakes. It should be underlined that the such considerations are limited to ordinary buildings. Nonstructural components inserted in strategic facilities, such as hospitals, must remain operational even for rare earthquakes (Gatscher and Bachman, 2012).

An important advantage is connected to the study of the seismic demand on NSCs due to frequent earthquakes. Indeed, floor response spectra obtained from dynamic analysis for rare earthquakes show that nonstructural components acceleration demand depends on the ductility demand level of the primary structure (Medina et al., 2006; Petrone et al., 2014). However, the ductility demand is not easily predictable during the design phase: the structural overstrength reduces the ductility demand compared to the one assumed during the design phase (D'Ambrisi and Mezzi, 2009, 2005). For frequent

earthquakes it can be assumed that the primary structure does not exhibit large excursions in plastic range. In this case it is not necessary to rigorously assess the level of ductility and the structural overstrength for evaluating the acceleration demand on nonstructural components.

Finally, different studies available in literature (Singh et al., 2006b; Sullivan et al., 2013) evidenced that rare earthquakes induce large floor accelerations in buildings, that are typically underestimated by the code formulas. The question arises how to design a nonstructural component in order to withstand such a large acceleration demand, that may be larger than 10 - 20 times the peak ground acceleration (Singh et al., 2006b).

3.2.3 METHODOLOGY

3.2.3.1 DESIGN OF THE BENCHMARK STRUCTURES

Five multi-story RC frame structures are designed according to Eurocode 8 (EC8) (CEN, 2004b) provisions. These benchmark structures are characterized by a different number of stories, i.e. one, two, three, five and ten stories, and by a 3 m interstory height and two 5 m wide bays in each direction.

Modal response spectrum analyses are performed considering a 0.25 g design ground acceleration on stiff soil a_g . The horizontal elastic response spectrum is defined referring to a 5% damping ratio and a 1.2 soil factor, i.e. soil type B. The seismic design meets the ductility class “high” (DCH) requirements: the assumed behavior factor is 4.95 for one-story building and 5.85 for multi-story frames. According to EC8, a halved moment of inertia is considered for the primary elements, in order to take into account the effect of cracking. The design fundamental periods of the benchmark structures are listed in Figure 114.

The mass is lumped at each story considering the actual column and beam cross sections. The dead weight of the slab is evaluated according to the typical RC slab dimensions used in European constructions. The mass per square meter ranges from 0.87 t/m² at the 1st floor of the 1-story structure to 1.39 t/m² at the 1st floor of the 10-story structure.

The dimensions of the column cross sections are strongly influenced by the restricted value of normalized design axial force; indeed, the average compressive stress over the concrete compression strength must not exceed 0.55. The limitation is especially valid for tall structures.

3.2.3.2 MODELING

Dynamic analyses are carried out for a set of seven earthquake records, on both linear and nonlinear models. Both linear and nonlinear analyses are performed on the central 2D frame of the benchmark structures (Figure 114). RC slabs and rigid diaphragms are considered for each floor; a third of the seismic mass is assigned to a master joint at each floor. Analyses are performed using the OpenSees program (McKenna and Fenves, 2013).

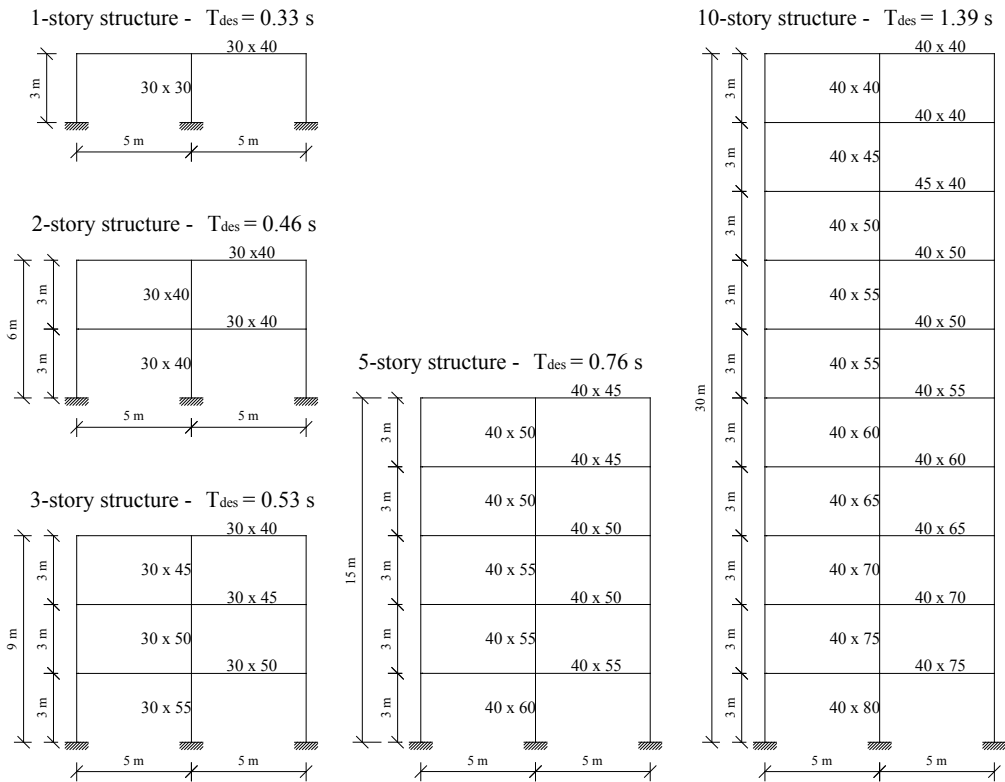


Figure 114. Lateral view of the considered building models and their design fundamental period (T_{des}). Dimensions of the cross sections are in [cm].

The primary elements are modeled as elastic beam-column elements in the linear model of the structures: the gross moment of inertia is considered. Concrete is modeled as an elastic material with a Modulus of Elasticity equal to 31476 MPa, according to the C25/30 class concrete assumed during the design phase.

A distributed plasticity approach is selected in order to define the nonlinear model of the structures. This approach allows investigating pre- and post-cracking behavior of the elements. Primary elements are modeled as nonlinear force-based elements (McKenna and Fenves, 2013). For each element appropriate cross sections are defined

considering the actual geometry and steel reinforcement. The cross section is divided into fibers and a stress-strain relationship is defined for each of them. Different constitutive laws are applied to three different kinds of fibers: unconfined concrete law is associated to cover fibers, confined concrete law is associated to core fibers, steel law is associated to the longitudinal reinforcement fibers. The stress-strain relationship for both unconfined and confined concrete are evaluated according to Mander et al. (1988). Tensile concrete strength is also considered.

The class B450C for the steel is used and a bilinear with hardening relationship is adopted. The mechanical characteristics for the steel and the concrete are calculated according to Eurocode 2 (CEN, 2004a).

3.2.4 GROUND MOTION RECORDS

A set of accelerograms representative of the frequent earthquake ground motion at the considered site is defined basing on the motivations included in Section 3.2.2. Eurocode 8 does not provide a formulation for the definition of the spectrum corresponding to a frequent earthquake. The Italian Building Code, instead, provides detailed hazard maps (a grid of more than 16,000 points) corresponding to different probabilities of exceedance in 50 years; the maps allows defining the spectrum that envelopes the uniform hazard spectrum at the site characterized by a given probability of exceedance. The maps are defined upon a probabilistic seismic hazard assessment (PSHA) of Italy performed by Stucchi et al. (2011).

In order to be consistent with the spectrum adopted during the design phase, the selected point of the Italian grid exhibits a 475-y return period spectrum very close to the one assumed during the design phase. The point, located close to the epicenter of (6.9 M_w) 1980 Irpinia earthquake, is characterized by a peak ground acceleration on stiff soil equal to 0.25 g for a 10% probability of exceedance in 50 years, i.e. a return period equal to 475 years. According to the Italian Building Code, a frequent earthquake is characterized by a 63% probability of exceedance, i.e. a 50-year return period; for the selected grid point the peak ground acceleration on stiff soil, characterized by a 63% probability of exceedance in 50 years is equal to 0.078 g. The 50-year return period spectrum is shown in solid thin line in Figure 115.

A suitable set of 7 European accelerograms (Table 38) recorded on soil type B is then provided, according to the EC8 recommendations (Maddaloni et al., 2012), matching the 50-year return period spectrum:

- the mean of zero-period spectral response acceleration values is larger than 0.094 g, i.e. the peak ground acceleration (PGA) considering a soil type B;

- the mean elastic spectrum of the selected ground motions is larger than 90% of the target elastic response spectrum (Figure 115) in the range of periods between $0.2T_{1,\min}$ and $2T_{1,\max}$, where $T_{1,\min}$ and $T_{1,\max}$ are, respectively, the minimum and the maximum fundamental period of the benchmark structures.

Waveform ID	Earthquake ID	Earthquake Name	M_w	Epicentral distance [km]	Direction	PGA [m/s^2]
761	292	Umbria Marche (aftershock)	5.6	21	x	1.07
2017	664	Drama	5.2	19	y	0.83
49	34	Friuli	6.5	42	y	0.86
2006	700	Almiros (aftershock)	5.2	14	y	0.71
231	108	Montenegro (aftershock)	6.2	21	x	1.63
336	159	Preveza	5.4	28	x	1.40
293	146	Campano Lucano	6.9	33	y	0.97

Table 38. Information about earthquakes used for dynamic analyses (Ambraseys et al., 2002).

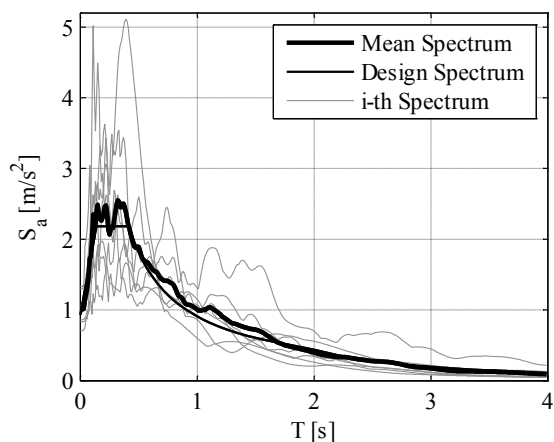


Figure 115. Comparison between design and mean natural spectrum at damage limit state.

3.2.5 RESULTS AND DISCUSSION

3.2.5.1 ELASTIC AND INELASTIC FLOOR RESPONSE SPECTRA

Dynamic analyses on the elastic and inelastic models are performed. The floor response spectrum at a given story is evaluated as the mean of the floor response spectra evaluated subjecting the structure to the 7 accelerograms reported in Table 38.

A 5% damping ratio is considered. This spectrum yields the maximum acceleration to which a nonstructural component is subjected, assuming that it is schematized as a single degree of freedom with a natural period T . The floor response spectra resulting from elastic and inelastic models are plotted and compared in Figure 116.

Both in elastic and inelastic models, peaks are exhibited in the floor spectra for a period close to the natural periods of the primary structure. This phenomenon is caused by the filtering action of the primary structure that modifies the frequency content of the base input at the different stories; the floor motion is characterized by a large frequency content for frequencies close to the natural frequencies of the structure. The nonstructural component at a given floor, which is characterized by a natural period close to the structural one, is subjected to the large accelerations, denoted by the peak in the floor spectra.

However, for inelastic models the peaks do not correspond to natural periods because the primary elements, subjected both to vertical loads and horizontal seismic action, exhibit a stiffness reduction due to the cracking, leading to the natural period elongation phenomenon.

The influence of higher modes is more evident for tall buildings, whose floor spectral accelerations, associated to the higher modes, are greater than the ones corresponding to the first mode. This phenomenon is more evident for inelastic models, in which the reduction of the floor spectral ordinates mainly involves the first mode peak, whereas the peaks corresponding to the higher modes are only slightly reduced. It is interesting to note that the reduction of the spectral ordinates is significant despite the structural elements are not yielded; the nonlinearity due to the cracking of the elements is significantly beneficial in terms of the seismic demand on nonstructural components.

It should be noted that the frequent seismic action considered in this study produces a demand on nonstructural components that is much smaller than the demand caused by the design rare seismic action considered in Petrone et al. (2014) on the same benchmark structures. Considering inelastic models, the seismic demand on nonstructural component due to a frequent seismic action does not exceed 0.9 g, whereas the demand due to rare earthquakes may be close to 3 g (Petrone et al., 2014).

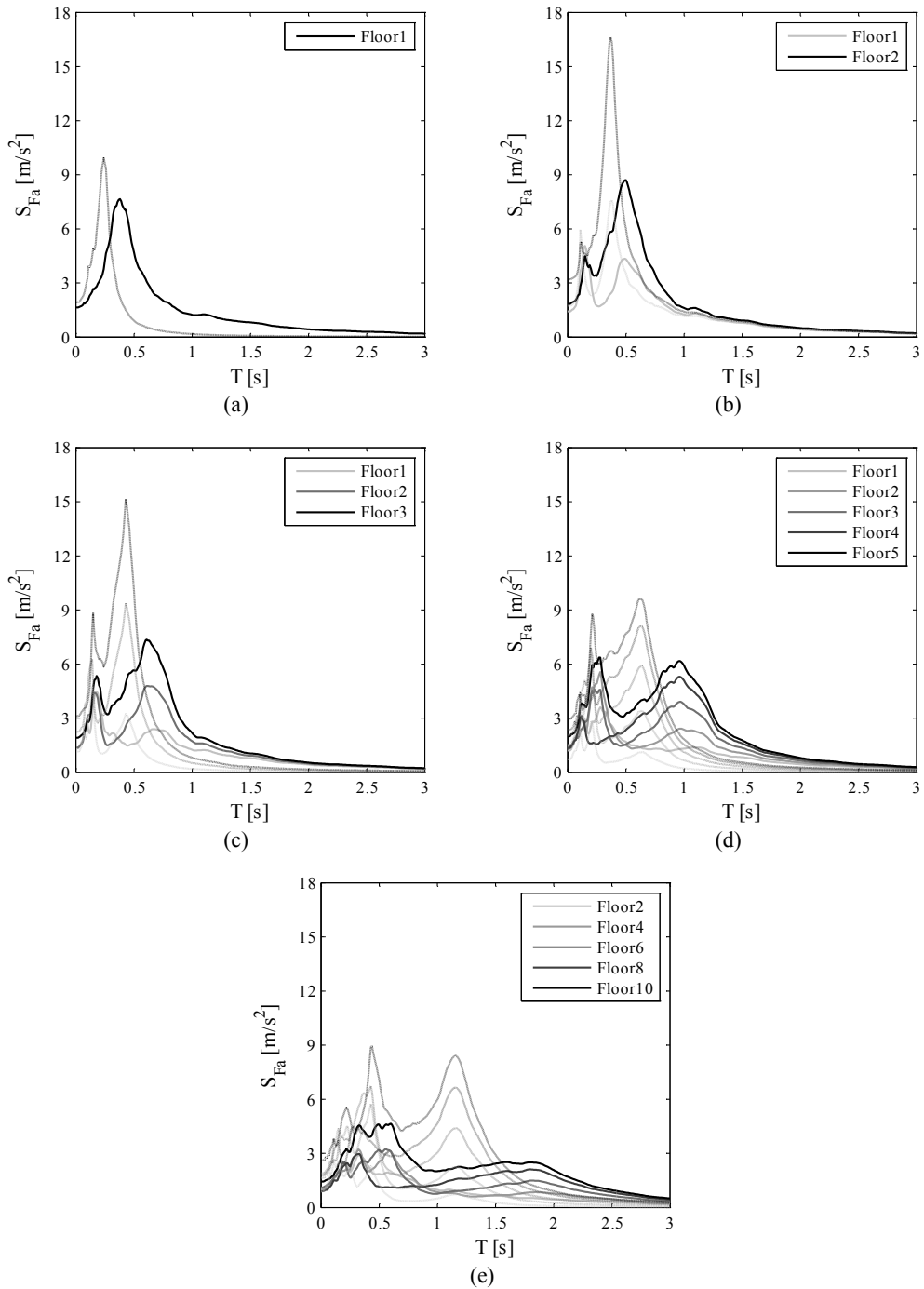


Figure 116. Floor response spectra in elastic (dotted lines) and inelastic (solid lines) models for (a) 1-story, (b) 2-story, (c) 3-story, (d) 5-story and (e) 10-story structures.

3.2.5.2 FLOOR AMPLIFICATION EVALUATION

The trends of the ratio between the peak floor acceleration (PFA) and the peak ground acceleration (PGA) are plotted in Figure 117, in order to study the acceleration amplification at the different story levels.

Both elastic and inelastic models show almost linear trends, excepting the 10-story structure, in which the shape of the PFA/PGA trend is influenced by the second mode displacement shape at the top stories. A reduction of the PFA/PGA ratio is exhibited in the inelastic models with respect to the elastic ones, due to the cracking of the primary elements; however, at lower stories of the tallest buildings, i.e. 5- and 10-story structures, a slight increase is recorded. This latter phenomenon could be caused by the great influence that higher modes have when structural nonlinearity, i.e. cracking, occurs (Fischinger et al., 2011; Rejec et al., 2012).

The PFA/PGA trends are compared to the provisions included in ASCE 7 (American Society of Civil Engineers, 2010) and EC8 that define a linear trend that goes from 1 at the base of the structure to 2.5 and 3 at the top for EC8 and ASCE 7 respectively. Both EC8 and ASCE 7 envelopes overestimate the numerical outcomes; it is noted that inelastic models are considered, since they, through the inclusion of the cracking in the elements, better predict the actual behavior of the structures. An envelope that goes from 1 at the base of the structure to 2 at the top would better fit the results.

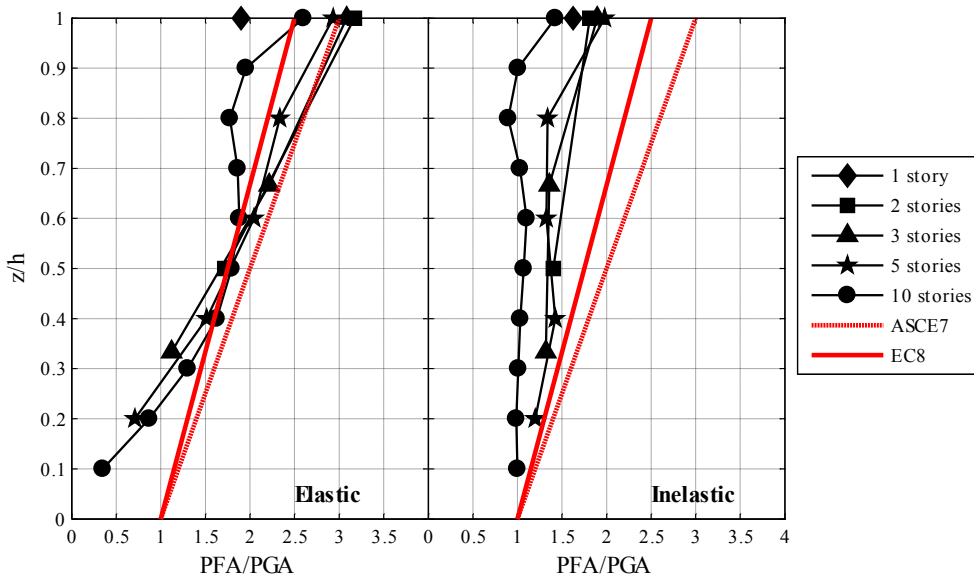


Figure 117. Ratio between peak floor acceleration (PFA) and peak ground acceleration (PGA), versus the relative height (z/h) compared to the provisions included in ASCE7 and EC8.

3.2.5.3 COMPONENT AMPLIFICATION EVALUATION

The trends of the ratio a_p between the maximum floor spectrum acceleration ($S_{fa,max}$) and the PFA with respect to relative height are shown in Figure 118, in order to study the component acceleration magnification of the floor accelerations. The outcomes corresponding to the elastic and inelastic models are compared: only slight differences are exhibited. The a_p ratio ranges from 3.0 to 5.2 in elastic models whereas it ranges from 2.6 to 4.8 in inelastic models. The component acceleration magnifications in tall buildings are generally smaller than the ones in short structures.

The trends are compared to the provisions included in ASCE7 and EC8, that define a trend that goes from 2.5 at the base of the structure to 2.5 and 2.2 at the top for ASCE7 and EC8 respectively (Figure 118). Hence, a noteworthy underestimation of the a_p values in the current building codes is clearly evidenced, as shown in Medina et al. (2006).

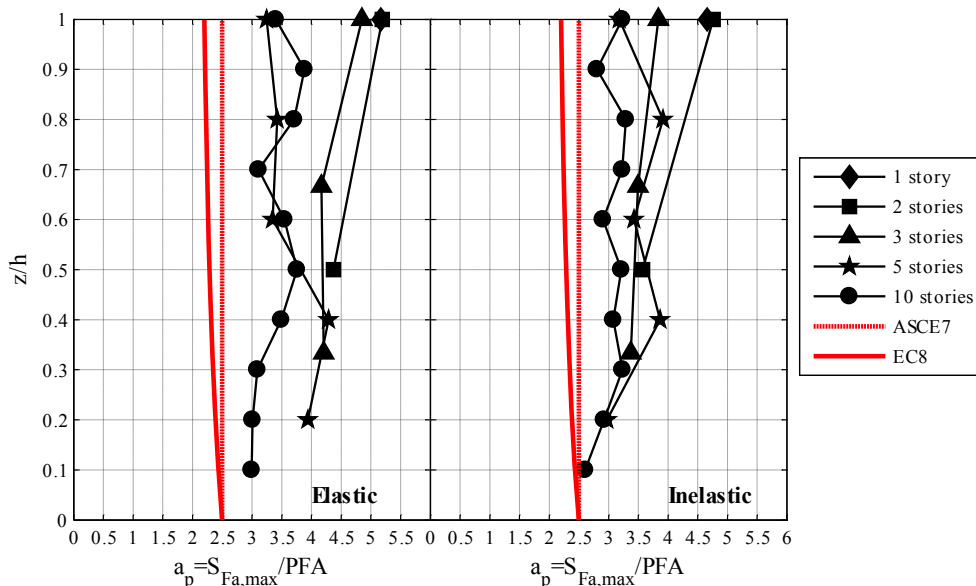


Figure 118. Floor acceleration magnification on nonstructural components versus the relative height (z/h) compared to the provisions included in ASCE7 and EC8.

3.2.5.4 COMPARISON WITH EC8 FORMULA AND LIMITATIONS

Eurocode 8 (CEN, 2004b) provides that the floor spectral acceleration, i.e. the maximum acceleration on a SDOF nonstructural component, is evaluated as:

$$S_{Fa,EC8}(T) = \alpha \cdot S \cdot \left[\frac{3 \cdot (1 + z/H)}{1 + (1 - T/T_1)^2} - 0.5 \right] \cdot g \geq \alpha \cdot S \cdot g \quad (21)$$

where:

- α is the ratio between the peak ground acceleration on stiff soil and the gravity acceleration g ;
- S is a soil amplification factor;
- z/H is the relative structural height at which the component is located;
- T is the nonstructural component period;
- T_1 is the fundamental period of the primary structure, assumed during the design phase.

The Eurocode 8 floor response spectrum could be then compared to the floor spectra resulting from the analyses, assuming in the formulation (21) a peak ground acceleration on stiff soil equal to 0.078 g , i.e. the 50-year return period peak ground acceleration. In Figure 119 the floor spectra are compared to Eurocode 8 floor spectra for the different structures considered in this study. In order to take into account the realistic behavior of the primary structures, floor spectra in inelastic models are considered.

This comparison underlines that Eurocode 8 typically underestimates the acceleration demand on nonstructural component for a wide range of periods, especially for periods close to the structural natural periods. Eurocode floor spectra give a good approximation, typically safe-sided, of the floor spectra for period sufficiently larger than the fundamental period of the structure. They also give a good approximation of the period (T_{des} in Figure 114) at which the maximum floor spectral acceleration occurs; this is caused by the assumption of halved inertia during the design phase, in order to take into account the effects of cracking.

Higher mode effects are not considered in the formulation (21): a significant underestimation is recorded in the range of periods close to the higher mode periods of vibration. The effective floor spectrum acceleration can be significantly underestimated, especially for tall buildings, i.e. the 5- and the 10-story structures, in which higher modes are predominant. An urgent need to include higher modes in the code formulation is clearly evidenced.

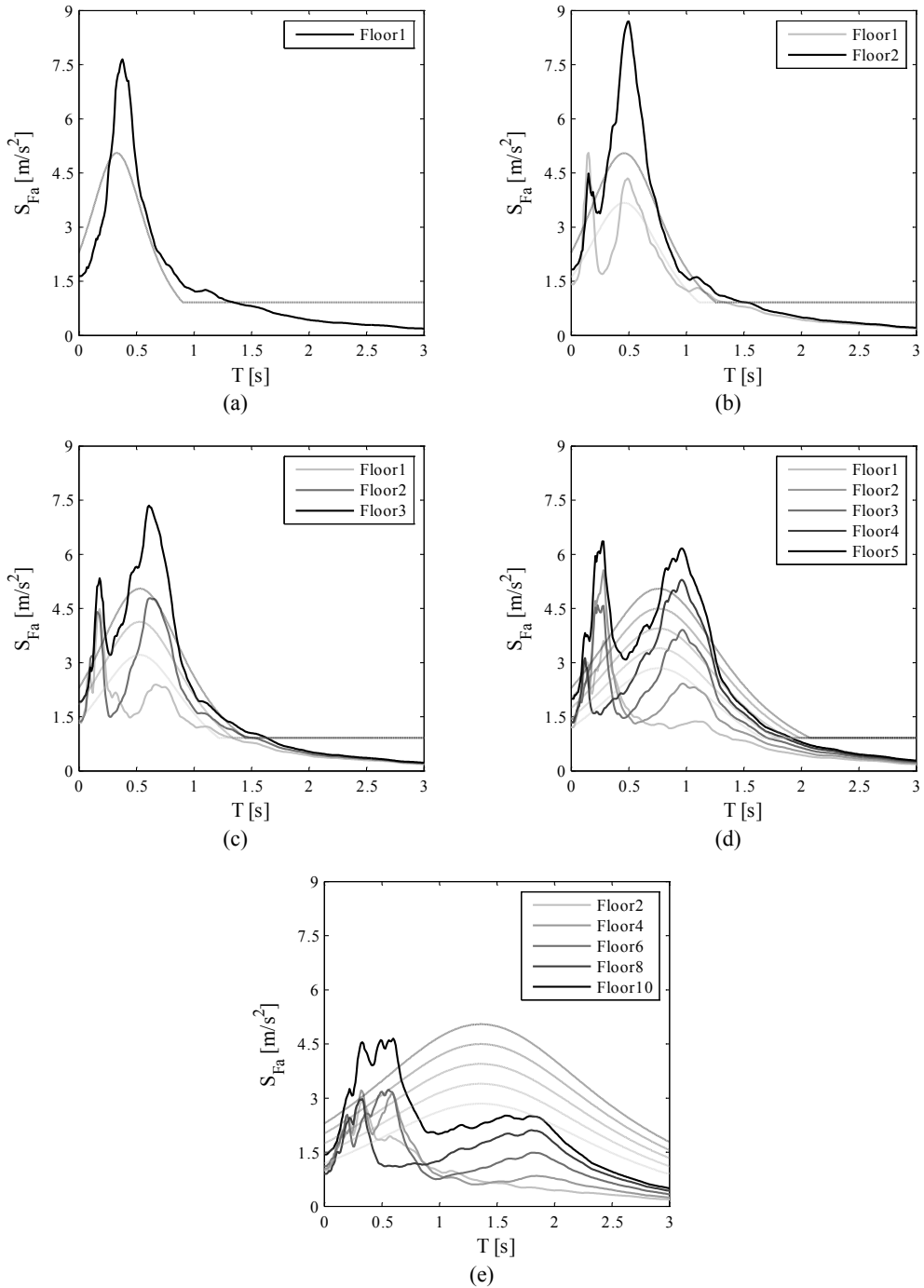


Figure 119. Floor response spectra (solid lines) on inelastic models compared to EC8 floor spectra (dashed lines) for the (a) 1-story, (b) 2-story, (c) 3-story, (d) 5-story and (e) 10-story structures.

3.2.5.5 DEFINITION OF A CODE FORMULA

The previous sections clearly evidenced the inadequacy of the Eurocode provisions for the evaluation of the seismic demand on acceleration-sensitive nonstructural components. The main issues of the EC8 formulation can be summarized in: (a) the slight overestimation of the peak floor acceleration (see Section 3.2.5.2), (b) the significant underestimation of the component acceleration magnification at a given floor (see Section 3.2.5.3), (c) the non-inclusion of the higher mode effects in the formulation, that lead to a significant underestimation of the floor spectral acceleration for small periods (see Section 3.2.5.4). However, the shape of the Eurocode floor spectrum is found to suitably catch the shape of typical floor response spectra. In this Section a novel formulation is proposed (Figure 120): it is based on Eurocode formulation and to some suggestions included in (Fathali and Lizundia, 2011).

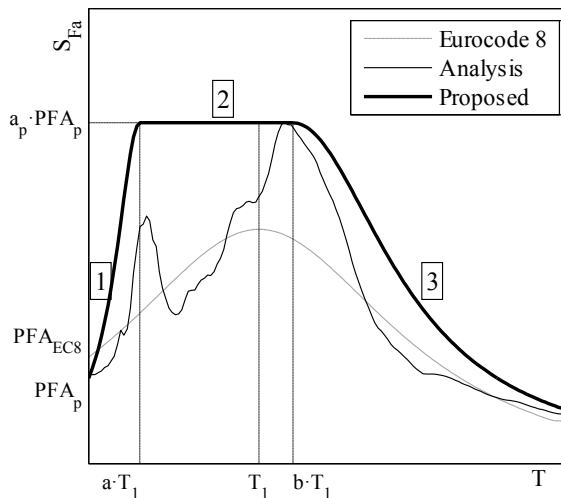


Figure 120. Proposed floor spectral shape compared to the Eurocode 8 floor spectral shape and to a typical analytical floor spectrum.

A formula similar to the one already included in the Eurocodes is defined, both for the sake of simplicity and in order to facilitate the implementation in future building codes.

- A three-branch floor response spectrum is defined (branches from 1 to 3 in Figure 120), in order to include the peaks corresponding to higher mode effect. Branches no. 1 and no. 3 have a shape similar to Eurocode 8 floor spectrum. The definition of the flat branch no. 2 is also capable to include the uncertainty in the evaluation of the structural periods.
- The formula included in EC8 is slightly modified in order to directly distinguish the different terms, i.e. ground acceleration, floor amplification and

component amplification, that influence the definition of the floor response spectrum as follows:

$$S_{Fa,proposed}(T) = PGA \cdot \frac{PFA}{PGA} \cdot \frac{S_{Fa}(T)}{PFA} \quad (22)$$

- The PFA over PGA ratio trend is modified according to the evidence described in the Section 3.2.5.2. The proposed ratio trend goes from 1 at the base of the structure to 2 at its top.
- The amplification factor a_p is increased up to 5 for short buildings and is reduced for tall ones (Table 39), according to the analytical results (Figure 118).

The proposed response spectra is defined according to the following formulation:

$$S_{Fa,proposed}(T) = \begin{cases} \alpha \cdot S \cdot g \cdot (1+z/H) \cdot \left[\frac{a_p}{1+(a_p-1)\left(1-T/a \cdot T_1\right)^2} \right] \geq \alpha \cdot S \cdot g & \text{for } T < a \cdot T_1 \\ \alpha \cdot S \cdot g \cdot (1+z/H) \cdot a_p & \text{for } a \cdot T_1 < T < b \cdot T_1 \\ \alpha \cdot S \cdot g \cdot (1+z/H) \cdot \left[\frac{a_p}{1+(a_p-1)\left(1-T/b \cdot T_1\right)^2} \right] \geq \alpha \cdot S \cdot g & \text{for } T > b \cdot T_1 \end{cases} \quad (23)$$

The parameters a , b and a_p are defined according to the fundamental period of the structure T_1 according to Table 39. They are based on the indications included in (Fathali and Lizundia, 2011) and they are then calibrated in order to ensure a good matching between the analytical floor response spectra and the proposed floor spectra. The other parameters are the same as in Eurocode formula (21).

	a [-]	b [-]	a_p [-]
$T_1 < 0.5$ sec	0.8	1.4	5.0
$0.5 \text{ sec} < T_1 < 1.0$ sec	0.3	1.2	4.0
$T_1 > 1.0$ sec	0.3	1.0	2.5

Table 39. Values of the parameters of the proposed formulation for different ranges of structural periods.

The floor spectra are evaluated according to the proposed formulation (23) and compared to the analytical floor spectra evaluated on the inelastic models (Figure 121). The proposed floor spectra are typically safe-sided with respect to the analytical results. They are also capable to include the peaks related to the structural higher modes; the reduction of the seismic demand on very flexible nonstructural components is also caught.

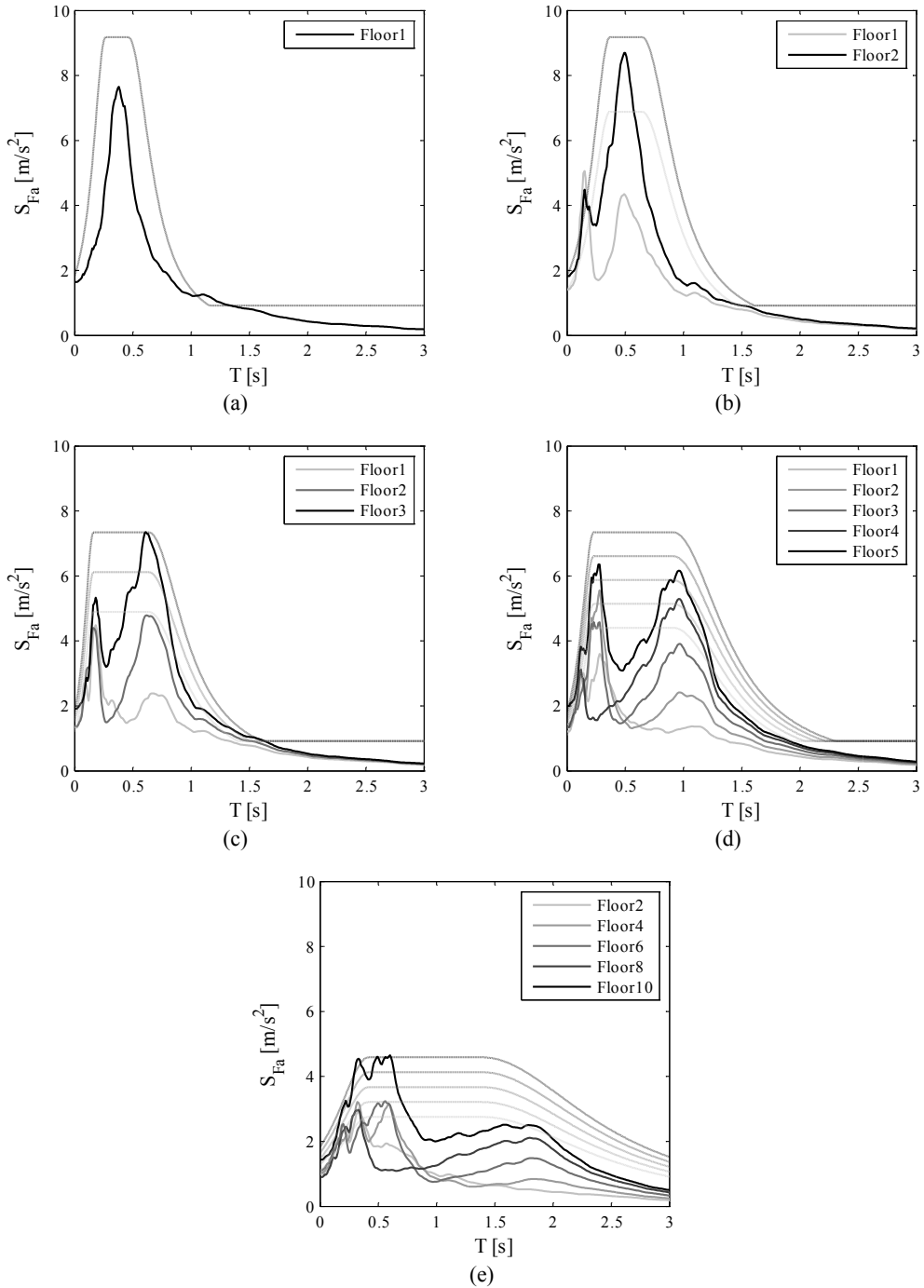


Figure 121. Floor response spectra (solid lines) on inelastic models compared to formulation (23) (dashed lines) for the (a) 1-story, (b) 2-story, (c) 3-story, (d) 5-story and (e) 10-story structures.

The proposed formulation yields conservative floor spectral accelerations for a wide range of periods, especially for periods close to the fundamental period; however, this overestimation could cover the uncertainty in the estimation of the structural period due to, for instance, the presence of stiff infill walls and partition walls (Petrone et al., 2013), as well as the uncertainty in the estimation of the nonstructural component period during the design phase.

3.2.6 CONCLUSIONS

Floor response spectra are evaluated through time-history analyses on a set of five RC frame structures with different number of stories. The floor spectra are evaluated according to a set of accelerograms compatible to a frequent seismic input motion. The investigation of floor response spectra induced by frequent earthquakes is motivated following a detailed analysis of the limit states definition in the actual European and Italian Building Codes.

Both elastic and inelastic models of the benchmark structures are considered. A period elongation phenomenon is clearly evidenced in floor spectra of the inelastic models, which is mainly caused by the cracking of the primary elements. The nonlinearity due to the cracking of the elements also induces a reduction of the floor spectral ordinates; the reduction of the floor spectral ordinates mainly involves the floor spectrum peak corresponding to the first mode, whereas the peaks corresponding to the higher modes are only slightly reduced. For tall buildings, the floor spectral accelerations associated to the higher modes are greater than those corresponding to the first mode.

The peak floor acceleration shows an almost linear trend with the structural relative height. The prediction included both in EC8 and ASCE 7 are conservative, i.e. they provide larger values of peak floor acceleration compared to the accelerations that result from the analyses.

The peak component acceleration, i.e. the maximum floor spectral acceleration value at a given story, normalized to the peak floor acceleration exhibits an almost constant trend with the structural relative height. Moreover, the taller the structure is, the smaller the component amplification factor becomes. A significant unsafe-sided prediction of both EC8 and ASCE 7 provisions is demonstrated. The comparison of the floor spectra of inelastic models with the EC8 provisions clearly underlines that Eurocode 8 typically underestimates the acceleration demand on nonstructural component for a wide range of periods. Eurocode floor spectra give a good approximation, typically safe-sided, of the floor spectra for periods sufficiently larger than the fundamental period of the structure. A significant underestimation is recorded

in the range of periods close to the higher mode periods of vibration of the benchmark structures.

A novel formulation is then proposed, based on the Eurocode actual formulation for an implementation in the future building codes. The proposed formulation is able to envelope the floor spectral peaks due to the higher modes. Moreover, it yields conservative floor spectral acceleration for a wide range of periods, especially for periods close to the fundamental period. However, such an overestimation could cover the uncertainty in the estimation of the structural and the nonstructural component periods during the design phase. Finally, it should be underlined that the conclusions of the present study are limited to a set of five regular RC structures designed according to Eurocode 8. A larger set of structures should be considered in a future study in order to validate the proposed formulation.

3.2.7 REFERENCES

- Ambraseys N, Smit P, Sigbjornsson R, Suhadolc P, Margaris B (2002) Internet-Site for European Strong-Motion Data. European Commission, Research-Directorate General, Environment and Climate Programme
- American Society of Civil Engineers (2010) ASCE/SEI 7-10: Minimum Design Loads for Buildings and Other Structures. Reston, Virginia, US
- CEN (2004a) Eurocode 2: Design of concrete structures - Part 1-1: General rules and rules for buildings. EN 1992-1-1. Brussels, Belgium
- CEN (2004b) Eurocode 8: design of structures for earthquake resistance - Part 1: general rules, seismic actions and rules for buildings. EN 1998-1. Brussels, Belgium.
- Consiglio Superiore dei Lavori Pubblici (2008) Decreto Ministeriale del 14/01/2008, Approvazione delle nuove norme tecniche per le costruzioni. G.U. n. 29 del 4/2/2008 (in Italian)
- D'Ambrisi A, Mezzi M (2005) A probabilistic approach for estimating the seismic response of elasto-plastic SDOF systems. *Earthquake Engineering & Structural Dynamics* 34 (14):1737-1753. doi:10.1002/eqe.509
- D'Ambrisi A, Mezzi M (2009) Probabilistic estimate of seismic response design values of RC frames. *Earthquake Engineering & Structural Dynamics* 38 (15):1709-1727. doi:10.1002/eqe.925
- Fathali S, Lizundia B (2011) Evaluation of current seismic design equations for nonstructural components in tall buildings using strong motion records. *The Structural Design of Tall and Special Buildings* 20:30-46. doi:10.1002/tal.736
- Fischinger M, Ercolino M, Kramar M, Petrone C, Isakovic T (2011) Inelastic seismic shear in multi-storey cantilever columns. Paper presented at the 3rd International Conference on Computational Methods in Structural Dynamics and Earthquake Engineering, COMPDYN 2011, 25-28 May 2011. Corfu, Greece,

- Gatscher JA, Bachman R (2012) Elements of 2012 IBC / ASCE 7-10 Nonstructural Seismic Provisions: Bridging the Implementation Gap. Paper presented at the 15th World Conference on Earthquake Engineering, Lisboa, Portugal,
- Maddaloni G, Magliulo G, Cosenza E (2012) Effect of the seismic input on non-linear response of R/C building structures. *Advances in Structural Engineering* 15 (10):1861-1877
- Mander J, Priestley M, Park R (1988) Theoretical Stress-Strain Model for Confined Concrete. *Journal of Structural Engineering* 114 (8):1804-1826. doi:10.1061/(ASCE)0733-9445(1988)114:8(1804)
- McKenna F, Fenves GL (2013) OpenSees Manual <http://opensees.berkeley.edu>. Pacific Earthquake Engineering Research Center, Berkeley, California.,
- Medina RA, Sankaranarayanan R, Kingston KM (2006) Floor response spectra for light components mounted on regular moment-resisting frame structures. *Engineering Structures* 28 (14):1927-1940. doi:10.1016/j.engstruct.2006.03.022
- Petrone C, Magliulo G, Manfredi G (2013) Shake table tests for the seismic assessment of hollow brick internal partitions. *Engineering Structures*:(under review)
- Petrone C, Magliulo G, Manfredi G (2014) Floor response spectra in RC frame structures designed according to Eurocode 8. *Journal of Earthquake Engineering* (submitted for publication)
- Rejec K, Isaković T, Fischinger M (2012) Seismic shear force magnification in RC cantilever structural walls, designed according to Eurocode 8. *Bulletin of Earthquake Engineering* 10 (2):567-586. doi:10.1007/s10518-011-9294-y
- Rodriguez ME, Restrepo JJ, Carr AJ (2002) Earthquake-induced floor horizontal accelerations in buildings. *Earthquake Engineering and Structural Dynamics* 31 (3):693-718. doi:10.1002/eqe.149
- Singh M, Moreschi L, Suárez L, Matheu E (2006a) Seismic Design Forces. I: Rigid Nonstructural Components. *Journal of Structural Engineering* 132 (10):1524-1532. doi:10.1061/(ASCE)0733-9445(2006)132:10(1524)
- Singh M, Moreschi L, Suárez L, Matheu E (2006b) Seismic Design Forces. II: Flexible Nonstructural Components. *Journal of Structural Engineering* 132 (10):1533-1542. doi:10.1061/(ASCE)0733-9445(2006)132:10(1533)
- Structural Engineers Association of California (SEAOC) (1995) *Vision 2000 - A Framework for Performance-based Design*. California Office of Emergency Services
- Stucchi M, Meletti C, Montaldo V, Crowley H, Calvi GM, Boschi E (2011) Seismic Hazard Assessment (2003–2009) for the Italian Building Code. *Bulletin of the Seismological Society of America* 101 (4):1885-1911. doi:10.1785/0120100130
- Sullivan TJ, Calvi PM, Nascimbene R (2013) Towards improved floor spectra estimates for seismic design. *Earthquakes and Structures* 4 (1):109-132. doi:10.12989/eas.2013.4.1.109

Chapter 4 *CONCLUSIONS*

Some research studies concerning nonstructural components are described in this thesis, based on several motivations: (a) the threat to life-safety that the collapse of nonstructural components can cause; (b) the attitude of these components in exhibiting damage (and the consequent evacuation of buildings) even for low-intensity earthquakes; (c) the huge economic loss connected to their damage.

Some experimental activities are carried out aiming at the evaluation of the seismic capacity of some nonstructural components, i.e. innovative plasterboard partitions, hollow brick partitions, standard high plasterboard partitions, hospital building contents and plasterboard continuous ceilings.

A proper test setup is defined for each test campaign in order to subject the specimen to the demand that it would experience in a building. Realistic boundary conditions of the specimen are reproduced. A testing protocol is defined according to AC 156, in case shake table tests are conducted, and FEMA 461 prescriptions, in case quasi-static tests are performed. A slight modification to the testing protocol provided by FEMA 461 is proposed, considering a set of European earthquakes in lieu of American ones, while a seismic input is derived based on AC 156 prescriptions for shake table testing. After each test of each campaign the visual damage is correlated to the occurrence of a given Damage State (DS) through the use of a damage scheme. A relationship between an Engineering Demand Parameter (EDP), e.g. the interstory drift ratio or the peak floor acceleration, and a predefined Damage State (DS), is established for the tested components. For instance, innovative plasterboard partition systems exhibit a good seismic behavior: a minor damage state is attained at 0.58% drift level, while a moderate damage state is attained at 0.98% drift level. Standard hollow brick partitions, instead, exhibits minor damage at 0.2% interstory drift, moderate damage at 0.34% interstory drift and major damage at 0.97% interstory drift.

In case the number of specimens within a test campaign is adequate, the fragility curve of the tested specimens, that expresses the attitude that the specimens have to exhibit damage at different seismic demand levels, is also evaluated. For instance, fragility curves are defined for a hospital examination room. Such fragility curves are derived based on a systemic approach, i.e. encompassing the performance levels of the components within the sample examination rooms. The DS1 and DS3 median peak floor acceleration values are 0.45 g and 1.06 g, whereas the logarithmic standard

deviations are 0.30 and 0.26, respectively. Based on six quasi-static tests on high plasterboard partitions, the fragility curves for three different damage states are evaluated. Their evaluation yields a median IDR value equal to 0.28%, 0.81% and 2.05% and a logarithmic standard deviation equal to 0.39, 0.42 and 0.46 for DS1, DS2 and DS3, respectively.

The damage progression is correlated to different properties of the test setup, such as its natural frequency, damping ratio and the dissipated energy. Macro-models of the tested specimens are also defined based on the experimental results for an easy implementation in a structural model of the tested nonstructural components.

The evaluation of the seismic demand on nonstructural components is also a main objective of this research study. Nonstructural components should be subjected to a careful and rational seismic design, in order to reduce the economic loss and to avoid threats to the life safety, as well as what concerns the structural elements. A parametric study on five RC frame structures, designed according to Eurocode 8, is conducted. It is found that the Eurocode formulation for the evaluation of the seismic demand on nonstructural components does not well fit the outcomes of the analyses. Some comments on the target spectrum provided by AC 156 for the seismic qualification of nonstructural components are also included and a modification is proposed. In particular, it is shown that in case the upper bound limitation on the Required Response Spectrum (RRS) is removed, the RRS well matches the floor response spectra resulting from the analyses on the benchmark structures.

The counterintuitive approach of current building codes to the design of nonstructural components is highlighted. For this reason the seismic demand on acceleration-sensitive nonstructural components caused by frequent earthquakes is also investigated. Finally, a novel formulation for the evaluation of such a demand is proposed for an easy implementation in future building codes based on the actual Eurocode provisions. The proposed formulation is able to envelope the floor spectral peaks due to the higher modes. Moreover, it yields conservative floor spectral acceleration for a wide range of periods, especially for periods close to the fundamental period.